RAINFALL INDUCED LANDSLIDE - DETECTION AND DEVELOPMENT OF EARLY WARNING SYSTEM

Ph.D. THESIS

by

ABHISHEK PRAKASH PASWAN

DEPARTMENT OF CIVIL ENGINEERING
DELHI TECHNOLOGICAL UNIVERSITY
DELHI – 110042 (INDIA)
NOVEMBER, 2023

RAINFALL INDUCED LANDSLIDE - DETECTION AND DEVELOPMENT OF EARLY WARNING SYSTEM

A THESIS

Submitted in partial fulfilment of the requirements for the award of the degree

of

DOCTOR OF PHILOSOPHY

in

CIVIL ENGINEERING

by

ABHISHEK PRAKASH PASWAN

Under the supervision of

PROF. A. K. SRIVASTAVA

DEPARTMENT OF CIVIL ENGINEERING
DELHI TECHNOLOGICAL UNIVERSITY
DELHI – 110042 (INDIA)
NOVEMBER, 2023

©DELHI TECHNOLOGICAL UNIVERSITY, DELHI-2023
ALL RIGHTS RESERVED

DELHI TECHNOLOGICAL UNIVERSITY
DELHI

CANDIDATE'S DECLARATION

I hereby certify that the work which is being presented in the thesis entitled **"RAINFALL INDUCED LANDSLIDE - DETECTION AND DEVELOPMENT OF EARLY WARNING SYSTEM"** in partial fulfilment of the requirements for the award of the Degree of Doctor of Philosophy and submitted in the Department of Civil Engineering of the Delhi Technological University, Delhi is an authentic record of my own work carried out during a period from December, 2018 to November, 2023 under the supervision of Prof. A. K. Srivastava, Professor, Department of Civil Engineering, Delhi Technological University, Delhi, India.

The matter presented in this thesis has not been submitted by me for the award of any other degree or in any other Institution.

(**ABHISHEK PRAKASH PASWAN)**

This is to certify that the above statement made by the candidate is correct to the best of my knowledge.

(Prof. A. K. Srivastava)
Supervisor

Date: November 09, 2023

ACKNOWLEDGEMENTS

I wish to convey my profound gratitude and heartfelt appreciation to the individuals who have been instrumental in supporting and assisting me in the successful completion of this thesis. It is with deep gratitude that I express my appreciation for their contributions, and I would like to dedicate the following words to acknowledge their invaluable assistance.

First and foremost, I extend my deepest gratitude, special thanks, and heartfelt appreciation to my supervisor, **Prof. A. K. Srivastava**. His unwavering support throughout my PhD journey has been nothing short of remarkable. There were moments when I felt lost and demotivated, but his guidance and presence were my guiding lights. Professor Shrivastava's exceptional ability to motivate, lead, and pursue new frontiers in academia are qualities I deeply admire. Words cannot adequately express the depth of my gratitude for his support and cooperation.

I am equally appreciative of the support I received from the department head and DRC chairman, Prof. Vijay K. Minocha, during my doctoral journey. I hold him in high regard and will always be respectful of his contributions. I extend my sincere thanks to the heads and faculty members especially Prof. Nirendra Dev, Prof. Munendra Kumar and Dr. Ritu Raj for providing me sensible guidance, faultless planning, helpful advice, and kind cooperation at various stages of my PhD journey.

Special gratitude goes to the members of the SRC, Prof. S. K. Singh from the Department of Civil Engineering at Punjab Engineering College, Chandigarh, and Prof. Kausar Ali from the Department of Civil Engineering at Aligarh Muslim University, Aligarh. I am also thankful to Prof. S. Anbu Kumar and Prof. Vijay Gautam from Delhi Technological University for their insightful and constructive feedback.

I am immensely grateful to the staff at the Rock Engineering Laboratory, Geotechnical Engineering Laboratory and Computer-Aided Design Laboratory within the Department of Civil Engineering. I extend my sincere thanks to lab technician Mr. Shashikant and lab assistants, Mr. Atul, Mr. Sanjay, Mr. Rakesh, and Mr. Pankaj, for their unwavering support during the experimental and simulation phases of my research.

My sincere appreciation extends to my senior and colleagues, Dr. Parvesh Kumar, Mrs. Archita Goyal, Dr. Manvendra Verma, Mr. Indrajeet Singh, Mr. Harshit Jayant, Dr. Deepak Singh, Mr. Prashant C. Ramteke, Dr. Sushant Kumar, Mr. Rahul Kumar, Mr. Nitin Lamba, Mr. Rajat Gautam, Mr. Dinesh K. Reddy and Mrs. Istuti Singh, for their valuable suggestions and assistance whenever I sought their guidance. Special thanks are also due for Dr. Shailendra Yadav to his insightful advice.

I would like to extend my heartfelt appreciation to Dr. Rahul Kumar Meena, my dear friend. Your unwavering support during my PhD journey, will forever remain etched in my memory. Your presence was akin to that of a supportive big brother, and I am immensely grateful for that.

I also want to express my gratitude to Mr. Prateek Roshan, whose consistent support from my PhD days through to my thesis submission was instrumental in my success. His priceless review comments, suggestions, and discussions were crucial pillars in the successful submission of my thesis. I owe a great debt of gratitude for his unwavering assistance. Furthermore, I extend my thanks to Mr. Gaurav Pandey, for his insightful comments that significantly contributed to the improvement of my thesis. Your feedback was invaluable, and I truly appreciate your input.

I am indebted to my juniors, Mr. Aniket Sharma, Mr. Wesam Al Agha, Vijay Kaushik, Shailesh Gupta, Mr. Rishabh Tyagi, and Mr. Amit Ram Ahirwar, for their constant support.

My deepest thanks go to my beloved parents, Shri Radhey Shyam Paswan and Smt. Urmila Devi, for their blessings and unwavering support. I extend my appreciation to my sisters, Mrs. (Dr.) Madhu Rashmi and Ms. Preeti Rashmi, my brother, Er. Ved Prakash Kaushal, my Bhabhi, Mrs. Vinulata, and my brother-in-law Dr. Ranjit for their moral and emotional support. Special thanks are reserved for my childhood friends, Mr. Atri Tripathi, Mr. Naveen Mani Tripathi, Mr. Anoop Gupta, and, who stood by me throughout this journey.

I am sincerely thankful and deeply grateful to all those who have supported and contributed to this significant milestone in my life.

(ABHISHEK PRAKASH PASWAN)

ABSTRACT

Landslides are a prominent natural disaster that impacts numerous mountainous areas worldwide, like the Himalayas, Andes, and Alps. It can cause injuries, loss of life, and widespread destruction of land and property, leading to substantial economic losses. Mountainous areas heavily rely on road transport, and when landslides obstruct these routes, it brings severe difficulties to the affected communities. Around 12.6% of India's total land area, equivalent to approximately 0.42 million square kilometers, is susceptible to landslide occurrences, with the north region being particularly susceptible. The Himalayan region is characterized by substantial rainfall, an extended monsoon season, heightened seismic activity, a relatively young geological profile, anthropogenic activities and formidable mountain terrain. These factors collectively result in the Himalayas being responsible for more than 70% of fatal landslides worldwide, with a significant share of these destructive events occurring within India. Despite the increasing information and awareness about landslides, the harm and destruction keep on rising with a massive increase in landslide occurrence throughout the rainy season. Therefore, conducting a well-targeted research study is of utmost importance to understand the mechanism of rainfall-induced landslides and their potential threat to human life and property.

Due to the unpredictable nature of landslides, understanding the complex mechanisms behind such events is crucial for effective monitoring and mitigation strategies. In this study, physical and numerical modelling methods have been utilized to effectively study the mechanism and determine the relative factor of safety under the given rainfall condition. Physical modelling offers a valuable approach to simulate and analyse the processes that trigger and control landslide occurrences under varying rainfall conditions. Hydro-mechanical parameters have been calculated, and a semi-similar material physical model test has been conducted to study the sliding mechanisms. In order to simulate the desired rainfall, a self-developed artificial rainfall generator is used. Furthermore, numerical modelling has been employed to determine the safety factor under dry and rainfall conditions. The study further affirms the validation of numerical simulations when compared to physical modelling. This validation is particularly valuable given the inherent complexities associated with physical modelling, making numerical modelling a more feasible alternative.

In this study, two landslide sites, Jhakri (N31º29’08”, E77º41’43”) in Shimla district and Kotrupi (N31º54“37.60, E76º53”26.30) in the Mandi district of Himachal Pradesh, lying in the northern region of the Indian subcontinent have been selected. Laboratory investigation has been performed to determine the geotechnical parameters of soil, which have further been utilised in physical and numerical modelling.

The physical modelling performed for the Jhakri landslide revealed that a rainfall depth of 80mm and an intensity of 30mm/hr led to debris type of slope failure. The numerical analysis confirmed the slope's stability with a safety factor of 1.23 pre-rainfall and its subsequent instability with a safety factor of 0.626 post-rainfall, highlighting the primary role of rainfall in triggering landslides.

Although numerical and physical techniques are frequently used, their limitations in dealing with unpredictable rainfall-induced landslides highlight the importance of sensor-based monitoring. This study introduces an inventive and cost-effective slope monitoring system that incorporates micro-electromechanical system (MEMS) based tilt and moisture sensors. It allows the collection of real-time data on tilt deformation and moisture content. The effectiveness of this monitoring system has been verified using a custom direct shear-based testing setup and physical slope modelling.

The developed low-cost monitoring system proved its efficiency in detecting both gradual and sudden movements during rainfall-induced landslides, with precise tilt angle measurements and moisture content readings contributing to its accuracy and precision. The tilt sensor can record even the slightest changes in the slope angle with a precision of 0.01 degree, enabling early detection of slope movement. Additionally, the volumetric water content sensor can detect variations with a precision of 1 percent, aiding in the identification of critical conditions that could lead to landslides.

The developed early warning system, designed for identifying impending slope failures, utilized a combination of tilt angle and moisture content variations. Through continuous monitoring, the system observed a gradual shift in the tilt angle of the slope over a two-hour period, displaying a variation ranging from approximately 0.5 degrees to 1.5 degrees. This specific range can be served as a predefined warning threshold. At the crucial second-hour mark, coinciding with the slope failure, there was a sudden and notable deviation 3 degrees to 3.5 degrees in the tilt angle. This deviation acted as a key indicator, marking the system's ability to accurately detect the onset of failure conditions.

Furthermore, the soil moisture sensor integrated into the system exhibited substantial variations of approximately 40% during periods of rainfall. These variations signalled a notable rise in soil saturation, reaching up to 95%, suggesting that elevated moisture levels may serve as a potential triggering factor for slope failure.

The physical and numerical analysis performed on the Jhakri landslide revealed a decrease in the safety factor from 1.045 pre-rainfall to 0.670 post-rainfall conditions, affirming the role of rainfall as the primary trigger for slope failure.

The results of the physical and numerical modelling very well establish the initiation of rainfall-induced landslides. The factor of safety is one of the crucial parameters in assessing the stability of slopes. The obtained safety factor values highlight the role of hydrology (rainfall) in activating and triggering the failure of slope mass. The findings, thus, corroborate the recent increase in landslide occurrences in the monsoon season. This study further demonstrated the greater significance of hydrological conditions, and recommends Bureau of Indian Standards for emphasizing the importance of assigning higher weightage than other contributing factors.

This study also proves the suitability and feasibility of numerical modelling to analyse different slopes, providing scientific guidance for monitoring and early warning so that preventive measures can be taken to reduce its effect. The proposed low-cost monitoring system for rainfall-induced landslides is effective and accurate and holds potential for wide-scale implementation in monitoring precarious slopes in hilly terrains.

LIST OF CONTENTS

LIST OF FIGURES

LIST OF TABLES

NOTATIONS AND SYMBOLS

ADC	Analog to Digital Converter
AE	Acoustic Emission
AHP	Analytical Hierarchy Process
BIS	Bureau of Indian Standards
EWS	Early Warning System
FEM	Finite Element Method
FL	Fuzzy Logic
FOS	Factor of Safety
GIS	Geological Information System
GPS	Global Positioning System
GSI	Geological Survey of India
GSM	Global System for Mobile Communication
GUI	Graphical User Interface
HCF	Hydraulic Conductivity Function
HPSDMA	Himachal Pradesh State Disaster Management Authority
ID	Intensity- Duration
IoT	Internet of Things
IPI	In-place Inclinometer
km	Kilometer
kPa	Kilo-Pascal
LEWS	Landslide Early Warning System
LHEF	Landslide Hazard Evaluation Factor
LHZM	Landslide Hazard Zonation Map
LVDT	Linear Variable Differential Transformer
m	Meter
MEMS	Micro Electro-Mechanical Sensor
min	Minute
MP	Morgenstern-Price
MW	Mega Watt
NDMA	National Disaster Management Authority

NH	National Highway
POP	Plaster of Paris
PWP	Pore Water Pressure
SAR	Satellite Radar Imagery
sec	Second
SOI	Survey of India
SWCC	Soil Water Characteristic Curve
USGS	United States Geological Survey
VWCF	Volumetric Water Content Function
WSN	Wireless Sensor Network

CHAPTER 1

INTRODUCTION

1.1 General

Landslides are a prominent natural disaster that impacts numerous mountainous areas worldwide, like the Himalayas, Andes, and Alps. It can cause injuries, loss of life, and widespread destruction of land and property, leading to substantial economic losses. Mountainous areas heavily rely on road transport, and when landslides obstruct these routes, it brings severe difficulties to the affected communities. Despite the increasing information and awareness about the landslide, the harm and destruction keep on rising with a massive increase in landslide occurrence throughout the rainy season. The region receives exceptionally high and intense rainfall during the monsoon season, which spans approximately six months from April-May to September-October. As the Himalayan region constitutes young fold mountain which makes them prone to seepage, which is the leading cause for an increased number of the landslides during the rainy season. Around 12.6% of India's total land area, equivalent to approximately 0.42 million square kilometres, is susceptible to landslide occurrences, with the North Region being particularly susceptible [1].

Landslides depend on factors like rainfall intensity, pore water pressure, duration of rainfall, and shear strength of the soil. By effectively monitoring these factors, it becomes possible to make approximate predictions of potential landslides. This enables authorities to allocate sufficient time for evacuation, implement necessary repairs and maintenance to critical infrastructure, and undertake measures to stabilize the slopes, mitigating the impact of landslides. It is observed that slopes at a steeper angle can remain stable, but with the influence of water, even the gentle slopes get failed as water plays a crucial role in decreasing soil suction which leads to a subsequent reduction in the soil's shear strength causing failure of slopes. This phenomenon could be attributed to the occurrence of landslides in the rainy season. In regions experiencing rapid development, various unaccounted activities pose a significant risk to slope stability. For instance, deforestation has become prevalent during the development process, resulting in a decrease in the soil's shear strength. This occurs because tree roots, which act as natural reinforcement by binding the soil particles together, are lost due to deforestation. Consequently,

the increased pace of development often results in the implementation of substandard construction practices, further compromising the stability of slopes.

Fig. 1. 1 displays India's landslide hazard zonation map as provided by the Geological Survey of India, which illustrates the general risk of landslides in India by highlighting different levels of hazard zones across several states. It is worth mentioning that the Himalayas in Northwest and Northeast India, along with the Western Ghats, are particularly susceptible to landslides, posing a significant threat to the surrounding area and hereby settled communities.

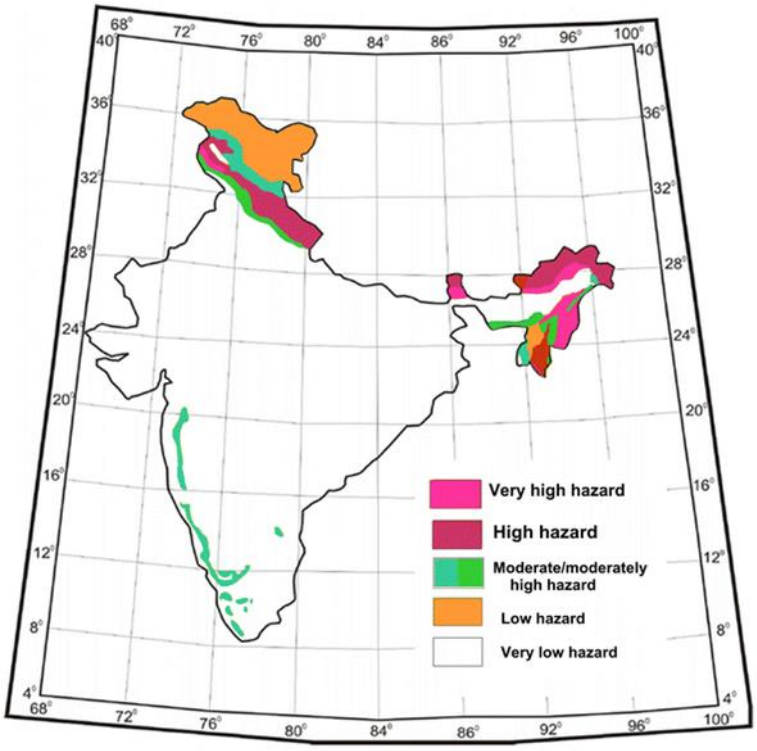

Fig. 1. 1: Landslide hazard zonation map of India [2]

The combination of steep slopes, heavy rainfall, and seismic activity contributes to the frequent occurrence of landslides necessitating effective measures for understanding, predicting, and mitigating landslide hazards.

1.2 Rainfall Induced Landslides

The global recognition of the substantial influence of rainwater infiltration on triggering landslides is well documented. When rainfall seeps into the soil, it increases the water content and reduces the matric suction, leading to higher unit weight of soil and decreased soil shear strength in the colluvium of the landslide-prone areas. The primary cause of landslides often stems from an increase in groundwater levels or the development of perched water tables. Since

most hill slope soils are unsaturated, the traditional approach of saturated soil mechanics is insufficient for assessing their stability. To understand the potential risk of rainfall-induced landslides, effective and appropriate modelling is crucial to study the changes in water content and matric suction due to rainwater infiltration. Numerous studies in the literature analyses rainfall-induced slope stability under different scenarios of rainfall intensity and duration [3], [4] and antecedent conditions [5]–[9]. These studies have emphasized the significance of unsaturated soil properties in elucidating the factors contributing to slope instability triggered by rainfall. The integrated effect of rainfall parameters and unsaturated soil action on infiltration and sliding mechanisms has also been explored. [10]–[12]. In these studies, the factors considered were soil parameters, HCC, and SWCC. In Fig. 1. 2, [13] provided a comprehensive illustration depicting the clarification of a landslide and its associated terminology. The figure explores various factors contributing to the understanding of landslides.

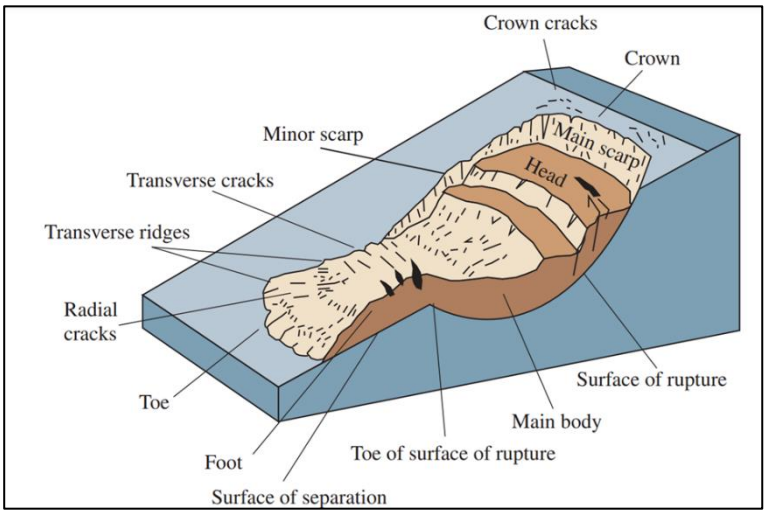

Fig. 1. 2: Earth flow labelled with different components of a landslide [13]

1.3 Variability of Geotechnical Properties

Geotechnical properties, such as soil strength, cohesion, and internal friction angle, play a crucial role in determining the stability of slopes. However, these properties can exhibit significant variability across different geological formations and regions. When geotechnical properties vary widely within a slope, it can lead to inconsistent Factor of Safety (FOS) values. The FOS is a crucial parameter used to assess slope stability, and its variation may indicate zones of potential instability. Higher variability in geotechnical properties can result in areas with lower FOS, being more susceptible to landslides. The variability of geotechnical properties also influences the initiation and propagation of landslides. Slope materials with contrasting strengths

can create zones of weakness and differential movement, increasing the likelihood of slope failure.

To mitigate the impact of geotechnical property variability on slope instability and landslides, comprehensive site investigations and geotechnical surveys are essential. Understanding the spatial distribution of properties can help for identifying appropriate stabilization measures further improving slope management practices. Moreover, advanced monitoring systems can help detect changes in slope behavior, allowing for timely responses and hazard mitigation strategies.

1.4 Physical Modelling of Rainfall Induced Landslides

Rainfall-induced landslides pose significant threats to communities and infrastructure worldwide. Understanding the complex mechanisms behind such events is crucial for effective risk assessment and mitigation strategies. Physical modelling offers a valuable approach to simulate and analyse the processes that trigger and control landslide occurrences under varying rainfall conditions. By replicating real-world scenarios in controlled laboratory settings, researchers can gain insights into the factors influencing landslide initiation, propagation, and behaviour. This study explores the importance of physical modelling in enhancing the understanding of rainfall-induced landslides and its potential applications for engineering practices and disaster management.

1.5 Numerical Modelling of Rainfall Induced Landslides

Numerical modelling has emerged as a powerful tool to simulate and analyse the complex interactions between rainfall, soil behaviour, and slope stability. By using advanced computational techniques, researchers can better assess landslide susceptibility, predict potential occurrences, and develop more robust mitigation strategies. This study delves into the realm of numerical modelling to explore the intricate dynamics of rainfall-induced landslides and its implications for safeguarding vulnerable regions.

1.6 Instrumentation Based Landslide Monitoring and Detection

Landslides triggered by heavy rainfall have been a recurring and catastrophic natural disaster in various regions worldwide. The increasing frequency and intensity of these rainfall-induced landslides have prompted the need for more effective monitoring and detection strategies to mitigate their devastating impacts on communities and infrastructure. In recent years,

advancements in instrumentation-based technologies have revolutionized the field of geotechnical engineering, providing new tools and methodologies to enhance the understanding of landslide mechanisms and offer improved early warning systems.

The study of landslide-prone areas, particularly those prone to rainfall-induced landslides, requires a multidisciplinary approach that combines geotechnical engineering, hydrology, and data science. In the past, landslide monitoring primarily relied on visual inspections and manual surveys, which had limitations in providing timely and accurate information about potential landslide occurrences. However, the advent of cutting-edge technologies, such as real-time sensor networks, now offers the ability to continuously and remotely monitor critical parameters that govern landslide initiation and movement. These advancements enable one to collect large volumes of data that can be analysed using sophisticated algorithms and modelling techniques to identify precursors and assess the potential risk of landslides in real-time with considerable accuracy.

Instrumentation-based monitoring and detection of rainfall-induced landslides, aims to explore the significance of employing advanced sensors, data acquisition systems, and analytical techniques to predict and respond to rainfall-triggered slope failures.

1.7 Motivation of The Study

The motivation behind studying rainfall-induced landslides stems from the significant threats they pose to lives and infrastructure. With India's diverse topography and monsoon climate, these landslides occur frequently, making it essential to comprehend their mechanisms and contributing factors. By conducting comprehensive research, one can develop effective early warning systems and risk management strategies. The goal is to enhance understanding, promote informed decision-making, and protect lives and property from the devastating consequences of these natural disasters. Fig. 1. 3 and Fig. 1. 4 shows recent incidences of landslides in the Northern Himalayan Region, which have hampered vehicular movement and caused loss of life and property. Fig. 1. 3 illustrates the substantial impact of landslides on several crucial national highways, disrupting vehicular traffic significantly. Meanwhile, in Fig. 1. 4a, the location of the landslide incident where rescue efforts are currently underway, resulting in a tragic loss of 27 lives. Furthermore, Fig. 1. 4b displays the aftermath of the landslide in the Kathua district of Jammu and Kashmir, which has led to the demolition of houses and the unfortunate loss of 8 lives.

(a)

(b)

(c)

(d)

Fig. 1. 3: (a) Vehicular movement from Chaura to Wangtu NH stopped after landslide on 14 July 2023 [14], (b) NH-5 blocked in Shimla districts on 23 July 2023 [15], (c) Gangotri NH blocked due to landslide on 20 July 2023 [16], (d) Mandi-Kullu National Highway blocked due to landslide on 18 July 2023 [17]

(a)

(b)

Fig. 1. 4: (a) Landslide incidence at Raigad, Maharashtra on 23 July 2023 [18], (b) Landslide in Kathua, J&K on 19 July 2023 [19]

1.8 Scope of The Thesis

Despite the severe consequences of landslides causing significant damage during the monsoon season in India, there has been a lack of attention given to landslide research. Rainfall

acts as the main triggering factor for landslides; the Himalayan region's newly folded mountains and seepage adversely affect slope stability, causing an increased number of slope failures during the monsoonal season [20]–[22]. The relationship between rainfall and landslide has been widely discussed in the existing studies [23]–[25]. Researchers have developed a threshold-based approach to assess the occurrence of landslides. Various methods can assess these thresholds: empirical methods [26], [27], probabilistic methods [28]–[31], and mathematical methods [32], [33]. With the advancement in technology, there are other tools, such as geological information system (GIS) and Global Positioning System (GPS) based on remote sensing and satellite data that can be used to develop a hazard zonation map [34]–[37] and to identify landslides through automatic process and calculation [38], [39]. These methods require a skilled team for deployment, which increases the cost. These are suitable for regional or larger areas for early warning, requiring a large amount of data; the rigorous processing of such large data and its inherent variability might lead to false alarms in some scenarios. Physical model methods are best suited to analyse the mechanism of rainfall-induced landslides for individual slopes due to their unpredicted nature and associated numerous triggering factors [40]–[43]. Numerical modelling methods are widely known to analyse the stability and seepage parameters for individual slopes, as it is not feasible to perform a physical model test for every individual slope due to its complex setup and procedure. Most of the existing studies performed numerical simulation but lacks validation with physical modelling results [8], [44]–[49]. However, the above methods can be combined for hazard risk zonation and to identify the critical slope. It can be seen that sometimes a steeper slope remains stable, whereas a gentle slope may fail under critical conditions. Keeping this in mind, it is important to consider individual slope monitoring for early prediction. As rainfall-induced landslides show an unpredictable nature of failure than the landslide initiated by the effect of gravity, scheduled field inspections at regular intervals alone may not be sufficient and effective [50]. With the advancement in electronic components and wireless networks, in-situ ground-based monitoring of slopes is another emerging method for real-time monitoring of slopes. These methods are also applicable to places not suitable for frequent visits. Different equipment and sensors have been used for monitoring and prediction of slopes. Extensometers are used to find the displacement of the moving slope from a stable portion [51]. However, this method needs extreme precision in selecting the critical slip surfaces to be installed. but the installation and maintenance costs are much higher, and thus cannot be suitable for low-cost purposes. The use of MEMS based sensors for the detection and monitoring of critical slopes is widely known due to their reasonable development and installation costs, and

are found to be effective in monitoring shallow slope failures [52]–[54]. Further slope stabilization methods can be applied to strengthen the slope to minimize the failure [55]–[57].

To overcome dependency on a single method or threshold value, a multi-method data fusion technique is suggested. This method integrates data from multiple method to enhance estimations and predictions, providing a more comprehensive and accurate approach to landslide monitoring and warning systems.

The examination of research literature focusing on the analysis and prediction of rainfall-induced landslides indicates a significant rise in landslide occurrences in the Indian Himalayan region during the monsoon season. Due to the distinct geological characteristics of the Himalayan region as a young mountainous area, featuring intricate soil and rock formations, the failure mechanisms here differ from those in other regions. This necessitates a comprehensive study of these failure mechanisms to facilitate appropriate preventive measures.

Unfortunately, there is a scarcity of studies investigating rainfall-induced landslides in the Indian Himalayan region, hindering the understanding of failure mechanisms. Additionally, conducting physical modelling for each critical slope is impractical due to resource constraints. Therefore, there is a need for numerical modelling methods, which offer a quicker means of determining critical failure planes and related safety factors. Despite the global use of numerical techniques, their reliance on input parameters and calibration for result analysis emphasizes the importance of validating results through physical modelling—a step lacking in previous studies.

Once critical failure planes are identified, precise slope monitoring becomes essential to reduce false alarms and enhance mitigation efforts. While instrumentation-based monitoring is widespread globally, the associated complexity, maintenance requirements, and high-cost limit its application for monitoring individual slopes, especially when extensive coverage for large-scale implementation is required. The recent advancements in MEMS-based sensors and IoT-enabled devices offer a cost-effective alternative to traditional monitoring methods. The developed system, featuring new-edge IoT connectivity, allows sensors to link with the internet for cloud-based data transfer and storage, facilitating subsequent analysis. In order to validate the functionality of the developed system, it is tested in a simulated real environment using physical modelling, demonstrating its working effectiveness with minimal missing data. However, the utilization of these technologies in the Indian Himalayan region requires careful evaluation due to the region's distinct geology and hydrological patterns. While MEMS-based sensors for low-cost monitoring are widely adopted globally, their exploration in India and the

Indian Himalayan region is still limited. This creates opportunities for future research to innovate and develop monitoring systems tailored to the unique conditions of the region, enhancing their effectiveness and capacity.

This study introduces an innovative strategy that integrates three methodologies: physical modelling, numerical modelling, and the installation of a self-developed cost-effective instrumentation-based monitoring device. This combined holistic approach aims to achieve precise slope monitoring, minimizing false alarms. Initially, physical and numerical modelling methods are employed to comprehend failure mechanisms and identify critical slopes. Subsequently, a sensor-based system is installed to enable accurate and real-time monitoring, enhancing the overall capability for mitigation measures.

Assumptions and limitations of the present study along with some possible scope for future research are outlined as follows:

1. Uniform values were used for the geotechnical input parameters and applied rainfall across the entire slope area. However, taking account of spatial changes in geotechnical and hydrological parameters could prove significant in making the analysis more realistic.

2. The current research approach does not consider the impact of common contributing factors such as human activities, runoff, erosion, evaporation, and plant roots. Future investigations in these domains should prioritize the incorporation of these elements alongside the occurrences of precipitation.

3. Transporting a large amount of material from the site to the laboratory for the experiment was unfeasible. Consequently, certain assumptions and limitations were inherent in material modelling. It is important to acknowledge the possibility of inaccuracies in material similarity, necessitating thorough checks during the interpretation of data.

4. The mass that failed moves downward under saturated conditions, causing erosion of the bed material and subsequently increasing the volume of flow. Therefore, the assumption in this study that the slope fails in a single layer with circular failure can be a significant limitation.

5. The system has undergone testing solely in a controlled laboratory setting. Before deploying it on-site, it is imperative to evaluate its performance in real-world conditions.

This assessment is critical to pinpoint any potential signal losses or internet connectivity issues, particularly in hilly and remote areas.

1.9 Objectives of The Study

The primary goal of this study is to comprehensively investigate the mechanisms behind landslides in the Himalayan region. To achieve this, a physical model has been developed in the laboratory. Additionally, numerical modelling has been used to study the failure mechanism, to assess the safety factor during rainfall, and to validate the physical model. This could enable the use of numerical modelling to analyse critical slopes and their mechanisms, which may not be feasible through physical modelling for every slope. Furthermore, the study aimed to create an early detection monitoring system for rainfall-induced landslides. By achieving these objectives, the research aims to gain a deeper understanding of the factors leading to landslides in specific sites and develop effective solutions for mitigation. After analysing the research gaps, the following objectives are proposed for the present research:

- To study the failure mechanism of rainfall-induced landslides by using the Physical modelling method.
- To investigate the failure mechanism of landslides using Numerical modelling techniques and subsequently validate the findings of the Physical modelling method.
- To design and develop an efficient and cost-effective landslide monitoring and Early Warning System using different sensors.
- To design and develop an Internet of Things (IoT)-based landslide monitoring system.
- To analyse the performance of the Early Warning System in a realistic environment by preparing a physical model of slope in the laboratory.

The significant findings of this study have been summarized, highlighting the key outcomes and insights gained from the research. These findings shed light on various aspects related to landslides, including their mechanisms, contributing factors, and monitoring measures. Based on these findings, recommendations for future studies and further research avenues have been provided. These recommendations aim to address any remaining gaps in knowledge and to encourage further exploration in the field of landslide research.

The critical outline of the proposed study is simplified and presented in the following flow chart (Fig. 1. 5):

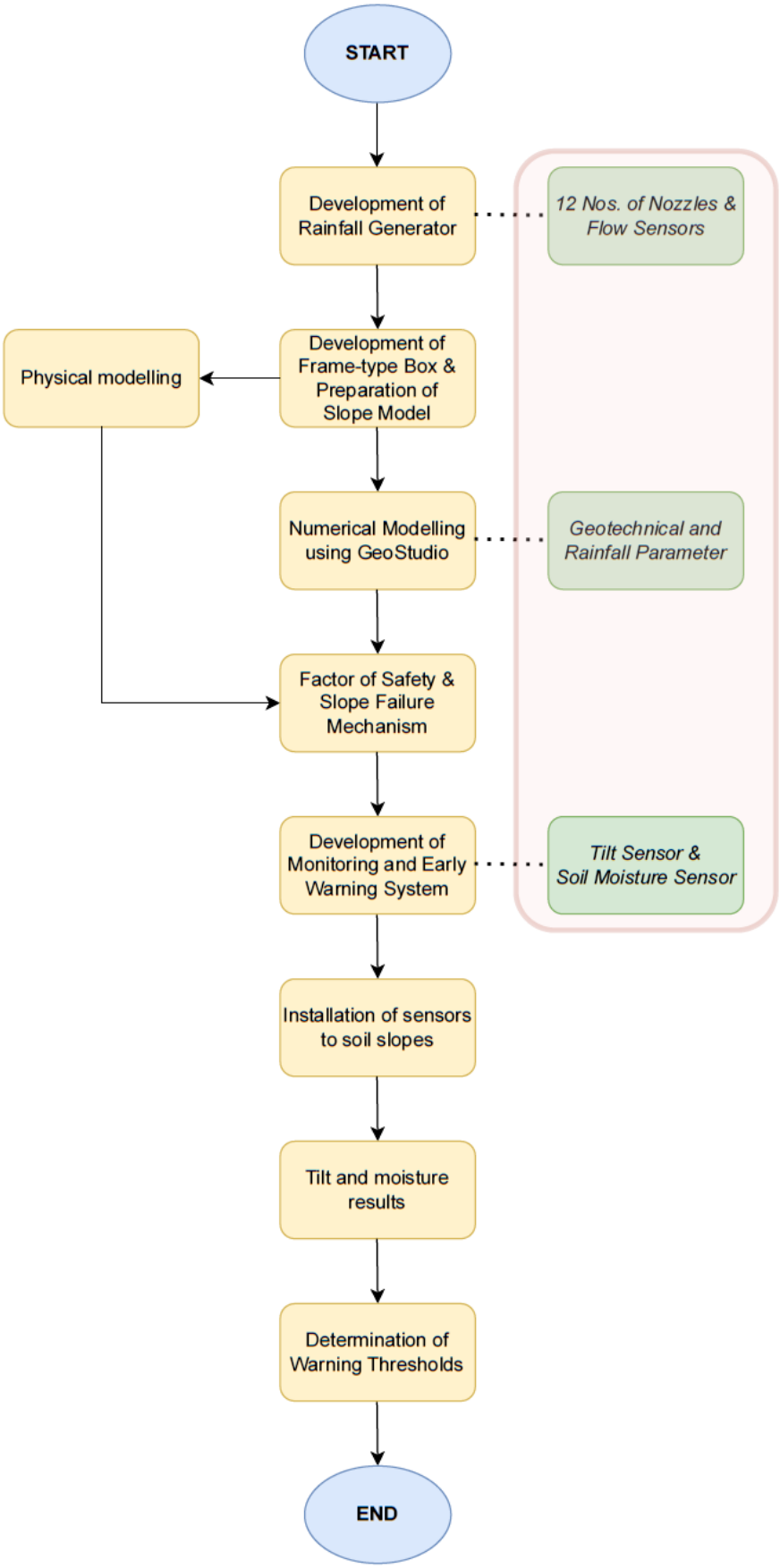

Fig. 1. 5: Flow chart of the study

1.10 Organization of The Thesis

This thesis consists of six chapters, outlined briefly as follows:

- **CHAPTER 1** gives a brief introduction on rainfall induced landslide the objective and scope of the present study.
- **CHAPTER 2** enumerates knowledge regarding numerical and experimental studies for determining threshold values for rainfall induced landslide on various slopes**.**
- **CHAPTER 3** summarizes the findings of an experimental study conducted on a physical model, detailing the results obtained at various slopes.
- **CHAPTER 4** summarizes the numerical study and the results obtained at various slopes.
- **CHAPTER 5** cover the details of design and development of monitoring system for determining threshold values.
- **CHAPTER 6** summarizes the observations, major conclusions drawn and recommendations proposed from the present study. Scope of future research work is also provided in this chapter.
- List of publications made during the present study are in the end of thesis.

CHAPTER 2

LITERATURE REVIEW

2.1 General

Landslides pose a significant threat to mountainous regions worldwide, necessitating extensive research on this phenomenon. This chapter presents a comprehensive literature review of previous studies related to landslides and establish connections with the findings of the current research. The review covers a wide range of internal and external factors that affect landslides and the mechanisms underlying their occurrence. Landslide events are caused by an interaction between internal variables, including land slope, soil composition, and rock characteristics, as well as external triggers like rainfall and earthquakes. The mechanics of landslides involve the convergence of these internal and external factors, with the initiation and movement of landslides occurring based on the prevailing conditions determined by these factors [58], [59].

In light of the above, this chapter provides an overview of relevant studies pertaining to landslides, examining a range of elements, encompassing both internal and external factors, along with the mechanisms behind the occurrence of landslides. By analysing the existing body of knowledge, this review aims to contribute to a deeper understanding of landslides and their dynamics.

2.2 Definition and Classification of Landslides

2.2.1 Definition

Bates & Jackson (1987) [60] defined that, a landslide is commonly defined as the process in which soil and rock material is transported down a slope under the influence of gravity. This movement typically occurs along a relatively confined zone or a surface of shear. The term “landslide” encompasses various types of mass movements, including but not limited to debris flows, rockfalls, and slope failures. These events can be triggered by a range of factors such as heavy rainfall, seismic activity, human activities, or geological conditions. Understanding the mechanisms and characteristics of landslides is essential for assessing and mitigating the associated risks. Extensive research has been conducted to investigate the causes, behaviour, and prediction of landslides, employing various techniques such as monitoring systems, geotechnical

analyses, and numerical modelling. By advancing the knowledge in this field, one can enhance the ability to anticipate and manage the impacts of landslides, ultimately promoting the safety and resilience of communities in landslide-prone areas.

Cruden & Varnes (1996) [61]**,** defined landslides as "Landslides encompass the downward displacement of rocks, debris, or earth along a slope." These events can exhibit a wide range of sizes, extending from isolated rock falls involving a single boulder to massive avalanches of debris carrying substantial volumes of rock and soil, with the potential to spread across vast distances measuring several kilometres. The scale and magnitude of a landslide can vary significantly and are influenced by factors such as the geological characteristics of the slope, weather conditions, and the underlying processes triggering the movement. This natural phenomenon can cause extensive damage to infrastructure, disrupt ecosystems, and pose a severe threat to human lives and livelihoods. Understanding the diverse dimensions of landslides, from minor rockfalls to colossal debris avalanches, is crucial for developing effective mitigation strategies and implementing early warning systems to mitigate the devastating consequences of these events.

Crozier (1999) [62] stated landslides are a specific category within the broader classification of slope processes known as mass movement. The term 'mass movement' encompasses all geological processes characterized by the downward or outward movement of materials composing a slope, influenced primarily by the force of gravity. Landslides, in particular, are mass movements characterized by relatively high velocities and distinct boundaries, typically formed by shear surfaces.

The distinction between landslides and other forms of mass movement lies in their speed of movement and the presence of well-defined boundaries. Unlike slower processes such as soil creep or solifluction, landslides exhibit rapid rates of displacement. This velocity is often associated with the presence of clear boundaries, typically manifested as shear surfaces within the slope material. These shear surfaces serve as identifiable markers, differentiating landslides from other types of mass movement.

By recognizing landslides as a subset of mass movement and understanding their distinctive characteristics, researchers and practitioners can gain insights into their behaviour, mechanisms, and potential hazards. This differentiation enables more accurate identification, assessment, and mitigation of landslide risks, leading to improved slope management and enhanced safety in areas prone to such events.

2.2.2 Classification

Landslides have been commonly classified based on the nature of their occurrence and the material characteristics of the sliding mass, as shown in Fig. 2. 1. Landslides are also categorised based on sliding velocity, ranging from extremely slow to extensively quick, as represented in Fig. 2. 2. It has been determined that landslides can be categorized into eight distinct groups according to their level of activity. These groups include active, suspended, reactivated, inactive, dormant, abandoned, stabilized, and relict mass movements [63], [64].

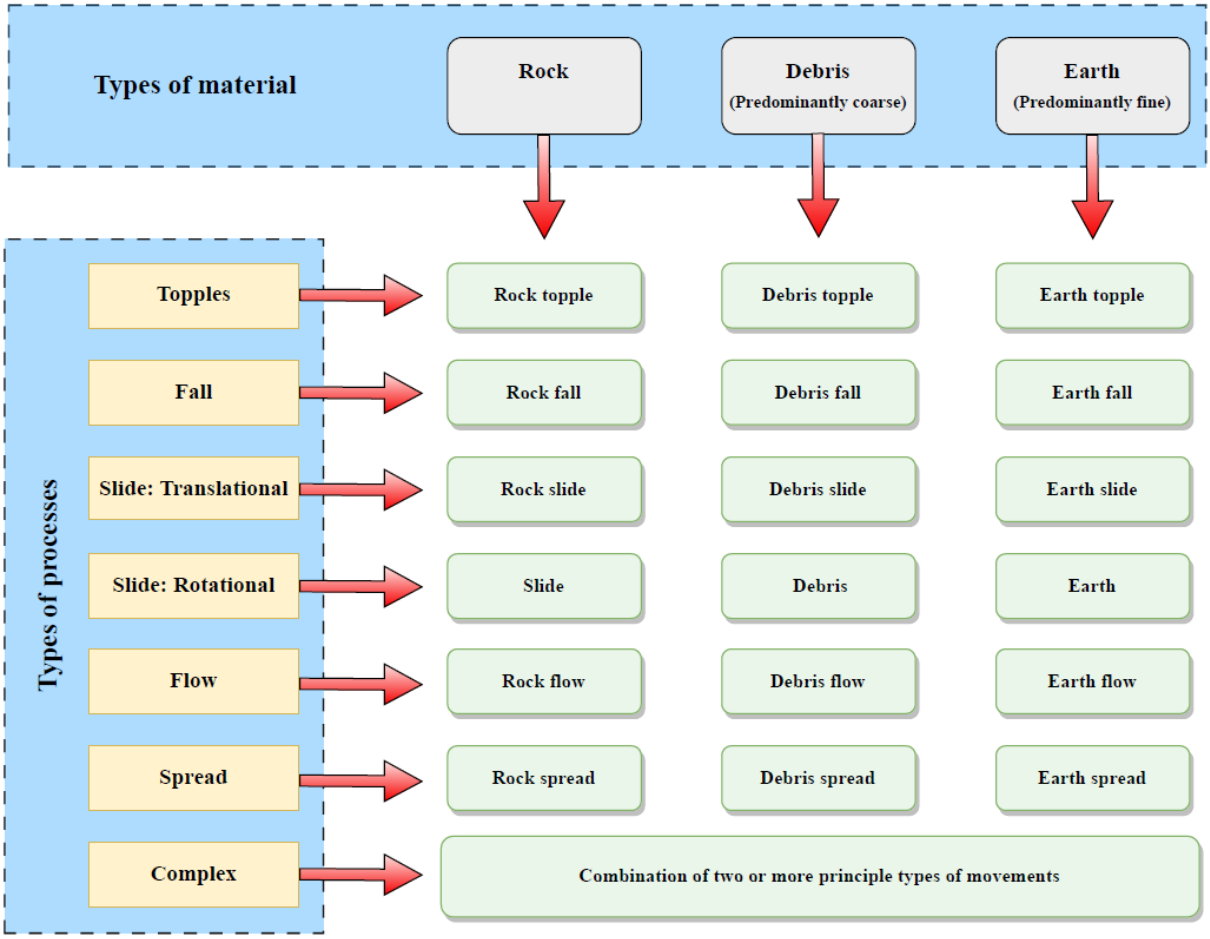

Fig. 2. 1: Classification of landslides based on process type and materials [61]

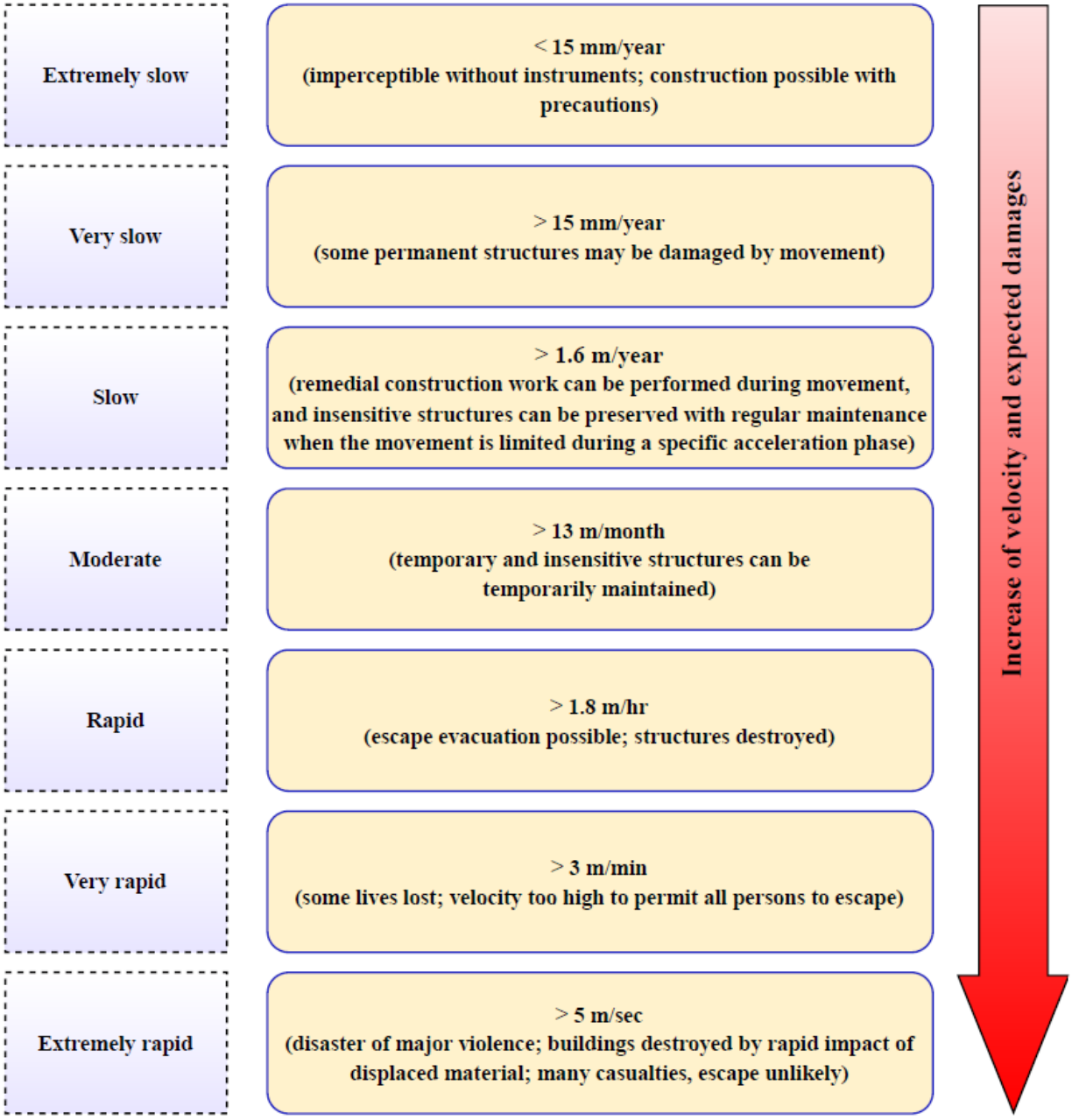

Fig. 2. 2: Mass movement classification based on velocity of displacement [64]

Geological mass movements exhibit various types of behaviours, each with distinct characteristics and triggers. These movements can significantly impact landscapes and pose risks to communities and infrastructure. Different types of mass movements are described (as shown in Fig. 2. 3):

I. **Falls:** Falls occur when masses of geologic materials, like rocks and boulders, detach from steep slopes or cliffs due to gravity and mechanical weathering. The movement involves free-fall, bouncing, and rolling along fractures, joints, and bedding planes.

II. **Topple:** Toppling failures occur when a unit or units undergo forward rotation around a pivotal point due to the combined effects of gravity and the forces exerted by neighbouring units or fluids within cracks.

III. **Flows:** There are five main categories of flows, each differing in fundamental ways:

   a. **Debris flow:** A rapid movement of a slurry-like mixture of loose soil, rocks, organic matter, air, and water downslope, commonly triggered by heavy precipitation, snowmelt, or other landslides.

   b. **Debris avalanche:** A debris flow characterized by an exceptionally high speed.

   c. **Earthflow:** Described as having an "hourglass" configuration, this phenomenon involves the liquefaction and subsequent flow of slope material, resulting in the creation of a depression at the upper end. It is frequently observed in materials that are fine-grained or contain clay.

   d. **Mudflow:** A swift movement of substances composed of particles measuring at least 50 percent in sand, silt, and clay sizes.

   e. **Creep:** The gradual and nearly imperceptible downward displacement of soil or rock caused by shear stress, without reaching the point of shear failure, is referred to as "creep." This phenomenon is often evidenced by the curvature of tree trunks, the bending of fences, and the formation of subtle soil ripples.

IV. **Lateral Spreads:** These phenomena take place on mild inclines or level ground, where motion is predominantly defined by horizontal expansion, often accompanied by the formation of shear or tensile fractures. Lateral spreading is often triggered by liquefaction, transforming saturated, loose sediments into a liquefied state, and can be induced by earthquakes or other factors.

It is essential to understand these various types of mass movements to effectively assess and mitigate their potential risks, especially in areas prone to landslides. A comprehensive understanding of their mechanisms can aid in the development of appropriate early warning systems and implementation of risk reduction strategies.

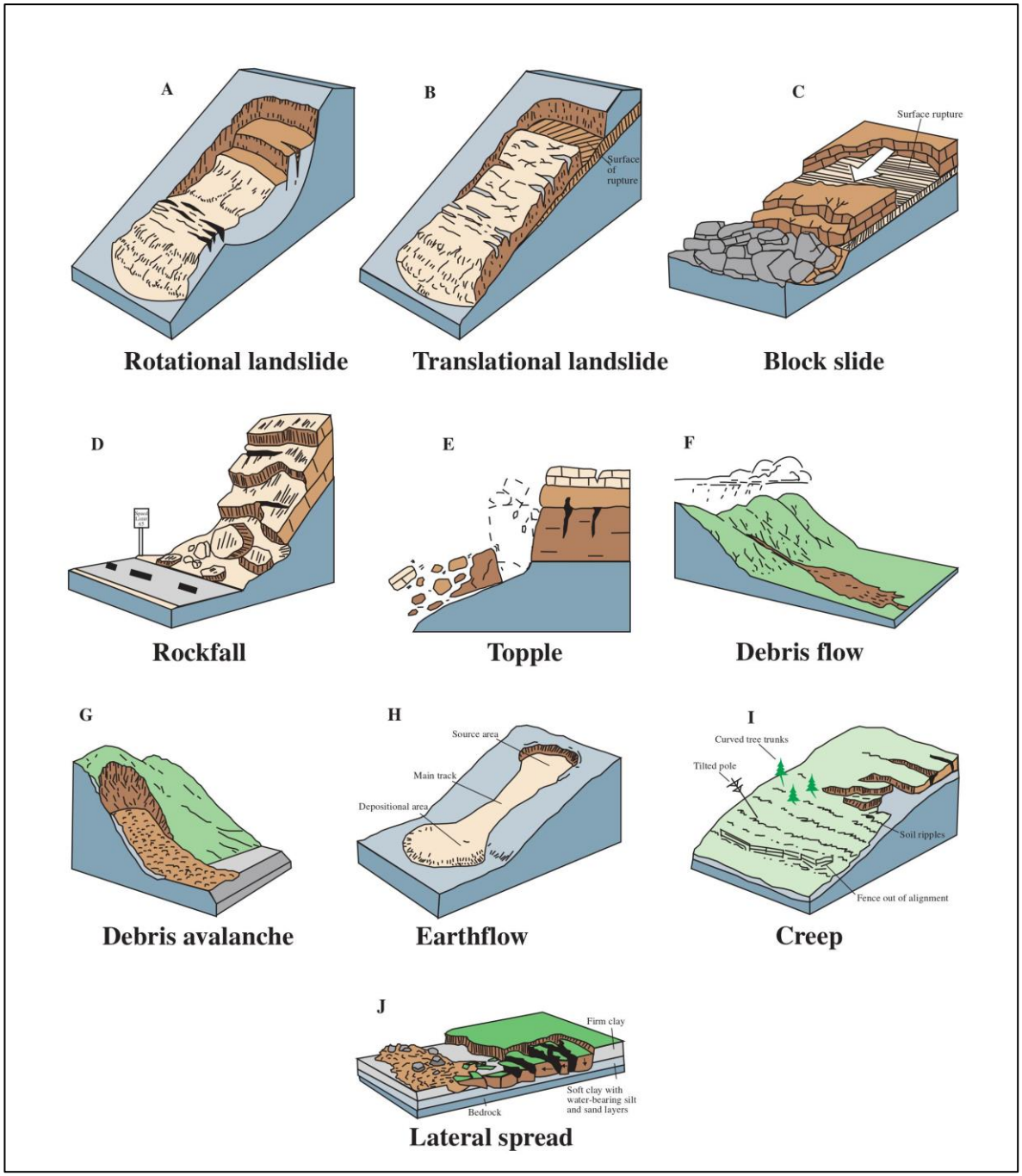

Fig. 2. 3: Major types of landslide movements [65]

2.3 Causative Factors

The causes of landslides can be classified into three main categories: geological, morphological, and human-induced factors. Geological causes include weak or sensitive materials, weathered materials, sheared or jointed materials, and the presence of adverse orientations in discontinuities. Morphological factors encompass tectonic or volcanic uplift, glacial rebound, erosion of slope toe or lateral margins by fluvial, wave, or glacial actions, and subterranean erosion. Human activities, such as excavation, loading, deforestation, irrigation,

mining, artificial vibration, and water leakage, also contribute to landslides. Fig. 2. 4 presents the causative factors for occurrences of landslide.

Among these causes, water saturation plays a significant role in triggering most damaging landslides globally. Slope saturation can occur due to intense rainfall, snowmelt, changes in groundwater levels, and water-level fluctuations along coastlines, dams, lakes, reservoirs, canals, and rivers. Landslides and floods are closely related, and debris flows and mudflows often coincide with floods, causing additional confusion. Landslides can lead to flooding by creating landslide dams that block valleys and stream channels, resulting in backwater flooding and downstream flooding if the dam fails. Moreover, landslides can cause overtopping of reservoirs and reduced capacity to store water.

Understanding the various causes of landslides is crucial for effective risk management, early warning systems, and disaster preparedness. The influence of water saturation, seismic activity, and volcanic events on landslides underscores the importance of proactive measures to minimize the devastating impacts of these natural hazards on human lives and infrastructure.

2.4 Landslide Study and Mitigation Approach

Studies related to landslides can be grouped into qualitative and quantitative methods. Qualitative methods involve analytical descriptions and expert opinions for prediction, while quantitative methods utilize mathematical descriptions and numerical simulations of landslides. These techniques can be further classified into local models, which highlight individual landslide processes, and region-specific models, which address landslide occurrences on a larger scale.

Landslide analysis has predominantly adopted a local approach in geotechnical engineering, particularly in slope stability assessments for natural and artificial slopes like road cuts, dams, embankments, and open-pit mines. This regional strategy provides:

i. A thorough understanding of the failure processes
ii. The effect of the triggering events
iii. The efficiency of remedial or stabilizing interventions.

By concentrating on specific sites, geotechnical engineering applications benefit from a thorough investigation of slope stability, ensuring the safety and reliability of various infrastructure projects. Fig. 2. 5 presents the approach for landslide early warning system.

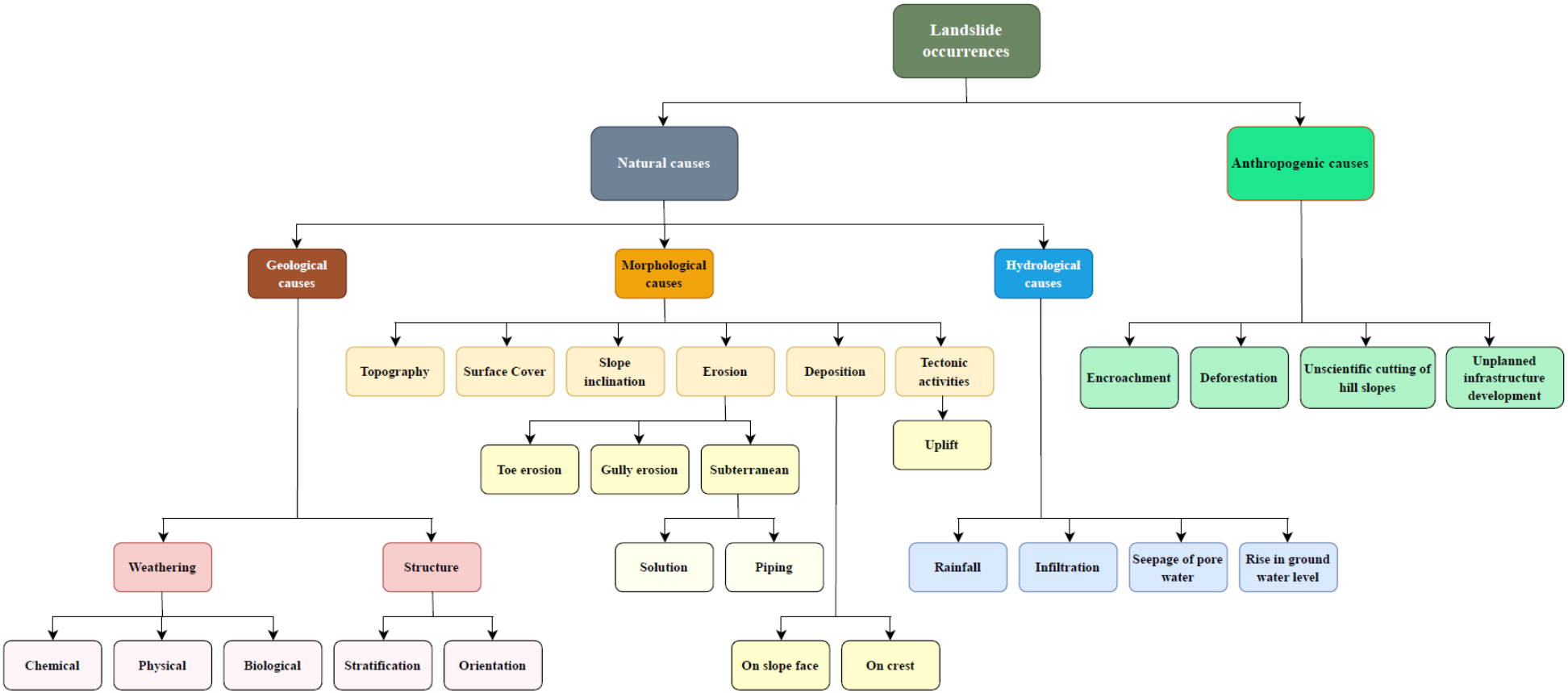

Fig. 2. 4 Causative factors for occurrences of landslide [65]

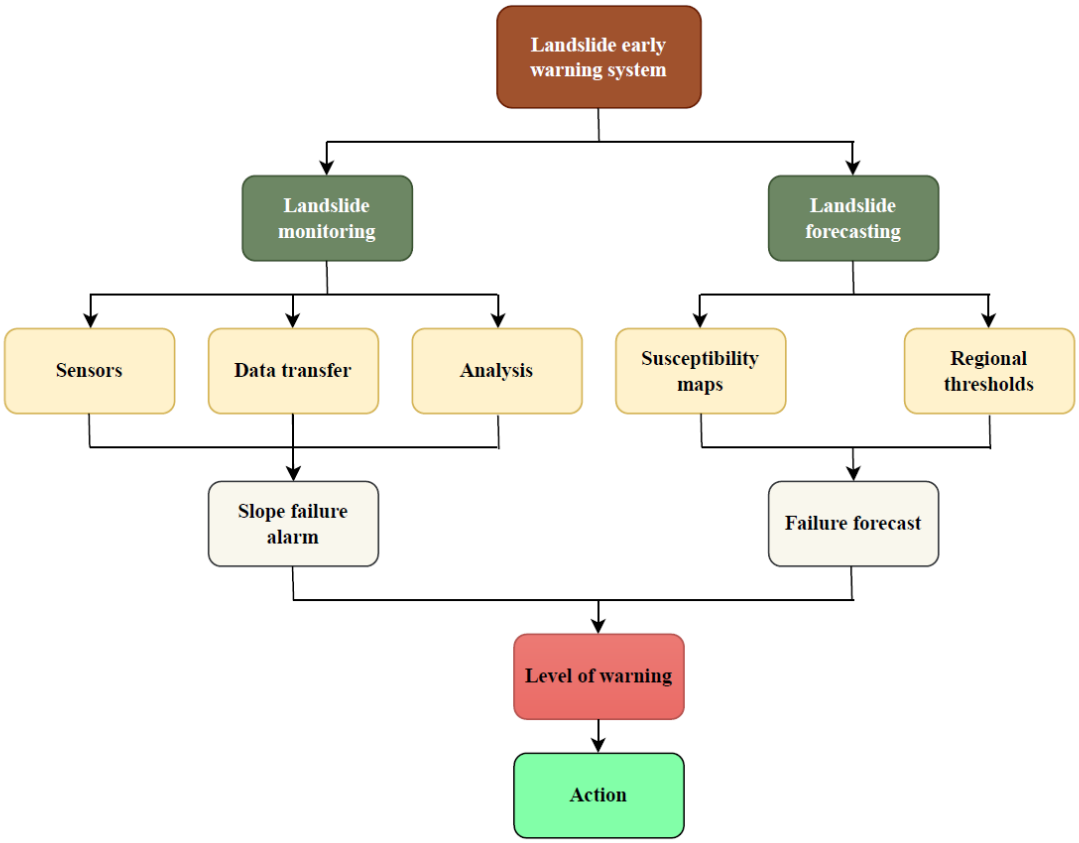

Fig. 2. 5: Approach for landslide early warning system (LEWS)

2.4.1 Literature Based on Instrumentation

Bhandari (2006) [66] discussed the Indian landslide scenario, including strategic issues and action points. The Central Road Research Institute (CRRI, India) initiated landslide instrumentation efforts in the 1970s, utilizing hydraulic standpipe piezometers for pore pressure measurements. The electrical resistivity method was employed to determine slip surfaces, while water level indicators monitored ground subsidence. A tilt measurement device measured crack widths and tilts in affected buildings. Continuous rain monitoring, estimation of infiltration and evaporation, linking rainfall to pore pressures and displacements, and stability analyses carried out in this study provided insights into exploring landslide possibilities. Deformation measurement is conducted using Satellite Radar Imaging (SAR) and the Global Positioning System (GPS).

Alcik et al. (2009) [67] developed a robust and simple algorithm for the Istanbul earthquake early warning system by utilizing exceedance of threshold time-domain amplitude and cumulative absolute velocity (CAV) levels in the study. The establishment of threshold levels

for the novel Bracketed CAV Window approach (BCAV-W) relied on an analysis of seismic ground motion records obtained from earthquake events occurring at fault distances less than 100 kilometers. Within this framework, three distinct alarm levels were defined, characterized by their respective critical velocity thresholds: 0.2 m/s, 0.4 m/s, and 0.7 m/s. In the BCAV-W protocol, when any recorded Cumulative Absolute Velocity (CAV) measurement surpasses the value of the first specified threshold, it is considered as a preliminary indication or 'vote' of seismic activity. To ensure the robustness of the detection system, a crucial condition must be met: the receipt of data from a minimum of three monitoring stations within a predefined selectable time interval. Once this condition is satisfied, the system proceeds to declare the first-level seismic alarm. This innovative approach represents a significant advancement in seismic monitoring and alarm systems, allowing for timely and accurate assessment of seismic activity based on ground motion records obtained from fault distances of less than 100 kilometers. The implementation of multiple threshold levels and a voting system enhances the reliability and precision of early earthquake detection. The BCAV-W approach is suggested, with threshold levels of 0.20, 0.40, and 0.70 m/s for the three alarm levels.

Ramesh (2014) [68] developed a comprehensive functional system comprising 50 geological sensors and 20 wireless sensor nodes. This wireless sensor network system gathers data on rainfall, moisture, pore pressure, movement, and various geological, hydrological, and soil properties. The integration of these sensors enabled a deeper comprehension of landslide conditions. By utilizing wireless sensor networks, an advanced three-level landslide warning system (Early, Intermediate, and Imminent) was developed within the system, enhancing landslide monitoring and prediction capabilities.

Uchimura et al. (2015) [69] presented a novel monitoring method for rainfall-induced landslides using tilt sensors for detection of abnormal deformation on slope surfaces. Tilt sensors were attached to steel rods and placed at depths of 0.5–1 m below the slope surface layer. A wireless sensor unit, combining MEMS tilt sensors and volumetric water content sensors, was developed and deployed on real slopes in the study areas of Japan and China for long-term monitoring. While tilt sensors were relatively new as an early warning technique, their monitoring data was less extensive compared to extensometers. The tilting behaviours in pre-failure stages might vary based on site conditions and sensor positions, necessitating further data collection to enhance the efficiency and applicability of this early warning method.

Biansoongnern et al. (2016) [70] developed an early warning system for landslides using microcontroller PIC12F683 and ATmega328 based on a low-cost Wi-Fi sensor network using a vibration sensor.

Smethurst et al. (2017) [71] explored the present and prospective functions of instrumentation and slope monitoring, including an examination of the prevailing monitoring infrastructure, frequently employed instrumentation, and the parameters that are typically measured. The existing monitoring infrastructure, commonly installed instrumentation, and measured parameters were discussed. The study also examined technological advancements and its potential impact on monitoring applications. Additionally, the article addresses the barriers and challenges hindering the widespread adoption of instrumentation in slope engineering. These challenges include integrating instrumentation economics into risk management, developing a better understanding of slope performance, identifying performance deterioration, and effectively managing and utilizing large volumes of data. Overall, the work provides insights into the evolving landscape of slope monitoring and the complexities associated with its implementation.

Intrieri et al. (2018) [72] developed a novel low-cost wireless network utilizing ultra-wideband impulse radiofrequency technology. The network, called Wireless sensor network for Ground Instability Monitoring (Wi-GIM), can measure distances between nodes using the same signals used for transmission, eliminating the need for separate measurement sensors. Wi-GIM consists of a wireless sensor network (WSN) that utilizes time-of-flight (ToF) measurements of Ultra-wideband impulses to determine inter-distances between nodes. The system's limitations include precision (up to 2-5cm with data filtering and averaging) and battery duration (a few weeks with hourly data acquisition, depending on air temperature). These limitations may be attributed to the prototype nature and the use of cost-effective components, which could be addressed through industrialization and the availability of advanced cost-effective modules.

Dikshit et al. (2018) [73] designed a dependable and sturdy system using microelectromechanical systems (MEMS) tilt sensors in conjunction with volumetric water content sensors for the purpose of monitoring both tilting angles and lateral displacement on slope surfaces. The goal was to create a dependable warning system with a low false alarm rate. The findings led to the development of an effective early warning system and the calibration of warning thresholds using empirical techniques for enhancing slope stability assessment and risk mitigation efforts.

Madhusudhan et al. (2018) [74] designed an Arduino-based sensor network technology that can develop large-scale systems for real-time monitoring of landslide-prone areas and give warning signals. The landslide detection system uses a vibration sensor to measure vibration, which monitors track and sends the necessary information to railway authorities to take necessary actions if chances of a landslide is detected.

Berg et al. (2018) [75] aimed to achieve three objectives: (i) gather a long-term dataset of continuous deformation measurements with high temporal resolution for a Peace River slope, (ii) enhance understanding of the behaviour of this creeping slope in response to climatic factors, and (iii) explore the effectiveness of an acoustic emission (AE) monitoring system in providing early warnings for accelerating deformation. Shape Accel Array (SAA) and acoustic emission (AE) instruments were installed alongside conventional inclinometers and piezometers. The measurements revealed that the landslide exhibited an "extremely slow" movement, averaging 5 mm per year. Seasonal activity with periods of acceleration and deceleration driven by pore-water pressures was observed. The measured AE correlated strongly with the rate and magnitude of displacement measured by SAA, indicating the efficiency of AE as an early warning tool for detecting deformation.

Dixon et al. (2018) [76] developed an affordable and reliable acoustic emission (AE) monitoring system to detect early signs of landslides. Physical model experiments were conducted to evaluate the system's effectiveness in measuring accelerating deformation, establishing a clear correlation between AE and displacement rates. Once the AE surpassed a predetermined threshold, an alarm is triggered to notify users of an imminent slope failure, allowing for timely evacuation or preventive measures to be taken. The developed system may serve as a practical solution for landslide detection and an early warning system to protect at-risk individuals. The system was simple and could be easily implemented by communities worldwide to safeguard vulnerable populations.

Kaur et al. (2019) [77] utilized a comprehensive strategy that involved the integration of random forest (RF) combined with probabilistic likelihood ratio (RF-PLR), fuzzy logic (FL), and the index of entropy (IOE) to quantify landslide susceptibility in Gangtok city, Sikkim state, India. Landslide inventories were compiled through the utilization of satellite imagery, Google Earth, and information sourced from the Geological Survey of India. Twelve conditioning factors, including slope, elevation, land use, geology, rainfall, and distance to roads, were used for

geospatial modelling. The resulting landslide susceptibility maps were classified into four hazard zones. The comparison of models revealed that RF-FL exhibited the highest accuracy of 69.36%, with a lower Type I error of 9.68% and Type II error of 19.35% compared to the other models.

Purnomo et al. (2019) [78] created a landslide monitoring system to detect soil movement and humidity, which are common causes of landslides. The project harnessed the capabilities of soil movement sensors, which effectively transformed spatial changes into stress measurements, and humidity sensors to record moisture levels. These sensors interfaced with a sophisticated 10-bit Analog to Digital Converter (ADC) embedded in the ATmega8535 microcontroller. The ADC facilitated the conversion of analog sensor data into digital format for further analysis. Once the data was digitized, the system seamlessly transmitted the acquired values, which included soil movement and humidity metrics, via a serial USB communication protocol. This protocol ensured a reliable and efficient means of conveying the information to a host computer or any other connected device for comprehensive data analysis and monitoring. This integrated setup allowed for real-time monitoring and analysis of the soil conditions, providing valuable insights into soil stability and moisture levels for a wide range of applications. This system enabled continuous monitoring and provided valuable data for landslide detection and prevention.

Ribeiro and Lameiras (2019) [79] presented an experimental evaluation of the performance of six low-cost MEMS accelerometers in identifying natural frequencies, damping ratios, and noise characteristics of a three-storey frame model and a reinforced concrete slab. The study utilized a low-cost Arduino-based data acquisition system. The findings indicated that the MEMS accelerometers exhibited an overall satisfactory performance.

Llorens et al. (2019) [80] developed a wireless multichannel seismic noise recorder system called Geophonino-W for array measurements. The system consists of components such as a microcontroller board (Arduino), conditioning circuit, Xbee module, SD card, and GPS module. Laboratory tests, including frequency response, synchronization, and battery duration, were conducted to evaluate the system's performance. The Geophonino-W was also compared with commercial systems and tested in field measurements. The study revealed that the MEMS accelerometers demonstrated a generally satisfactory performance.

Kafadar (2020) [81] presented an affordable and computer-aided system that utilized geophones to record, monitor, and analyse three-component microtremor data. In contrast to basic data

acquisition systems, the integrated system in question boasts an ingenious capability – it seamlessly incorporates the interpretation of microtremor data by leveraging the horizontal-to-vertical spectral ratio (H/V) method. This remarkable feature eliminates the need for external software, making data analysis more efficient. This advanced system facilitates the effortless estimation of both H/V peak frequency and amplitude, greatly enhancing its usability for researchers and professionals in various fields. It comes equipped with an array of impressive specifications, including a robust 200 Hz sampling frequency, an impressive dynamic range of approximately 72 dB, and an intuitive text data format. Furthermore, the system provides a comprehensive suite of data analysis tools to assist users in extracting meaningful insights from the collected data. Adding to its user-friendliness, the system is complemented by a graphical user interface (GUI) meticulously developed using the .NET Framework 4.5.2. This GUI streamlines the data acquisition and analysis process, ensuring a smooth and efficient workflow for users. In terms of hardware, the system is not just self-contained, but also incorporates various external components. These include signal conditioning circuits, a voltage converter circuit, an external analog-to-digital converter, and an Arduino Uno board. These additional components contribute to the system's robustness, reliability, and flexibility in addressing a wide range of data acquisition and analysis needs. This software facilitated communication, data transfer, monitoring, recording, and interpretation of seismic data between the external hardware and computer. The system demonstrated an overall satisfactory performance.

Abraham et al. (2020) [52] developed a Landslide Early Warning System (LEWS) that was meticulously designed and implemented in the challenging terrain of the Darjeeling Himalayas. This innovative system harnessed the power of a sensor network, featuring state-of-the-art Micro-electro-mechanical systems (MEMS)-based tilt sensors and volumetric water content sensors, to effectively monitor active slopes and predict potential landslides. The heart of this system was an Internet of Things (IoT)-based network, enabling seamless wireless communication between the various components involved. These components included the sensors themselves, data loggers responsible for data collection, and a centralized internet database for comprehensive analysis and storage. In a rigorous field trial conducted over three monsoon seasons, the functionality and reliability of the tilt sensors in this unique setting were fully demonstrated. This not only showcased their effectiveness in detecting slope movement but also revealed its adaptability to the specific environmental conditions of the Darjeeling Himalayas. One of the most significant outcomes of this study was the recognition of the importance of considering long-term rainfall patterns as opposed to merely focusing on

immediate weather events when defining rainfall thresholds. This revelation underscored the need for a more holistic approach to landslide prediction, one that takes into account the cumulative impact of sustained rainfall on slope stability.

Zhu et al. (2020) [82] introduced a novel calibration technique for improving the measurement accuracy of Micro-electro-mechanical system (MEMS) accelerometer-based inclinometers used in civil structure deformations. In this study, a novel approach was employed to enhance the accuracy of angle measurements. The methodology revolved around the development of a calibration model with a single parameter. This calibration model served as the cornerstone for obtaining highly precise angles. To determine the essential parameter for this calibration model, an image-processing-based method was meticulously designed and integrated into the system.

To validate the viability and reliability of this innovative technique, an ADXL355 accelerometer-based inclinometer was chosen as the benchmark instrument. The results of the validation process underscored the technique's robustness and dependability. Consequently, this paved the way for the utilization of the calibrated MEMS inclinometer as the primary tool for measuring the deflections of a scale beam model. The primary objective was to assess the performance of the proposed technique in the real-world context. Experimental findings demonstrated that this cutting-edge approach delivered highly accurate deformation measurements for MEMS inclinometers. The precision and reliability of the measurements obtained through this methodology represent a significant leap forward in the field of in-clinometry, promising a wide array of applications in various industries and scientific endeavours. This new calibration technique offered a promising approach to enhance the measurement accuracy of MEMS accelerometer-based inclinometers in civil engineering applications.

Qiao et al. (2020) [54] conducted a series of model and field tests to examine the tilting direction and pre-failure behaviour of slopes under various conditions. To explore the dynamics of surface tilting, an array of tilt sensors with varying rod lengths were employed in this study. The objective was to gain insights into the underlying mechanisms governing surface tilting behaviour. The findings from our experiments revealed an intriguing pattern in the readings obtained from these tilt sensors. Remarkably, the data demonstrated that surface tilting measurements obtained from tilt sensors lacking rods and those equipped with short rods directly above the slip surface exhibited a remarkable and consistent alignment. This outcome implied that the rotation of the surface in response to external forces followed a predictable pattern under these conditions.

Conversely, the results took an unexpected turn when tilt sensors with elongated rods were introduced into the equation. These particular sensors exhibited a conspicuous departure from the established rotational direction. The surface tilting behaviour observed in conjunction with the longer rods was notably distinct, showcasing a counterintuitive or opposing rotational direction.

This striking observation underscores the complexity of surface tilting dynamics and hints at the significance of rod length as a contributing factor. Further analysis and investigation are warranted to elucidate the precise mechanisms that underlie this intriguing phenomenon. These findings provided valuable insights into understanding contradictory surface tilting behaviours in real-life landslide monitoring cases and further established a correlation between slip surface depth and surface tilting. The authors also offered a standard for tilt sensor installation in field monitoring applications.

Supekar et al. (2018) [83] aimed to develop a warning system which could alert people about impending landslides and thunderstorms. The system collects data from input sensors, which was then transmitted to a controller. Using a GSM module, an alert message is sent to notify individuals. The sensor readings were displayed on an LCD screen as a percentage. By employing an SMS system, this approach could effectively alert people, potentially saving lives and protecting property. Integrated with Wireless Sensor Networks (WSN), the developed system could provide accurate and continuous data for analysis. The research highlights the importance of monitoring changing geotechnical conditions using sensors like soil moisture sensors, rain sensors, and strain gauges. Furthermore, it discussed the concept of data transmission via Global System for Mobile Communication (GSM) to a remote data centre.

Kanungo et al. (2017) [84] implemented a real-time and cost-effective landslide monitoring system as a measure for risk mitigation. In the Garhwal Himalayas of India, a Landslide Observatory was established at Pakhi Landslide. This observatory utilized wireless instrumentation to monitor ground deformation and hydrologic parameters in real time. The comprehensive monitoring system in place featured an array of sensors, notably in-place inclinometers (IPI), piezometers, wire-line extensometers, and an automated weather station (AWS). These sophisticated sensors were instrumental in continuously collecting valuable real-time data, which was subsequently leveraged to establish crucial warning thresholds. A thorough analysis of this data illuminated intriguing findings. One prominent observation was that the

stable region of the landslide, situated beyond the primary scarp, displayed minimal displacement, indicating relative geological stability. However, within the main body of the landslide, a more intricate pattern of movement emerged, particularly evident at various depths. This dynamic behaviour was most pronounced at the interface between colluvium and significantly weathered bedrock, highlighting the intricate interplay between geological features. Interestingly, the interface between the greatly weathered bedrock and the un-weathered bedrock also exhibited notable activity, suggesting a complex interaction that merits further investigation. The work presented signifies the diverse array of sensors within the monitoring system provided an invaluable window into the geological dynamics of the landslide, shedding light on localized areas of movement and stability within the study area. In addition to that, a correlation between intense rainfall events and displacement patterns across the inclinometer sensors was also presented.

Artese et al. (2015) [85] developed a cost-effective and compact integrated sensor for position and inclination measurement and monitoring at the University of Calabria. The sensor was specifically designed for monitoring landslides and structures. The sensor's measurement accuracy and range could be adjusted by selecting bubble vials with different characteristics. Equipped with a computer, the instrument could independently process data from a single sensor or a network of sensors. It could also generate alert signals if predetermined thresholds set by the monitoring centre were exceeded. It provided a detailed description of the sensor's hardware and software, calibration process, laboratory tests, and initial field data acquisitions.

Intrieri et al. (2013) [86] presented a landslide Early Warning Systems (EWSs) and provided practical guidelines for designing such systems, specifically targeting end-users with limited experience in this area. The guidelines were based on two flow chart-based tools developed as part of the Safe Land project, aimed at ensuring simplicity and adaptability to various types and settings of landslides for the individual slope scale. The authors highlighted that it is almost impossible to account for all possible real-life scenarios in a landslide early warning system. Therefore, it is crucial for end-users to customize the process according to the specific characteristics of the interest area where the landslide EWS is to be implemented. The article emphasizes the need for flexibility and adaptation to local conditions. The guidelines served as a useful resource for stakeholders involved in the design and implementation of landslide EWSs, enabling them to tailor the systems to meet the unique requirements and challenges of their respective areas.

Intrieri et al. (2012) [51] presented in detail the full process of implementing an early warning system for rockslides in the Central Italy region. The research delved into a comprehensive analysis of the early warning system, encompassing a wide spectrum of critical components. These facets included geological comprehension, the formulation of risk scenarios, a thorough kinematic characterization of landslide dynamics, the meticulous selection and subsequent installation of monitoring equipment, the establishment of alert thresholds, and the development of civil protection strategies. This multifaceted system was composed of an array of monitoring instruments, featuring 13 wire extensometers, 1 thermometer, 1 rain gauge, and 3 cameras. In practice, the early warning system functioned in a sophisticated manner. It utilized the data collected by its instruments to monitor and assess the prevailing conditions. When the velocity thresholds of two or more sensors were surpassed, the system automatically triggered attention levels, which, in turn, led to an escalation in the intensity of monitoring and surveillance efforts. This real-time response mechanism allowed for a swift and proactive approach to potential landslide events, enhancing the system's overall effectiveness in safeguarding vulnerable areas and communities from such natural hazards. In the event of a change in the landslide's behaviour, combined with the use of expert assessment and predictive techniques suggesting an impending failure, an alarm would be activated, resulting in the closure of the upper road.

Uchimura et al. (2010) [53] introduced a cost-effective and straightforward monitoring method for early landslide warning. Instead of using an extensometer, a tilt sensor was employed to detect abnormal deformation on the slope surface. Model tests were conducted to investigate the relationship between rotation angle measured by the tilt sensor and slide displacement along the slope surface. The results showed that rotation data responded approximately 30 minutes prior to failure, suggesting its potential as an early warning signal. However, the behaviour of rotation varied between cases, necessitating careful definition of warning criteria. In the investigation of a model slope constructed with loosely packed sand, the methodology employed for failure detection exhibited noteworthy efficacy. One facet of this approach involved the measurement of slide displacement along the surface of the slope, which proved instrumental in the early detection of instability and potential failure at the toe of the slope. This critical assessment allowed for the timely recognition of impending issues at the base of the slope. Furthermore, the study expanded its focus to encompass the monitoring of rotational movements occurring on the slope's surface. This facet of the research provided valuable insights into the development of progressive failures further up the slope. By scrutinizing the rotation dynamics of the slope, the study was able to identify the onset and progression of instability along the entire slope, offering

comprehensive and in-depth insights into its behaviour. Moreover, the research delved into the deployment of advanced wireless sensor units equipped with tilt sensors and volumetric water content sensors. These sensor units were strategically placed on a real-life slope in Kobe City, providing a genuine and representative testing environment. Through the deployment of these sensors, the study aimed to establish a robust system for long-term monitoring, aiming to capture the slope's behaviour over extended periods and facilitate the early detection of potential instabilities. This comprehensive investigation not only demonstrated the efficacy of measuring slide displacement and monitoring rotational behaviour in detecting slope failures but also ventured into the realm of advanced sensor technology for real-world slope monitoring, paving the way for improved safety and risk management in geological and geotechnical contexts. By combining data from tilt sensors and volumetric water content sensors, a simple approach to defining warning criteria was proposed.

A brief summary of the existing literature based on instrumentation studies is provided in Table 2. 1.

Table 2. 1: Literature based on instrumentation

S. No.	Authors	Work done
1.	Bhandari (2006) [66]	Used a tilt measurement device and hydraulic standpipe piezometer to determine the slip surfaces, ground subsidence and PWP
2.	Ramesh (2014) [68]	Developed a monitoring system comprising 50 geological sensors and 20 wireless sensor nodes. This network system gathered data on rainfall, moisture, PWP, movement, and other geological, hydrological and soil properties
3.	Uchimura et al. (2015) [69]	Presented a novel monitoring method using tilt sensors for detection of deformation on slope surfaces. The sensors were attached to steel rods and placed at a depth of 0.5 to 1 m below the surface
4.	Biansoongnern et al. (2016) [70]	Developed an LEWS using microcontroller PIC12F683 and ATmega328 based on a low-cost Wi-Fi sensor network using a vibration sensor

5.	Smethurst et al. (2017) [71]	Carried out examination of the prevailing monitoring infrastructure conditions and the parameters that influences the functioning of instrumentation for slope monitoring
6.	Intrieri et al. (2018) [72]	Developed a low-cost wireless network using impulse radiofrequency technology. The system can measure distances between nodes using the same signals used for transmission, eliminating the need for separate measurement sensors.
7.	Dikshit et al. (2018) [73]	Designed MEMS based warning system including tilt and VWC sensors to monitor tilt angles and lateral displacement of slope surfaces
8.	Madhusudhan et al. (2018) [74]	Designed an Arduino-based sensor network technology that can develop large-scale systems for real-time monitoring of landslide-prone areas and give warning signals
9.	Dixon et al. (2018) [76]	Developed an acoustic emission (AE) based monitoring system and conducting physical model experiments to check the system effectiveness
10.	Ribeiro and Lameiras (2019) [79]	Utilized a low-cost Arduino-based data acquisition system comprised of six low-cost MEMS accelerometers to measure natural frequencies, damping ratios, and noise characteristics of a three-storey frame model and a RC slab
11.	Abraham et al. (2020) [52]	Developed an IoT based LEWS for terrain of Darjeeling Himalayas. The system included MEMS based tilt and VWC sensors.
12.	Qiao et al. (2020) [54]	Conducted a series of model and field tests to examine the tilting direction and pre-failure behaviour of slopes under varying conditions by using an array of tilt sensors with varying rod lengths.
13.	Supekar et al. (2018) [83]	Developed a warning system for landslides and thunderstorm using a GSM module for emergency alerts
14.	Kanungo et al. (2017) [84]	Devised a real-time landslide monitoring system comprised of an array of sensors, in-place inclinometers (IPI),

		piezometers, wire-line extensometers, and an automated weather station (AWS)
15.	Artese et al. (2015) [85]	Developed a cost-effective and compact integrated sensor for position and inclination measurement and monitoring equipped with a computer, the instrument could independently process data from a single sensor or a network of sensors

2.4.2 Literature Based on Rainfall Intensity-Duration

Harilal et al. (2019) [87] attempted to set rainfall thresholds as a component of creating a more effective early warning system for landslides. The establishment of landslide rainfall thresholds involved a meticulous examination of daily rainfall records procured from the India Meteorological Department (IMD) encompassing six distinct weather stations situated in the region of Sikkim. An exhaustive scrutiny of both the daily precipitation data and historical records of landslide occurrences spanning the time frame from 1990 to 2017 was diligently undertaken. This comprehensive analysis formed the foundation for determining the specific precipitation levels at which landslides become a significant concern in the Sikkim region. A regional rainfall threshold specific to the Sikkim region for rainfall-triggered landslides was established using an intensity-duration (I-D) relationship, expressed as $I = 43.26D^{(-0.78)}$, (where I represents rainfall intensity in millimetres per day, and D denotes the duration in days) for the rainfall-triggered landslides in the Sikkim region, and a local threshold of $I = 100D^{(-0.92)}$ was developed for the Gangtok area.

Kanungo and Sharma (2014) [21] developed localized rainfall thresholds for landslides by analysing daily precipitation data within the geographical expanse of the Chamoli-Joshimath region situated in the Garhwal Himalayas, India. After analysing 81 landslides out of 128 that occurred between 2009 and 2012, an empirical intensity-duration threshold of $I = 1.82D^{(-0.23)}$, (where I is the intensity of rainfall in millimetres/hour and D is time duration taken in hours unit) was determined for landslide occurrences. Also, the research attempted an extensive investigation into the influence of antecedent rainfall, uncovering a crucial threshold for landslide initiation in the study region. The findings revealed that a minimum antecedent rainfall of 55 mm over a 10-day period and an even more substantial antecedent rainfall of 185 mm spanning 20 days were both indispensable factors for triggering landslides in this specific geographical area. These findings shed light on the essential role that antecedent rainfall plays in the initiation of

landslides, providing valuable insights for understanding and mitigating landslide risks in the studied locale. Further refinement of these thresholds using hourly rainfall data and additional years of data was recommended.

Dikshit et al. (2020) [6] carried out the evaluation of landslide risk by utilizing a rainfall threshold model, which incorporated both daily and cumulative antecedent rainfall measurements for instances of landslides. The process of establishing threshold values for predicting landslides in a particular area encompassed a comprehensive examination of daily rainfall and prior precipitation data, incorporating records of precipitation and landslide occurrences from 2010 to 2016. This comprehensive examination revealed that a 20-day antecedent rainfall period demonstrated the highest degree of correlation with landslide events within the area. To ensure the robustness and reliability of these threshold values, they were subsequently subjected to validation, incorporating data from the year 2017, which was excluded from the initial threshold estimation process. The validated threshold values, having proven their efficacy in predicting landslides, were leveraged to establish temporal probabilities for landslide occurrence using a Poisson probability model. This critical step allows for a more comprehensive understanding of the temporal dynamics of landslides, offering insights into the likelihood of such events at different points in time. The validated results suggested that the model could be used as a preliminary early warning system.

Abraham et al. (2020) [27] developed an early warning system based on empirical rainfall thresholds correlated with landslide initiation. The research focused on selecting appropriate rainfall parameters and developing regional-scale thresholds using intensity and duration conditions. Four different approaches were considered, including using the nearest rain gauge, selecting the most extreme rainfall event irrespective of location, modifying intensity definition, and defining local-scale thresholds based on meteo-hydro-geological conditions. The results indicated that choosing the rain gauge on the basis of most severe rainfall parameters yielded the best performance. The findings highlighted the significance of sensitivity in intensity-duration threshold models to variables like the choice of rain gauge, the definition of intensity, and zone subdivision.

Dikshit et al. (2020) [20] presented a comprehensive review of studies conducted in the Indian Himalayas, encompassing forecasting, monitoring, hazard analysis, and susceptibility assessment. The analysis highlighted the need for additional research, such as incorporating

climate change factors and obtaining high-quality data for computational models. It also revealed a geographical bias in the studies, with certain regions receiving more attention than others. The review could be a valuable resource for stakeholders and researchers working or planning to work in the Indian Himalayas, emphasizing the research gaps and strengths, and promoting future advancements in landslide risk reduction in the region.

Abraham et al. (2020) [88] applied an algorithm-based model, the SIGMA ("Sistema Integrato Gestione Monitoraggion Allerta") model to Kalimpong town in the Darjeeling Himalayas, a region highly susceptible to landslides. The research encompassed a dual-fold investigation with the primary goals of (i) ascertaining the specific precipitation thresholds necessary for triggering landslides within the geographical region of Kalimpong, and (ii) evaluating the suitability and adaptability of the SIGMA model within the context of a physically diverse environment. This multifaceted study was designed to shed light on the critical factors influencing landslide occurrences in Kalimpong, while simultaneously examining the practicality and effectiveness of the SIGMA model when applied to a region characterized by its unique physical characteristics. Daily rainfall and landslide data from 2010 to 2015 were used for model calibration, and 2016-2017 data were used for validation. The findings of the study indicate that the SIGMA model exhibited a remarkable level of precision in forecasting all documented landslide occurrences within the specific geographical area under investigation. This high level of accuracy was quantified at 92%, affirming the model's effectiveness in landslide prediction. Additionally, the likelihood ratio for the model's predictions stood at an impressive 11.28, further underscoring its reliability and potential for practical application in landslide risk assessment and management within this region. These findings confirmed the potential of integrating SIGMA with rainfall forecasting to establish a reliable landslide early warning system for Kalimpong town.

Yang et al. (2020) [89] defined empirical rainfall thresholds based on intraday rainfall and antecedent rainfall up to 7 days before landslide occurrences. The research region was partitioned into six distinct alert zones, wherein an analytical approach employing logistic regression was applied to scrutinize the daily rainfall and landslide data recorded during the monsoon seasons spanning from 2003 to 2010. In this extensive examination, the dataset underwent rigorous calibration to establish a spectrum of probability thresholds. The most suitable threshold was determined via a meticulous analysis involving the receiver operating characteristic (ROC) method. Within the purview of this investigation, the study encompassed the integration of two distinct sets of criteria, complemented by their respective indicators. This comprehensive

approach led to the formulation of three distinct rainfall thresholds within a sophisticated warning model, catering to a total of four alert classes. Validation using data from 2011-2015 confirmed the suitability and robustness of the thresholds. The optimal threshold, with a probability range of 4-10 %, was suitable for issuing a moderate warning, while thresholds for high and very high warnings corresponded to probabilities ranging from 30-55 % and 75-95 %, respectively. The performance of these thresholds remained consistent over different time periods, indicating their practical applicability and reliability.

Dikshit et al. (2019) [90] developed an effective early warning system based on determination of rainfall thresholds for triggering landslides. The article focused on Chukha Dzongkhag, a region along the Phuentsholing-Thimphu highway, which experiences frequent landslides during the monsoon season. The study calculated event rainfall-duration thresholds using a equation based on available rainfall and landslide data from 2004 to 2014. The results indicated that a cumulative rainfall of 53 mm over a 24-hour period could trigger landslides. Additionally, the study explored the impact of antecedent rainfall ranging from 3 to 30 days on landslide occurrences and identified thresholds of 88 mm for a 10-day period and 142 mm for a 20-day period. Further improvements could be made with additional data and hourly rainfall measurements.

Teja et al. (2019) [23] introduced an algorithm-based model that identified the precipitation conditions responsible for landslide occurrences. Traditional empirical models for rainfall-induced landslides rely on statistical approaches and power-law equations, but they often fail to account for uncertainties in threshold calculations. The methodology involved an automated tool that determines rainfall-duration thresholds, along with associated uncertainties, at various exceedance probabilities. After applying this approach to the Kalimpong region of the Darjeeling Himalayas using rainfall and landslide data from 2010 to 2016, the study revealed that a cumulative event rainfall of 36.7 mm over a 48-hour period could trigger landslides in the area.

Abraham et al. (2019) [4] focused on defining a rainfall threshold at a regional local scale and determining the occurrence of landslides within the Idukki district. Using data from 2010 to 2018 on rainfall and landslides, an intensity-duration threshold equation, $I = 0.9D^{(-0.16)}$, was derived. This research also delves into the investigation of how antecedent rainfall conditions play a pivotal role in the initiation of landslides, with a specific focus on cumulative rainfall over various durations leading up to the failure event. The results of this study unveiled a significant

trend: as the number of days preceding a landslide event expanded, a discernible shift was observed in the distribution of landslide occurrences toward instances with elevated antecedent rainfall conditions. In particular, the data demonstrated that the likelihood of a landslide event was substantially influenced by the cumulative rainfall experienced in the lead-up to the failure event. An intriguing insight from this investigation pertains to the escalating influence of antecedent rainfall conditions as one extend the temporal scope. When considering a shorter timeframe of just 3 days prior to a landslide event, the occurrence of landslides exhibited a biasness of 72.12 % towards higher antecedent rainfall conditions. However, this biasness intensified dramatically as the authors extended the analysis window to a longer period of 40 days, reaching an astonishing 99.56 %. In essence, these findings highlight the intricate relationship between antecedent rainfall and landslides, emphasizing the critical importance of understanding the temporal dynamics of rainfall conditions leading up to such natural disasters. The obtained mathematical expressions, when coupled with a rainfall prediction framework, have the potential to be utilized for the purpose of issuing advanced warnings for landslides within the study region.

Naidu et al. (2018) [91] studied a combined cluster and regression analysis to establish the precipitation threshold responsible for initiating landslides within the susceptible Amboori region of Kerala, India. The rainfall data for 2, 3, and 5 days prior to the landslides were clustered to identify critical events that could potentially trigger landslides. Regression analysis was then applied to the cluster of critical events to develop threshold equations. The analysis revealed that the best fit was obtained by considering the precipitation occurring in the five days leading up to a given day (x-variable) with the daily rainfall on that specific day (y-variable), resulting in the threshold equation $Y = 80.7 - 0.1981X$. The intercept specified by the equation indicated that a minimum daily rainfall of 80.7 mm was required to trigger landslides when the 5-day antecedent rainfall was zero. The slope stability analysis using the Probabilistic Infinite Slope Analysis Model (PISA-m) identified areas in Amboori with lower Factors of Safety, indicating vulnerability to landslides. The study suggested that integrating rainfall threshold analysis with FOS values from slope stability analysis could lead to the development of a simple, cost-effective, and all-encompassing early detection system for shallow landslides in areas like Amboori and its counterparts.

Dikshit and Satyam (2018) [92] established rainfall thresholds for landslide occurrence in Kalimpong using the power law equation, with an intensity–duration threshold relationship of $I = 3.52\ D^{(-0.41)}$, (I represent rainfall intensity in mm/h and D represents duration in hours). The

findings of this study suggest that rainfall events featuring an intensity of 0.95 mm/h, coupled with a duration lasting a full 24 hours, present a significant hazard in terms of triggering landslides. Moreover, it was observed that, in the context of antecedent rainfall over periods of both 10 and 20 days, landslide incidents were contingent on rainfall intensities of 88.37 mm and 133.5 mm, respectively, within the region. These results underscore the critical role of rainfall characteristics in landslide susceptibility and offer valuable insights for hazard mitigation and management strategies in the area. This data could contribute to the implementation of early warning systems focused on rainfall thresholds and forecasting, which could be further improved with additional precipitation and landslide data as they become available.

Melillo et al. (2018) [93] created an all-encompassing utility known as CTRL-T, which stands for "Calculation of Thresholds for Rainfall-induced Landslides-Tool." CTRL-T streamlines the process of objectively reconstructing rainfall events and pinpointing the triggering conditions associated with landslides. Additionally, it calculates rainfall thresholds at varying exceedance probabilities. The tool incorporates adjustable parameters to account for variations in morphological and climatic settings. Testing was conducted in Liguria region, Italy, which is highly susceptible to landslides. It is anticipated that CTRL-T would have a significant impact on rainfall threshold determination not only in Italy but also in other regions, leading to a reduction in the risk associated with rainfall-induced landslides.

Rosi et al. (2016) [94] established rainfall thresholds for rainfall-triggered landslides in Slovenia acquiring data from around 900 landslide incidents and concurrent rainfall measurements from 41 rain gauges. An objective procedure, based on a software developed for a different region (Tuscany, central Italy), was employed to establish the thresholds. At the outset, a singular national threshold was established, and subsequently, the geographical expanse of the nation was partitioned into four distinct zones, delineated in accordance with the prominent river basins that traverse the land. The thresholds' effectiveness was assessed using various statistical parameters, demonstrating favourable performance, albeit with some uncertainties potentially arising from data quality limitations.

Papa et al. (2013) [95] proposed a methodology to overcome previous limitations specifically for debris flows and mud flows induced by shallow landslides or debris avalanches. A frequently employed strategy proposed by researchers involves evaluating the potential occurrence of debris flows through a comparative analysis of observed and projected rainfall in relation to critical

rainfall threshold (CRT) curves. Nonetheless, the practicality of deriving CRT curves empirically from historical rainfall data can become quite intricate, especially in situations where there is a scarcity of documented debris flow events or when environmental conditions undergo significant transformations over time.

The development of CRT curves is achieved through a rigorous process of mathematical and numerical simulations, wherein the infinite-slope stability model takes centre stage. This model considers the escalation of groundwater pressure resulting from rainfall as the dominant factor influencing slope stability. In essence, it provides a theoretical framework to quantify the vulnerability of slopes to debris flows, offering valuable insights into the interplay between rainfall, terrain characteristics, and the predisposition of the landscape to mass movement. This approach enabled the derivation of CRT curves even in situations where historical rainfall data is limited or when environmental conditions are dynamic.

Tiranti and Rabuffetti (2010) [96] presented the development of a forecasting tool tailor-made for predicting shallow landslides induced by heavy precipitation in the Piemonte region. An empirical model was constructed based on historical documents correlating rainfall with past landslide occurrences. The research aimed to establish rainfall thresholds for landslide triggering by considering the geological characteristics of different territories. Calibration of the system was carried out using data from 160 landslides with detailed hourly information and triggering time from the period 1990 to 2002. The study identified two distinct zones: alpine environments with metamorphic rocks, igneous rocks, dolostones, or limestones requiring higher critical rainfall values, and hilly environments with sedimentary bedrock requiring lower critical rainfall values. Verification of the model was performed using data from 429 landslides with known dates of occurrence, demonstrating a high level of accuracy and operational effectiveness without missed alarms and minimal false alarms.

Gupta et al. (2010) [97] proposed a rainfall threshold, suggesting that if the normalized cumulative rainfall exceeded 250 mm over a period of more than 15 days, landslide might likely would occur. By examining rainfall and landslide data from 1998 to 2006, it was observed that the relationship between cumulative rainfall (E) and rainfall duration (D) could not be accurately modelled using typical exponential relationships. This threshold indicates that surpassing the cumulative rainfall limit resulted in saturation and failure of the debris zone, leading to landslides in the affected area.

Caine (1980) [98] compiled data from various locations around the world, identifying 73 different combinations in both the duration and intensity of rainfall that resulted in shallow landslides and debris flows. The author utilized an extensive dataset to establish a first-ever global rainfall intensity-duration (ID) threshold for the commencement of landslides and consequent debris flows. This pioneering research represents a significant milestone in the understanding of the conditions required for these geological events to occur on a worldwide scale. The threshold curve he formulated is represented by the equation $I = 14.82 * D^{(-0.39)}$, where I stand for rainfall intensity in millimetres/hour, and D represents rainfall duration in hours. This pioneering work has since laid the foundation for understanding the relationship between rainfall patterns and the triggering of shallow landslides and debris flows, providing valuable insights for future research and disaster mitigation strategies.

Guzzetti et al. (2008) [26] compiled an extensive global database comprising 2,626 instances of rainfall-triggered shallow landslides and debris flows by conducting a comprehensive review of the existing literature. The rainfall and landslide data collected played a pivotal role in updating the previously established minimum rainfall duration and intensity thresholds, which were initially set forth by Nel Caine in 1980. This update was critical in enhancing the understanding of the conditions that lead to shallow slope failures.

By employing a sophisticated approach, the rainfall intensity-duration (ID) values were plotted on logarithmic coordinates. This method allowed to uncover an intriguing relationship between duration of precipitation and the minimum aggregate rainfall intensity required to trigger shallow slope failures. It is observed that as the duration of rainfall extends, there's a linear decrease in the minimum average intensity necessary for triggering such events. This phenomenon was evident within a specific range of durations, spanning from short periods of just 10 minutes to prolonged durations lasting up to 35 days. Objective statistical methods were employed to determine the minimum ID threshold required to trigger shallow landslides and debris flows. These techniques ensured that the findings were rooted in sound empirical evidence, contributing to the reliability and robustness of the results. It is worth noting that regional variations in rainfall patterns can significantly impact the risk of shallow landslides and debris flows. Therefore, to account for these variations across different climatic regions. The rainfall data were normalized using key parameters, such as mean annual precipitation and rainy-day norms, which were derived from a global climate dataset. This normalization process allowed make the findings

more universally applicable, ensuring that the established thresholds were relevant and adaptable to various geographical locations. The resulting global ID thresholds were found to be significantly lower than Caine's original threshold and other thresholds proposed in the existing literature. These thresholds hold the potential to be employed in a global operational landslide EWS based on worldwide precipitation measurements, particularly in the absence of local or regional thresholds. presents threshold equation presented by various authors.

Baum and Godt (2010) [9] highlighted that the establishment and functioning of effective early warning systems for debris-flow or rapid landslide events relies on various essential resources. The available resources encompass a range of essential components for the development of effective landslide susceptibility prediction systems and early warning mechanisms. These components include dependable landslide susceptibility maps, location-specific warning thresholds, meteorological and geotechnical monitoring networks, as well as robust computer and communication networks that facilitate seamless operations. In order to provide accurate and timely warnings, it is imperative to establish rain gauge networks, soil moisture monitoring systems, and pore pressure sensors in regions prone to landslides, especially those frequently affected by debris flows. These regions often face the challenges of rapidly changing weather conditions and short lead times, particularly in areas that have experienced wildfires or have sparse vegetation cover. This necessitates the need for continuous and real-time monitoring operations to ensure the safety of vulnerable communities. A critical piece of the puzzle for a comprehensive landslide warning system is the development of a standardized national-scale shallow landslide hazard map. Such a map would serve as the cornerstone for a coordinated national initiative aimed at enhancing landslide warning systems across the country. Additionally, the creation of a comprehensive landslide database is crucial to support these efforts. This database would not only improve the understanding of landslide occurrences but also provide invaluable data for the development and refinement of early warning strategies.

Capparelli and Versace (2011) [99] discussed the FLaIR (“Forecasting of Landslides Induced by Rainfall”) and SUSHI (“Saturated Unsaturated Simulation for Hillslope Instability”) models. FLaIR is a hydrological model that determines the probability of landslide occurrence by considering a mobility function based on landslide characteristics and antecedent rainfall. SUSHI is an integrated model that encompasses hydraulic processes at the slope level, encompassing Darcy flow in saturated conditions and addressing variations in subsoil pore pressure over time and space. This model comprises a hydraulic component for studying water movement during

rainfall infiltration and a geotechnical slope stability component founded on the principles of Limit Equilibrium Methods. These models provided valuable tools for understanding and predicting landslide events induced by rainfall.

Lepore et al. (2013) [100] introduced a rainfall-triggered landslide module into an ecohydrological model called tRIBS-VEGGIE, a physically based spatially distributed ecohydrological model. The developed framework offered a reliable tool for assessing the possibility of landslides brought on by rainfall by combining the ability of the hydrologic model to reflect soil moisture dynamics with the infinite slope model. This development enhanced the modelling capabilities of tRIBS-VEGGIE, enabling more accurate assessments of rainfall-induced landslide hazards.

Martha et al. (2015) [101] studied the devastating landslides and consequential damage in the Bhagirathi and Alaknanda River valleys, particularly in Kedarnath town, resulting from extreme rainfall between June 15 and 17, 2013. Through the analysis of high-resolution satellite data, the study confirmed that two closely occurring events led to the destruction in Kedarnath town.

Matziaris et al. (2015) [41] defined specific rainfall thresholds that trigger landslide initiation across a spectrum of diverse initial conditions. To achieve this, a series of model tests were meticulously designed and executed. These tests employed plane-strain slope models constructed from finely granulated silica sand. These models were intentionally fabricated at various densities to represent a broad range of natural soil conditions. The models were subsequently subjected to gravity equivalent to ‘1g’ to simulate real-world conditions. In order to closely mimic the real-world circumstances that can lead to landslides, these prepared models were placed within a specially designed centrifuge container. This container, capable of generating forces equivalent to 60 times Earth's gravity (60g), offered a controlled environment for experimentation. To induce slope failure and gather data under different circumstances, a rainfall simulator was employed. The rainfall simulator was programmed to generate a variety of rainfall events characterized by distinct intensities, durations, and groundwater conditions. By systematically subjecting the slope models to these simulated rainfall scenarios, the researchers aimed to gain valuable insights into the critical conditions that result in slope instability and ultimately lead to landslides. This comprehensive investigation not only expanded the understanding of landslide initiation but also provided essential data for assessing the risks associated with varying initial conditions and rainfall patterns. The study sought to understand

the impact of these factors on landslide initiation and provide valuable insights into the mechanisms governing slope failure under rainfall-induced conditions.

Yang et al. (2015) [102] carried out a comprehensive set of field and laboratory studies to uncover the precise mechanisms behind the initiation of these shallow landslides during the torrential rains. Portable dynamic cone penetration tests were employed to ascertain the thickness of the soil layer. These tests revealed a gradual thinning of the soil layer from the upper slopes to the lower ones, with a thickness of approximately one meter. Furthermore, in-situ infiltration assessments illuminated the low hydraulic conductivity of this slender soil layer. During episodes of heavy rainfall, it was evident that the majority of the precipitation would run off the surface instead of infiltrating the soil.

Findings from consolidated-undrained triaxial compression tests indicated specific soil properties, with the effective friction angle measured at 36.9° and cohesion at 6.3 kPa. These results demonstrated the robust shear strength of the soil, suggesting that under normal rainfall conditions, the steep slopes on the northeastern rim of the Aso caldera would remain stable.

In the quest to understand the likely trigger for the shallow landslides, it became apparent that the initial failure process commenced with toe erosion due to surface runoff during periods of heavy rainfall. The erosion of the slope's base resulted in a critical state as the pore-water pressure within the slope continued to rise, ultimately setting the stage for these devastating events.

Gupta et al. (2016) [103] Ground-penetrating radar technology was done for ground investigation and the study showed that rocks were overlain by thin debris cover of the order of 5–10 m. The paper concluded that the rocks were unstable and the landslide was initiated due to the excessive precipitation in the region.

KS and K (2016) [104] focused on the examination of slope instability and the underlying elements contributing to the vulnerability of landslides within the upper Alaknanda valley, located in the state of Uttarakhand, India. The research findings indicated that both landslides and flash floods were triggered by atmospheric precipitation. Furthermore, these natural events could be reliably forecasted provided that up-to-the-minute rainfall data is accessible, and specific thresholds are established for various catchment areas. These thresholds should be determined based on several key factors, including the slope of the terrain, geological characteristics, the distribution of quaternary deposits, the extent of the catchment area, and the

land use patterns within those areas. The findings emphasize the critical role of real-time rainfall information and the need for a nuanced, context-specific approach to predicting and managing the risks associated with landslides and flash floods in diverse geographic regions. This approach takes into account the unique environmental and geographical features that contribute to the susceptibility of different catchments, paving the way for more effective disaster mitigation strategies.

A brief summary of the Intensity-Duration relationships proposed by various researchers is provided in Table 2. 2.

Table 2. 2: Intensity-Duration relationship proposed by various researchers

S. No.	Author	Equation
1.	Caine (1980) [98]	$I = 14.82\ D^{(-0.39)}$
2.	Innes (1987) [105]	$I = 4.93\ D^{(-0.50)}$
3.	Crosta and Frattini (2003) [106]	$I = 0.48 + 7.2\ D^{(-1)}$
4.	Guzzetti et al. (2008) [26]	$I = 2.20\ D^{(-0.44)}$
5.	Harilal et al. (2019) [87]	$I = 43.26\ D^{(-0.78)}$
6.	Kanungo and Sharma (2014) [21]	$I = 1.82\ D^{(-0.23)}$
7.	Dikshit and Satyam (2017) [107]	$I = 3.72\ D^{(-0.48)}$
8.	Dahal and Hasegawa (2008) [7]	$I = 73.9\ D^{(-0.79)}$

Where, "I stand for rainfall intensity in millimetres/hour, and D represents rainfall duration in hours."

2.4.3 Literature Based on Susceptibility Mapping

Mondal and Mandal (2023) [108] applied the Weight of Evidence (WoE) model to assess landslide susceptibility (LS) in the Darjeeling Himalaya region of Eastern India. Fifteen landslide-triggering factors, including elevation, geology, slope angle, and rainfall, were used as spatial databases. Remote Sensing (RS) and Geographical Information System (GIS) methods were employed to develop the WoE model and create a landslide susceptibility zonation (LSZ) map. The LSZ map revealed varying levels of LS, ranging from very low to very high. The obtained accuracy of the model was evaluated using identified landslide locations, yielding a prediction accuracy of 78.90%. The study confirmed the significance of the WoE model as a statistical tool for LS mapping in the region and provides valuable insights for effective landslide hazard mitigation.

Liao et al. (2010) [109] created early warning system for rainfall-induced shallow landslides on Java Island, Indonesia, integrates three vital components. First, a susceptibility mapping module uses geospatial data, including topography, soil properties, and local landslide records, to identify high-risk areas. Second, the authors employed a satellite-based precipitation monitoring system from http://trmm.gsfc.nasa.gov for real-time rainfall data. Lastly, a specialized physically-based modelling approach called SLIDE was applied, tailored to predict rainfall-triggered landslides. This comprehensive system enhances landslide prediction accuracy, bolstering disaster preparedness and risk mitigation for the region. By integrating these components, the early warning system demonstrated its potential for improving landslide prediction and mitigation efforts in the region.

Nanda et al. (2023) [110] focused on delineating landslide susceptibility zones along National Highway 1D in the northwestern Himalaya region. Various geo-environmental factors such as slope angle, land use/land cover, distance to faults, precipitation, soil, slope aspect, lithology, altitude, distance to streams, and distance to road were considered to create a comprehensive landslide susceptibility map. The Analytical Hierarchy Process (AHP) was used to generate a weighted pairwise comparison matrix, which was combined with the geo-environmental factors using the index overlay module in ArcGIS 10.2. Analysis of past landslide events identified approximately 913.55 km^2 area as high and very high susceptibility zones, characterized by challenging terrain, frequent landslides, and significant impacts. The study highlighted the need of urgent mitigation measures along the Sona Marg to Kargil Road stretch to minimize human and economic losses caused by frequent disruptions from landslides.

Gokul et al. (2023) [111] focused on assessing landslide susceptibility in the high-range local self-governments (LSGs) of Kottayam district, Western Ghats, after a significant landslide incident in the Koottickal area in 2021. The analytical hierarchy process (AHP) and fuzzy-AHP (F-AHP) models were used to evaluate landslide susceptibility and compare existing susceptible maps. Influencing parameters like slope, geomorphology, soil texture, and satellite image-derived indices, land use/land cover (LULC), were considered. The resulting landslide-susceptible zones were classified as low, moderate, and high. The TISSA model demonstrated the best performance in validating the maps. Key factors contributing to landslides were identified as slope, soil texture, LULC, geomorphology, and the normalized difference road landslide index (NDRLI). Highly susceptible LSGs include Koottickal, Poonjar-Thekkekara,

Moonnilavu, Thalanad, and Koruthodu. These findings aided decision-makers in identifying vulnerable infrastructure and establishing emergency evacuation routes.

Makonyo and Zahor (2023) [112] utilized Geographical Information Systems (GIS) and Remote Sensing (RS) techniques to identify landslide susceptibility areas in Lushoto district, Tanzania. Remote datasets, including Digital Elevation Models (DEMs) and Landsat 8 imageries, were integrated with past landslide coordinates obtained through GPS for analysis. Various GIS techniques were employed to evaluate factors influencing landslides, such as rainfall, elevation, soil type, slope angle, lithology, faults, proximity to roads, rivers, and Normalized Difference Vegetation Index (NDVI). These factors were weighted and ranked using the Analytical Hierarchy Process (AHP). The results showed that rainfall, slope angle, elevation, and soil types significantly influenced landslides, while proximity to faults, lithology, roads, rivers, and NDVI had minimal impact. The model achieved an overall accuracy of 81% in determining landslide susceptibility levels.

Liu et al. (2023) [113] utilized Synthetic Aperture Radar Interferometry (InSAR) technology to determine the average annual deformation rate in Yunnan Province over a four-year period. The deformation rate, combined with various factors such as elevation, slope, lithology, rainfall, and distance from roads and rivers, was used to assess landslide susceptibility. The random forest model was employed for accurate analysis, and the results showed that incorporating the annual mean deformation rate enhanced prediction accuracy. Approximately 10% of the province was identified as high susceptibility areas, which accounted for 68% of the landslides. The random forest model exhibited high accuracy, with a prediction accuracy of 0.80 and an AUC value of 0.87, making it a reliable method for evaluating landslide susceptibility in Yunnan Province.

Bhadran et al. (2023) [114] applied a GIS-coupled fuzzy “Multi-Criteria Decision Making” (MCDM) technique to assess landslide-susceptible zones in the Southern Western Ghats highland segment. Fuzzy numbers were used to determine relative weights for nine landslide influencing factors, and ArcGIS was utilized to establish and delineate these factors. The “Analytical Hierarchy Process” (AHP) enabled pairwise comparison of fuzzy numbers, resulting in standardized causative factor weights. Thematic layers were assigned normalized weights, producing a landslide susceptibility map. Validation using area under the curve values (AUC) and F1 scores confirmed the model's validity. Results showed that 27% of the study area was highly susceptible, 24% moderately susceptible, 33% low susceptible, and 16% very low

susceptible. Plateau scarps in the Western Ghats were identified as highly susceptible areas. The model's high predictive accuracy, demonstrated by AUC scores (79%) and F1 scores (85%), established the reliability of the landslide susceptibility mapping for future hazard mitigation and land use planning in the region.

Zhang et al. (2022) [115] compared four neural network models, namely convolutional neural network (CNN), gated recurrent unit (GRU), multi-layer perceptron (MLP), and multi-scale convolutional neural network (MSCNN), for landslide susceptibility mapping (LSM) in Lanzhou city, China. Historical landslide/non-landslide locations and eight landslide-related influencing factors were used. The models were trained and validated using a 7:3 split. Performance assessment includes statistical indicators, confusion matrix, Kappa coefficient, F1-score, and evaluation through receiver operating characteristic (ROC) and Precision-Recall (PR) curves. Results indicated that the MSCNN model outperforms the others, demonstrating higher Recall, Kappa, and F1-score values. Comparatively, models considering neighbourhood features, like CNN and MSCNN, showed better performance than those considering sequence features. The study suggested prioritizing neighbourhood features in future LSM models to accurately represent landslide occurrence characteristics.

Shano et al. (2021) [116] focused on landslide susceptibility mapping as a crucial step in environmental planning. By analysing 1554 landslides and nine causative factors, including conditioning and triggering factors, the study identified influential factor classes. These include slope ranged between 12 and 45°, convex and concave curvature classes, aspect classes in specific directions, and elevation classes within a certain range. Factors such as distance to streams and lineaments within specific ranges also significantly contributed to landslide occurrences. The land use/land cover factor exhibited varying levels of direct and indirect influence on landslides. The resulting landslide susceptibility map was classified into different classes, providing valuable information for local, zonal, regional, and federal governments in disaster management and prevention, land use planning, and risk mitigation efforts. The model's reliability was verified through a receiver operating characteristic curve analysis, yielding an 82% accuracy rate, further supported by field observations.

Saha et al. (2020) [117] focused on the delineation of landslide susceptibility zones (LSZ) in Kurseong municipality and its surrounding hill slope in the Darjeeling Himalayan region of India. Nine parameters, including slope, altitude, rainfall, geological structure, distance from river channels, distance from lineament, soil type, land-use/land-cover, and aspect, were utilized

to map the LSZ using analytic hierarchy process (AHP), frequency ratio (FR), binary logistic regression (BLR) models, and their ensemble combinations (AHP-FR, AHP-BLR, and FR-BLR) with the assistance of ArcGIS, SPSS, and ERDAS software. The LSZ maps produced by the different models were classified into five susceptibility classes. The evaluation of map accuracy involved the utilization of receiver operating characteristics (ROC) and kappa statistics to calculate the area under the curve (AUC). The results exhibited that all models achieved considerable accuracy, with AUC values ranging from 78.86% to 84.73% and kappa statistics ranging from 0.789 to 0.868. The LSZ mapping yielded significant insights for land-use planning and the development of strategies to mitigate future landslide hazards.

Sestras et al. (2019) [118] utilized bivariate statistical analysis to assess the dynamic potential of a geographical area, considering the statistical correlations between independent variables such as factors like slope, geology, and land use, and their influence on dependent variables related to landslide occurrences. The evaluation of result validation's extent was ascertained by computing the AUROC (Area under the Receiver Operating Characteristic) score, which yielded a notable value of 0.854, highlighting the model's apt representation. The examination of landslides susceptibility has revealed that the hilly terrain surrounding the Cluj-Napoca metropolitan area in Romania has been categorized into the spatial classes of landslides occurrence.

Chen et al. (2019) [119] carried a comparative analysis of three advanced machine learning methods like “kernel logistic regression (KLR), naive Bayes (NB), and radial basis function network (RBF Network) models”, to assess their effectiveness in modelling landslide susceptibility in Long County, China. The research involved identified 171 landslide locations through historical reports, aerial photographs, and field surveys. These landslide locations were randomly divided into training and validation sets. Twelve landslide conditioning factors, including slope, curvature, elevation, distance to various features, lithology, NDVI, land use, and rainfall, were considered for modelling. Correlations between these factors and landslide occurrences were analysed using normalized frequency ratios, and multicollinearity was assessed. Feature selection was conducted using chi-squared statistic and cross-validation techniques. The trained models were then used to create landslide susceptibility maps, and their performance was evaluated using receiver operating characteristics (ROC) curve, area under the curve (AUC), accuracy, F-measure, mean absolute error (MAE), and root mean squared error (RMSE). The KLR model demonstrated the most stable and best performance, making it a promising technique for landslide susceptibility mapping. However, all three models showed

reasonably good performance and could be efficiently utilized for landslide susceptibility analysis.

Mondal and Mandal (2019) [120] focused on assessing landslide susceptibility in the Darjeeling Himalaya region by employing the index of entropy (IOE) model. The IOE model examined the relationship between landslide occurrences and various causative factors. The model incorporated fifteen distinct data layers related to landslide conditioning, encompassing factors such as elevation, aspect, slope, curvature, geology, soil type, lineament density, proximity to lineaments, drainage density (DD), distance to drainage, stream power index (SPI), topographic wetted index (TWI), precipitation, normalized differential vegetation index (NDVI), and land use and land cover (LULC). The relative importance of each causative factor was determined, with soil type identified as the most influential factor and NDVI playing the least significant role in landslide susceptibility. Using the IOE model, a landslide susceptibility map was generated in a GIS platform, achieving a prediction accuracy of 78.2% as validated by the ROC curve. The study concluded that the IOE model demonstrated reliability and authenticity in assessing landslide susceptibility based on the estimated frequency ratio values across susceptibility zones.

Chen et al. (2017) [121] compared three statistical models, namely the "weight of evidence model (WoE), logistic regression model (LR), and support vector machine method (SVM)", to determine landslide-prone areas in the Zhouqu to Wudu segment of the Bailong River Basin in Southern Gansu, China. Six environmental factors, comprising elevation, slope, aspect, proximity to fault lines, rock composition, and population density, were chosen as independent variables through the application of principal component analysis (PCA) and Chi-square testing. Three distinct models were employed to investigate the correlation between the distribution of landslides and these factors, ultimately estimating landslide susceptibility (LS). The models' efficacy was assessed using the Small Baseline Subset Interferometric Synthetic Aperture Radar technique and the Receiver Operating Characteristic (ROC) curve. The results showed that the SVM model had better prediction accuracy and classification ability, with areas of high LS levels exhibiting more deformation points. The WoE and LR models provided insights into the factors contributing to landslide occurrence, such as elevation, settlement density, and distance from fault. The SVM model could be utilized to identify potential landslide zones for land planning and landslide hazard mitigation in the Bailong River Basin.

Lin et al. (2017) [122] presented a statistical model for global landslide susceptibility mapping using logistic regression. Five factors, including relative relief, extreme precipitation, lithology, ground motion, and soil moisture, were selected based on an extensive review of the literature. Logistic regression was conducted using 70% of randomly selected landslide and non-landslide points, while the remaining data were used for model validation. The accuracy of the predictive models was evaluated using criteria such as the receiver operating characteristic (ROC) curve method. The results indicated that all five factors were significant in explaining landslide occurrences on a global scale. The confusion matrix analysis showed an approximately 80% correct classification rate for landslides, and the area under the curve (AUC) was nearly 0.87. During the validation process, these statistics improved to approximately 81% and 0.88, respectively. The findings suggested that the model exhibited strong robustness and stable performance. Additionally, the model revealed that soil moisture has a dominant influence on global landslide occurrences, while topographic factors play a secondary role.

Chalkias et al. (2016) [123] presented an integrated landslide susceptibility model, called the Landslide Susceptibility Index (LSI), which combined expert-based knowledge and bivariate statistical analysis. An examination of various factors linked to the occurrence of landslides, such as elevation, slope aspect, slope angle, land cover, rock type, Mean Annual Precipitation (MAP), and Peak Ground Acceleration (PGA), was conducted within a Geographic Information System (GIS) framework. This comprehensive approach produced a susceptibility map for landslides that categorized the study area based on the likelihood of landslides. Using a separate validation dataset of landslide occurrences, Receiver Operating Characteristics (ROC) analysis was used to assess the accuracy of this map. The model demonstrated a predictive ability of 76%, underscoring that the combination of statistical analysis and expert insights can yield a reliable assessment of landslide susceptibility at a regional level. The LSI model offered a valuable tool for landslide risk management and mitigation strategies in the study area.

Saha et al. (2013) [124] focused on generating a comprehensive Landslide Susceptibility Zonation (LSZ) map for the Ganeshganga watershed, known for the Patalganga landslide, to facilitate effective landslide prevention and mitigation measures. The creation of the Landslide Susceptibility Zone (LSZ) map involved the utilization of a binary logistic regression (BLR) model. This model incorporated various thematic layers designed to represent the contributing factors associated with landslide occurrences. These layers encompassed a spectrum of parameters, including slope, aspect, lithology, tectonic structures, land use, distance to drainage,

as well as anthropogenic influences such as proximity to roads. The data necessary for constructing these thematic layers were derived from a combination of remote sensing imagery, comprehensive field surveys, supplementary datasets, and Geographical Information System (GIS) techniques. The BLR model generated coefficients for each of these causative factors, which, when combined with a constant term, were instrumental in the formulation of the final Landslide Susceptibility Map. This map was then categorized into four distinct susceptibility zones, each with varying degrees of susceptibility, ranging from high to very low. In order to assess the accuracy and reliability of the resulting map, a rigorous validation process was undertaken. Receiver Operator Characteristic (ROC) curve analysis was employed to gauge the performance of the LSZ map. Remarkably, the map exhibited an impressive accuracy rate of 95.2% when applied to an independent set of test samples. This validation outcome underscores the robustness of the LSZ map as a tool for assessing landslide susceptibility and represents a significant step forward in understanding and mitigating the risk of landslides in the study area. Moreover, a robust correlation was evident in the alignment of preexisting landslide locations and the forecasted areas with a susceptibility to landslides.

Roy et al. (2013) [125] focused on assessing landslide susceptibility in the Darjeeling Himalayas using a bivariate statistical technique. Seven factor layers with 24 categories, derived from Cartosat and Resourcesat - 1 LISS-IV MX data, were used to analyse the factors contributing to landslides in the region. The Information Value Method was employed to allocate weights to each category, and the cumulative sum of these weighted values was utilized in the production of a landslide susceptibility map. The results indicated that 8% of the area was classified as highly susceptible to landslides, 32% as moderately susceptible, and the remaining 60% as low susceptibility zones. The prediction model's robust performance was exemplified by its impressive area under the receiver operating characteristic curve (0.89), indicating a notably high level of accuracy. This study highlighted the effectiveness of the bivariate statistical technique in landslide susceptibility assessment in the Darjeeling Himalayas.

2.4.4 Literature Based on Numerical Modelling

Chandrasekaran et al. (2013) [126] conducted Finite Element Analyses on the case histories employing PLAXIS2D software to comprehend the failure mechanism and the factors contributing to it. They also performed slope stability analysis by employing the strength reduction technique to identify the critical slip surface and assess the factor of safety.

Paswan and Shrivastava (2022) [127] focused on an area prone to recurrent rainy season landslides, aimed to understand the triggering mechanisms. Extensive fieldwork and laboratory experiments were conducted to compute hydro-mechanical parameters. A semi-similar physical model test was performed to investigate the sliding mechanism and key factors. Numerical modelling using GeoStudio was carried for studying seepage and slope stability parameters for validating and comparing the results. A simulation system for artificial rainfall was developed to emulate the quantity and intensity of rain and rainfall thresholds for triggering landslides. The physical model failed at a rainfall depth of 80 mm with a fixed intensity of 30 mm/h. The numerical analysis indicated that the slope exhibited stability with a safety factor of 1.23 prior to the onset of rainfall. However, upon replicating rainfall conditions, the slope experienced failure at identical intensity and depth, displaying a similar failure plane and a diminished safety factor of 0.626. This study confirmed rainfall as the primary triggering factor for landslides and demonstrated the suitability of numerical modelling for slope analysis, providing valuable insights for monitoring and early warning systems to mitigate landslide impacts.

Dahal et al. (2009) [50] examined the failure occurrences in the granitic terrain of northeast Shikoku Island, Japan, during the 2004 typhoon. It explored the relationship between rainfall and failures and discusses synoptic descriptions of the failures. By utilizing data from laboratory experiments and field observations, the study conducted sensitivity and stability analyses, considering different slope angles, strength parameters, and saturated residual soil thicknesses. The main objective was to apply a standardized method for stability analysis of translational slides under extreme rainfall conditions. The findings contributed to a better understanding of landslide behaviour and provided insights for assessing slope stability during severe rainfall events.

Singh and Kumar (2021) [128] focused on the slope stability assessment along a section of the pilgrimage route NH-154A, which connects the holy shrines of Bharmour and Manimahesh in addition to linking hydroelectric dams and power stations via a tunnel. The study involved the identification and investigation of soil slopes along the road corridor, specifically targeting failed soil slope sections. Geotechnical studies were conducted, including the collection of soil samples from selected sites. The study area featured slopes with inclination angles ranging from 40° to 80°. Circular failure charts (CFC) were employed to determine the factor of safety values based on relevant slope parameters. The findings of this study have implications for mitigating unstable slopes along the highway stretch. Factors such as slope steepness, proximity to the river Ravi,

rainfall, and human disturbances resulting from road widening are identified as significant triggers for slope instability along NH-154A.

Harris et al. (2012) [129] validated the numerical models employed in creating a rainfall-induced landslide early warning system by conducting a back analysis was conducted on a roadway embankment. Field measurements were taken using volumetric water content sensors and a rainfall gauge to monitor the soil's response to rainfall. Slope stability analysis was performed to calculate the factor of safety for the slope.

Dahal (2012) [130] conducted an assessment of landslide processes and their associated hazards in Nepal. They approached the evaluation of rainfall-induced landslides from three different angles: through hydrological and slope stability modelling, the determination of rainfall thresholds for triggering landslides, and the overall assessment of landslide hazards.

Lee et al. (2014) [131] described mechanism of rainfall-induced landslide in the Hulu Kelang area using field observation and numerical modelling and concluded that daily rainfall information was insufficient for predicting landslides in the area.

Zhang et al. (2019) [132] investigated the interaction between internal erosion and infiltration in soil slopes composed of mixed coarse and fine particles. A combined model integrating unsaturated flow and internal erosion was formulated to assess how internal erosion impacts pore water pressure distributions and the stability of slopes. Parametric studies were conducted to assess the impact of erosion and hydraulic parameters. The results demonstrated that internal erosion primarily occurs within the zone of the wetting front, accelerating its advancement and reducing slope stability. The coefficient of erosion flux rate (B_{er}) was identified as the main factor influencing internal erosion. Larger values of B_{er} exhibited a more pronounced effect on the movement of the wetting front. Parameters i* and A_{er} have less significant effects compared to B_{er}. Significantly, it is worth noting that when the intensity of rainfall exceeds the saturated coefficient of permeability, it has a pronounced effect on both water infiltration and the stability of slopes. In contrast, if the rainfall intensity remains below the saturated coefficient of permeability, the significance of internal erosion in these processes becomes negligible. This phenomenon underscores the critical role that rainfall flux plays in the complex interplay between water infiltration and slope stability, with the threshold of the saturated coefficient of permeability serving as a pivotal point determining the extent of internal erosion's influence.

Consequently, understanding and monitoring the relationship between rainfall flux and permeability is essential for managing erosion-related challenges in various environments. Additionally, higher air-entry values of the soil diminished the impact of internal erosion on infiltration and slope stability.

Singh et al. (2018) [45] adopted an integrated geotechnical and numerical approach to analyse the stability of road-cut slopes along the highway. The geotechnical analysis conducted in this study served to ascertain the specific soil characteristics that exert a significant influence on slope stability. Furthermore, a unique antecedent rainfall threshold was formulated to quantitatively capture the intricate connection between precipitation and slope failure in the context of the particular event under investigation. To comprehensively assess the stability of the slope both prior to and following failure, a two-dimensional limit equilibrium method was meticulously employed. This method allowed for an in-depth examination of the structural integrity of the slope, both in its pre-failure state and in the aftermath of a failure event, shedding light on crucial insights into the slope's overall performance under varying conditions. The results indicated that slope geometry was a major influencing factor in the failure pattern. Furthermore, proactive strategies such as implementing benching and soil nailing were proposed and confirmed through a limit equilibrium analysis to guarantee both sustained stability and secure transportation. This study highlighted the need for comprehensive stability investigations and provided valuable insights for managing slope failures along NH-5 in the Jhakri region.

Kumar et al. (2018) [133] quantified the global factor of safety (FOS) and compared the conventional Limit Equilibrium (LE) Model with the advanced Numerical Model for rock slopes in Amiya, Nainital, Uttarakhand, India, using the Mohr-Coulomb failure criterion. Rock-mass characteristics were determined based on physio-mechanical properties estimated from field samples using the joint weakening coefficient for LE and numerical analysis. An examination of stability was carried out using various methods, such as the Swedish slip circle, the Ordinary method of slices, the Modified Bishop method, the Janbu method, Finite difference static analysis, Finite element static analysis, and Finite difference dynamic analysis. The results indicated global Factor of Safety (FOS) values of 0.65, 1.34, 1.38, 1.29, 1.57, 1.144, and 0.84 for each respective method. The results indicated that the slope was generally stable, and failure was likely only in the event of downslope movement with a minor seismic event. The combination of LE and numerical approaches proved to be more effective for determining critical slip surfaces and FOS.

Jamir et al. (2017) [134] focused on three slope sections (S-1, S-2, S-3) to analyse displacement and shear strain patterns. Using 2D Finite Element Method (FEM) and Shear Strain Reduction (SSR) analysis, the potential slope instability of Kharsali village was assessed. Results indicated that the southern edge (S-1) housing the Shani Temple was critically unstable with a Stress Reduction Factor (SRF) of 1.5. The S-2 section was identified as the most vulnerable with a critical SRF of 1.08, as evidenced by failure surfaces and displacements. Conversely, the S-3 section in the northern part of Kharsali was relatively stable, with the highest critical SRF of 2.76. An un-metalled road near S-3 had experienced a failure surface and subsidence. Overall, S-2 section of the village was the most susceptible to slope failure.

Senthilkumar et al. (2017) [135] investigated geotechnical characterization and analysis of the landslide. Field and laboratory investigations were conducted, including mapping, topographical survey, borehole and geophysical investigations, as well as testing of soil and rock samples. The results revealed that the slope at Marappalam consisted of a loose and soft soil layer with low permeability, interspersed with boulders, which contributed to debris flow. Scanning electron microscopic (SEM) and x-ray diffraction (XRD) analyses were performed to examine the influence of weathering on slope failure. Numerical analysis using the LS-RAPID landslide simulation program identified the failure mechanism of the landslide. The analysis showed that the slope became saturated due to intense rainfall (405 mm) on November 10, 2009, following 5 days of antecedent rainfall (303 mm). This saturation led to a decrease in matric suction, an increase in pore water pressure, a reduction in shear resistance, and ultimately resulted in progressive failure.

Jeong et al. (2017) [136] analysed rainfall-induced landslides on partially saturated soil slopes, specifically investigating the 2011 Umyeonsan landslides in Seoul, Korea. The study employed a comprehensive approach that combined laboratory tests, field tests, and numerical analysis to understand the factors contributing to landslide occurrence. The results from investigations conducted in the Umyeonsan region revealed a strong correlation between landslide activity and rainfall, soil properties, slope geometry, and vegetation. Numerical analysis further confirmed the influence of these factors on landslide occurrence. The study gave special attention to rainfall penetration analysis to determine the depth of the wetting band, which was critical for understanding shallow and deep-seated slope failures in large-scale landslides. The simulated results aligned closely with the findings from the investigations, demonstrating the suitability of the applied method for simulating landslides in unsaturated soils. Overall, this research enhanced

the understanding of rainfall-induced landslides on partially saturated soil slopes and provided valuable insights for landslide risk assessment and mitigation.

Gupta et al. (2016) [137] studied the Surabhi Resort landslide located in Mussoorie township, Garhwal Himalaya, and employed the shear strength reduction technique for finite element analysis of the failed slope. Two slope models, debris and rock mass, were analysed to assess the potential future failure of the slope. The critical strength reduction factor (SRF) was found to be 0.28 for the debris model and 0.83 for the rock mass model. A low SRF value indicated significant progressive displacement in the detachment zone. This displacement was further confirmed by cracks in the Surabhi Resort building and subsidence zones in the Mussoorie International School. The findings of this study aligned with previous research conducted using different methodologies. The results highlighted the vulnerability of the slope and emphasized the need for mitigation measures to prevent future slope failures in the area.

Acharya et al. (2016) [44] investigated the relationship between topographic hollows, flow direction, flow accumulation, and pore-water pressure development in slope failure occurrences. A small catchment in Niihama city, Shikoku Island, Japan, which experienced seven slope failures triggered by heavy rainfall during a typhoon in October 2004, was chosen for analysis. Through fieldwork and laboratory experiments, hydro-mechanical parameters were computed for unsaturated and saturated conditions. Seepage and slope stability modelling were conducted in the GeoStudio environment using precipitation data from the event. The results revealed that porewater pressure exhibited rapid transient behaviour in silty sand, with larger topographic hollows exhibiting higher maximum porewater pressures near their bases. The study also identified a threshold relationship between topographic hollow area and maximum porewater pressure, indicating that a topographic hollow of 1000 sq. m area could generate a maximum porewater pressure of 1.253 kPa. Furthermore, the porewater pressures required to trigger slope instability were found to be relatively smaller in the upper part of the topographic hollows compared to the lower part.

Igwe et al. (2014) [138] examined the dominant mechanisms of slope failures and potential obstacles to reduce landslide hazards in the Iva Valley area of Enugu, Nigeria. The landscape was characterized by numerous landslide scars and gullies, with slope deposits consisting of unconsolidated, friable sands interspersed with thin layers of montmorillonitic claystone. The study identified 43 landslide events, primarily shallow movements with slip-surface depths

below 2 meters. The examination demonstrated that landslides predominantly occur during the commencement of the rainy season, marked by short yet strong precipitation. A holistic methodology that encompasses on-site mapping, laboratory examinations, and computational assessments unveiled a multitude of elements that contribute to instability. These factors encompass the presence of baren slopes prior to the rainy season, intense rainfall, erosion, overgrazing, soil properties, and the distinctive lithological arrangement at the location. Shearing tests demonstrated strain-softening behaviour of the soils until reaching a low steady-state strength. A computer code simulated a similar landslide using input parameters obtained from field and laboratory studies. The study highlighted the increased vulnerability of marginalized communities due to urbanization and unplanned settlements on slopes. The research contributed to a regional study aimed at generating data for future landslide susceptibility mapping to protect vulnerable populations.

Rahardjo et al. (2007) [8] established the role of rainwater infiltration in causing landslides, but there were differing opinions on the importance of antecedent rainfall. This research entailed a comprehensive set of parametric investigations aimed at assessing the various factors that impact the stability of a uniform soil slope under changing rainfall scenarios. The factors under scrutiny included soil properties, rainfall intensity, initial water table location, and the geometrical characteristics of the slope. The outcomes of these analyses shed light on the dominant and subsidiary roles played by these factors in slope instability. The results of this study unveiled that the stability of the slope was predominantly influenced by two key factors: soil properties and the intensity of rainfall. Specifically, variations in soil properties, such as cohesion and internal friction, had a substantial impact on the slope's stability. Additionally, the intensity of rainfall, when subject to change, significantly affected the slope's structural integrity. However, the influence of the initial water table location and the slope geometry on the stability of the soil slope was found to be of secondary importance. These two factors, while still contributing to the overall behaviour of the slope, appeared to exert a lesser influence compared to soil properties and rainfall intensity. One particularly noteworthy discovery from this study was the identification of a threshold rainfall intensity level that was specific to different durations of rainfall. This threshold marked the point at which the factor of safety reached its global minimum. In other words, the slope was most susceptible to instability when subjected to this critical rainfall intensity, which was unique for each duration of rainfall. The research has elucidated the primary and secondary factors affecting the stability of a uniform soil slope under changing rainfall conditions. The findings offer valuable insights into the intricate interplay of

soil properties, rainfall intensity, initial water table location, and slope geometry, shedding light on the critical threshold of rainfall intensity that poses a significant risk to slope stability under varying conditions. Furthermore, the study connected these parametric findings to field observations by other researchers and established that the significance of antecedent rainfall was dependent on soil permeability.

Collins and Znidarcic (2004) [139] focused on the slope stability issues related to rainfall-induced slope failures. It investigated at how the stability of initially unsaturated slopes was affected by both positive and suction pore water pressures. Infinite slope assessment methods were paired with these factors to create a predictive framework for slope falls induced by rainfall events. This formulation served as a fundamental analysis approach for assessing the stability of soil slopes subjected to surface infiltration, considering factors such as slope geometry, soil strength, and infiltration parameters. The research presented a systematic approach to employing analytical formulation to anticipate alterations in the safety factor for slopes undergoing infiltration. This method provides a structured framework for predicting how the infiltration process may affect slope stability. By utilizing this analytical procedure, engineers and geologists can gain valuable insights into the potential safety risks associated with slopes in the presence of water infiltration. This predictive technique is useful for assessing and mitigating slope stability concerns in geotechnical engineering, ultimately contributing to safer infrastructure development and management. A detailed case study analysis was presented to validate the method, providing quantitative information on the timing and depth of failure in relation to soil, slope, and rainfall characteristics. Overall, this research contributed to the understanding and prediction of rainfall-induced slope failures, enabling improved slope stability assessments.

Cheng and Lau (2013) [140] utilized SLOPE 2000 software to accurately identify the critical failure surface, which could be either circular or non-circular. A comprehensive comparative investigation was undertaken to assess the contrasting characteristics of circular and non-circular failure surfaces, along with an examination of 2D circular and 3D spherical failure surface analyses. This thorough analysis investigated the effects of multiple variables, such as slope inclinations, soil properties, and external loading condition and their influence on slope stability. The results demonstrated that non-circular failure surfaces consistently exhibit greater criticality than circular ones in 2D analysis. Additionally, the 3D analysis using spherical failure surfaces yielded larger factors of safety than the corresponding 2D analysis. Moreover, significant differences in failure mechanisms were observed between 2D and 3D analyses. These findings

emphasized the importance of considering non-circular failure surfaces and performing 3D analyses in slope stability assessment and design processes.

Fredlund et al. (1994) [141] estimated the coefficient of permeability in unsaturated soils using the soil-water characteristic curve primarily influenced by the pore-size distribution. A previously proposed equation by the authors described the curve across the entire suction range (0 to 106 kPa) and enabled the prediction of permeability in unsaturated soils. This equation eliminated the need for evaluating the residual water content when predicting permeability. The proposed permeability function integrated the relationship between suction and water content. The equation proved to be an exceptionally accurate fit when applied to existing literature data, encompassing measurements for both the soil-water characteristic curve and the coefficient of permeability. This remarkable success underscores the precision with which the presented model aligns with empirical observations, highlighting its robust performance in this context. The integration in the equation could be performed from zero water content to saturated water content, allowing for the use of normalized water content or degree of saturation data in predicting the permeability function.

Ng et al. (2001) [142] employed three-dimensional (3D) numerical simulations to explore how groundwater reacts in an initially unsaturated cut slope at Lai Ping Road in Hong Kong when subjected to different rainfall patterns, durations, and return periods. Field monitoring data was used to establish initial and boundary conditions. The computed results revealed that rainfall patterns had a notable impact on pore-water pressures near the ground surface, with the influence diminishing as depth increased. Among the analysed rainfall patterns, a 24-hour duration with an advanced storm pattern was found to be the most critical, leading to the highest pore-water pressure in the slope. The impact of rainfall patterns on pore-water pressures exhibited a distinct sensitivity to the initial groundwater conditions, where higher initial water tables played a pivotal role in mitigating the effect. Additionally, it was observed that the escalation of pore-water pressure was notably pronounced when the return period was extended from 10 years to 100 years. Still, this escalation was less prominent when transitioning from a 100-year return period to a 1000-year one. It is important to note that the influence of rainfall on pore-water pressure distribution manifested differently depending on the duration and intensity of the precipitation events. In short-duration, intense rain, the primary influence was concentrated in the upper soil layers, impacting shallow depths. On the other hand, prolonged and more moderate rainfall exhibited a more profound effect on groundwater, with deeper soils experiencing a more

pronounced impact. This variation in response highlights the complex interplay between rainfall characteristics, initial groundwater conditions, and the temporal scale at which the evaluation of the influence of these factors on pore-water pressures have been examined. Prolonged rainfalls exhibited less significant differences in pore-water pressure distribution compared to short-duration, intense rainfalls.

Dudeja et al. (2017) [143] focused on the slope stability analysis and geotechnical assessment of a section of the Yamunotri pilgrimage route in India. The way included a possible location for a 204 m high concrete gravity dam intended to span the Yamuna River and generate power. Various slide zones were identified, classified as planar, wedge, or circular failures based on discontinuity orientation, structural features, and debris materials. A comprehensive investigation was undertaken through fieldwork and laboratory examinations to assess various aspects of circular failure slides in weathered quartzites, phyllites, and shale formations. This multidimensional analysis explored morphological dimensions, structural characteristics, orientations, and geotechnical parameters. The primary objective of these investigations was to provide a solid foundation for conducting a rigorous stability analysis of these geological phenomena. The cohesion, angle of internal friction, and other geotechnical properties were assessed. The slopes have an average inclination of 40°–43° with sparse vegetation. The materials in and around the slide zones consist of sands with significant fines. The factor of safety, computed based on strength, soil, and slope properties, indicated stability in dry conditions but decreased below unity with increasing saturation during rainfall, rendering the slopes unstable. Steep slopes, proximity to stream channels, weathering, jointing, rainfall, and road widening were identified as causative factors and triggers for slope failures along the route.

Kanungo et al. (2013) [144] focused on landslide and slope failures in the Indian Himalayas, specifically along a 1.5 km road stretch located 9 km from Pipalkoti on the Chamoli-Badrinath highway (NH-58). The study area was divided into different zones based on field surveys, contour maps, and hillshade analysis. Three specific zones were selected for investigation and modelling, including a potential debris slide, a stable debris slope, and a potential rock slide. Field mapping, data collection, and laboratory testing of soil and rock samples were conducted to determine the physical and mechanical properties of the slopes. Numerical simulations using a 2D finite element plain strain approach were employed to model the failure process and assess the stability of the slopes. The results of the analysis demonstrated high instability in the rock and debris slide slopes, accurately depicting observed failure patterns. The stable slope was

validated to be stable through the analysis. The findings from this study contributed to landslide hazard assessment in the study area.

Sarkar et al. (2012) [145] carried a study around the Amiyan area near Kathgodam, Nainital, Uttarakhand, which belongs to the Lower Siwalik formation and is susceptible to landslides. The authors investigated the slope instability in this area through extensive field surveys and laboratory experiments to determine the physicomechanical properties of the rock mass. Numerical simulations, using both two-dimensional and three-dimensional slope stability models, were employed to analyse the failure mechanism and zone of influence. The computed deformations and stress distribution aligned well with field observations, highlighting the vulnerability of the Amiyan slope and the need for appropriate protective measures. The study emphasized the importance of three-dimensional slope stability analysis in understanding slope behaviour and facilitating effective slope protection.

Hammouri et al. (2008) [146] compared the limit equilibrium method and the finite element analysis for slope stability analysis, considering homogeneous and inhomogeneous slopes under conditions such as rapid drawdown, undrained clay soils, and tension cracks. The examination was performed with the utilization of PLAXIS 8.0, employing the finite element method, in addition to SAS-MCT 4.0, which follows a limit equilibrium approach. The focus was on determining the safety factor and identifying the critical slip surface using both methods. By comparing the results obtained from the two methods, the study aimed to evaluate their effectiveness and accuracy in slope stability assessment. The limit equilibrium method, known for its simplicity, was compared to the more complex finite element analysis. The findings of the study provided insights into the similarities and differences between the two methods, enabling a comprehensive assessment of slope stability and informing the selection of the most suitable method for future slope stability analyses.

Singh et al. (2008) [147] investigated and compared the limit equilibrium method and finite element analysis for slope stability assessment, specifically considering homogeneous and inhomogeneous slopes under various conditions such as rapid drawdown, undrained clay soils, and tension cracks. PLAXIS 8.0 (based on Finite Element Method) and SAS-MCT 4.0 (based on Limit Equilibrium approach) were utilized to perform the analyses. The primary focus was to determine the safety factor and identify critical slip surfaces using both methods. By comparing the results obtained from the two approaches, the study aimed to assess their effectiveness and

accuracy in slope stability analysis. The simplicity of the limit equilibrium method was contrasted with the complexity of the finite element analysis. The findings of this study provide valuable insights into the similarities and differences between these methods, enabling a comprehensive evaluation of slope stability. The outcomes could assist in selecting the most appropriate method for future slope stability analyses.

Zhu et al. (2003) [148] proposed a generalized framework that integrated various existing limit equilibrium methods for slope stability analysis with general slip surfaces. The framework established in this study formulates force and moment equilibrium equations by incorporating the factor of safety and initially hypothesizing a normal stress distribution across the slip surface. This distribution is subsequently adjusted by including a function that relies on two auxiliary variables. The primary objective is to derive analytical solutions for the factor of safety by manipulating these equations. By introducing this framework, the authors utilised various assumptions regarding interslice forces into a single, comprehensive expression that governs the normal stress distribution along the slip surface. This unification streamlines the analysis process and facilitates a more cohesive approach to slope stability assessment. An iterative procedure has been meticulously developed to ensure the efficient convergence of the factor of safety solution. This procedure typically demonstrates rapid convergence, often requiring only a few iterations to yield an accurate result. Moreover, it is recognized that there are specific numerical challenges associated with the computation of the factor of safety, particularly when utilizing the Janbu method. To address these challenges, the authors proposed typical computation schemes, which alleviate numerical difficulties and enhance the accuracy of a factor of safety calculations. An additional advantage of the presented framework is its adaptability for practical implementation. It can be readily incorporated into computer programs, enabling the assessment of slope stability using various conventional methods of slices. This adaptability enhances the accessibility and usability of the framework in real-world engineering and geotechnical applications.

A brief summary of the existing studies based on numerical modelling is provided in Table 2. 3.

Table 2. 3: Literature based on Numerical modelling

S. No.	Authors	Work done
1.	Chandrasekaran et al. (2013) [126]	Conducted FEA in Plaxis2D software to understand the failure mechanism and the factors contributing to slope

		stability by employing the strength reduction technique to identify the critical slip surface and assess the FOS
2.	Harris et al. (2012) [129]	Conducted back analysis using volumetric water content sensors and a rainfall gauge to monitor the soil's response to rainfall
3.	Singh et al. (2018) [45]	Analysed the stability of road-cut slopes along the highway by employing a two-dimensional limit equilibrium method. The authors formulated a unique antecedent rainfall threshold.
4.	Kumar et al. (2018) [133]	Quantified the global FOS and compared the conventional LE Model with the advanced Numerical Model for rock slopes in Uttarakhand, India, using the Mohr-Coulomb failure criterion
5.	Jamir et al. (2017) [134]	Analysed displacement and shear strain patterns on three slope sections (S-1, S-2, S-3) using 2D FEM and SRR methods to determine the potential of slope instability
6.	Senthilkumar et al. (2017) [135]	Conducted numerical analysis using the LS-RAPID landslide simulation program to identify the failure mechanism of the landslide
7.	Acharya et al. (2016) [44]	Carried fieldwork and laboratory experiments and computed hydro-mechanical parameters for unsaturated and saturated conditions to determine seepage and slope stability using GeoStudio software
8.	Rahardjo et al. (2007) [8]	Conducted comprehensive set of parametric investigations to assess various factors that impact the stability of a uniform soil slope under changing rainfall scenarios
9.	Fredlund et al. (1994) [141]	Estimated the coefficient of permeability in unsaturated soils using the SWCC primarily influenced by the pore-size distribution
10.	Kanungo et al. (2013) [144]	Carried numerical simulations using a 2D FE plain strain approach to assess the stability of the slopes by selecting three specific zones including a potential debris slide, a stable debris slope, and a potential rock slide

11.	Hammouri et al. (2008) [146]	Compared LE method (SAS-MCT 4.0) and FEA (Plaxis 8.0) for slope stability analysis, considering homogeneous and inhomogeneous slopes under conditions such as rapid drawdown, undrained clay soils, and tension cracks

2.4.5 Literature Based on Physical Modelling

Guan et al. (2023) [149] examined the failure mechanisms of landslide dams by conducting experiments and analysing debris composition and geomorphic parameters. The interaction between the dam and the backwater lake played a crucial role in dam breaching. Soil properties, such as shear strength and seepage, regulated the failure modes of dams. Overtopping, seepage instability, and head cutting contributed to the failure of fine-grained and widely graded dams, while coarse-grained dams remained stable. Geomorphic parameters influence infilling time and affect failure modes through seepage. Peak outflow rates were predicted using regression analysis with lake volume, dam height, and soil properties. This research enhanced concepts of breach mechanisms and allowed for predicting peak outflow rates based on dam parameters.

Cogan and Gratchev (2019) [150] examined the combined effects of rainfall intensity, slope angle, and slope moisture content on landslide initiation. Previous research focused on individual factors, while this study considered their amalgamation. Experiments using a flume device were conducted to model single soil layer slope failures. The tests were categorized based on rainfall intensity (40, 70, and 100 mm/h), with variations in slope angle (45-55°) and initial moisture content (5-12%). Failure times occurred when pore-water pressure peaked and moisture content equalized. Changes in failure time were observed with alterations in slope angle and initial moisture content. The study developed an intensity-duration threshold function of $I = 80.065\ D^{(-0.596)}$, based on the summarized initial failure times.

Li et al. (2016) [42] investigated the startup conditions and sliding mechanism of rainfall-induced loess-mudstone interfacial landslides through a semi-similar material physical model test. The study investigated landslides that transpired within the confines of Qingshuihe County, in the Inner Mongolia region of China. The primary driving force behind these events was rainwater infiltration along the loess strata. This gradual seepage of rainwater softened the soil in proximity to the loess-mudstone interface, which, in turn, diminished the frictional constraints that were holding the soil layers in place. A crucial element in this geological narrative was the presence

of mudstone, which functioned as a critical barrier within the subsurface geological makeup. The relatively impermeable mudstone presented a stark contrast in terms of permeability coefficients when compared to the overlying loess strata. This disparity in permeability was a significant factor in the chain of events leading to the landslides. As the rainfall persisted and continued its steady infiltration, the softened zone near the loess-mudstone interface underwent a progressive expansion. This expansion, over time, culminated in a state of fluidization, a condition in which the soil lost its mechanical integrity and essentially transformed into a fluid-like state. This, in turn, precipitated the occurrence of interfacial landslides. In essence, the interplay of rainwater infiltration, soil softening, differences in permeability coefficients, and the ultimate transition to a fluidized state at the loess-mudstone interface was the intricate sequence of events that resulted in the observed landslides within the study area. The startup conditions were influenced by rainfall intensity, duration, and the thickness of overlying loess. The study provided scientific guidance for prevention, monitoring, early warning, and control of geologic landslide hazards.

Zhang et al. (2017) [151] investigated the response of a loess-mudstone landslide model to seismic activity using centrifuge shaking table tests and 2D seismic input waves. The model was subjected to different amplitudes of simulated seismic signals, and the dynamic response was analysed in terms of relative peak ground acceleration (PGA). The results showed that relative PGA increased with increasing landslide height, with maximum values at the crest and slightly larger values at the toe compared to the middle of the slope. The outer surface exhibited the highest PGA, while the sliding surface had the weakest. Horizontal values of PGA were generally larger than vertical values, and the seismic input amplitude strongly influences the landslide's dynamic response. The study highlighted the deformation and failure mechanisms of the slope, such as displacement, cracks, collapsed soil deposition, and shallow sliding. Both centrifuge model testing and numerical modelling provided consistent results in terms of dynamic responses and failure characteristics induced by seismic activity.

Wen and He (2012) [152] studied irrigation practices in loess areas of northwest China which have led to frequent landslides, specifically loess–red mudstone landslides. The presence of salt sinters at the landslide toes suggested that irrigation water's leaching effect on soluble salts in weathered red mudstone (WRM) may weaken its shear strength, contributing to landslide occurrence. Tests on WRM samples near landslides in Lanzhou city revealed that leaching by irrigation water reduced the residual shear strength and friction angle by up to 65% and 62% respectively after six leaching cycles, accompanied by significant dissolution of soluble salts.

Particle size distribution indicated that leaching mainly caused disaggregation of coarser particles and weakened interparticle forces among clays. Clay mineralogy may affect particle disaggregation.

Zhou et al. (2014) [153] investigated the soil behaviour and failure mechanisms of loess slopes in Heifangtai Plateau, Gansu Province, China, which is prone to frequent landslides. High-quality soil samples were collected behind a landslide's failure plane. Three sets of stress path tests were conducted, simulating the process of loess slope failures. The tests included undrained compression (UC), drained shear, and wetting on anisotropically consolidated saturated and unsaturated samples. Results revealed strain-softening behaviour in saturated loess during undrained compression, sudden failure at low confining stress during drained shear, and progressive deformation during wetting in unsaturated loess. The study discussed the failure mechanisms of loess slopes based on these experimental findings.

Wang et al. (2021) [154] focused on the detection, shear characteristics, and formation mechanism of loess-mudstone landslides in the loess Plateau of China. Field investigations, ring shear tests, and numerical simulations were conducted on loess specimens collected from the Dingjiagou landslide in Yan'an city. Results revealed that moisture content decreased the peak and residual strength of slip zone soils, while increased normal stress enhances shear strength. Heavy precipitation was found to play a significant role in slope instability compared to excavation. Well-developed cracks in loess soils and underlying mudstone soils contributed to the formation of loess-mudstone landslides. The study proposed three stages of formation: local deformation, penetration, and creeping-sliding stages, providing valuable insights for understanding and mitigating such landslides.

Li et al. (2022) [155] conducted a physical model test to simulate loess landslide failure under rainfall conditions. Pore-water pressure and soil pressure sensors were used to monitor the failure process. The results demonstrated the random nature of loess landslide failures and highlighted the inadequacy of single-scale or linear mechanical models. However, by considering micro and macro scales, the failure process of loess landslides could be effectively described. The study suggested analysing loess landslide mechanics from various perspectives, including liquid bridge, force chain, soil mechanics tests, physical models, real landslides, and tectonic stress, to enhance scientific understanding and effectiveness in future research.

Ling and Ling (2012) [156] investigated landslides triggered by heavy precipitation, specifically focusing on rainfall associated with hurricanes. Using centrifuge model simulations, the researchers replicated a landslide event that occurred during Typhoon Nabi in Japan in 2005. The simulations involved a sand-clay soil mixture and incremental application of rainfall until it surpassed field measurements. Instability was analysed using an infinite slope analysis, and the mechanism of rainfall-induced failure was discussed. The results demonstrated that rainfall increments below 200 mm caused localized failures, while a cumulative rainfall of 400 mm led to a widespread slope failure. The instability was attributed to reduced soil cohesion and increased pore pressure resulting from infiltration during rainfall.

Zhang et al. (2012) [12] investigated the infiltration-deformation-failure process of slopes with cracks under rainfall-induced deep-seated landslides. Centrifuge model tests were conducted, measuring suction, displacement, and wetting front behaviour. The results showed that the wetting front curved significantly near the cracks, and deformation was mainly influenced by soil saturation and crack-affected water infiltration. The displacement process of slopes with cracks exhibited stages of small displacement, rapid increase, and stability. With increasing distance, cracks showed lesser impact on infiltration and deformation. Vertical deformation was prominent near vertical cracks, while horizontal deformation was less significant. Rainfall style and intensity also impacted the slope's deformation-failure behaviour. Vertical cracks on the slope top were less likely to trigger global landslides compared to oblique cracks.

Askarinejad et al. (2012) [157] performed small-scale physical modelling experiments using a geotechnical drum centrifuge to examine the factors that lead to landslides triggered by rainfall. The tests were carried out in a controlled setting concerning temperature, humidity, wind, and the amount and duration of rainfall. The purpose was to examine potential failure mechanisms proposed for full-scale landslide experiments. The model included different shapes and hydraulic properties of the bedrock to simulate drainage and exfiltration. Close-range photogrammetry and high-speed cameras were used to track ground movements, monitor volumetric changes, and analyse deformation vectors and strains using the PIV method. The paper also discussed the design details of the climate chamber used in the experiments.

Peranic et al. (2022) [158] presented the monitoring of downscaled slope models under simulated rainfall in ‘1g’ to understand the hydraulic response. The study focused on the sensor network used to monitor soil moisture and pore-water pressure (PWP) changes. The results demonstrated

that the sensor network effectively monitors soil moisture and PWP changed during rainfall infiltration and under fully saturated conditions. The simultaneous monitoring of soil moisture and PWP allowed for the reconstruction of stress paths. The study also discussed hydraulic hysteresis, surface erosion, and challenges in achieving and maintaining the desired initial moisture distribution in slope models.

Zhan et al. (2022) [159] conducted a rainfall-induced landslide model test to investigate the change in hydrological indices during the evolution process. The results showed that volumetric moisture content reached its maximum value before failure, accompanied by an increase in pore-water pressure. A sudden change in volumetric moisture content occurred during failure. Pore-water pressure and volumetric moisture content were commonly used as indicators for landslide early warnings, with pore-water pressure-based models often outperforming moisture content-based models. However, some failures occurred even with small positive pore-water pressure due to heavy rainfall. To address this, a model focusing on volumetric moisture content and its time variation was established, providing reliable early warnings for landslides triggered by saturated conditions or low pore-water pressure.

Prodan et al. (2023) [160] examined the failure mechanism of a landslide induced by simulated rainfall through the utilization of small-scale slope modelling. The models, constructed with varying soil types (sand and sand-kaolin mixtures) but having the same slope angle, were subjected to simulated rainfall while monitoring parameters like water content, pore-water pressure, matric suction, slope deformation, and failure development. The findings revealed that rainfall infiltration increases water content, reduces suction, and weakens the slope's effective stress and shear strength, leading to movement and slope failure. Observations indicated that sandy slopes experience retrogressive failure due to rising groundwater, while sand-kaolin mixtures exhibit crack instabilities caused by matric suction dissipation from rainfall infiltration in unsaturated conditions.

Peranic et al. (2022) [161] introduced a model platform developed at the University of Rijeka, Croatia, to conduct physical simulations of downscaled slopes subjected to rainfall infiltration under gravitational forces less than ‘1g’. The need for a comprehensive understanding of rainfall-induced landslides was emphasized due to climate change and urban expansion. Observing how slopes responded hydromechanically to rainfall loads was essential to better understanding the mechanisms behind them. The platform included a sensor network for precise monitoring of soil

moisture and pore water pressure during rainfall simulations. The study highlighted the importance of such models in providing accurate insights into relevant variables. Two examples of monitoring data were analysed, demonstrating the applicability of the model platform in studying scaled slope models exposed to rainfall.

Arbanas et al. (2020) [162] used scaled physical models to study landslide behaviour originated in Japan during the 1970s. Laboratory experiments using scaled models, also known as flume tests, were conducted in Canada, Japan, and Australia in the 1980s and 1990s under normal gravity conditions. The work aimed to model the behaviour of landslide remediation structures in scaled physical models under static (rainfall-triggered) and seismic (earthquake-triggered) conditions, as well as their combined effects. This research presented preliminary results from a rainfall simulation test on a sandy slope, including observations of water content, pore-water pressure, and surface displacement using structure-from-motion techniques. The article also examined the commencement and progression of the observed instability within the sandy slope model.

Wang et al. (2022) [163] derived a new debris flow rainfall threshold based on real-time rainfall intensities in Beijing. Severe flooding and debris flows occurred in Beijing's mountainous areas during three storms on July 21, 2012, July 20, 2016, and July 16, 2018. These events provided an opportunity to evaluate rainfall intensity thresholds for debris flow occurrence. Different threshold types based on average intensities during the rainfall period and entire duration were estimated. Results indicated that various threshold types differ in their ability to distinguish storms with positive and negative debris flow responses, with the real-time threshold performing the best. The results also indicated that the initiation of debris flows in Beijing was associated with a combination of rainfall intensity and cumulative precipitation, requiring both to reach a threshold level for initiation.

Zhang et al. (2022) [164] presented a method for determining rainfall types based on their impact on slope instability, aiming to enhance early warning systems for rainfall-induced slope failures. Through simulations of slope instability scenarios under various rainfall conditions and soil properties, threshold curves for slope failure were obtained. Examining these graphical representations allowed for categorizing rainfall patterns into two distinct types: those characterized by short-duration and high-intensity (referred to as SH) and those described by long-duration and low-intensity (referred to as LL). The findings from the analysis revealed a

compelling connection between the specific rainfall types and their impact on the onset of slope failure. The authors observed that varying intensity-duration (I-D) conditions pronounced affected the initiation of slope failure under LL-type rainfall. In contrast, such conditions did not exert a significant influence under SH-type rainfall. Expanding further on the results, the work highlights the intricate relationship between rainfall characteristics and their role in slope failure. The SH-type rainfall, characterized by its brief but intense downpours, has a relatively consistent effect on slope stability. In contrast, the LL-type rainfall, characterized by prolonged and gentler precipitation, demonstrated a more complex response to variations in intensity and duration. This insight suggests that slope stability during rainfall events is a multifaceted phenomenon, influenced not only by the overall amount of rainfall but also by the specific characteristics of the rain, including its duration and intensity. Understanding these aspects in rainfall patterns and their impact on slope stability is crucial for effective slope management and risk mitigation in geotechnical engineering and related fields. Soil shear strength parameters do not affect rainfall type classification, although they can shift the threshold curve of slope failure. This research contributed to understanding rainfall's role in slope failure initiation, aiding the development of future early warning systems.

Arnhardt et al. (2007) [165] focused on investigating the entire information chain, from data gathering through wireless sensor networks to information retrieval, specifically for landslides and mass movements. The importance of early warning systems in disaster prevention for natural hazards is increasing, especially in areas where mitigation strategies are limited. However, data gathering and system interoperability pose significant challenges. The project emphasized the need for cost-effective and easily deployable measurement systems, as well as modern information systems with interoperability and service-oriented architecture concepts. The proposed wireless network served as a foundation for additional techniques such as sensor fusion and malfunction identification. The obtained geodata was processed according to user requirements and could be integrated into local, regional, or global information structures, ensuring flexibility and accessibility for a wide range of users.

Gidon and Sahoo (2023) [166] performed real-time monitoring of slopes for accurate assessment of slope behaviour and analysis based on received data. In India, 15% of the landmass is prone to landslides according to the “National Disaster Management Authority” (NDMA). By measuring pore water pressure, site displacement, and hydrological conditions, a deeper understanding of slope behaviour and failure mechanisms can be gained. Proper instrumentation

during monitoring revealed the failure surface caused by rainwater seepage, aiding in the reduction of catastrophic effects. Tensiometers placed at various slope levels highlighted the significance of pore water pressure during rainfall. Finite element analysis validated field study results, identifying potential slip surfaces and enabling the development of reliable slope stabilization techniques. Advanced warning criteria could be established by identifying a threshold level through the system.

Menon (2023) [167] introduced a methodology for identifying the key parameters affecting rainfall-induced landslides. Two laboratory-scale slope models were constructed using a tilting fume setup and rainfall simulators to study landslide processes. Various sensors and cameras were employed to monitor the landslides. The results obtained from this study contributed to the identification of effective monitoring parameters for the development of a landslide early warning system (LEWS). The study focused on the measurement of pore water pressure parameters and continuous capture of instantaneous photographs during artificial rainfall simulations. The findings suggested that while pore-water pressure monitoring is not ideal for developing an early warning system due to the unpredictable nature of pressure values in heterogeneous soil and sloping angles, a sudden release of pore pressure occurs after mass failure, as observed in the results.

Kuradusenge et al. (2021) [168] determined rainfall and soil water content thresholds for the landslide early warning system (LEWS) using Internet of Things (IoT) technology. shallow landslides pose a significant threat, often triggered by rainfall in mountainous regions. The rainfall threshold for landslide occurrence varies based on geographical characteristics. Determining soil water content is crucial for landslide prediction and early warning systems. Real-time monitoring with rain gauges, soil moisture sensors, and rainfall simulating tools was conducted. Results showed that landslide occurrence is influenced by rainfall amount, intensity, soil moisture, and internal and environmental factors. A comprehensive investigation conducted at a particular geographical location has yielded valuable insights regarding the temporal dynamics of slope failure. It was determined that the onset of slope failure at this specific site necessitates a minimum duration of 8 hours and 41 minutes. This critical temporal threshold was observed in conjunction with specific meteorological and soil conditions. Specifically, this threshold emerged under sustained rainfall, an intensity of 8 millimetres per hour, and notably high soil moisture levels exceeding 90% as measured by deeper sensors. These findings hold significant implications for advancing Landslide Early Warning Systems (LEWS). By

identifying the temporal threshold associated with slope failure in this specific geographic context, the authors established a crucial reference point for predictive modelling. These values, derived from empirical research, can be employed as pivotal components within LEWS algorithms, enhancing the system's accuracy and reliability in predicting impending slope failures in similar regions. This represents a substantial step forward in bolstering the effectiveness of LEWS, ultimately contributing to improved landslide risk management and mitigation strategies.

Table 2. 4 shows the summary of existing literature based on Physical modelling.

Table 2. 4: Literature based on Physical modelling

S. No.	Authors	Work done
1.	Guan et al. (2023) [149]	Examined the failure mechanisms of landslide dams by conducting experiments and analysing debris composition and geomorphic parameters
2.	Cogan and Gratchev (2019) [150]	Examined the combined effects of rainfall intensity, slope angle, and slope moisture content on landslide initiation using a flume device to model single soil layer slope failures
3.	Li et al. (2016) [42]	Investigated the startup conditions and sliding mechanism of rainfall-induced loess-mudstone interfacial landslides in China through a semi-similar material physical model test
4.	Wang et al. (2021) [154]	Conducted field investigations, ring shear tests, and numerical simulations to understand the detection, shear characteristics, and formation mechanism of loess-mudstone landslides in the loess Plateau of China
5.	Li et al. (2022) [155]	Carried a physical model test to simulate loess landslide failure under rainfall conditions by using PWP and soil pressure sensors to monitor the failure process.
6.	Askarinejad et al. (2012) [157]	Performed small-scale physical modelling experiments using a geotechnical drum centrifuge to examine the factors that lead to landslides triggered by rainfall including different shapes and hydraulic properties of the bedrock to simulate drainage and exfiltration by utilising close-range photogrammetry and high-speed cameras to track ground

		movements, monitor volumetric changes, and analyse deformation vectors and strains using the PIV method
7.	Peranic et al. (2022) [158]	Presented the monitoring of downscaled slope models under simulated rainfall in '1g' to understand the hydraulic response and developed a sensor network to monitor soil moisture and PWP changes
8.	Prodan et al. (2023) [160]	Examined the failure mechanism of a landslide induced by simulated rainfall through the utilization of small-scale slope constructed with varying soil types (sand and sand-kaolin mixtures) modelling and by monitoring parameters like water content, pore-water pressure, matric suction, slope deformation, and failure development
9.	Arbanas et al. (2020) [162]	used scaled physical models and conducted flume tests under normal gravity conditions to study landslide behaviour observed in Japan
10.	Zhang et al. (2022) [164]	Proposed a method for determining rainfall types based on their impact on slope instability to develop LEWS for rainfall-induced slope failures. Threshold curves for slope failure were obtained through simulations of slope instability scenarios under various rainfall conditions and soil properties
11.	Menon (2023) [167]	Constructed two laboratory-scale slope models utilising a tilting fume setup and rainfall simulators to study landslide processes. PWP parameters were noted and instantaneous photographs were captured during artificial rainfall simulations by employing sensors and cameras to monitor the landslide process.

2.4.6 Literature Based on Statistical and Probability Modelling

Abraham et al. (2020) [30] proposed a Bayesian analysis method that calculated the likelihood of landslides happening based on various combinations of rainfall intensity and the antecedent soil moisture levels. The "Système Hydrologique Européen Transport" (SHETRAN) hydrological model simulated soil moisture, and event rainfall-duration (ED) thresholds are used to characterize rainfall severity. The approach was applied in Kalimpong, a landslide-prone area in the Darjeeling Himalayas, to define two-dimensional Bayesian probabilities for landslide

occurrence. The research illustrated the practicality of utilizing the SHETRAN model for simulating moisture conditions, offering a viable strategy for enhancing the accuracy of empirical threshold predictions tailored to the local context.

Uwihirwe et al. (2020) [169] endeavoured to employ empirical-statistical methods, utilizing both landslide and precipitation data, to achieve two main objectives in Rwanda, Central-East Africa. Firstly, they sought to pinpoint the precipitation-related variables with the greatest capacity for explaining landslide occurrences. Secondly, they aimed to establish threshold levels for landslides based on both triggering events and their underlying causes. To accomplish these goals, they employed a combination of the Bayesian probabilistic approach, maximum true skill statistics, and the minimum radial distance technique to identify informative threshold levels indicating the likelihood of landslide occurrences.

Dikshit et al. (2017) [107] employed a probabilistic approach in the Kalimpong region of Darjeeling Himalayas using rainfall and landslide data from 2010 to 2016. The frequency of landslides in the Indian Himalayan regions has increased, leading to severe consequences in terms of loss of life and property. This necessitated the development of strategies to mitigate the impact of landslides. The findings highlighted the correlation between landslides and rainfall event parameters, particularly rainfall intensity. Additionally, a comparative analysis was conducted between empirical and probabilistic thresholds to assess their effectiveness in landslide prediction.

Lari et al. (2014) [28] introduced a general framework for probabilistic landslide hazard analysis that provides hazard curves and maps for all types of landslides. The technique assessed the likelihood that a given slope site would experience a landslip within a specific time frame. Hazard maps were generated by selecting a fixed probability of exceedance. The approach considers landslide onset frequency, runout frequency (for long-runout landslides), and local landslide intensity. The methodology was used to analyse rockfall risk in an area damaged by the 2011 earthquake in Christchurch, New Zealand. Hazard curves and maps were crucial for designing mitigation structures, land planning, and risk management policies.

Glade et al. (2000) [29] highlighted that rainfall-induced landslides pose significant risks and are vital geomorphic processes worldwide. In this study, the authors investigated landslide susceptibility in three regions within New Zealand's North Island, known for their vulnerability

to landslides. They employed the empirical “Antecedent Daily Rainfall Model” to establish regional rainfall thresholds that trigger landslides. This model integrates antecedent rainfall data and rainfall that occurs on the day of the event. Moreover, it incorporates a decay coefficient derived from the physical characteristics of storm hydrograph recession. These three regions in New Zealand's North Island were chosen for their distinct geological and climatic factors, making them ideal study areas to understand landslide triggers better and develop early warning systems. The research not only focused on identifying rainfall thresholds but also aimed to shed light on the complex interplay between antecedent rainfall conditions and the specific rainfall patterns during an event. The decay coefficient, which derived from storm hydrograph recession behaviour, provided a valuable key to comprehending the dynamic processes associated with landslides in these regions. Statistical techniques were applied to identify thresholds that effectively distinguish landslide occurrence conditions. The resulting regional models provided a means to assess the probability of landslide events based on rainfall conditions, highlighting regional variations in susceptibility to landslide-triggering rainfall based on physical conditions and landslide databases.

Wu and Song (2018) [170] evaluated landslide susceptibility in Danba County, China, a probability statistic model called the certain factor was employed. Landslide events in the region were frequent but poorly understood. The resulting susceptibility map achieved accuracies of 0.8211 and 0.8288 in the experiment and verification areas, respectively, validated by the area under the prediction rate curve. Spatial clustering analysis using Moran's statistic and local indicator of spatial association (LISA) was conducted to identify landslide-prone areas. The high Moran's index of 0.959 and the consistent LISA identification with previous investigations confirmed the rationality and effectiveness of the proposed method in locating landslide-prone regions and facilitating decision-making.

Rollo and Ramoello (2021) [171] employed a probabilistic approach, utilizing an updated database of ground motions recorded during Italian earthquakes, to assess slope seismic performance. The advantage lies in accounting for the aleatory variability of ground motions and predicting seismic-induced slope displacements. Hazard curves were presented, displaying the annual rate of exceeding permanent slope displacement. The approach was applied regionally, creating seismic landslide hazard maps for Southern Italy's Irpinia district, characterized by high seismic hazard. These maps could aid practitioners and government agencies in regional

planning, identifying and monitoring zones susceptible to earthquake-induced slope instability, necessitating further site-specific studies.

2.4.7 Indian Standard Provisions

The Bureau of Indian Standards (BIS) has established guidelines pertaining to the broader assessment of landslide hazards on a regional scale of 1:50,000, as detailed in IS 14496, Part 2 (1998, reaffirmed in 2002) in India. The approach employed by BIS for evaluating landslide susceptibility zoning involves the use of a heuristic method known as Landslide Hazard Evaluation Factor (LHEF) rating scheme. BIS has identified six primary factors contributing to landslide occurrence in hazard zoning: lithology, structural characteristics, slope morphology, relative relief, land use and land cover, and hydrological conditions. Table 2. 5 shows landslide hazard evaluation factor (LHEF) presented by BIS [172].

Table 2. 5: Landslide hazard evaluation factor (LHEF)

Sr. No.	Causative factor	Maximum LHEF Rating
1.	Lithology	2
2.	Structure	2
3.	Slope morphometry	2
4.	Relative relief	1
5.	Land use and land cover	2
6.	Hydrological condition	1

The National Disaster Management Authority (NDMA) has presented an official document titled "Management of Landslides and Snow Avalanches" in the year 2009. This document provides definitions for various terms used in the field of landslide studies. It defines Landslide Hazard Zonation (LHZ) mapping as a valuable tool to identify regions prone to landslides, evaluating the likelihood of such events occurring over a specified timeframe. The creation of an LHZ map involves analysing regional geology, geomorphic conditions, slope stability (both current and potential), and land usage data.

The significance of scale is emphasized within the document when conducting LHZ mapping. Maps at scales of 1:1,00,000 or 1:50,000 are unsuitable for comprehensive regional assessments,

as they offer only preliminary insights and lack sufficient detail. It is recommended to use larger scale maps, such as 1:10,000 or higher, for in-depth investigations at the local level. The document also underscores the absence of a comprehensive landslide inventory, which poses challenges in validating landslide hazard maps. No institution within the country possesses a robust database of landslide inventory. Recognizing the importance of establishing a reliable landslide inventory database, the Geological Survey of India (GSI) has recently launched an initiative to create landslide inventory maps and databases encompassing regions prone to landslides in the country.

Furthermore, the document details specific case studies involving geotechnical assessments and monitoring of various landslide sites. Prominent examples of such investigations encompass the meticulous scrutiny of various landslide occurrences across different regions of India. Notable among these is the thorough assessment of the Kaliasaur landslide, which is situated in proximity to Srinagar along National Highway 58 (NH-58). Additionally, in the picturesque region of Nainital, the Sher Ka Danda and 9.5-mile landslides have garnered considerable attention and research efforts. Moving towards the eastern Himalayas, the B2 and Lanta Khola landslides in Sikkim have also been subjects of in-depth investigation. Further west, in the pristine landscapes of Kinnaur district, Himachal Pradesh, the Powari landslide at kilometer 367 on National Highway 21 (NH-21) has drawn scientific interest for its unique characteristics. Similarly, the Patalganga landslide near Pipalkoti, along National Highway 58 in Uttarakhand, has been thoroughly examined to understand its underlying geological and environmental factors. The Department of Science and Technology (DST) has taken proactive steps by initiating multiple research projects in response to the growing need for comprehensive research in this field. Noteworthy among these endeavours are those focused on NH-1A in Sonapur, Meghalaya, which has experienced its share of geological challenges. Additionally, the ancient and sacred Tirumala Hills have become a subject of scientific scrutiny to comprehend the geological dynamics in that region better. The DST has also undertaken research projects at eight specific sites in Uttarakhand, each providing valuable insights into the complexities of landslide occurrences in diverse terrains. These research initiatives undertaken by the Department of Science and Technology are part of a broader effort to enhance the understanding of landslides and the geophysical processes that lead to them in various parts of India, ultimately contributing to developing effective mitigation and preparedness strategies.

2.5 Research Gaps

After a detailed and extensive literature survey in the area of rainfall-induced landslides, the following research gaps are identified:

1. Previous studies have primarily relied on mathematical or numerical models to analyse rainfall-induced landslides. However, a research gap exists in the limited exploration of physical modelling methods to simulate the key parameters of parent landslides. Physical modelling techniques can provide valuable insights into the behaviour and mechanisms of landslides under different rainfall conditions, particularly in the context of the Himalayan terrain.
2. Most of the existing studies have employed numerical methods for slope failure analysis but the effectiveness and significance of these techniques have not been adequately verified through physical modelling experiments. Therefore, the validation of numerical techniques using physical modelling is an unexplored domain of research to ensure better reliability and applicability of these models in assessing slope failure mechanisms in specific geographic contexts, particularly in the vicinity of the Indian Himalayas.
3. There is a lack of extensive research and development of EWS that utilize strain gauges for stress detection prior to failure. This highlights the need for further exploration of this particular approach to enhance the effectiveness for various failure events.
4. A limited number of studies have been conducted on the simultaneous utilization and integration of multiple sensors, such as strain gauges, soil moisture sensors, rain gauges, and tilt sensors to collectively assess probable initiation factors for landslides. Therefore, further research is much needed to explore and investigate in this context for the development of more accurate and reliable monitoring systems.
5. A research gap exists in the need for low-cost monitoring systems instead of previous instrumentation-based EWS, which were costly and impractical to install and monitor for every critical slope. Additionally, the inability to recover and reuse the monitoring instruments after slope failure events further emphasizes the requirement for cost-effective alternatives. This research gap highlights the necessity of exploring and developing low-cost monitoring systems that are affordable. Such systems would enable more widespread implementation and continuous monitoring of critical slopes, contributing to enhanced slope stability assessment and timely warning of potential failure events.

CHAPTER 3

PHYSICAL MODELLING

3.1 General

Debris flows are fast-moving landslides that are dangerous to life and property because they move quickly, destroy objects in their paths, and often strike without warning. Debris flows are most common during seasons of heavy rain, and they usually begin on slopes or mountains. Debris flows, also known as mudslides, mudflows, or debris avalanches, are a form of landslide [50]. It is tough to explain the mechanism of debris flow landslide, only with a numerical or mathematical model because of sudden failure, complexity, and random behaviour [42]. So, the slope failure mechanism has been studied by adopting a physical model test as it is most effective and widely used method to explore the sliding mechanism of soil slices, to investigate the rainfall water movement through the pores, to analyse the rainfall-induced slope instability, and thereby helping in providing insights for early warning and control of landslides [42], [157], [186].

3.2 Material Similarity and Similar Condition

The concepts of 'similar theory' are used for the indoor model experiment. The experimental set-up and materials are prepared by criterion based on the similar theory. Similarity ratio is adapted accordingly, which is the prototype ratio to model for the parameters: geometric similarity ratio, quality similarity ratio, loading similarity ratio, and boundary condition similarity ratio [42], [187], [188].

The scale-based physical model is mostly used models than any other mechanical model to study the landslide mechanism. A model test used for the study of landslides should have its similarity characteristics, including dead load similarity, slope material similarity, rainfall duration similarity, and boundary condition similarity. These factors are effective parameters in the physical model test used to study the landslide mechanism.

The soil available in the laboratory (Delhi Technological University (DTU) soil) constitutes 80% sand, and 20% fine-grained soil, i.e., silt and clay. The soil of the study area constitutes 60% sand and 40% fine-grained soil. So, to meet the similarity condition, sand and clay are added to

the DTU soil. As in the study area, there are stones and boulders that are also present in debris material, so fraction of stones and boulders of different sizes are mixed to meet up with similarities. By material similarity theory, the similarity ratio of inner friction angle, modulus of elasticity, cohesion, and poisson's ratio are taken similar to the prototype, as $C\varphi = C_E = Cc = C\mu = 1$.

3.3 Physical Modelling Set-Up

A physical modelling test has been set-up in the study bearing identical engineering properties based on the existing studies. The essential engineering properties of soil obtained through similar materials are tested in the laboratory and derived through the 'dimensional technique'. The 'similar conditions' of the physical model experiment were brought in line with the similar theories. The start-up conditions and failure mechanism of the rainfall-induced landslide are studied through the physical model experimental method. Fig. 3. 1 shows the schematics of the experimental set-up of the physical modelling and Fig. 3. 2 shows the frame type box with soil slope.

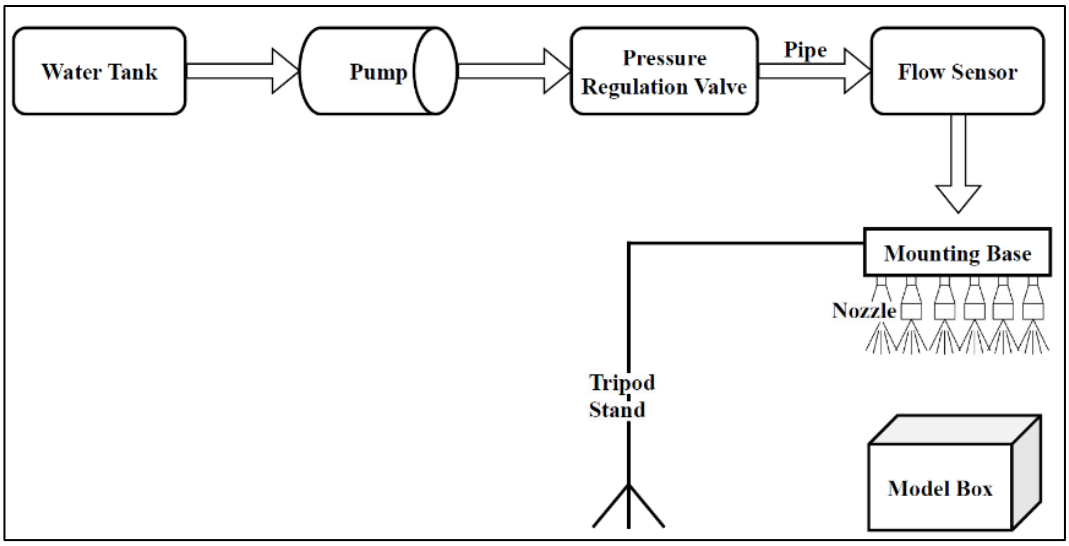

Fig. 3. 1: Schematic diagram of the experimental set-up

The following assumption has been made while performing the physical modelling: -

i. The engineering properties of parent soil and experimental soil are the same.
ii. All the sides are impermeable, ensuring no seepage except the toe drain.
iii. The impact factor of rainfall on the slope is negligible as the sprinkler used is not jet type.
iv. Rainfall distribution on the slope is uniform.
v. The effect of vegetation and evaporation has not been considered.

3.3.1 Fabrication of Frame-Type Box

The frame type box model is designed using a transparent acrylic sheet of 15 mm thickness with a steel frame for experimental work. The 'similarity ratio' of geometry, C_G is taken equal to 'n' (C_G = n). In this test, the geometry scale is taken as 1 in 100 as the prototype is large. The experimental platform is a cuboidal tank, which measures 97 cm long, 57 cm wide, and 48.5 cm high. Drain holes are also provided at the toe side to flush the runoff water.

Fig. 3. 2: Frame-type box model with soil slope

3.3.2 Fabrication of Rainfall Simulator

There are two main empirical methods based on precipitation measurement to define its threshold [11], [26], [189], which are: -

i. Rainfall obtained for a particular event (intensity–duration (ID), total event precipitation (E), precipitation event–duration (ED), and precipitation event–intensity (EI) thresholds) and
ii. Antecedent precipitation activity which is outlined as the threshold amount of rainfall that would cause slope failure.

In this study, three parameters have been considered to simulate rainfall: -

a. intensity of precipitation '*q*',
b. duration of precipitation '*t*' and
c. interval of precipitation.

The rainfall duration and interval each vary with the time factor 't'. The relationship between the intensity of rainfall 'q' and the total rainfall '*Q*' is –

$$q = \frac{Q}{t} \qquad \text{Eq. 5. 1}$$

A self-designed rainfall simulation system, as shown in Fig. 3. 3, has been employed to replicate varying rainfall patterns that portrays real-world conditions. The artificial rain generator has been fabricated using a water storage tank, submersible pump, control valve, flow sensor, and raindrop nozzle, all working together to generate the necessary amount of rain. The rain generation process utilizes multiple sprinkler nozzles incorporated into a rainfall simulator to replicate the precipitation. The nozzles employed have a spray design with a fixed opening, resulting in potential variation in droplet size based on input flow pressure.

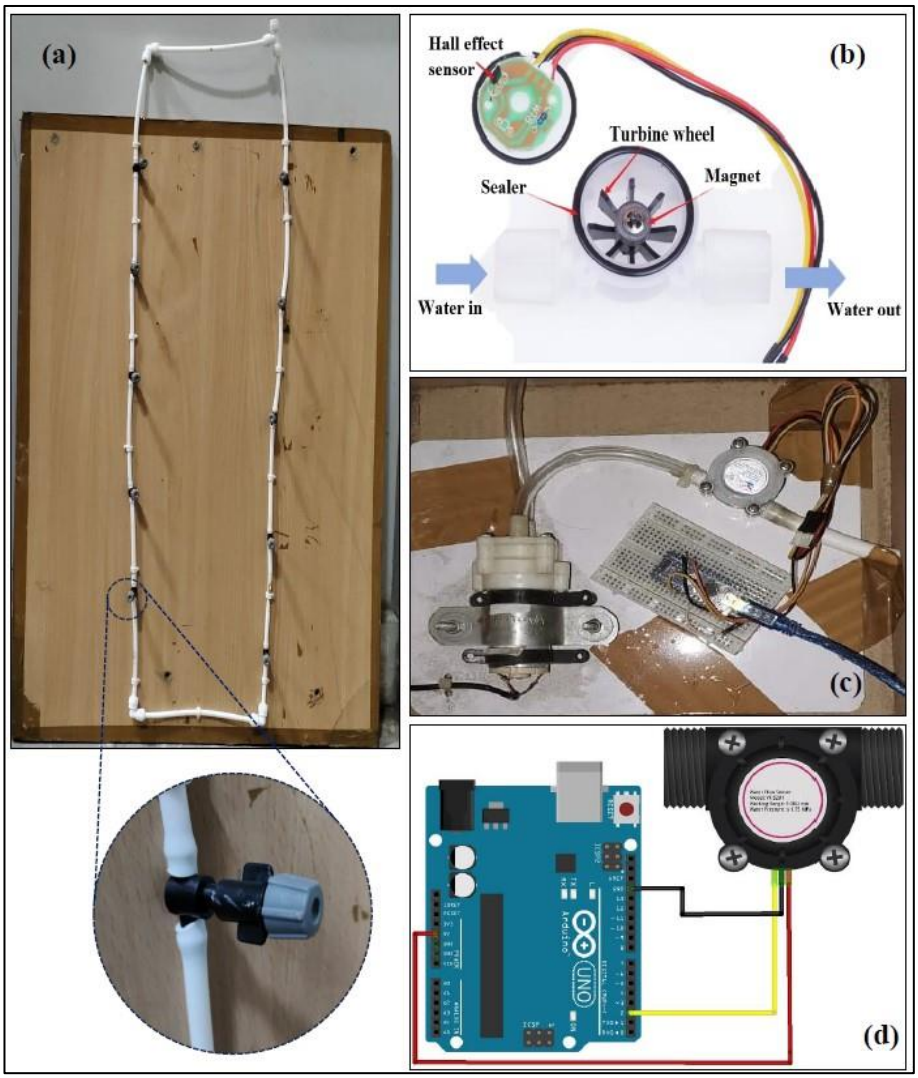

Fig. 3. 3: Components and circuit diagram for rainfall simulator

The rainfall generator has been outfitted with a flow sensor that interfaces with a microcontroller, enabling data collection when connected to a computer. Regulating the water flow during

simulations is facilitated by a sluice valve affixed to the rainfall simulator, complete with calibrated scales. Adjustment of the water flow is achieved by manipulating a hand wheel, allowing for increased or decreased flow as required. Additional markings were introduced based on experimental requirements.

To achieve the desired cumulative depth of rainfall, a fixed-opening sprinkler has been positioned 12.5 cm above the slope within the rainfall simulator. The droplet size could not be altered due to the sprinkler's fixed design. The negligible impact of the sprinkler's dispersion is assumed, given that the simulator did not employ a jet-type mechanism. This setup has been chosen to ensure feasibility and consistency throughout the experimentation process.

3.4 Study Area

This section discusses two study locations. The first study site is situated along NH-5 within Jhakri town in the Shimla district of Himachal Pradesh, India, referred to as the "Jhakri landslide." The second study site is situated near Kotrupi village along the Mandi – Joginder Nagar – Pathankot National Highway (NH-154), known as the "Jhakri landslide." These locations are selected for analysing the failure mechanism and evaluating the effectiveness of the developed system through physical modelling. The two slopes considered in this study possess distinct geometric and material characteristics, suitable for carrying comprehensive exploration of the landslide phenomenon, its underlying factors and failure mechanisms.

Soil samples have been collected from the failure sites from both the study area-I and II. These collected samples have been brought and tested in the laboratory for the determination of the geotechnical parameters of interest which serves as the input parameters for the physical and numerical modelling. The primary soil characteristics essential for simulating the in-situ conditions of the slope and for assessing the slope stability used in the present study are dry unit weight, moisture content, permeability, cohesion and friction angle. Suitable laboratory tests have been conducted for the determination of aforementioned parameters as per the guidelines and procedure outlined by Bureau of Indian Standards. The obtained values of these parameters are mentioned in the result section.

3.4.1 Study Area-I (Jhakri Landslide)

The study location is on NH-5 in Jhakri town of Shimla district in Himachal Pradesh, India (Fig. 3. 4a). The study area is covered under the topo sheet no. 53/E11 (1973) by the Geological Survey of India (GSI). NH-5 is a major national highway-connecting corridor for

Shimla districts to other areas of Himachal Pradesh. There are two hydroelectric projects of 1500 MW and 343 MW capacity operated by Satluj Jal Vidyut Nigam (SJVN) Ltd in this area (Singh et al. 2018b). The location is situated near the Sutlej River that is the rainfall catchment basin of the study area. Jhakri area near the NH-5 (HPSDMA Himachal Pradesh, 2011) is highly affected by rainfall-induced landslides.

The study area is situated in the Himalayan region and is characterized by two major thrust zones, namely the 'Main Boundary Thrust (MBT)' and 'Main Central Thrust (MCT)'. In this region, there is the presence of moderately to highly weathered quartz-mica schist, which appears white to light yellow. Stratigraphically, the Shali formation is found beneath the Rampur formation, where the lower part consists of volcanic material and the upper part comprises Rampur Quartzite. Various thrust zones in the study area undergo neo-tectonism, and the Jhakri thrust zone serves as the boundary between the Wangtu Gneiss Complex and Quartzite present in the study area. The Jhakri thrust zone has been active for more than 4.5 million years [190]–[192]. Lithology provides information about the rock formations in the study area (Fig. 3. 4b), and the lithological formations were identified through the interpretation of resource maps obtained from Bhukosh, GSI [193].

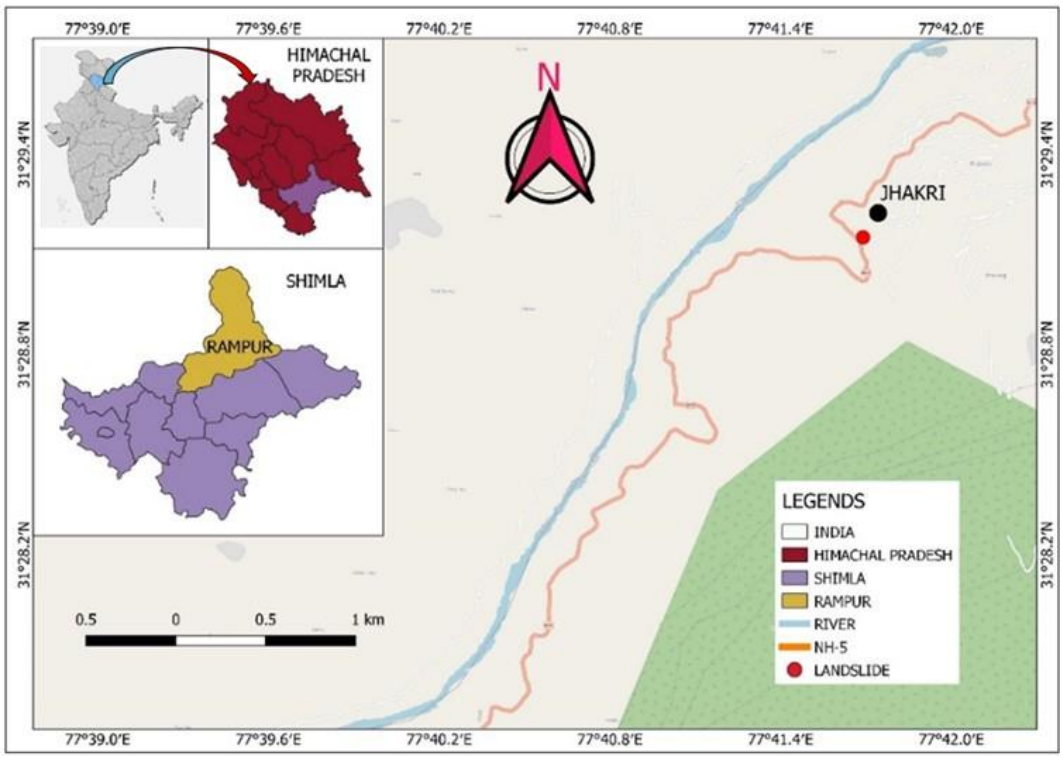

(a)

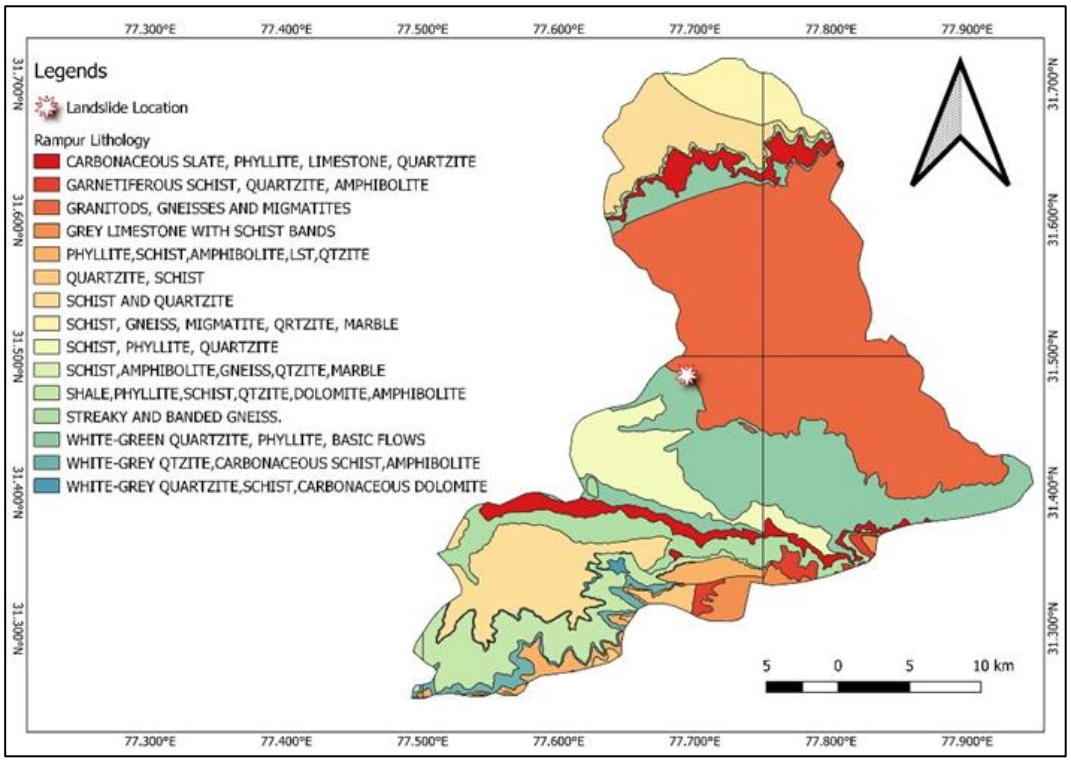

(b)

Fig. 3. 4 (a) Location map of the study area-I situated in Rampur district of Shimla, Himachal Pradesh, India, and (b) Lithological map of study area-I (Jhakri landslide)

3.4.1.1 Description of The Slope

The studied slope is near a tributary of river Sutlej. The digital elevation model of Rampur is shown in Fig. 3. 5a, while the Fig. 3. 5b shows the elevation profile of the study area. The slope has a height of 55.3 m, with a slope angle of 35° as observed during the study. The slope material contains loose aggregate deposits composing highly weathered rock particles. The soil material is non-uniform in grain size containing various sizes of rock and stones. Surface runoff has been prominent, which can be justified by the presence of erosional gullies and slope surface. The Jhakri area has experienced many devastating landslides in the past. The sloping section of the Jhakri area along NH-5 has a wide history of failure. It frequently obstructs the road because of the mass of the debris and rolling boulders.

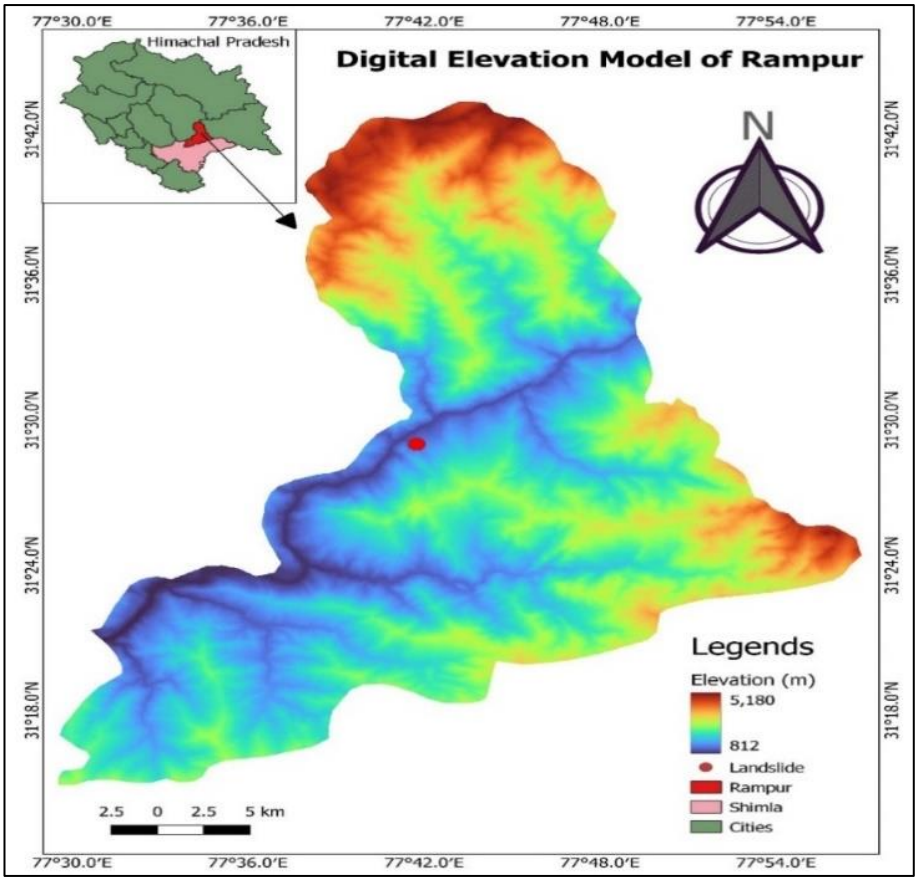

(a)

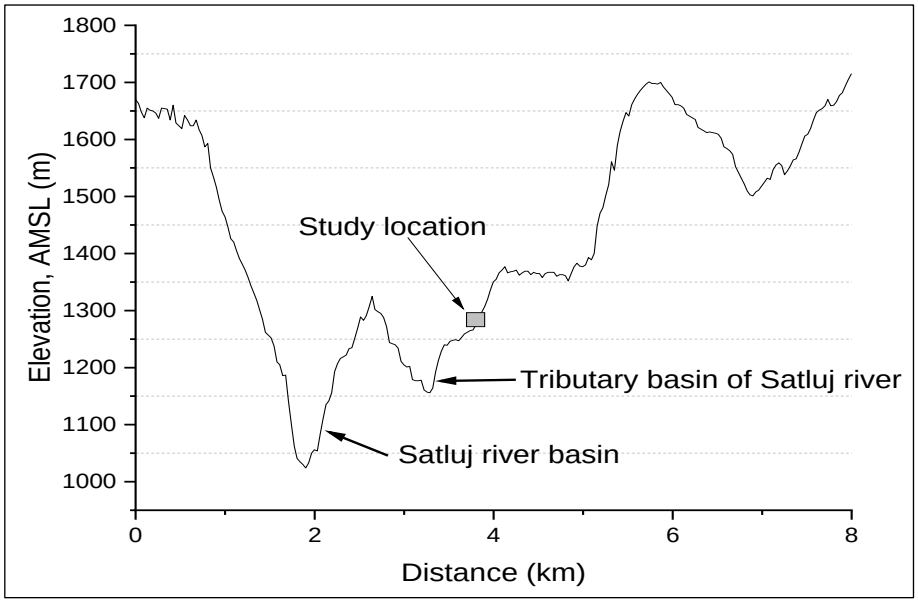

(b)

Fig. 3. 5: (a) DEM of Rampur, Shimla and (b) Elevation profile of the study area

3.4.1.2 Geotechnical Investigation of Slope Material

To determine the material properties of the failure slope, soil samples have been collected from different locations of the slope from the study area. By performing particle size distribution test in laboratory according to BIS standards [194], the obtained results shows that the material consists of 60% sand, 36% silt, and 4% clay. Some fractions of stones have been also available in a non-homogeneous way, and the gradation of slope material eventually comes as non-uniform due to the presence of wide range of particles. The soil is classified as silty sand in nature.

3.4.1.3 Rainfall Characteristics

The study area comes under the catchment region of Sutlej valley. Primarily the rainfall in this area is because of the S-W monsoon due to the orographic mechanism. The S-W monsoon appears during months of June-September resulting in maximum precipitation depth [195].

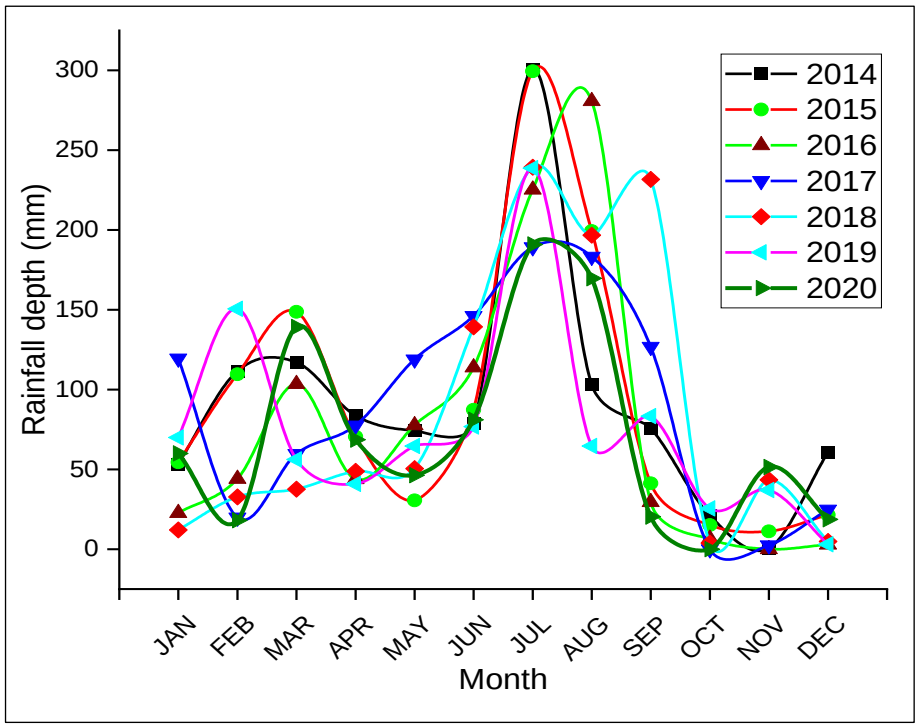

(a)

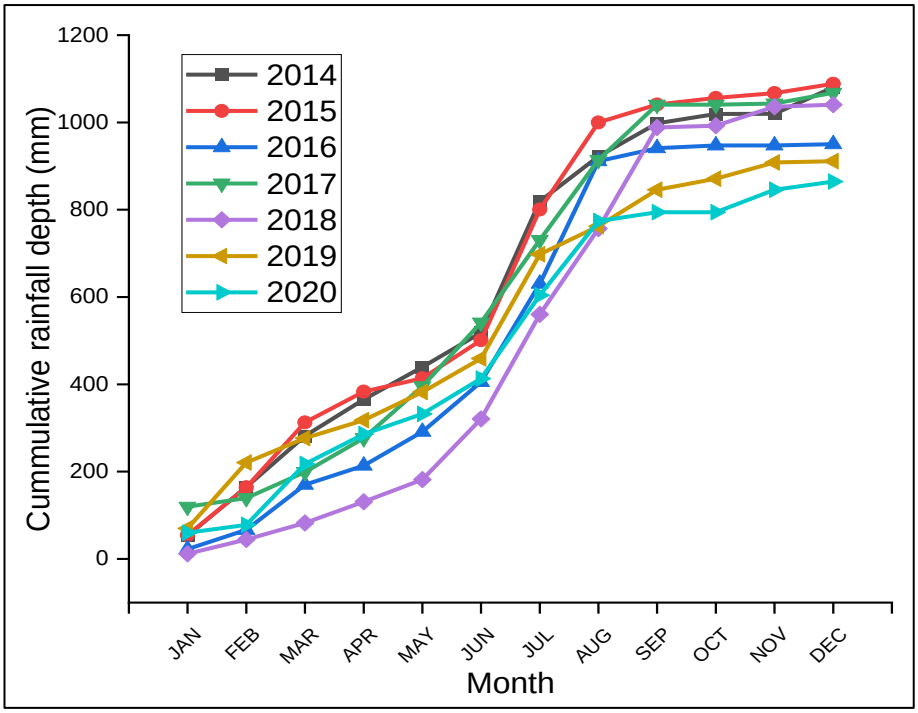

(b)

Fig. 3. 6: (a) Monthly precipitation variation, and (b) Cumulative rainfall variation

Fig. 3. 6a shows the monthly precipitation variation for the Shimla district from year 2014 to 2020. The precipitation data for the particular area have been taken from the Shimla regional centre of the Indian Meteorological Department (IMD). By analysing the monthly rainfall variation for seven consecutive year (from 2014 to 2020) it can be observed that the maximum rainfall received is in between months of June and July followed by some slight rainfall every month which helps in development of positive pore water pressure which acts as key factor in initiation of landslide. It explains the reason behind increased number of landslides in monsoonal season and also provide an indication towards the focused study during the monsoonal season. Fig. 3. 6b shows the cumulative rainfall variation for seven successive years which defines the maximum rainfall depth for the particular year which helps in deciding the threshold rainfall depth for landslide.

3.4.1.4 Mechanism of Landslide

According to Indian standard code IS 14496 (Part 2) [196], slope & geometry, lithology, state of stress, pore pressures, structure, material properties, and boundary conditions all contribute to the landslide mechanism. Because of the high number of landslides that occur in the area during the monsoon season, this research focuses on the characteristics of rainfall that occur when a slope fails. The slope section under investigation has a moderate slope gradient

and a semi-circular failure surface. Because of the lower height, the failed section is critically stable in the dry state, but saturation may further reduce the stability. As rainwater infiltrates the soil, it activates the shallow failure in four stages [197] as shown in Fig. 3. 7. Sharma et al. (2013) [198] have suggested that increased water content from heavy monsoon rains could worsen slope conditions.

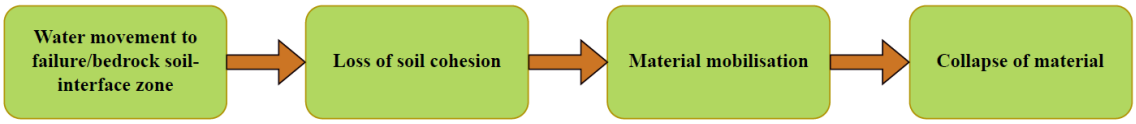

Fig. 3. 7: Stages of shallow landslide failure

3.4.2 Study area–II (Kotrupi Landslide)

The study location (Fig 3.8) is in the vicinity of Kotrupi village on the Mandi – Joginder Nagar – Pathankot National Highway (NH-154); the Kotrupi landslide has caused extensive damage [199]. On either side of the slide, Padhar and Joginder Nagar tehsils of Mandi district (Himachal Pradesh) are approximately 4 and 21 kilometers away, respectively. The study area is covered by the Geological Survey of India (GSI) toposheet No. 53A/13. Geographical coordinates with latitude N 31º 54’ 37.60” and longitude E 76º 53’ 26.30” indicate the location of the landslide [199].

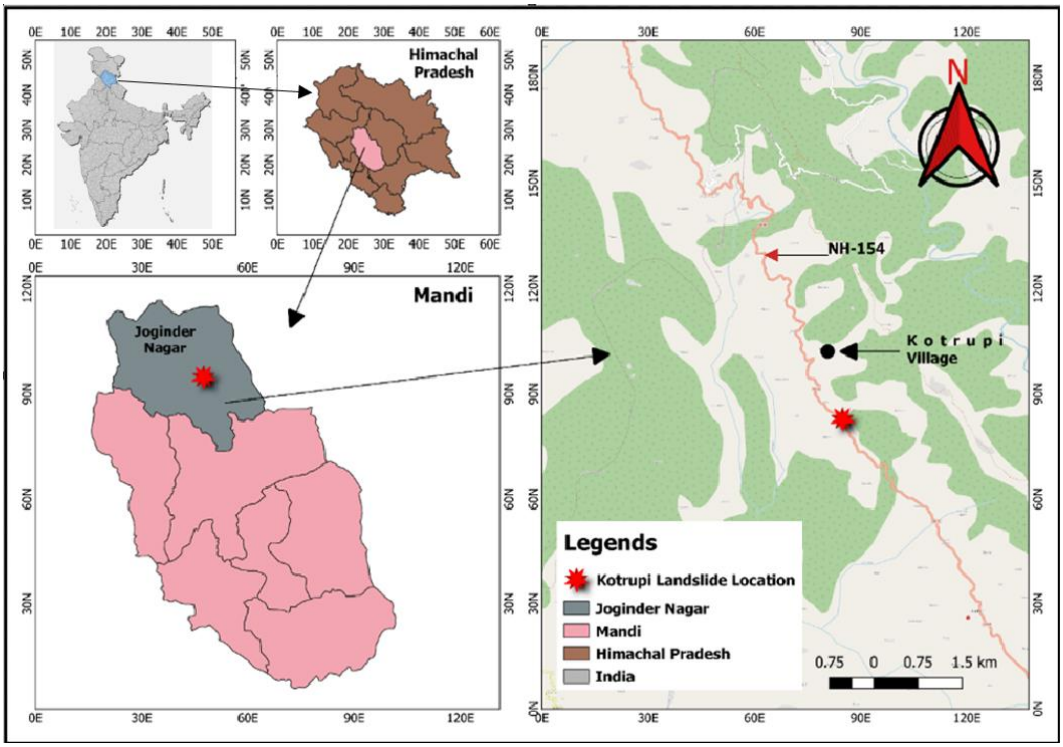

(a)

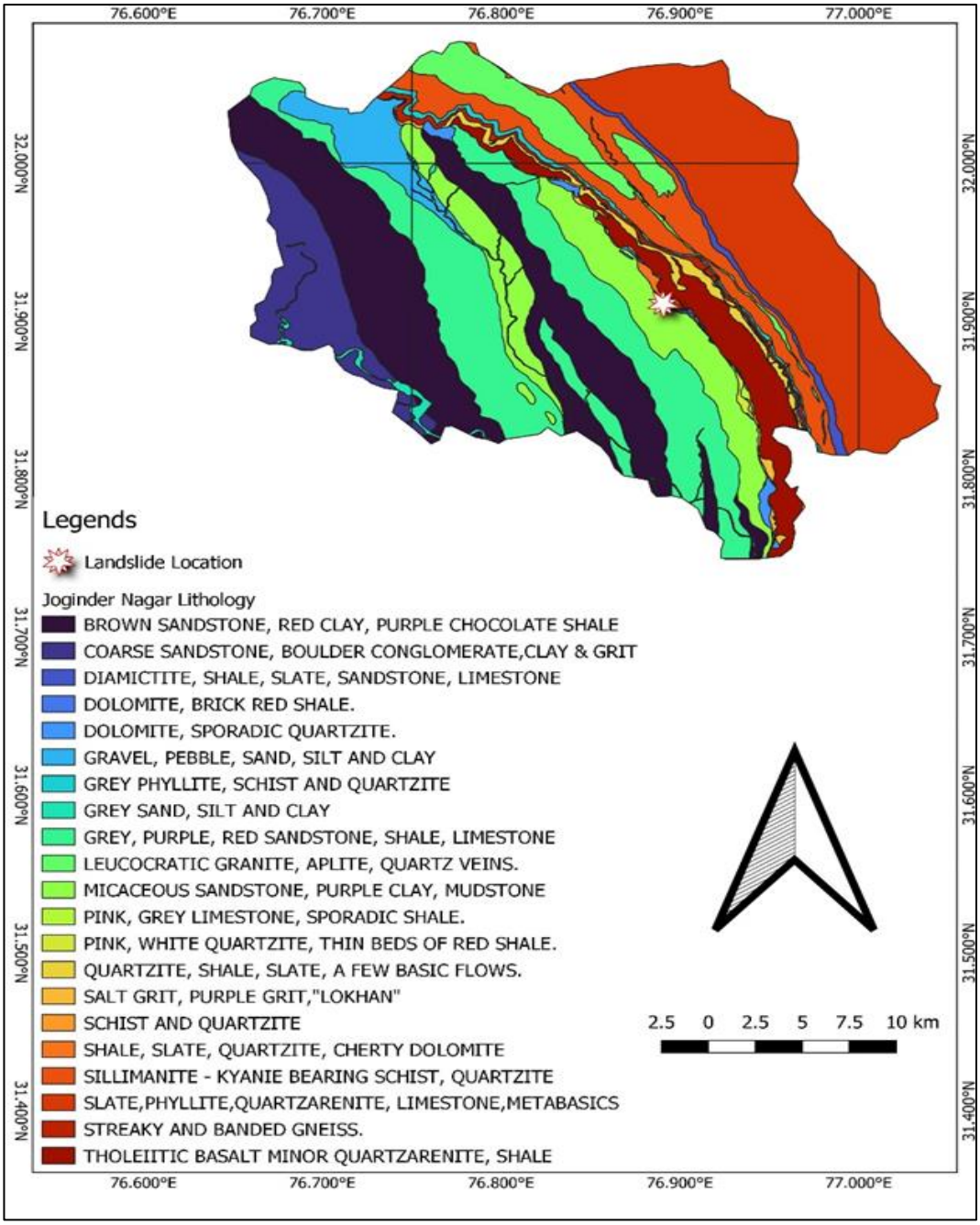

(b)

Fig. 3. 8: (a) A map showing the location of the research location, and (b) Lithological map of study area-II (Kotrupi landslide)

Siwaliks and the Shali Group of rocks, which are mostly made up of dolomites and red brick shale, micaceous sandstone, purple clay, and mudstone, come together at the location where the MBT (Main Boundary Thrust) occurs. The hardness of these rocks is comparatively low; thus, they are affected by much larger deformation and failure due to the thrust activity, making the region particularly more vulnerable to landslides. The satellite image was used to create a map

of the contours. It is possible that parts of the lineaments are neo-tectonically active because of the deep incision of the tributaries, which are located near the main boundary push that separated Siwalik groups from lower Himalayan rocks. The research region contains rocks from the Shali Group and the Dharamshala Group. Phyllite, slate, and phyletic quartzite comprise mainly Shali Group rocks. The upper part of the slide is dominated by pyritic quartzite. Red shale and siltstone make up the Dharamshala Group, separated from the Shali Group by the Shali Thrust. Fig 3.8b shows the lithology of the study area, describing the thrust boundary, joints/fractures, and types of rock and minerals [200].

3.4.2.1 Landslide Event and Mechanism

On Sunday, August 13th, 2017, a major landslide happened in the Mandi district of Himachal Pradesh in the village of Kotrupi (near the Kotrupi Bus Stop). The road connecting Mandi and Pathankot was affected by the landslide. According to reports [201], a section of the slope completely collapsed, burying two Himachal State Transport buses and a few other cars, and at least 47 people were killed in the tragedy. Nearly three hundred meters of the highway have been entirely buried by debris, shutting off contact on this vital corridor. Landslides can be classified into various types, such as rotational slides, falls, lateral spreads, debris flow, and topples [65]. There have been scars from small landslides in the Kotrupi region prior to the actual landslide. Debris flow slides occur when significant soil mass has flowed down a steep channel with debris. The Kotrupi landslide was one of the types of debris failure [201].

3.4.2.2 Description of Study Slope

The area includes part of the catchment basin of the Beas River, and several tributaries joining it. The Uhl river, Rana Khad, Arnodi Khad, and Luni Khad are minor tributaries of the Beas River. Physio-graphically, the area falls in the Lesser Himalayan Zone occupied by the Dhauladhar range in the north-eastern part. The topography is rugged, displaying high ridges and deep valleys. Fig. 3. 9 shows the satellite view of the study area, indicating landslide crown and runout. The slope is moderate to steeply inclined with occasional breaks in slope. The slope is moderate to highly dissected, as evidenced by minor streamlets on either side of the slope. The slope that is affected by the failure has a 45º-50º inclination. The landslide's crown is located at an elevation of 1620 meters. The main landslide is approximately 230 meters tall, with a 210-meter width. The slide is 300 meters long from top to bottom. The landslide's runout distance was 1155 meters [201], [202]. Fig. 3. 10 shows the digital elevation model (DEM) of Joginder

Nagar, indicating the landslide location. The DEM is created using SRTM data with the help of the QGIS tool.

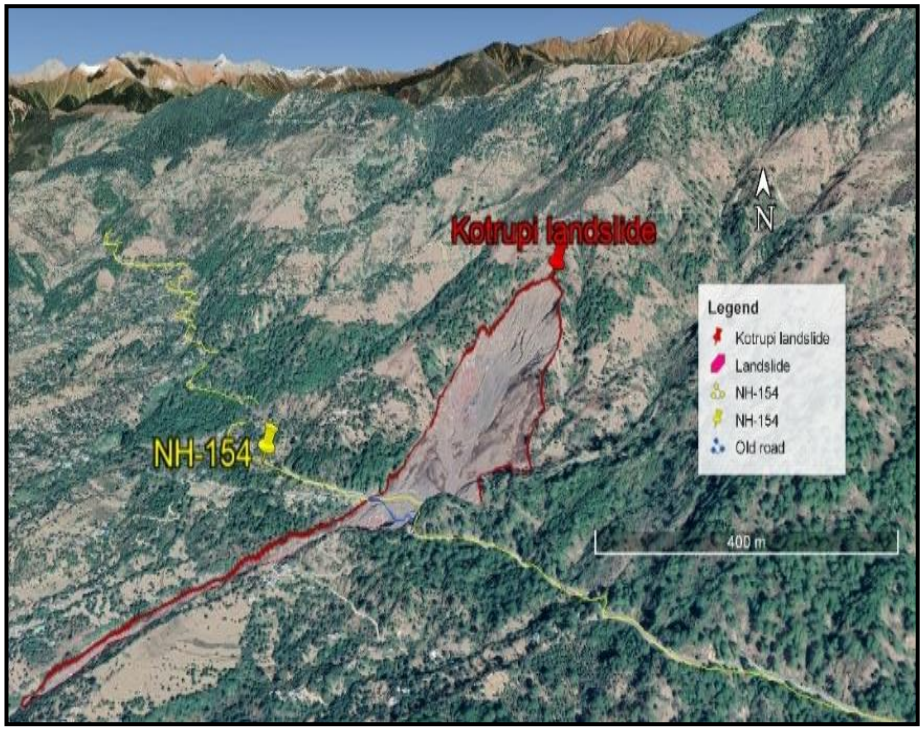

Fig. 3. 9: Satellite view of the study area

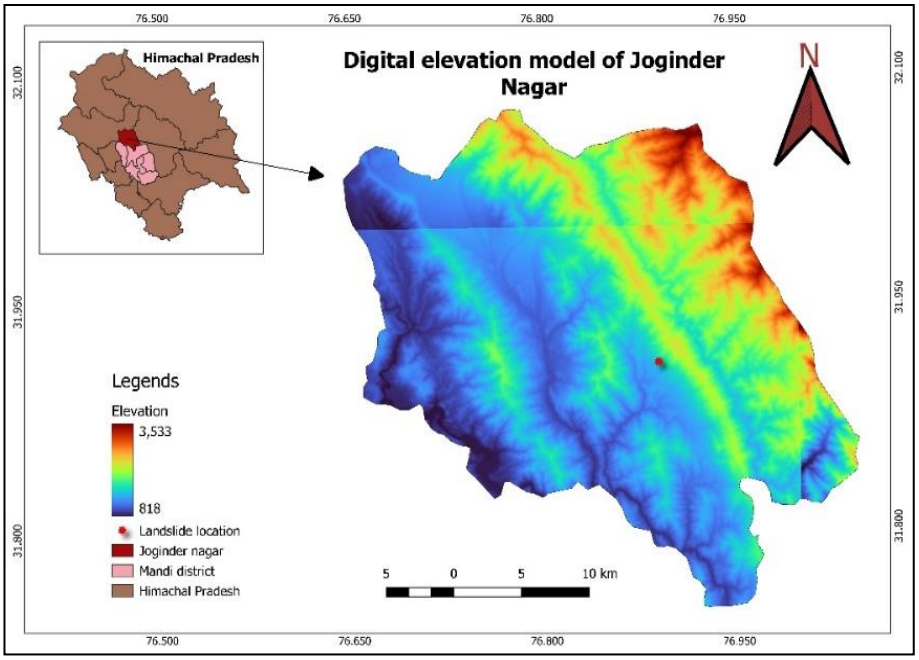

Fig. 3. 10: SRTM-DEM of Joginder Nagar, Mandi, Himachal Pradesh

3.4.2.3 Geotechnical Characteristics of The Slope Material

Slope forming material has been collected during the field survey to find the hydro-mechanical and geotechnical parameter. In order to minimize the differentiability of location in simulation of the material properties and also to stablish the better understanding towards the behaviour of Kotrupi landslide, materials have been collected at various locations throughout the landslide area. Grain size analysis, Atterberg's limits, natural water content, specific gravity, compaction test, and triaxial test were carried out using the disturbed samples that were taken from the site in accordance with the IS code. After performing grain size analysis, the material is categorized by three fractions i.e., sand, silt, and clay. The material collected from the site is classified as a non-uniform gradation because it contains a wide variety of possible particle sizes, including plants, big stones and boulders. Indian standard code IS: 2720 is followed to perform sieve and hydrometer analyses to determine grain size [194] and from the results the values of coefficient of uniformity (C_u) and coefficient of curvature (C_c) have been obtained as 6.2 and 0.67 respectively. The fineness modulus of the material lies in between 5 to 12 percent, thus, the soil is classified as poorly graded sand containing less amount of silt (SP-SM). Provisions of Indian standard code IS:2720(part 5) have been referred to perform Atterberg's limit tests [203]. Atterberg's limit results are summarized in the results section of the paper. IS code: 2720(Part-7) has been referred to perform light compaction tests to determine the dry density of the soil [204]. Based on the geotechnical investigation performed during the field and laboratory testing, the material obtained from Kotrupi landslide location mostly contain poorly graded sand (SP). The landslide's shear strength parameters can be calculated using either the drained or the undrained stresses, the total or the effective stresses [200]. In the case of a debris-type landslide, the unconsolidated-undrained (UU) test has been recommended for soil characterization [205]. Following IS: 2720, part-11, the tests are conducted at 50 kPa, 100 kPa and 200 kPa to determine the shear strength parameters (c_u and ϕ_u) [206].

3.5 Results and Discussions

3.5.1 For Study Area-I (Jhakri Landslide)

3.5.1.1 Laboratory Test Result

The soil taken from the DTU campus (named DTU soil) is mixed with Yamuna sand and clay to meet the 'similar condition' of parent soil. Laboratory investigation has been done to find the properties of soil for the analysis of slope stability. Various physical and engineering properties of the soil are obtained by conducting different tests according to Bureau of Indian

standards 2720 [203], [204], [207]–[211]. Based on the results the soil is classified as silty sand in nature. The natural water content of the soil is 6.7%. The values of the bulk unit weight, dry unit weight, and saturated unit weight of the soil are 14 kN/m^3, 13.3 kN/m^3, and 18.27 kN/m^3, respectively. Permeability coefficient (k) was 0.0023 m/hr, cohesion (c) is 9.5 kPa, and friction angle (φ) is 32°.

3.5.1.2 Physical Modelling Test Result

As the considered slope has recurring landslide history and may undergoes failure in future. The study proves that the slope is unstable under heavy rainfall condition and the area receives high intensity rainfall during monsoonal season thus the threshold for the particular slope has been determined for the critical events seen during the physical model experiment for warning purposes.

The rainfall intensity for the adopted slope area, which is 0.6099 m^2, is fixed to 30 mm/hour simulating a high-intensity rainfall. The effect of rainfall on the slope with 10 mm rainfall depth variation is shown below to visualize the failure pattern of the slope. The images shown in Fig. 3. 11 are clearly describing the progressive stage of a rainfall-induced landslide in the experiment performed. It presents the complete process of occurrence, development, and sliding of the landslide under rainfall. Fig. 3. 11a and b indicate for 30 mm depth of rainfall, water percolation occurs. Due to the high volume of runoff water generated by heavy rain, the effects of weathering and erosion can be seen on the slope face. With continued rainfall of 50 mm depth, the non-uniform vertical settlements can be seen to initial marking. The formation of gullies occurred due to further weathering and erosion by runoff water. This pointed towards the importance of a drainage system to ensure the stability of the slope. The runoff is drained out by the drain hole provided at the toe side of the slope to ensure no ponding condition. This effect is shown in Fig. 3. 11c. With rainfall of 80 mm, water infiltrating through the cracks and the pores leads to the development of positive pore pressure by accumulating water between the soil layers. The friction resistance on the interface gets reduced, resulting in the development of fracture along the sliding surface, causing in a landslide as in Fig. 3. 11d. Further number of physical modellings can be done to get the threshold for various landslides to generate the regional threshold for warning and prediction purposes.

Existing studies have shown that the intermittent, low intensity, and shorter duration rainfall may help in stabilization of slope up to a certain extent by the development of negative pore pressure

between the soil pores [131], [212]. The threshold has been defined for the particular slope as the study is site specific which do not represent the threshold for all the landslides.

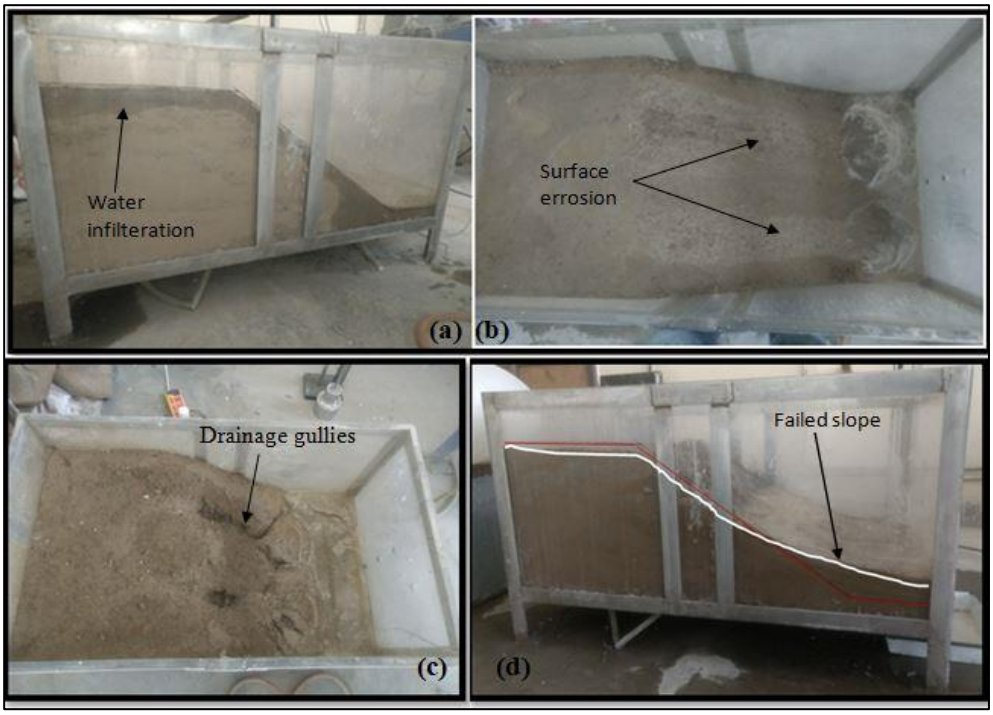

Fig. 3. 11: Effect on the slope for (a, b) 30 mm rainfall, (c) 50 mm rainfall, (d) 80 mm rainfall

3.5.2 For Study Area-II (Kotrupi Landslide)

3.5.2.1 Soil Properties

Dry and saturated unit weights of the soil have been obtained as 16.7 kN/m^3, and 20.3 kN/m^3, respectively. The saturated permeability coefficient (k) is 0.00023 m/sec, cohesion (c) is 21 kPa, and friction angle (φ) is obtained as 31°. The soil in Kotrupi has been primarily made up of very coarse sand as poorly graded sand (SP) in USCS classification. The presence of moisture from the infiltration that the slope has experienced has resulted in the development of apparent cohesion. As a result, the apparent cohesiveness between different soil particles is revealed by the cohesion value that is achieved through triaxial testing. Additionally, the presence of fine soil, as measured by silt content (SM), has been of assistance in the development of the cohesion value. The liquid limit of slope material is found to be 32%. Detailed laboratory experiments have been performed to find out the geotechnical characterization of the Kotrupi landslide as it has been seen that they vary in a wide range, although the results from this study fall in the region which justifies the laboratory results [199], [200], [213], [214].

3.5.2.2 Monitoring Results

The variable rainfall intensity (as shown in Fig. 3. 12) is attained by controlling the valve attached to the inlet of rainfall generator and the input rainfall intensity. It depicts the input variation of rainfall intensity along with accumulated rainfall depth with respect to time. Variable interval is also introduced for next successive rainfalls to make water infiltrate properly.

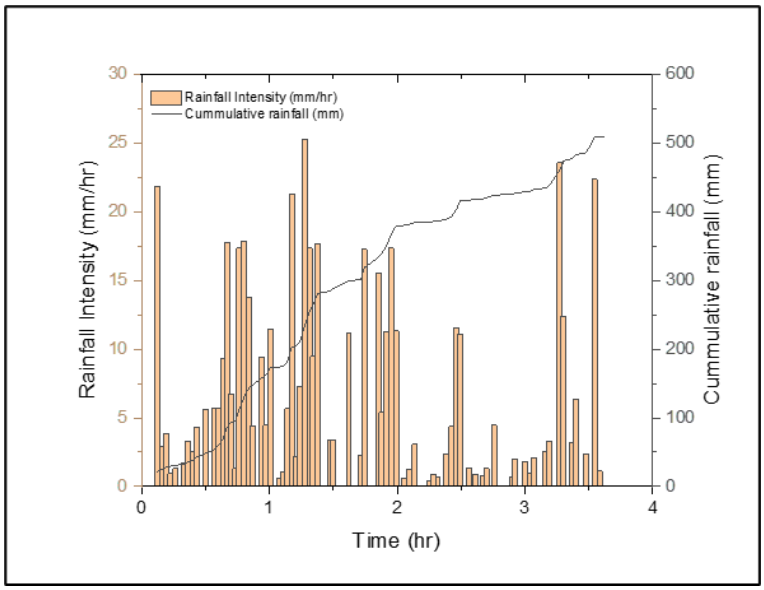

Fig. 3. 12: Input rainfall parameter

The purpose of the physical slope model is to analyse the impact of rainfall on slope stability and to assess the operational effectiveness of the newly devised landslide monitoring system. To examine the impact of pre-monsoonal rainfall, a simulated antecedent rainfall of 10 mm is enacted at an intensity of 1 mm/hr. The outcomes presented in Fig. 3. 13a indicate the occurrence of substantial deep percolation. This finding supports the notion that extended periods of low-intensity rainfall can lead to deep saturation, potentially culminating in a landslide with a deep-seated nature. This may result in compaction and consolidation of soil near the junction point of wet and dry soil, which in turn decreases the permeability. Fig. 3. 13b shows the generation of small cracks on top of the slope which is observed after one week time. Fig. 3. 13c shows the effect after four weeks, and wide cracks can be seen on top as well as the slope section that may be generated due to the occurrence of soil shrinkage after wetting and drying. The duration of generated cracks may differ according to the temperature and humidity of the surrounding environment. Further rainfall on the slope results in faster and deeper percolation of water through the cracks, which helps in creating the fluidization zone between the dense and loose soil layer during the monsoonal season. The tilt sensors have been mounted on top of a steel

scale. At the bottom, a soil moisture sensor is attached and placed into the soil after creating a borehole using a drill machine (Fig. 3. 13d).

The rainfall has been simulated by a self-developed rainfall generator equipped with a flow sensor and a microcontroller to record the flow. Fig. 3. 14 shows the variation of water content against the input rainfall. As the water content increases or varies according to the input rainfall, the variation in the water content affects the slope stability; thus, the variation in the tilting angle can be seen in Fig. 3. 15. As the slope is much more likely to fail in the y-direction due to gravity action, the angle deviation is much more significant in the y-direction. There is also some deviation detected in the x-direction due to some rotation and settlement.

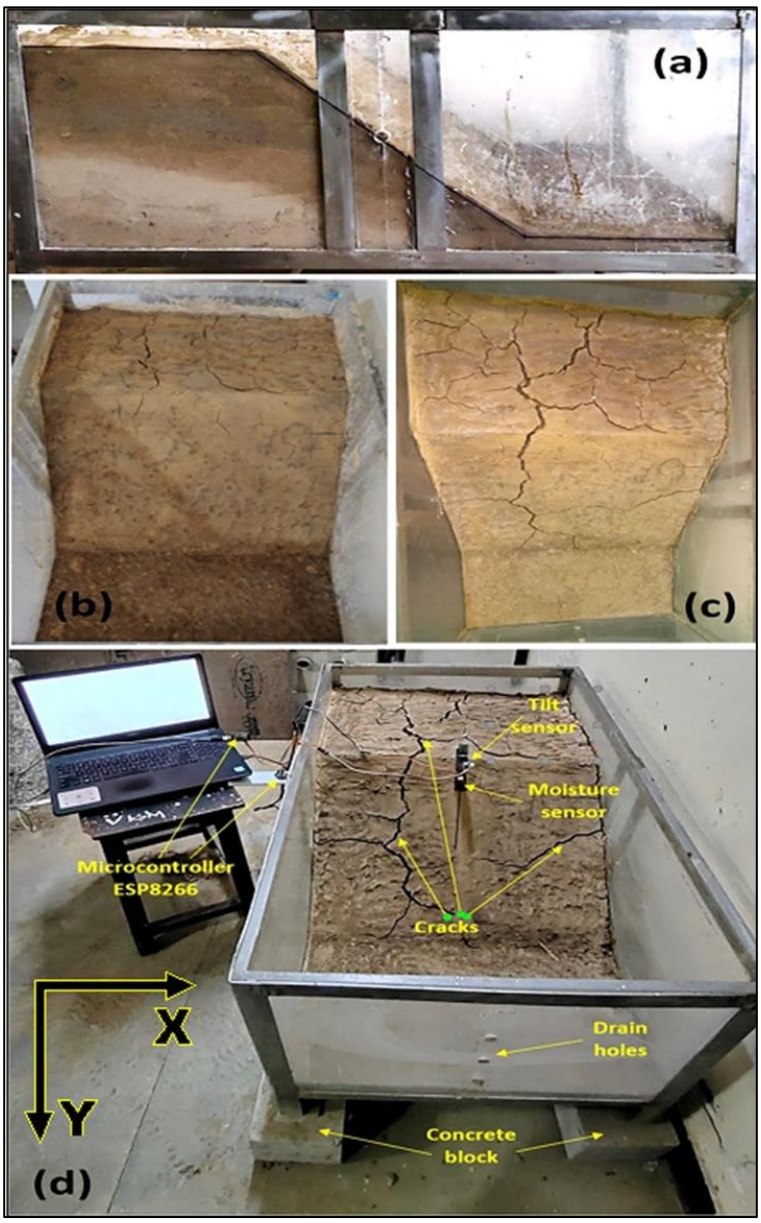

Fig. 3. 13: Physical model setup (a) Percolation of water, (b) Visible small cracks, (c) Formation of larger cracks, and (d) Placement of sensors

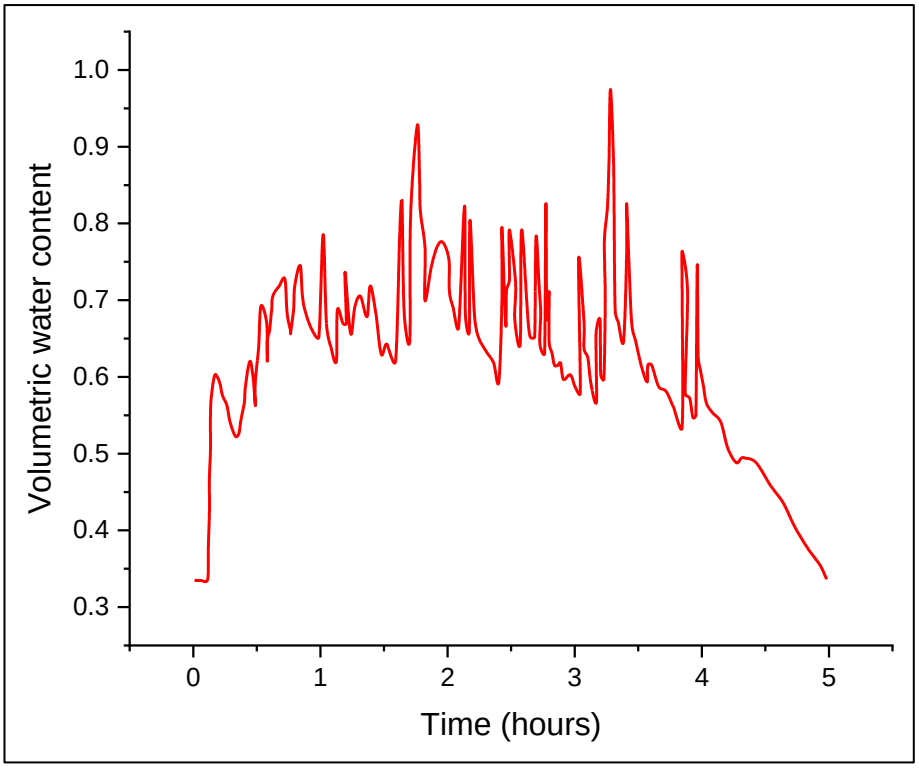

Fig. 3. 14: Output volumetric water content

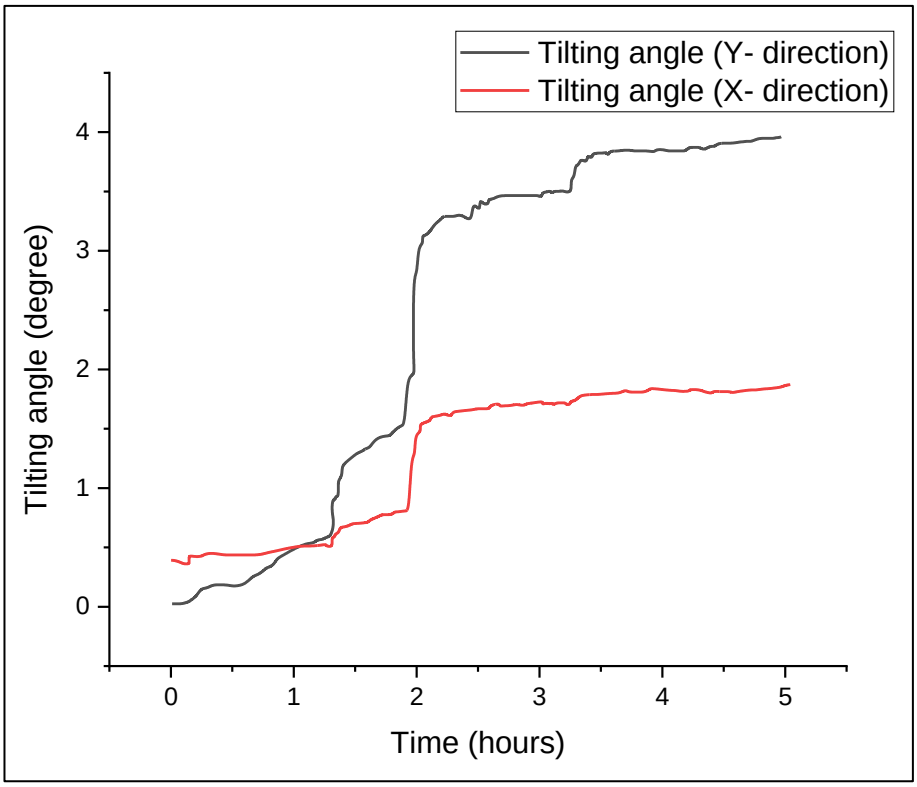

Fig. 3. 15: Variation of angle in X- and Y- direction

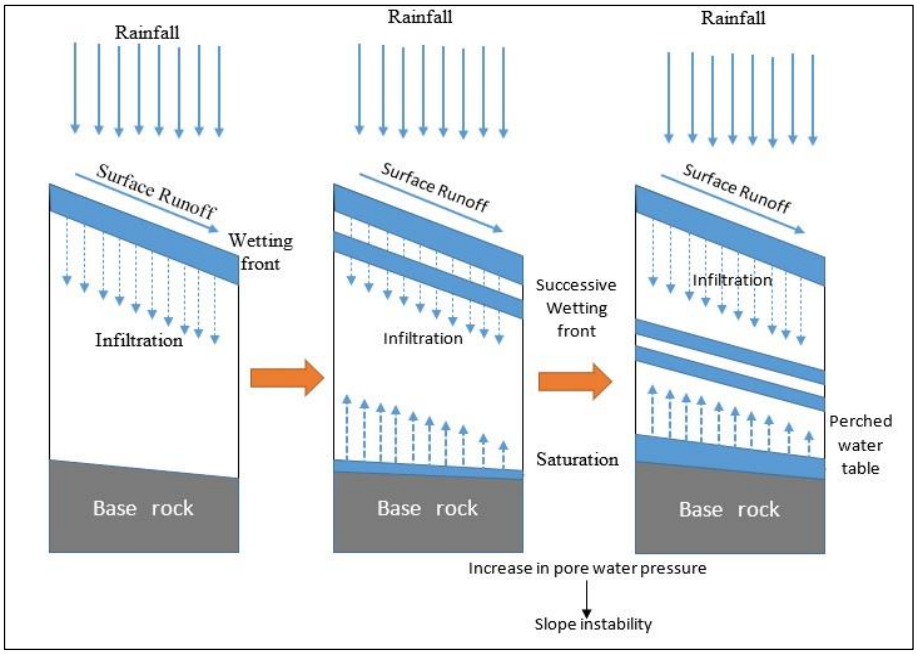

Fig. 3. 16: A sequential schematic of landslide initiation

The Fig. 3. 16 depicts the progression of landslide initiation in a step-by-step manner. In this case, the rainwater percolation results in the saturation of the interface zone, resulting in the development of a perched water table and the subsequent appearance of successive wetting fronts. Positive pore-water pressure results in a decreased shear strength and effective stress of the soil. An increase in rainfall causes the soil layers to penetrate deep into one another, causing the fluid zone to form near the surface, decreasing shear strength and resulting in landslides.

In previous studies, only a few researchers studied rainfall-induced slope failure mechanisms using the physical modelling method. Li et al. (2016) [42] concluded that the physical modelling method is very efficient to visualize the rainfall-induced landslides for a specific study area by performing the laboratory modelling test. It is tough to analyse it only by the mathematical or numerical model. Therefore, it highlights the need to perform numerical analysis along with physical modelling to compare the results for validation purposes. So, to study the failure mechanism of a slope in the Himalayan region, a self-designed experimental platform has been developed to perform the physical model simulating the phenomenon of rainfall-induced landslides. The experimental platform includes an artificial rainfall generator, a loading mechanism, and a frame type box for modelling slope. The slope material has been made in the laboratory by ‘similar material’ theory as it was not possible to take that much material from the site to the laboratory. The intensity for the rainfall generator was fixed to 30 mm/hr. Each time, 10 mm rainfall is delivered to the slope to minimize the error induced while calculating the

threshold for intensity duration relationship. The threshold has been determined as the total depth of rainfall delivered to the model to cause the failure of the slope under consideration. The observations of the physical model experiment using ‘semi-similar’ material revealed that it is notably a highly efficient technique to visualize the pore-water penetration process in a soil mass. The sliding mechanisms of the slope have been studied, indicating that rainfall is one of the key factors triggering the slope failure and the obtained results helps understand the mechanism of slope failure.

Based on the observations during the physical modelling test and obtained results it has been noted that the rapid sliding failure occurred at 80 mm rainfall depth, making it the threshold value for the studied slope. However, weathering failure starts at 30 mm, which can be considered as the warning threshold. As heavy rainfall occurs, water infiltrates into the soil layer and creates fluidization zones between the slopes, increasing pore water pressure. The soil layer within the lower part will become fully saturated first because the thickness of the soil layer at the toe side is significantly less. As the hydraulic conductivity (k) of the soil is significantly less than rainfall intensity, most of the rainfall converts into surface runoff, which leads to the erosion of the slope's surface. This stage starts at 30 mm rainfall depth. Further, an increase in rainfall depth, i.e., at 50 mm rainfall depth, soil surface erosion increases rapidly, and formation of gullies can be seen on the slope, considered as the initiation of slope failure, which can be regarded as extreme warning threshold and the restriction must be applied for any movement nearby the slope. Again, continuous increase in rainfall depth vigorous erosion may occur, which results in removal of the soil in the lower part of the slope, which provides the frictional resistance to the slope stability. Further, the water level between the layers keeps increasing due to the continuous rainfall and infiltration, i.e., the pore water pressure in the soil keeps rising. After reaching a critical stage, sliding failure occurs. When the pore-water pressure crosses the limiting value, a shallow landslide is triggered by heavy rainfall. This stage occurred at 80 mm rainfall depth, and the safety factor is found significantly less.

Many researchers have worked around the globe in order to test the feasibility of tilt based monitoring system [52], [54], [69]. The present study validates the effective monitoring of rainfall induced landslide using tilt sensor. The physical modelling method is used to simulate the soil slope to study the effect of pre- and post- monsoonal rainfall on slope and also to test the monitoring sensor in realistic environment [42], [215], [216]. Fig. 3. 13 also shows that wetting and drying can lead to formation of cracks during pre-monsoonal rainfall which can cause the water to infiltrate deep and may cause the failure [44]. Uchimura et al. (2010) [53] stated that the

change in water content is a better representation than just the water content for slope monitoring and as Fig. 3. 14 depicts that the variation in the volumetric water content is vigorous, which may cause the slope to be unstable. Fig. 3. 15 also depicts that the sudden variation in tilt angle is observed when the input precipitation continues for around two hours which validates that the slope failure gets triggered due the heavy rainfall. It also proves the unpredictable nature of the landslide failure which require continuous monitoring for prediction and early warning measures. This study also proved the possible failure mechanism occurring in rainfall induced landslide (Fig. 3. 16) [216].

3.6 Summary

In this study, an inventive and cost-effective slope monitoring system that incorporates MEMS-based tilt and moisture sensors were developed. A block shear test model has been set-up to check the effectiveness and feasibility of the developed system. A physical modelling methodology has been adopted to study the failure mechanism.

1. In this study, two landslide sites, Jhakri (N31º29’08”, E77º41’43”) in Shimla district and Kotrupi (N31º54‟37.60, E76º53”26.30) in the Mandi district of Himachal Pradesh, in northern India were selected to study the failure mechanism.
2. Hydro-mechanical parameters were calculated, and a semi-similar material physical model test was conducted to analyse the mechanisms of sliding. In order to simulate the desired rainfall, a self-developed artificial rainfall generator is used.
3. The tilt and volumetric water content sensors employed in the system provide accurate and precise measurements. The tilt sensor records even the slightest changes in the slope angle with a precision of 0.01 degree, enabling early detection of slope movement. Additionally, the volumetric water content sensor can detect percentage variations with a precision of 1 percent aiding in the identification of critical conditions that could lead to landslides.

CHAPTER 4

NUMERICAL MODELLING

4.1 General

A numerical model is a mathematical simulation of a real physical process. Numerical modelling is purely mathematical and in this sense is very different than scaled physical modelling in the laboratory or full-scaled field modelling.

Numerical analysis has revolutionized the field of geotechnical engineering by providing powerful tools to assess the stability of slopes, a critical aspect in infrastructure and construction projects. Slopes are prevalent features in natural landscapes and human-made structures, making their stability crucial for safety and sustainability. Traditional methods often involve simplified assumptions that might not capture the complexities of real-world scenarios. Numerical analysis addresses this limitation by employing computational techniques to model and simulate the intricate behaviours of slopes under various conditions. The process involves discretizing the slope into smaller elements or grids, employing mathematical equations to represent the governing physical phenomena such as soil mechanics, groundwater flow, and structural interactions. These equations are then solved iteratively using computers, enabling a comprehensive understanding of slope behaviour, failure mechanisms, and potential risks.

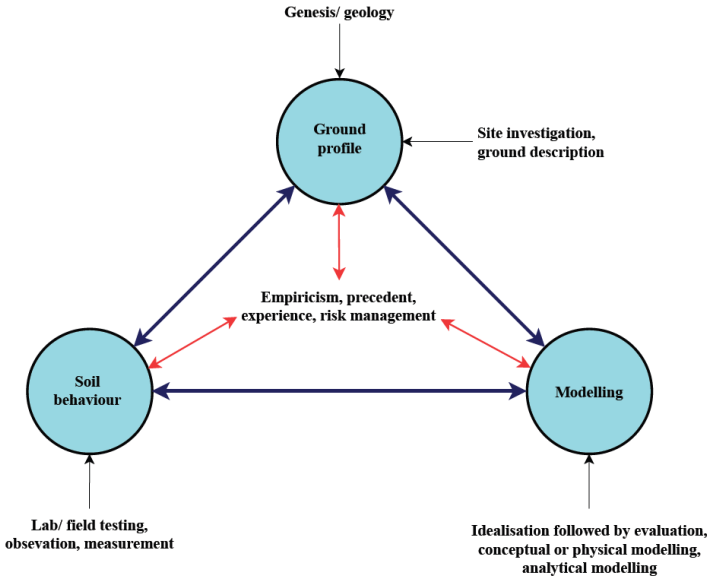

Fig. 4. 1: Framework for numerical modelling recognized as the Burland triangle

Burland (2012) [217] proposed a conceptual framework for geotechnical engineering, comprising three core elements: the ground profile, soil behaviour, and modelling. Fig. 4. 1 depicts these elements as the vertices of a triangle, and is recognized as the Burland triangle. The aspect of soil behaviour comprises a range of assessment techniques encompassing laboratory experiments, in-situ evaluations, and field measurements. On the other hand, the ground profile element predominantly revolves around site characterization, which entails the comprehensive delineation and depiction of the prevailing site conditions. Notably, modelling in geotechnical engineering can take on various forms, including conceptual, analytical, and physical representations. As Burland observed, these diverse modelling approaches offer valuable insights into the behaviour of geotechnical systems. Nevertheless, in the contemporary context, due to the remarkable advancements in computing capabilities and the availability of sophisticated software tools, the term "modelling" has predominantly come to signify numerical modelling. Acknowledging this shift towards numerical modelling as the primary mode of modelling, one can discern its pivotal role in geotechnical engineering, as exemplified by the Burland triangle. This triangle emphasises the utmost significance of numerical modelling in understanding and analysing geotechnical phenomena, highlighting its status as a cornerstone in modern geotechnical practices.

Advantages of Numerical Modelling Over Physical Modelling:

- **Rapid Setup:** Numerical models can be established quickly compared to the time-consuming construction of physical models. While physical models may take up to months to create, numerical models can be formulated within minutes, hours, or days.
- **Versatility:** Numerical models offer flexibility in exploring diverse scenarios, unlike physical models that are typically constrained to a specific set of conditions.
- **Gravity Handling:** Numerical models effortlessly account for gravity, a challenge in physical models where gravity scaling is impossible without specialized equipment like centrifuges.
- **Safety:** Numerical modelling eliminates the risk of physical harm, unlike physical modelling which involves potentially hazardous heavy equipment, necessitating heightened safety concerns.

- **Location-Specific Data:** Numerical modelling provides data and insights throughout the entire cross-section, whereas physical modelling yields visual responses and data only at discrete instrumented points.

- **Boundary Condition Adaptability:** Numerical models can accommodate various boundary conditions, while physical models often face limitations in the types of boundary conditions they can simulate.

In this particular numerical examination, a two-dimensional method has been employed to analyse the precipitation-induced landslide's triggering to validate the results. Creating an accurate representation of the actual topographical features of the failed slope proved to be a formidable challenge. Therefore, in order to arrive at a definitive and well-informed conclusion, a simplification has been made by assuming a linear or straight slope. This approach aligns with the findings of numerous prior research studies, which have also utilized this simplification to gain valuable insights [42], [132], [218], [219]. Several key assumptions have been considered to adopt a two-dimensional methodology for arriving at an unequivocal conclusion, as documented in the GEO-SLOPE International Ltd. report of 2012 [220]. The first underlying assumption suggests that slope failure occurs primarily within a single geological layer, attributing this behaviour to the relatively smaller size and high compaction of the soil particles within the slope. This assertion lays the groundwork for the analytical framework used to understand and evaluate the stability of such geological formations. The failure pattern is circular. Maximum failure depth can only be extending to the soil depth. The bottom-most layer underneath the soil mass is assumed to be impermeable; that is, there will be no percolation possible through the soil layer to bedrock. The hydrological and mechanical parameters of soil are the same as the failed soil for saturated and unsaturated cases and the maximum rate of water percolation is equal to soil permeability.

Slope stability analysis has been widely used to deal with complex calculation, investigation, prototype modelling, testing, design, and stability analysis of natural, artificial rock, and soil slopes. The researcher and design engineer typically use the slope stability analysis to assess the safe design of artificial or natural slopes. Slope stability is the resistance of the inclined surface between the layers of soil to failure by sliding or collapsing. The main objectives of slope stability analysis are finding the critical failure section, analysing potential failure mechanisms, and designing slopes considering safety, reliability, and economics [44], [221].

In this study, the soil slope is analysed using GeoStudio 2020 software. First, the unsaturated slope is analysed for its stability using Slope/W module, which is based on the limit equilibrium method, and then the stability of the slope is analysed after the rainfall. The rainfall modelling has been done in Seep/W module based on the finite element method, and then the results obtained from it have been used in Slope/W module to check the stability of saturated slope after the rainfall using the Morgenstern and Price method [222].

4.2 Stability Analysis

4.2.1 General

Numerous solution approaches have evolved for the method of slices throughout time. In essence, they share strong resemblances. Variations among these methods arise from specific factors: the inclusion and fulfilment of static equations, incorporation of interslice forces, and the presumed connection between interslice shear and normal forces. An illustrative depiction in Fig. 4. 2 shows a standard representation of a divided sliding mass and the potential forces exerted on each slice. These forces encompass both normal and shear components and are distributed across the slice's base and sides.

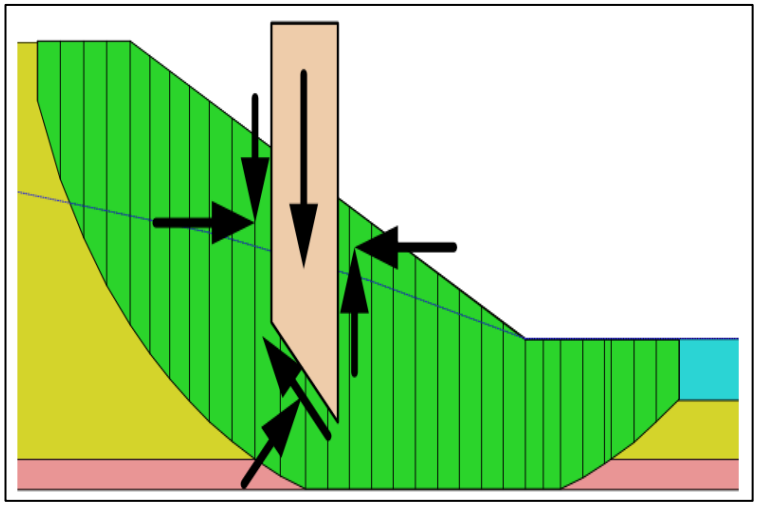

Fig. 4. 2: Slice discretization and slice forces in a sliding mass

Table 4. 1 provides an inventory of the techniques accessible within Slope/W module, along with an indication of the static equilibrium equations upheld by each method. Meanwhile, it also furnishes a condensed overview of the interslice forces incorporated, accompanied by the presumed correlations between interslice shear and normal forces.

Table 4. 1: Equations of statics and interslice force characteristics

Technique	Force Equilibrium	Moment Equilibrium	Interslice Normal (E)	Interslice Shear (X)
Fellenius/Ordinary	×	✓	×	×
Simplified Bishop	×	✓	✓	×
simplified Janbu's	✓	×	✓	×
Spencer	✓	✓	✓	✓
Morgenstern- Price	✓	✓	✓	✓
Corps of Engineers–1	✓	×	✓	✓
Corps of Engineers–2	✓	×	✓	✓
Janbu Generalized	✓	✓	✓	✓
Sarma–vertical slices	✓	✓	✓	✓

4.2.2 Limit Equilibrium Method

A general limit equilibrium (GLE) formulation was developed by Fredlund at the University of Saskatchewan in the 1970's [223], [224]. This formulation encompasses the key elements of all the methods listed in Table 4. 1. The GLE formulation incorporates a unique approach founded on a pair of safety factor equations, which in turn provide flexibility in accommodating various interslice shear-normal force scenarios. One of these equations calculates the factor of safety concerning the equilibrium of moments (referred to as F_m), whereas the second equation pertains to the factor of safety concerning the equilibrium of horizontal forces (referred to as F_f). This dual-factor approach empowers the GLE formulation to comprehensively assess stability across a spectrum of load and geometric conditions, making it a versatile tool in geotechnical engineering analyses. The idea of using two factor of safety equations was actually first published by Spencer (1967) [225].

The interslice shear forces in the GLE formulation are handled with an equation proposed by Morgenstern and Price (1965) [226]. The equation where, X is interslice shear force; E is the interslice normal force; λ is the percentage of the function used; f(x) is a function.

$$X = E\,\lambda f(x) \qquad \text{Eq. 4. 1}$$

The limit equilibrium method of slices is a widely employed technique in geotechnical engineering for assessing the stability of soil slopes. It involves the application of iterative methods to solve the nonlinear factor of safety equations. Specifically, in the Morgenstern-Price variation of this method, additional iterations are necessary to determine the slice forces that lead to equal values of the factor of safety (F_m) and factor of safety (F_f) for each individual slice. These iterative processes are essential to fulfil the following two critical conditions:

- **Force equilibrium for each slice:** This condition ensures that the forces acting on each slice must maintain the force equilibrium implying that the forces must be balanced, preventing the slice from experiencing net translation or rotation.
- **Uniform factor of safety for each slice:** This condition aims to achieve uniformity in the safety factor across all slices, which is of utmost concern because a variable factor of safety could lead to localized failure within the slope.

It is crucial to note that the forces calculated through these iterations might not accurately represent the actual in-situ slope conditions. Instead, these are forces that satisfy the required two condition of each slice. This means that the interslice and forces acting along the slip surface may not reflect the real-world situation. Consequently, determining a realistic thrust line for the interslice shear-normal resultant can be challenging. In some instances, the forces calculated for individual slices may result in a line of thrust that lies outside the boundaries of the slice. This clearly indicates that the derived slice forces do not always correspond to the actual physical forces at play in the slope. However, there is a silver lining to this complexity. Although the local slice forces may not precisely represent in-situ conditions, the global safety factor remains realistic. This is because when all the mobilized driving forces and the base resisting shear forces are integrated, the local irregularities are effectively smoothened out. This results in a global factor of safety that accurately represents the stability of the entire sliding mass, making it an acceptable and reliable indicator of the slope's overall stability.

4.2.3 Morgenstern-Price Method

Morgenstern and Price (1965) [226] adopted an approach akin to the Spencer method, but with a slight variation that set it apart - the incorporation of diverse user-defined interslice force functions. This innovative modification allows for a greater degree of customization and adaptability, empowering users to tailor their approach according to their specific requirements. The Morgenstern-Price method allows users to define custom interslice functions for their analyses. The various functions at their disposal are the constant, half-sine, clipped-sine, trapezoidal, and data-point specified functions. It is worth noting that the constant and half-sine functions stand out as the most frequently employed choices in practice. Interestingly, when a Morgenstern-Price analysis uses the constant function, it effectively parallels a Spencer analysis, emphasizing the relevance of these two approaches. By default, the Slope/W software module employs the half-sine function as the interslice function for the Morgenstern-Price method. The selection of the half-sine function is based on its characteristic of concentrating interslice shear forces toward the central region of the sliding mass, effectively reducing interslice shear effects at the crest and the toe areas. This default preference is a testament to its historical effectiveness in various geotechnical scenarios and is a rational choice for initial analysis configurations. The limit equilibrium factor of safety equation with respect to moment equilibrium is:

$$F_m = \frac{\sum (c'\beta R + (N-u\,\beta)R\tan\emptyset')}{\sum Wx - \sum Nf \pm \sum Dd} \qquad \text{Eq. 4. 2}$$

The limit equilibrium factor of safety equation with respect to horizontal force equilibrium is:

$$F_f = \frac{\sum (c'\beta\cos\alpha + (N-u\,\beta)\tan\emptyset'\cos\alpha)}{\sum N\sin\alpha - \sum D\cos\omega} \qquad \text{Eq. 4. 3}$$

Where, "c' is effective cohesion; φ' is effective angle of friction; u is pore-water pressure; N is slice base normal force; W is slice weight; D is concentrated point load; α is inclination of slice base; β, R, x, f, d, ω are geometric parameters."

4.2.4 Mohr-Coulomb Material Strength Theory

Slope/W module in GeoStudio software, which uses the limit equilibrium method, has been used to examine the slope's stability. Several methods exist for calculating the slope's safety, but the Morgenstern-Price method has been used in this study. Due to its ability to maintain both force and moment equilibrium, this approach is frequently employed in engineering applications. A relationship between interslice shear (X/E) and normal force (E) is established by the interslice

force function [f(x)], where f(x) is the scaling factor. As it reduces interslice shear at the toe and crest and concentrates shear force in the middle of the sliding mass, the half-sine interslice force function has been used in the current study. The slope stability analysis is performed using a modified Mohr-coulomb soil strength method that also takes into account the variation in shear strength due to matric suction in the soil [227]. The governing equation for this model is given below.

$$\tau = c' + (\sigma_n - u_a)\tan\varphi' + (u_a - u_w)\tan\varphi^b \quad \text{Eq. 4. 4}$$

Where, "τ denotes the soil's shear strength, *c'* denoting the effective value of cohesion strength, $(\sigma_n - u_a)$ denotes the net effective value of normal stress, σ_n denotes the total stress; $(u_a - u_w)$ denotes negative pore water pressure also known as matric suction, u_w denotes the value of pore-water pressure, φ'denotes the friction angle of soil, and φ^b denotes angle between the rate at which shear strength increases in relation to the negative pressure."

4.3 Seepage Modelling

4.3.1 General

Flow rate is a crucial factor for measuring seepage losses from reservoirs and identifying potential water sources for various uses. The pressure of pore-water related to groundwater movement holds particular significance in geotechnical engineering. Pore-water pressure, regardless of whether it is positive or negative, greatly influences soil stress conditions. This, in turn, directly impacts shear strength and soil volume changes. In recent decades, research has emphasized the need of moisture flow dynamics in unsaturated surface soils, especially concerning soil cover design.

Traditionally, the groundwater flow analyses cantered on saturated soil conditions, typically categorized as confined or unconfined scenarios. For instance, confined flow issues were relevant beneath structures, while unconfined flow was observed in homogeneous embankments. Analysing unconfined flow problems posed challenges due to determining the phreatic surface's location, which marks the shift from positive to negative pore-water pressures. Neglecting any flow above the phreatic line was common. Yet, ignoring water movement in unsaturated soils above this surface is no longer acceptable. Neglecting it limits the analyses results and disregards a vital aspect of moisture flow.

Considering unsaturated soil movement above the phreatic surface is pivotal. The associated modelling facilitates incorporation of unsaturated soil flow conditions into numerical models, enabling a broader range of seepage problems to be tackled. Energy differences relates to the total water head, including elevation and pressure head (pore-water pressure) and drive water flow. The term “seepage” often refers to flow primarily influenced by gravity, like reservoir seepage to downstream areas. In other scenarios, like consolidation, excess pore-water pressures from external loading are the main driving force.

The formulation used for seepage analysis also applies to dissipating excess pore-water pressures. Modelling water flow in soil can be intricate due to soil's natural heterogeneity, changing boundary conditions, and variable permeability. When soil becomes unsaturated, permeability becomes a function of negative pore-water pressure, leading to nonlinear problems requiring iterative techniques for computation.

These complexities make numerical analysis essential for seepage problems analysis. Understanding these intricacies aids in comprehending and addressing various seepage scenarios in geotechnical engineering.

4.3.2 Geometry and Meshing

Finite element numerical methods are structured around the idea of breaking down a continuous material into smaller units, characterizing the behaviour of these units, and then integrating their behaviour to represent the entirety. This division process is called discretization or meshing, with the units referred to as finite elements.

Within the GeoStudio software, defining the model's geometry precedes the crucial discretization step. Notably, advancements in automatic mesh generation algorithms have reached a stage where they can now offer a highly functional default discretization, demanding only minimal input from the user. Nevertheless, exercising caution reviewing this default mesh is advisable, as the software allows for convenient adjustments. Users have the flexibility to make modifications by simply altering a single global element size, adjusting the divisions of the mesh along geometry lines, or specifying edge sizes for individual mesh elements. This allows users with the capacity to fine-tune the discretization to suit their specific modelling requirements, ultimately ensuring a more accurate and customized simulation experience.

4.3.3 Material Models and Properties

In this segment, the diverse soil hydraulic attributes essential for solving the seepage partial differential equation can be elucidated. Gaining a comprehensive grasp of the significance and impact of these soil properties on outcome characteristics is crucial. This underscores the significance of distinct parameters and the consequences of insufficiently defining them. Accurate soil property specification plays a pivotal role in achieving a proficient solution to the finite element equations.

4.3.3.1 Soil-Water Characteristic Curve (SWCC) Function

In unsaturated soils, the amount of water held within voids varies with the matric suction, defined as the disparity between air (U_a) and water (U_w) pressures. Considering the inherent temporal and spatial differences, it becomes imperative to establish a comprehensive function that elucidates the dynamic changes in soil water content across diverse pressure conditions. This function should encapsulate the intricate relationships between soil moisture and the multilayered influences exerted by time and geographical factors. The volumetric water content function explains how much water the soil can hold under changing matric pressure. It specifies the proportion or volume of voids that remain water-saturated during drainage. The function's crucial attributes include the air-entry value (AEV), depicting the onset of significant drainage due to negative pore-water pressure, and the slope in both positive and negative pressure domains (m_w), alongside the residual water content (S_r).

The AEV hinges on pore size and distribution, influencing the drainage threshold. Representing the function's slope is pivotal for seepage analysis, accounting for water release via void drainage and soil compression-induced water displacement. In the positive pressure realm, m_w equates to m_v, the coefficient of volume compressibility. The negative pressure slope mirrors the rate of water volume change within the soil as pressure varies, spanning AEV to residual water content.

Moreover, it is worth noting that the residual volumetric water content serves as a critical indicator that delineates the stage at which any additional decrease in negative pore-water pressure has minimal impact on the soil's water content. This pivotal point can be quantified in terms of saturation, calculated by dividing the residual volumetric water content by the soil's porosity. In other words, the degree of saturation reflects the proportion of pore space within the soil structure still occupied by water even after negative pore-water pressure has reached a certain threshold. This concept is vital in geotechnical engineering and hydrology as it provides insights into the water retention characteristics of soils and their behaviour under varying environmental

conditions. While Seep/W excludes evaporative drying, Vadose/W incorporates it through coupled heat, mass, and vapor flow considerations.

Obtaining a direct measurement of volumetric water content function in a laboratory is not overly complex but does demand time and access to a suitable geotechnical facility. Nevertheless, deriving a grain-size distribution curve is a common practice and can be efficiently carried out, proving both cost-effective and rapid. In transient analysis, volumetric water content function is a vital input parameter. It makes sense to estimate this data using either a closed-form solution requiring user-defined curve-fitting parameters or a predictive strategy using a measured grain-size distribution curve, given the probable challenges involved in obtaining it. Within Seep/W, four techniques exist for constructing a volumetric water content function, discussed in the forthcoming paragraphs. These encompass predictive methods grounded in grain size, employing pre-built software functions, and utilizing closed-form equations based on established curve fit parameters.

5.3.3.1.1 Estimation Method-I (Grain Size-Modified Kovacs)

Aubertin et al. (2003) [228] introduced a method for predicting the volumetric water content function approach with tailored modifications to suit hard-rock mine tailings and clay type soils. The method proposed estimates the volumetric water content function using fundamental material properties, serving as a valuable tool for preliminary analysis. However, it is important to exercise caution, particularly for clay materials, and rely on measured material properties for final design rather than estimates.

The process begins by establishing a degree of saturation function, subsequently transformed into a volumetric water content function. This is achieved by defining two key components of the degree of saturation. The first component relates to water storage through capillary forces at relatively minor negative pore-water pressures. The second component influences volumetric water content at significant negative pressures, primarily influenced by adhesion. Both components derive from negative pore-water pressure and material properties like particle size, shape, and porosity. The degree of saturation, based on capillary and adhesive aspects, is as follows:

$$S_r = \frac{\theta_w}{n} = S_c + S_a^* (1 - S_c) \qquad \text{Eq. 4. 5}$$

$$S_a^* = (1-S_a)+1 \qquad \text{Eq. 4. 1}$$

Where, "S_r is the degree of saturation; θ_w is the volumetric water content; n is the porosity; S_c is the degree of saturation due to capillary forces, and S_a^* is the bounded degree of saturation due to adhesion (S_a)."

5.3.3.1.2 Estimation Method-II (Sample Functions)

GeoStudio software offers a wide range of predefined water content functions for various soil types. While these sample functions facilitate rapid model setup, it is the user's responsibility to define the saturated and residual water content based on the field insights. These functions serve to expedite testing, enable swift function adjustments, gauge result sensitivity to function shape, and prompt consideration of acquiring more precise data if necessary. Historically, genuine functions were often adopted as definitive design material properties without due consideration of their applicability. This approach falls short of modelling practice as shown in Fig. 4. 3.

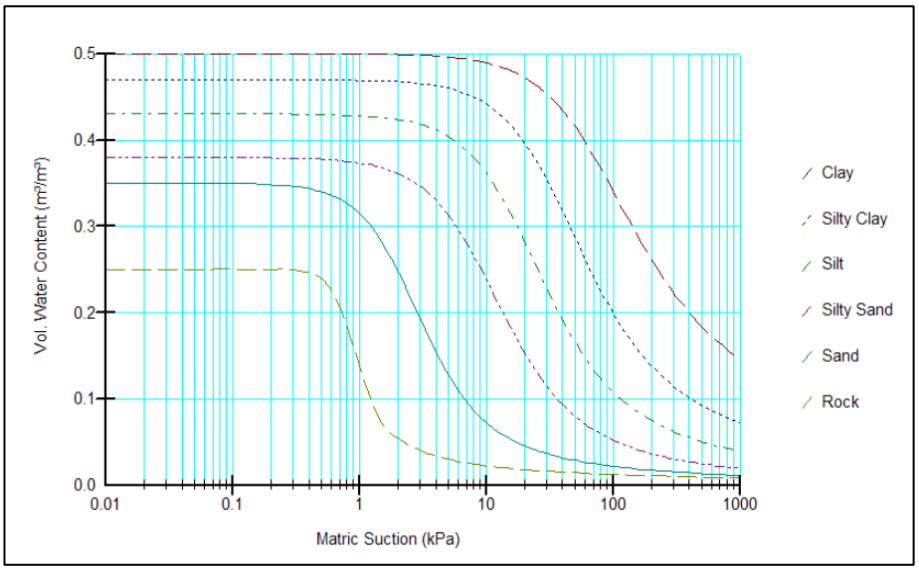

Fig. 4. 3: Sample functions [227]

5.3.3.1.3 Estimation Method-III (Fredlund and Xing, 1994)

The approach by Fredlund and Anqing Xing (1994) [229] presents a self-contained solution enabling the creation of the volumetric water content function across a broad spectrum of negative pressures, from zero down to minus one million kPa. This is achieved by leveraging the user's familiarity with a set of three parameters. The underlying equation is articulated as follows:

$$\theta_w = C_\Psi \left[\frac{\theta_s}{\left[\ln\left(e + \left(\frac{\Psi}{a} \right)^n \right) \right]^m} \right] \quad \text{Eq. 4. 2}$$

$$C_\Psi = 1 - \frac{\ln\left[1 + \frac{(u_a - u_w)}{(u_a - u_w)_r} \right]}{\ln\left[1 + \frac{(10^6)}{(u_a - u_w)_r} \right]} \quad \text{Eq. 4. 3}$$

Where, "θ_w is the volumetric water content; C_Ψ is the correction function and can be taken 1 [230]; θ_s is the saturated volumetric water content; e is the natural number (2.71828); Ψ is the negative pore-water pressure; and a, n, m are the curve fitting parameters; $(u_a - u_w)$ is matric suction (kPa); $(u_a - u_w)_r$ residual matric suction corresponding to the residual water content (kPa); u_a is pore-air pressure (kPa); u_w pore-water pressure (kPa)."

The parameter 'a' is a pivotal point in the volumetric water content function, measured in kPa. Typically, it slightly exceeds the AEV. The variable 'm' controls the residual water content, and 'n' regulates how steeply the volumetric water content function slopes.

The functionality of the Fredlund and Anqing Xing (1994) [229] approach requires prior knowledge of specific parameters a, n, and m. These values can typically be derived through an appropriate fitting algorithm applied to observed data points, a feature available in Seep/W module. It is crucial to note that this method is not designed for predicting volumetric water content functions based on grain-size curves. Instead, its purpose is to generate a continuous and consistent function across the entire range of negative pore-water pressure values (from 0 to 10^7 kPa).

5.3.3.1.4 Estimation Method-IV (Van Genuchten, 1980)

In the year 1980, Van Genuchten [228] introduced a four-parameter equation that serves as a closed-form solution for forecasting the function of volumetric water content. The underlying equation is outlined below:

$$\theta_w = \theta_r + \frac{(\theta_s - \theta_r)}{\left[1 + \left(\frac{\Psi}{a} \right)^n \right]^m} \quad \text{Eq. 4. 4}$$

Where; "θ_w is the volumetric water content; θ_s is the saturated volumetric water content; Ψ is the negative pore-water pressure; and a, n, m are the curve fitting parameters. While the

terminology of the a, n, and m parameters resembles that of Fredlund and Xing (1994), their meanings vary slightly. Notably, the “a” parameter is distinct from the air-entry value; it serves as a pivotal point influencing the “n” parameter's impact on the function's slope. Additionally, the “m” parameter governs the steepness of the curve as it transitions to the lower plateau.”

4.3.3.2 Hydraulic Conductivity Function (HCF)

The hydraulic conductivity function reflects the soil's ability to carry water in saturated and unsaturated circumstances. Water fills every pore between solid particles in saturated soil. Beyond the air-entry threshold, air infiltrates the larger pores, rendering it to non-conductive pathways that elongate the flow route's complexity (Fig. 4. 4). Consequently, the soil's hydraulic conductivity diminishes. As pore-water pressures decline, more pores contain air, further reducing hydraulic conductivity. This underscores that water movement through a soil profile hinges on its water content, represented by the volumetric water content function. It is difficult and expensive to measure hydraulic conductivity directly. However, various predictive techniques, utilizing grain-size distribution or measured volumetric water content with saturated hydraulic conductivity, can derive this function. Seep/W incorporates predictive methods for estimating hydraulic conductivity once volumetric water content and saturated permeability (K_{sat}) are defined.

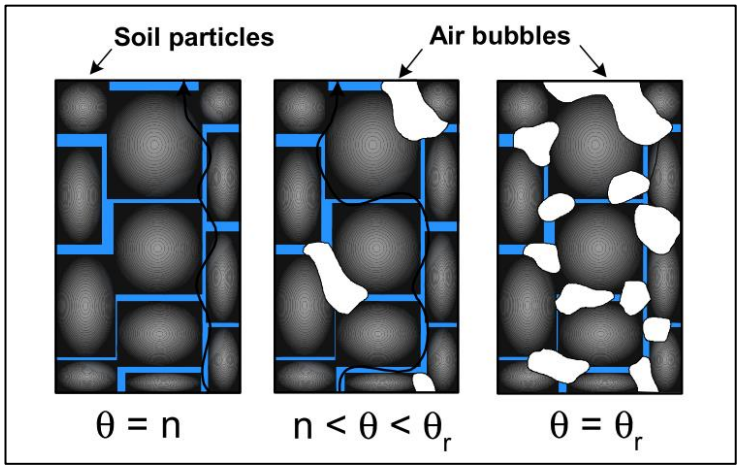

Fig. 4. 4: Flow paths from saturated to residual condition [231]

In cases involving an unsaturated zone, it is imperative to establish a hydraulic conductivity function for all materials within the scenario. Even if this function is an approximation, employing it yields more realistic outcomes compared to a flat, unvaried input. Specifically, in unsaturated seepage analysis featuring negative surface fluxes (like evaporation), and the potential for extreme negative pressures, the conductivity function should encompass a pressure

range surpassing several hundred thousand kPa (or equivalent) of negative pressure. Neglecting the comprehensive coverage of this entire spectrum leads to the imposition of the minimum specified value as the standard for progressively more adverse pressure conditions. In simpler terms, failing to account for the full range of pressures underestimates the hydraulic conductivity.

When one opts for a consistently uniform hydraulic conductivity function to represent unsaturated soil, implying a consistent conductivity value across different moisture levels, it tends to yield outcomes that lack realism. This means that assuming the same conductivity irrespective of the varying moisture content in the soil can produce inaccurate or misleading results in the context of hydraulic behaviour. This approach can misplace the phreatic surface and exaggerate the proportion of flow through the unsaturated zone. The issue stems from a horizontal conductivity function enabling water to traverse the unsaturated zone as easily as the saturated zone. However, real-world conditions differ, as water encounters more resistance when flowing through unsaturated soil due to its lower hydraulic conductivity compared to saturated soil.

4.3.4 Rainfall Infiltration Analysis

The Seep/W module based on the 2D finite element method has been used to obtain the pore water pressure generated by the rainfall of desired intensity for the defined material property, slope cross-section, initial and boundary conditions. It uses a numerical discretization technique to solve Darcy's equation for unsaturated or saturated slope conditions and runs the following water flow governing equation to compute 2D seepage [44], [129], [139], [232].

$$\frac{\partial}{\partial x}\left(k_x \frac{\partial H}{\partial x}\right)+\frac{\partial}{\partial y}\left(k_y \frac{\partial H}{\partial y}\right)+q = m_w^2 \gamma_w \frac{\partial H}{\partial t} \qquad \text{Eq. 4. 5}$$

Where, "k_x is used to represent the horizontal x-direction infiltration coefficient, k_y is used to represent the horizontal y-direction infiltration coefficient, H denotes total head of water, q denotes the applied rainfall intensity, m_w denotes the slope for the SWCC (soil-water characteristic curve), and γ_w denotes the water's unit weight."

4.4 Results and Discussions

GeoStudio 2020 software has been used to simulate 2D rainfall in Seep/W, which is directly linked to Slope/W for the analysis of slope stability, in order to investigate the failure pattern of the physical model. Using GeoStudio 2020 Slope/W stability software, this study performs a Morgenstern-Price Method assessment of the soil slope's stability. The factor of safety has been

calculated using Morgenstern-Price [222] method from the various limit equilibrium methods. It is one of the most widely used methods. It allows for a special variable interslice force function to be used, allowing the interslice inclination to vary on every slice along the slip surface while also satisfying both force and moment equilibrium. The geometry and material properties (Cohesion, friction angle, and unit weight) of the slope have been taken according to the model test as mentioned in the laboratory result section.

The assessment of slope stability is a comprehensive process that involves a detailed examination of existing conditions, with a primary focus on determining the stability of a slope by analyzing the interaction between forces favouring sliding and those resisting movement. The slope is taken to be satisfactorily stable when the calculated resistive forces are more significant than the sliding forces, resulting in a Factor of Safety (FOS) greater than 1. In instances where structural design is a crucial consideration, strict adherence to elevated FOS values is vital following the guidelines specified in IS 14243-2 (1995). Enforcing these higher FOS values becomes crucial, particularly in construction scenarios where critical structural elements are at play. This precautionary measure provides an additional margin of safety, ensuring that the structural integrity is not compromised. This approach effectively mitigates the risk of potential failure, thereby enhancing overall safety standards in construction projects. By emphasizing adherence to heightened FOS values, the assessment process contributes significantly to preventing slope instability-related issues and strengthens the robustness of construction projects.

4.4.1 For Study Area-I (Jhakri Landslide)

In this section, Jhakri slope has been analysed using the GeoStudio. Geometrical parameter of the slope has been drawn. The slope has a height of 36.2 m, with a slope angle of 35° as observed during the field study. Figure 5.6a shows the geometry of the slope.

4.4.1.1 Material Property

The slope/W employs geotechnical parameters to assess the factor of safety. In this case, the soil is categorized as silty sand. The natural water content of the soil stands at 6.7%. Key values for the soil include bulk unit weight (14 kN/m^3), dry unit weight (13.3 kN/m^3), and saturated unit weight (18.27 kN/m^3). Additionally, the permeability coefficient (k) is 0.0023 m/hr, cohesion (c) is 9.5 kPa, and the friction angle (φ) is 32°.

The two main input parameters for this analysis are volumetric water content function (VWCF) also widely known as the soil-water characteristic curve (SWCC) function and hydraulic

conductivity function (HCF). VWCF shows the relationship between volumetric water content vs. matric suction (Fig. 4. 5a), and the HCF shows the relationship between water conductivity and matric suction (Fig. 4. 5b).

Matric suction expresses the water-retaining capacity of the soil. The function has been defined using the GeoStudio software with the help of material properties like grain size distribution and the material's hydraulic conductivity. For soils with identical grain-size distributions, the SWCC function was employed, while the HCF function was calculated from the SWCC using the criteria as discussed [229]. The criteria eliminate the requirement for additional prediction approaches to assess residual water content. The SWCC function and the HCF function were combined with the field measurements of saturated water content and soil permeability during the simulation. A limiting suction of -20 kPa was introduced in the analysis as an initial condition to avoid the excessively high negative pore-water pressure. The initial water table has been defined along with the impermeable bedrock [129], [220].

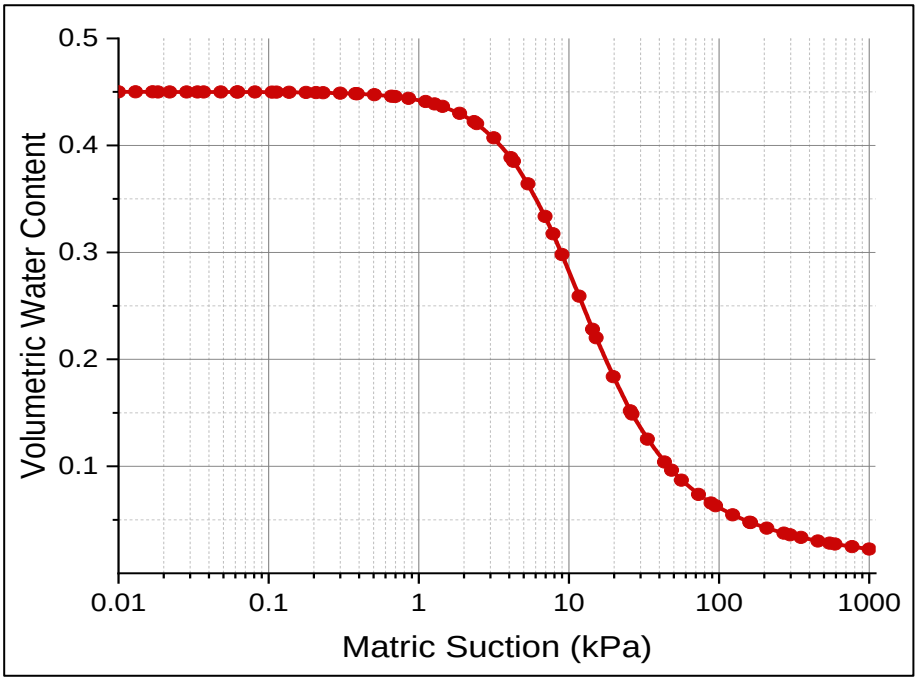

(a)

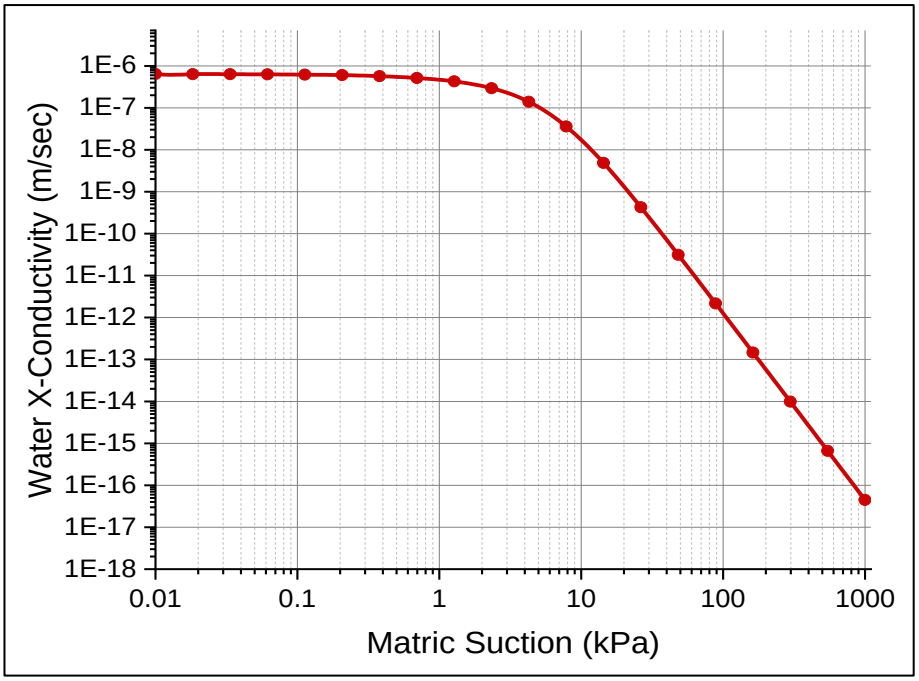

(b)

Fig. 4. 5: (a) Volumetric water content function, (b) Hydraulic conductivity function

4.4.1.2 Slope/W Results Before Rainfall

Slope stability analysis has been done to determine the factor of safety of the slope before the rainfall using soil parameters. Using the GeoStudio software, the factor of safety comes out to 1.23, which represents that the slope is very much stable on its own before the rainfall as the FOS of the slope is greater than 1. The critical slip failure pattern has been highlighted in Fig. 4. 6a, which can fail under certain circumstances. It also represents the hazard zonation map according to the factor of safety. Fig. 4. 6b shows the relationship between friction strength, shear resistance, and shear mobilization. As shear resistance is comparativily more than the mobilized shear, which directly indicates, the slope is stable.

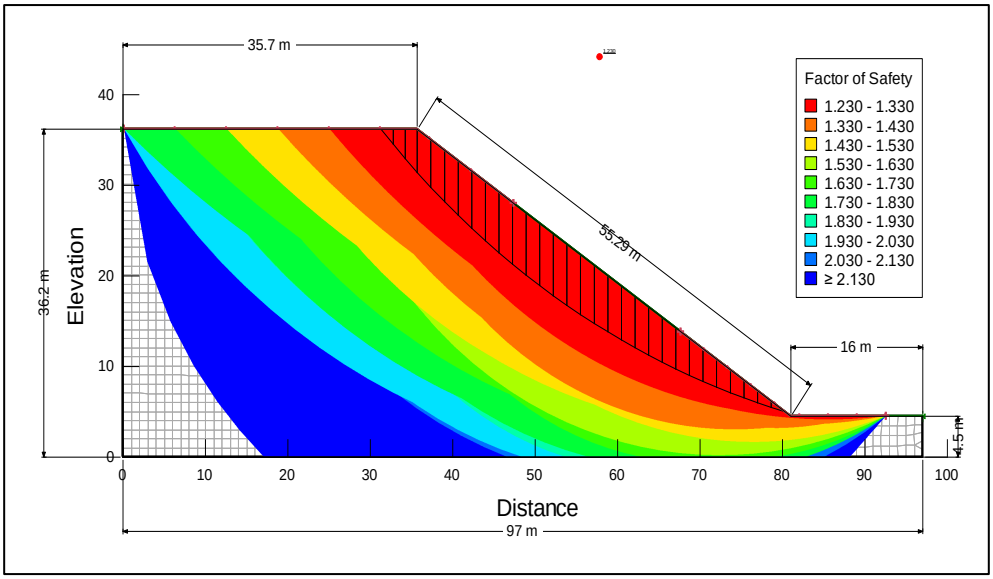

(a)

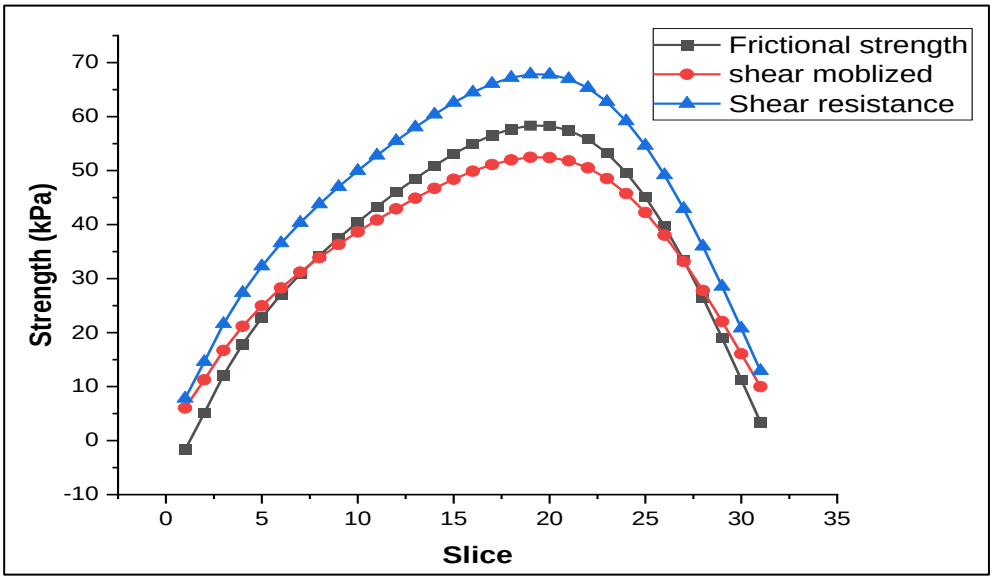

(b)

Fig. 4. 6: (a) Stability analysis of slope before rainfall, and (b) Variation of shear strength, mobilized shears, and shear resistance before rainfall

4.4.1.3 Seep/W Results After Rainfall

Rainfall simulation has been done in Seep/W software under steady-state to analyse the effect of rainfall on the slope. The analysis gives a result of pore water pressure developed under the effect of desired rainfall intensity for the particular slope. The rainfall intensity was fixed to 30mm/hr according to the physical modelling experiment, and the rainfall boundary condition is used as a data point function in which the time duration has been fixed to 20 min to simulate the

10 mm rainfall depth for the 30mm/hr rainfall intensity. The bottom and left side of the geometry model has been set to impervious as a rock bed so that no seepage can occur. The toe boundary condition has been set to zero pressure boundary condition, representing the drain path for the seepage water. Fig. 4. 7a represents the pore water pressure distribution according to depth. Fig. 4. 7b shows the flow vectors, which represent the direction of seepage flow. These figures also represent that the soil is fully saturated with the rainfall.

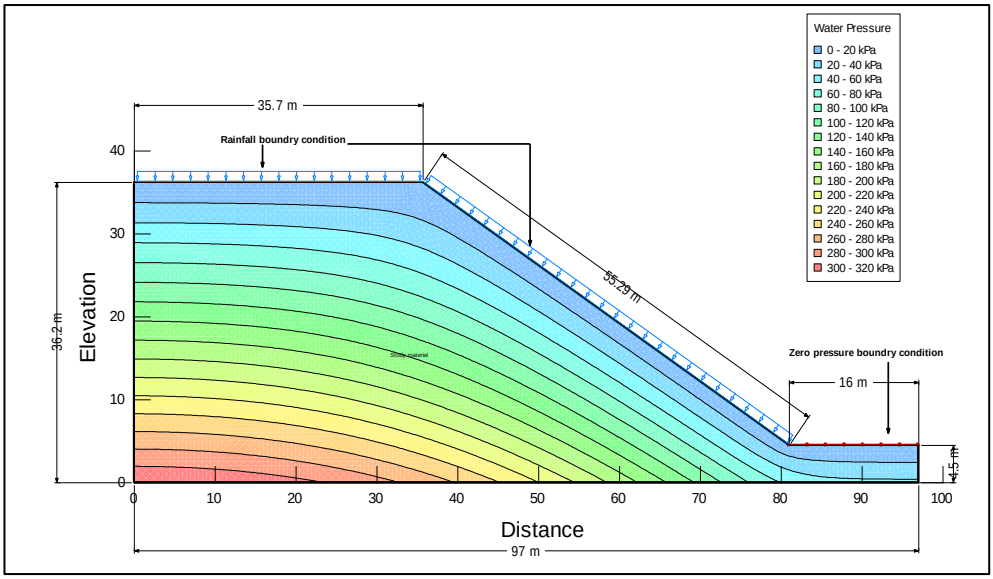

(a)

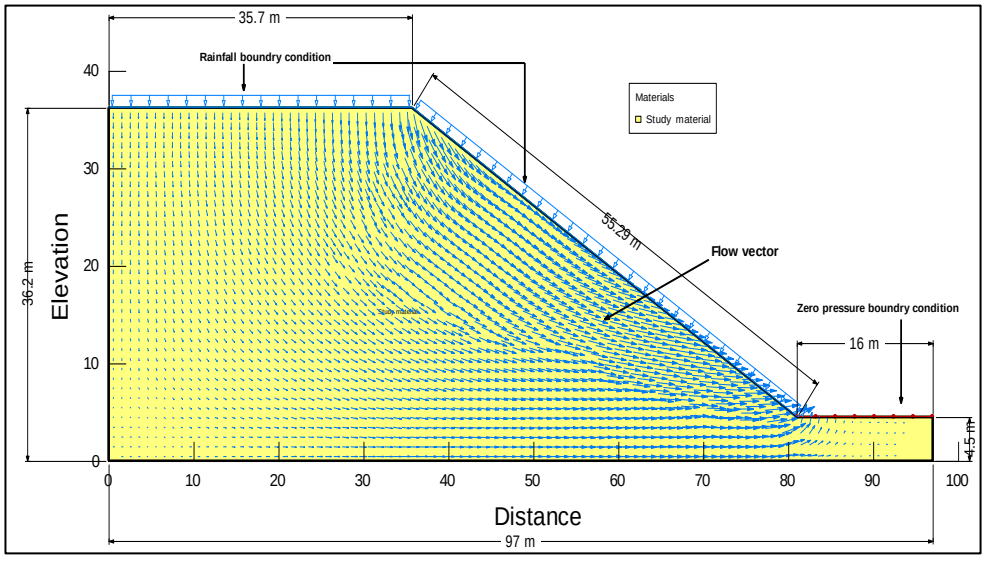

Fig. 4. 7: (a) Pore-pressure variation by rainfall, and (b) Flow vectors showing the flow direction of rainfall water

4.4.1.4 Slope/W Results After Rainfall

Rainfall simulation done in Seep/W is later linked to Slope/W to analyse slope stability so that factor of safety can be determined after the rainfall, which will further help in monitoring and early warning. The safety factor comes out to 0.626, which represents that the slope is very much critical to fail after the rainfall as the FOS of the slope is less than 1. The critical slip failure pattern has been highlighted in Fig. 4. 8a, which failed under the action of rainfall. It also represents the contour profiles according to the factor of safety after the rain. Fig. 4. 8b shows the relationship between friction strength, shear resistance, and shear mobilized. As shear resistance is much lower than the mobilized shear, it indicates the slope is unstable under the rainfall condition.

From the numerical modelling results, the factor of safety of the slope obtained before the rainfall is 1.23, and after the rainfall of the given intensity, it decreased to 0.626, which is less than 1, which justifies the physical modelling mechanism of failure for the rainfall simulated in the laboratory.

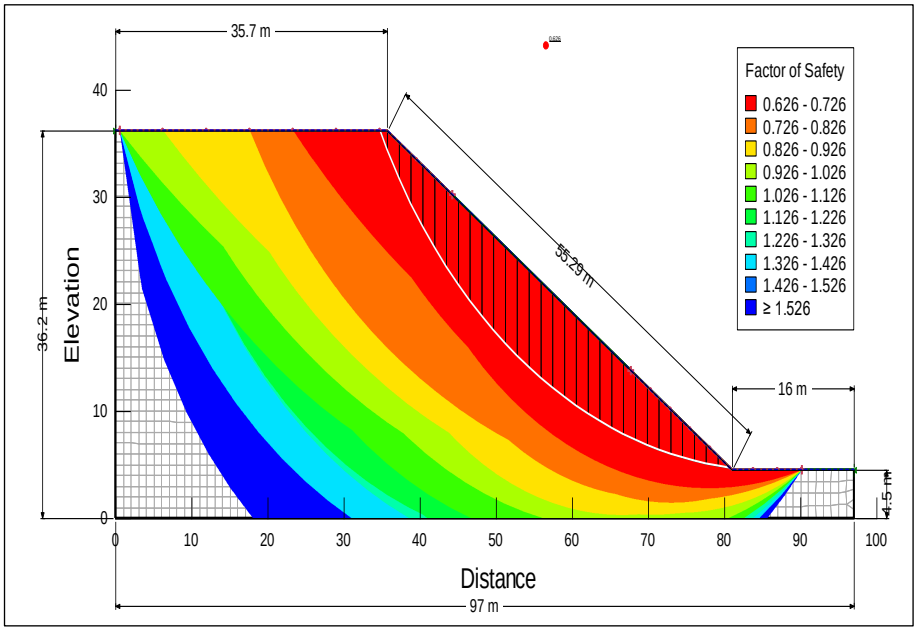

(a)

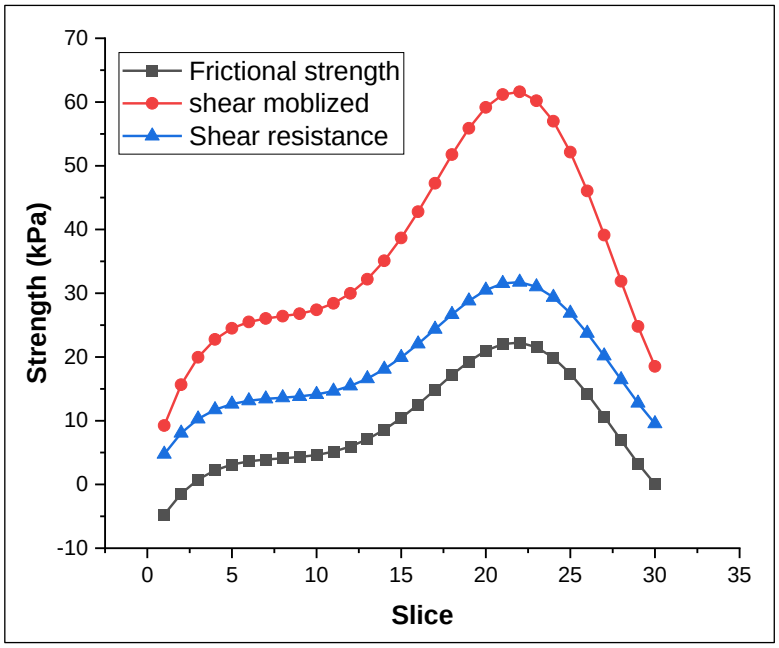

(b)

Fig. 4. 8: (a) Stability analysis of slope after rainfall, and (b) Variation of shear strength, mobilized shears, and shear resistance after rainfall

4.4.2 For Study Area-II (Kotrupi Landslide)

The studied slope has an inclination angle of 47.56º (approx. 47º) as shown in figure 5.10. The presence of moisture from the infiltration that the slope has experienced has resulted in the development of apparent cohesion. As a result, the apparent cohesiveness between different soil particles is revealed by the cohesion value that is achieved through triaxial testing. Additionally, the existence of fine soil, as measured by silt content (SM), has been of assistance in the development of the cohesion value.

4.4.2.1 Material Property

The slope/W employs geotechnical parameters to assess the factor of safety. In this case, the soil is categorized as silty sand. The natural water content of the soil stands at 6.7%. Key values for the soil include dry unit weight (16.7 kN/m^3), and saturated unit weight (20.3 kN/m^3). Additionally, the permeability coefficient (k) is 0.0023 m/hr, cohesion (c) is 21 kPa, and the friction angle (φ) is 31°.

The two main input parameters for seepage analysis are volumetric water content function (VWCF) also widely known as the soil-water characteristic curve (SWCC) function and hydraulic conductivity function (HCF). VWCF shows the relationship between volumetric water

content vs. matric suction (Fig. 4. 9a), and the HCF shows the relationship between water conductivity and matric suction (Fig. 4. 9b).

The Volumetric Water Content Function (VWCF) is established through a data point function utilizing soil classification samples, categorizing the soil as silty sand. The saturated water content is set at 45%. The Hydraulic Conductivity Function (HCF) is determined using a data point function based on the Van Genuchten method, incorporating the previously defined VWCF. The saturated conductivity (k) is specified as 0.0023 m/hr, with the residual water content set at 10% of the saturated water content. The applied boundary conditions include a rainfall intensity as illustrated in Fig. 4.12 and a zero-pressure boundary, as illustrated in Figure 5.11.

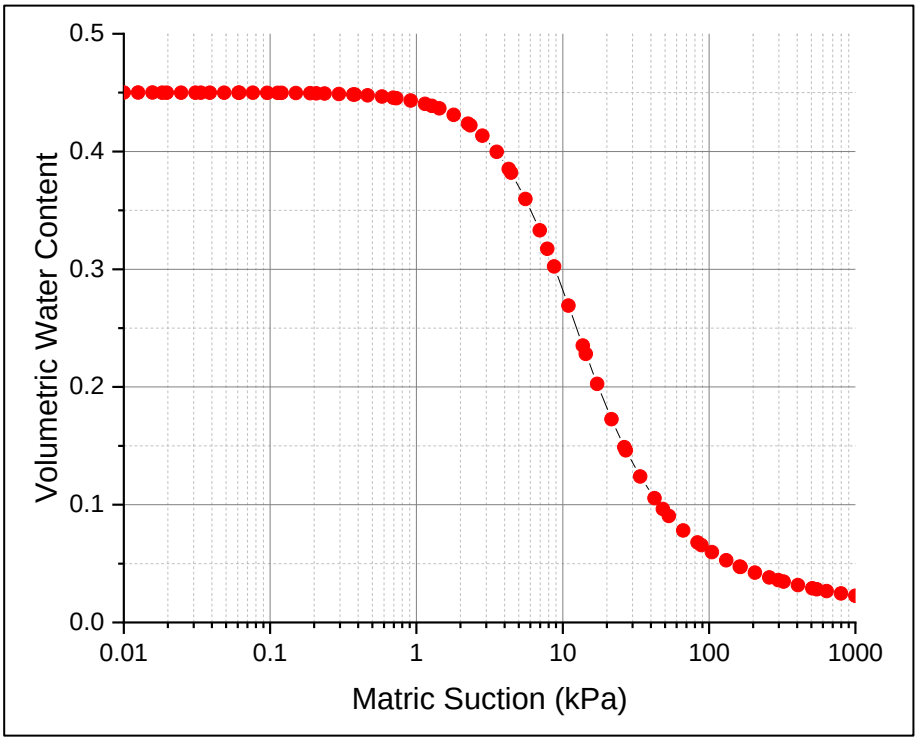

(a)

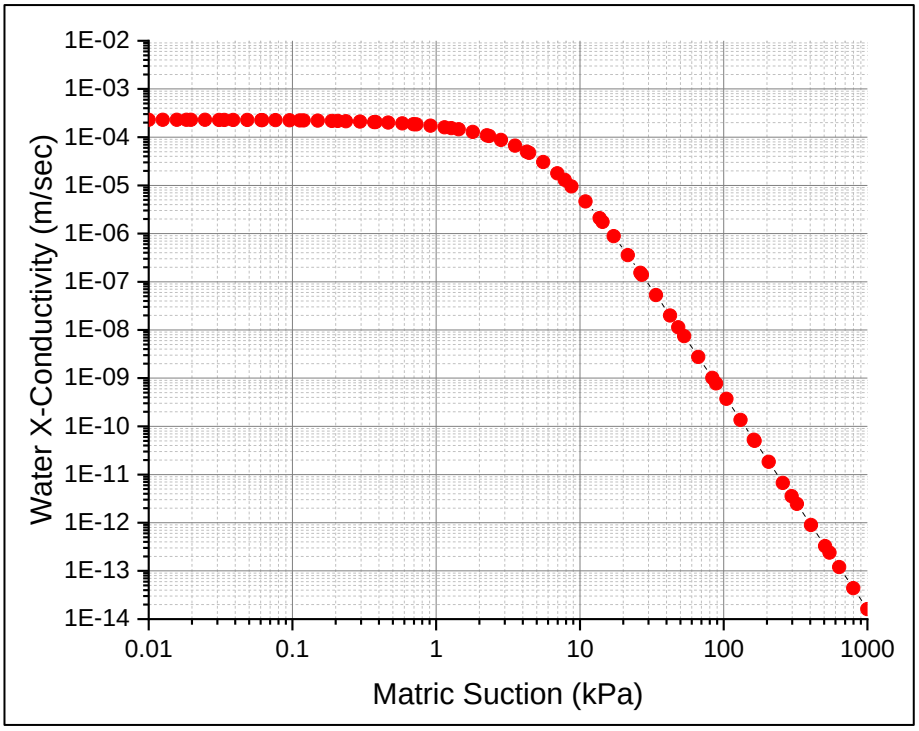

(b)

Fig. 4. 9: (a) Volumetric water content function, (b) Hydraulic conductivity function

4.4.2.2 Stability Analysis Results Before Rainfall

The geometry and material property used in physical modelling analysis is used for simulation. The slope before the rainfall has been analysed using Slope/W module using Morgenstern Price method [222] to assess the safety factor in dry natural condition. Fig. 4. 10**Error! Reference source not found.** shows the variation of factor of safety and for critical slip surface it came out to be greater than 1 which shows that the slope was stable before rainfall.

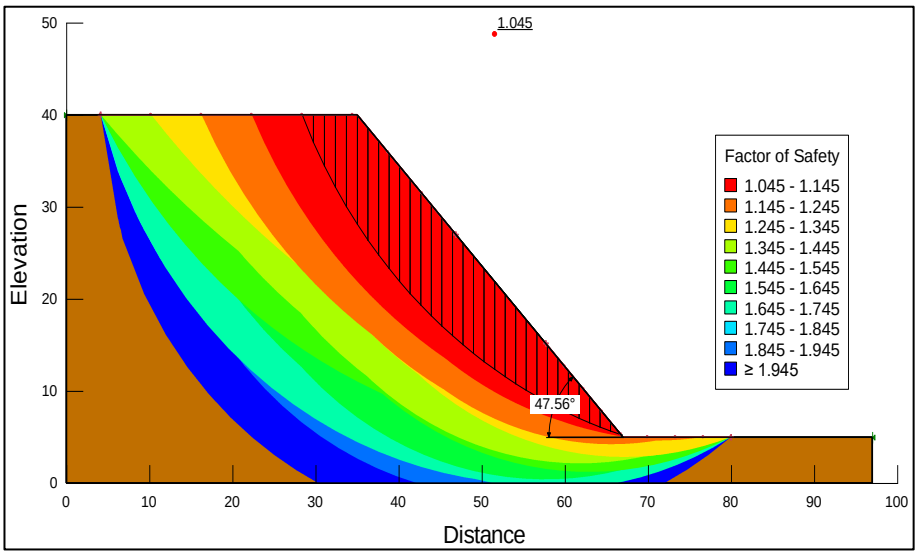

Fig. 4. 10: Variation of factor of safety prior to rainfall condition

4.4.2.3 Seepage Analysis Result After Rainfall

Seep/W module is used to investigate the seepage and pore water pressure parameters of slope under the effect of rainfall. Fig. 4. 11 shows the variation of pore pressure with slope elevation. Presence of negative pore pressure can be seen on upper section which help in stable slope. It also depicts the flow vectors which is the path followed by seepage water and it can be seen that in the nearby slope area the intensity of flow vectors is very dense which might be the cause for the resulting failure. The seepage analysis convergence plot (Fig. 4. 12) shows that the analysis has reached its final solution [231].

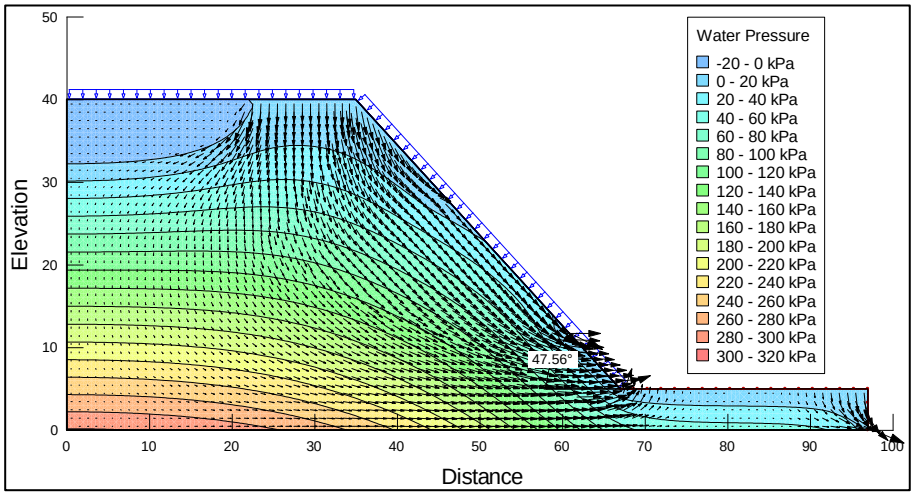

Fig. 4. 11: Variation of pore pressure with input rainfall condition

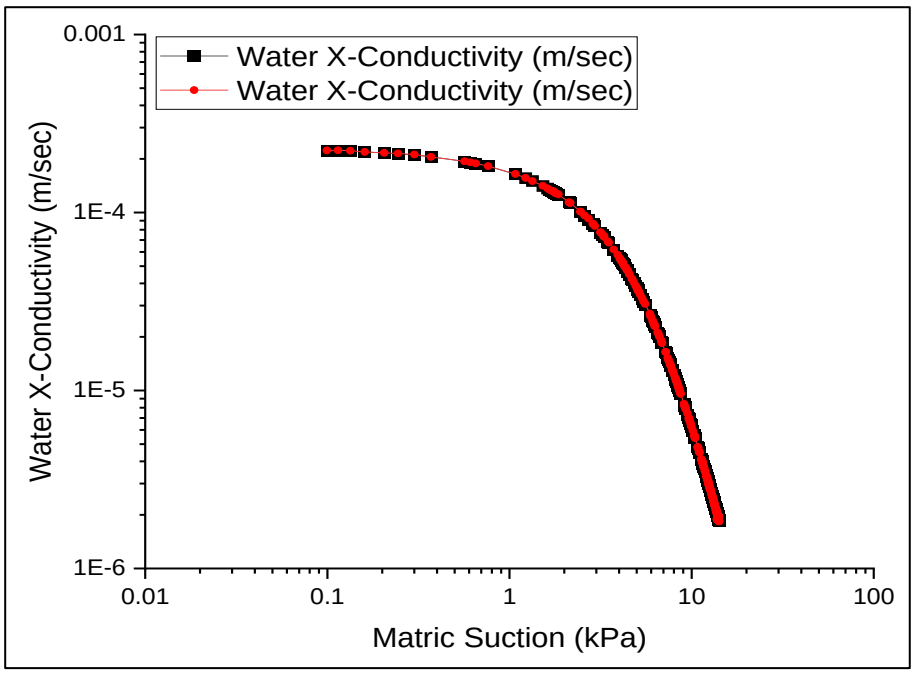

Fig. 4. 12: Convergence plot for seepage analysis

4.4.2.4 Slope/W Results After Rainfall

The safety factor has been later investigated using the seepage analysis results in slope/W module, and from Fig. 4. 13**Error! Reference source not found.**a, it can be inferred that the FOS decreased below 1, supporting the theory that the slope failure has been due to seepage of rainwater. The failure pattern is also identified in the investigation of the physical model.

The fluctuation in shear resistance, shear mobilised stress, and pore pressure are shown in Fig. 4. 13b. It can be deduced that the slope failed because the mobilised shear stress is greater than the shear resistance available.

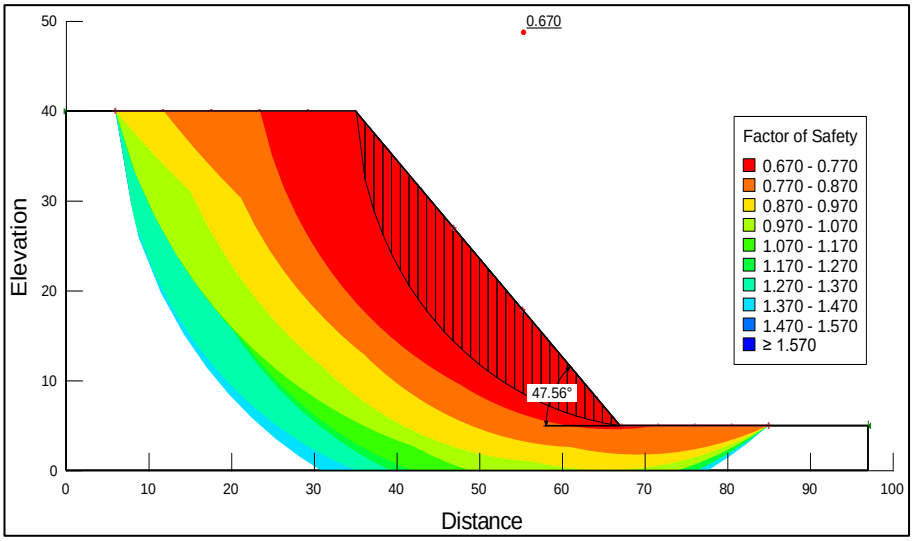

(a)

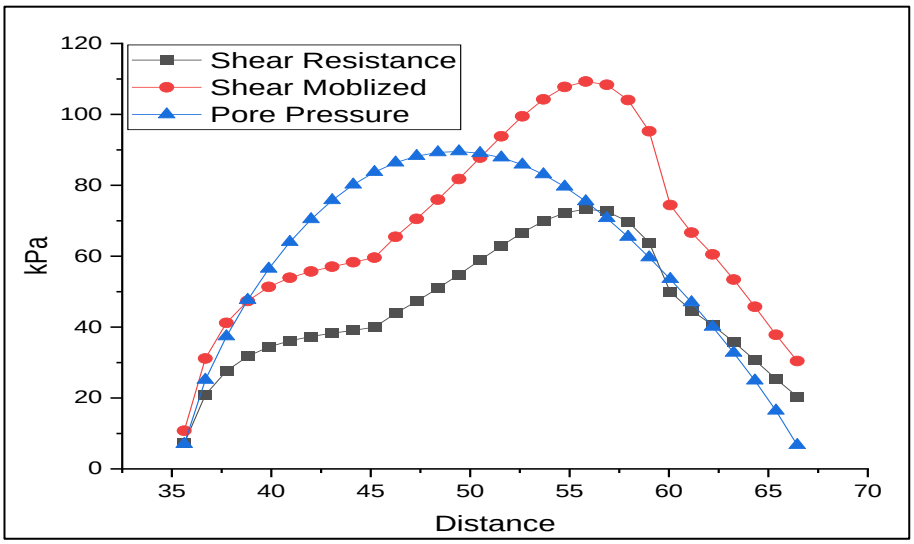

(b)

Fig. 4. 13: (a) Variation of factor of safety after rainfall, and (b) Variation of shear resistance, shear mobilized and pore pressure

This chapter aims to provide a significant insight for numerical analysis. Many researchers studied and analyzed the behavior and mechanism of landslides using physical modelling methods under various rainfall conditions [40]–[42], [150], [157]. Since it is practically not feasible and not scientific to test each critical slope individually with a physical model, [216] validated the physical modelling with numerical modelling results. Furthermore, numerous studies have been conducted using numerical modelling methods, demonstrating their suitability and feasibility [8], [44], [45], [139]. In this study, two landslides have been considered to analyze the pore pressure parameter and its factor of safety variation under rainfall conditions by numerical modelling using GeoStudio 2020 software, and the results show that the slope was stable in dry conditions [136], [147], [233]. However, some studies proved that the stability factor increased due to light and intermittent rainfall [234]. Further, the seepage analysis has been done under the monsoonal rainfall, which caused an increase in pore pressure. Prolonged and cumulative rainfall results in the formation of rills, erosional gullies, and trenches caused by vigorous seepage, which in turn results in weathering, making the slope more critical to fail. As a result, the landslide's occurrence can largely be attributed to the rain. A slope's strength is determined by frictional resistance when the soil is dry; however, as water seeps into soil pores, negative pore pressure (also known as matric suction) increases the stability of the slope; however, slope failure occurs when water seeps into the soil to a point where it becomes saturated and loses its frictional strength [42], [89], [212]. The results of the numerical modelling very well demonstrated the effectiveness in determining the variation of FOS and PWP under rainfall conditions, and thus, can be used to identify the critical slopes against failure.

4.5 Summary

In the current investigation, numerical simulations have been conducted utilizing GeoStudio 2020 software. Initially, an analysis of the slope has been performed under natural dry conditions, prior to the occurrence of rainfall. Subsequently, an assessment of seepage and stability parameters is carried out following the onset of rainfall. The numerical analysis is conducted to validate the findings of the physical modelling.

1. For study area-I (Jhakri), the factor of safety is calculated to be 1.23, indicating that the slope is inherently stable prior to any rainfall, as its safety factor exceeds 1. Rainfall analysis was conducted using the Seep/W software in a steady-state condition to examine how rainfall impacts the slope. The FOS comes out to 0.626, signifying the substantial

susceptibility of slope failure following rainfall, given that the factor of safety for the slope is below 1.

2. Similarly, for study area- II (Kotrupi) the values of factors of safety for the considered slope have been calculated both prior to and following the occurrence of rainfall. It has been observed that prior to rainfall, the Factor of Safety (FOS) value is 1.045 (exceeded 1), signifying the stability of the slopes. However, following rainfall simulation, there has been a significant decrease in FOS value, reducing to 0.67 (dropping below 1), which indicated slope instability.

3. The investigation also examined variations in shear resistance, shear-induced stress, and pore pressure within the selected slopes in both study regions-I and II. It has been determined that the slope failure occurred due to the fact that the mobilized shear stress exceeded the available shear resistance.

CHAPTER 5

SYSTEM DESIGN AND IMPLEMENTATION

5.1 General

Monitoring focuses on systematic surveillance, regular measurements, recording of activities and evaluation of positional and orientational changes caused by external forces. Slope monitoring is vital for understanding soil parameters like erosion, water content, drainage, vegetation, geomorphology, and historical data. Deformation and tilt observations are essential for calculating rock and soil stability, deformation evaluation, prediction, and issuing warnings. Different monitoring systems require specific devices based on application, method, installation time, site accessibility, weather conditions, required accuracy, and frequency. Collaborative efforts from experts in geology, geophysics, hydrology, geodesy, remote sensing, and other academic fields are necessary for effective landslide and slope monitoring.

Implementing an “early-warning system (EWS)” is a highly beneficial approach for mitigating risks and reducing the impact of disasters. By effectively alerting the public in advance, such a system can save lives and minimize both the economic and physical consequences of catastrophes. However, to ensure its success, active engagement of the public is essential. This involves creating awareness among the population about potential dangers, educating them on the precautionary measures in place, and ensuring the system is continuously prepared to respond promptly when needed. The involvement of the public in the early-warning system has been proven effective in various scenarios, yielding positive outcomes in terms of disaster management and overall community safety.

Drawing a clear distinction between the terms “monitoring system” and “early-warning system (EWS)” is essential. The monitoring system for landslides involves the continuous gathering and examination of data related to slope conditions and movements. By consistently monitoring factors such as slope stability, weather patterns, and ground displacement, this system provides valuable information to assess the potential risks of landslides and ensure timely responses when necessary. Monitoring plays a crucial role in identifying early warning signs of instability,

enabling authorities to take proactive measures to mitigate hazards and protect lives and infrastructure in landslide-prone areas.

The EWS for landslides is an integral part of landslide risk management. Through continuous data analysis and monitoring, the system identifies critical thresholds that, when surpassed, trigger pre-established civil safeguards. These safeguards may include issuing warnings to communities at risk, implementing evacuation plans, or activating protective measures to minimize the impact of impending landslides. By combining advanced monitoring technologies with quick and decisive responses, the EWS aims to reduce the potential consequences of landslides and enhance overall safety and resilience in vulnerable regions.

By employing such devices, a comprehensive monitoring system provides valuable data to understand the behaviour and characteristics of landslides over time. On the other hand, an early-warning system (EWS) is dedicated to detecting potential hazards and triggering timely alerts to mitigate the risks associated with landslides. While the monitoring system continuously gathers data for analysis, the early-warning system focuses on identifying critical thresholds or precursor signals that could indicate an imminent landslide event. By clearly defining these two concepts, stakeholders can implement effective strategies for both monitoring and early warning, thereby enhancing landslide risk management and reducing potential impacts. Fig. 5. 1 shows a community-centric landslide early warning system presented by Intrieri et al. (2013) [86].

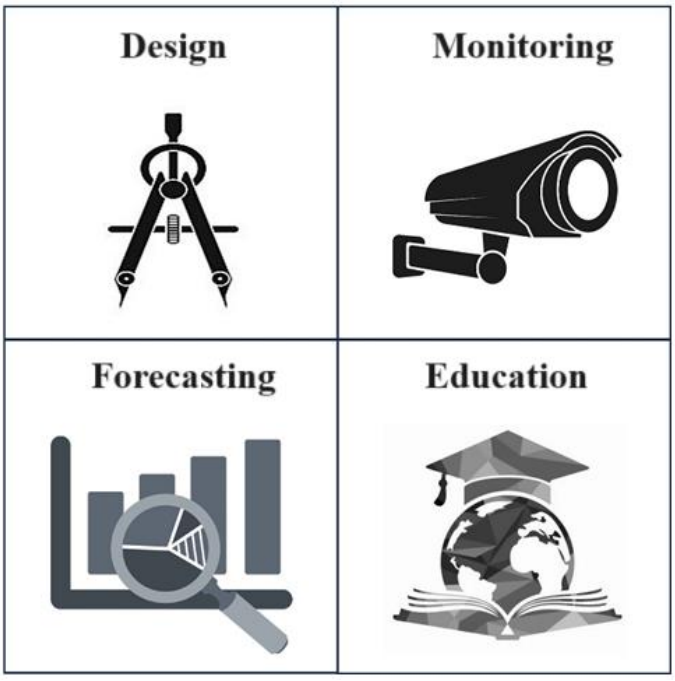

Fig. 5. 1: A community-centric landslide early warning system [86]

The essential elements of a comprehensive landslide warning system can be as follows:

1. **Risk Knowledge:**

The warning system necessitates geological analyses and scenarios to identify temporal and spatial progression scenarios, considering physical movement size, threatened regions, and potential timeframes for landslides. Setting threshold values, understanding people requirements, and establishing effective communication protocols are essential components.

2. **Monitoring:**

Continuous data collection from devices measuring landslide warning signs, like extensometers, inclinometers, and geophones, is critical. Data is processed either continuously or at specified intervals based on predicted conditions.

3. **Analyses and Forecasting:**

Regular data validation and comparison with threshold values are conducted through intelligent systems or expert staff. Automated and manual warning signal issuance are both employed.

4. **Civilian Protection:**

Prior to a landslide, people in hazardous areas must receive instructions on potential dangers and how to respond in emergencies. Strategies for handling false alarms are emphasized. Post-warning signal, procedures are established to inform civil safeguard personnel responsible for safety measures. The civilian safeguarding program is constantly updated to adapt to changing scenarios.

This chapter focuses on the development of a comprehensive landslide monitoring and warning system aimed at safeguarding lives and properties. It encompasses the design, monitoring, analyses, and forecasting aspects of the system. This section provides detailed coverage of the employed sensors and the main elements of the system used to monitor the landslide-prone zone. By integrating advanced technology and sensor data, the proposed early warning system aims to improve landslide detection and prediction, enabling timely and effective measures to protect communities and infrastructure in vulnerable areas.

5.2 System Design and Components

Landslides cause damage to structures like roads, buildings, and power supplies, affecting society significantly [173]. Detecting the movement patterns and impact requires sensitive and precise sensors. The velocity and power of the movement determine the sensor requirements,

such as measuring range, sampling rate, and sensitivity. The sensors should be weather-resistant and durable since landslides occur in various weather conditions. Keeping the cost of the monitoring system low is crucial, which necessitates the use of small, low-cost sensors for large area monitoring. Additionally, low-energy consumption is essential for continuous monitoring as landslides often have irregular activity. Ensuring reliable and steady operation of the sensors is vital for effective landslide monitoring in the long term.

The design of the proposed landslide monitoring system consists of three major components: a sensing unit which includes the sensors and microcontroller, a data logging unit, including a connection and networking module for the collection and storage of data, and a threshold analysis unit, which can be helpful in generating the warning. Fig. 5. 2 shows the schematics of the proposed system for landslide monitoring.

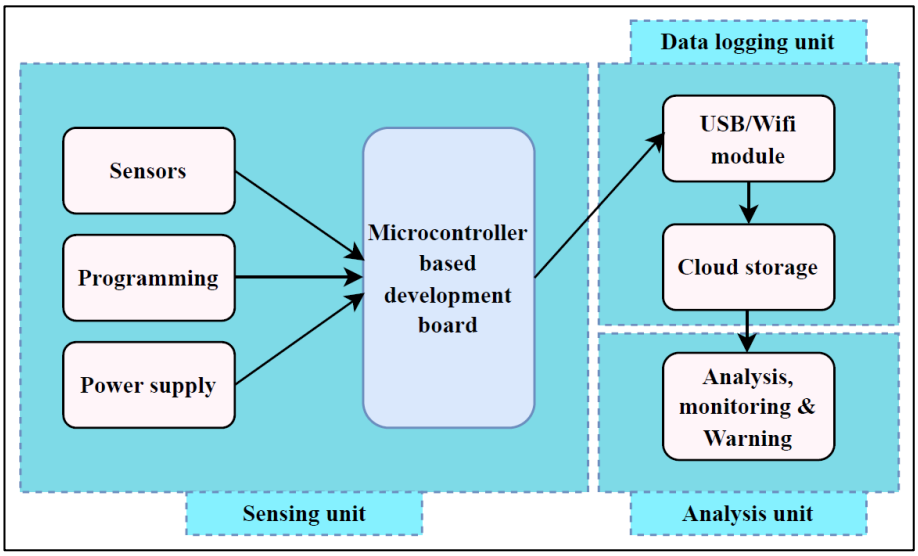

Fig. 5. 2: Design components of the proposed low-cost framework for landslide monitoring

5.2.1 Sensing Unit

The sensing unit is the first and foremost part of the proposed system for monitoring landslide initiation. It includes the sensors used to sense the required data for the analysis. This system uses Micro-Electro-Mechanical System (MEMS)-based sensors owing to their efficient working, durability, and cost-effective availability. This system is to be deployed in the field and cannot be reused if a landslide takes place, making MEMS-based sensors suitable choice for this purpose. The components of the sensing unit are discussed in the following sub-sections.

5.2.1.1 Tilt Sensor

It is necessary to choose a module (MPU6050), which consists of an accelerometer, gyroscope, and temperature sensor, to record the tilt variation in the x, y, and z directions. The 16-bit triaxial gyroscope and accelerometer are combined into the six-axis sensor as shown in Fig 5.3. The module is built around an MPU6050 InvenSense IMU (Inertial Measurement Unit) chip. In addition to this, there is a power LED that displays the current power status of the module (Fig 5.3a). The MPU6050 module is a Micro-Electro-Mechanical System (MEMS) that contains within it a three-axis accelerometer as well as a three-axis gyroscope (Fig 5.3b). This allows to measure the acceleration, velocity, orientation, and displacement of a system or object, in addition to a wide variety of other motion-related parameters. Fig 5.3c shows the circuit diagram of this sensor module. Fig 5.4 shows the block diagram of MPU6050 sensor module. Table 5.1 shows the specifications of the MPU6050 sensor module.

MEMS accelerometers are used in situations where there is a requirement to measure linear motion, such as movement, shock, or vibration, but there is no fixed reference point. The accelerometer tracks the object's linear acceleration while being tethered to it. The mass on a spring principle is the principle on which all accelerometers operate. Due to inertia, the mass seeks to remain immobile as the item to which they are attached accelerates. As a consequence, the spring undergoes stretching or compression, resulting in the production of a force that can be measured and is related to the acceleration that has been applied. Table 5. 1 shows the specification of MPU6050 module.

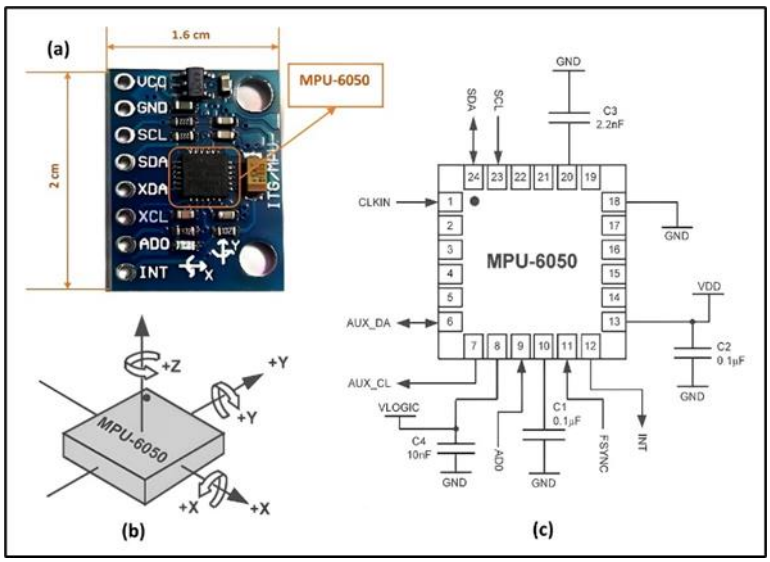

Fig. 5. 3: MPU6050 module (a) Sensor module, (b) Working axis details, and (c) Circuit diagram

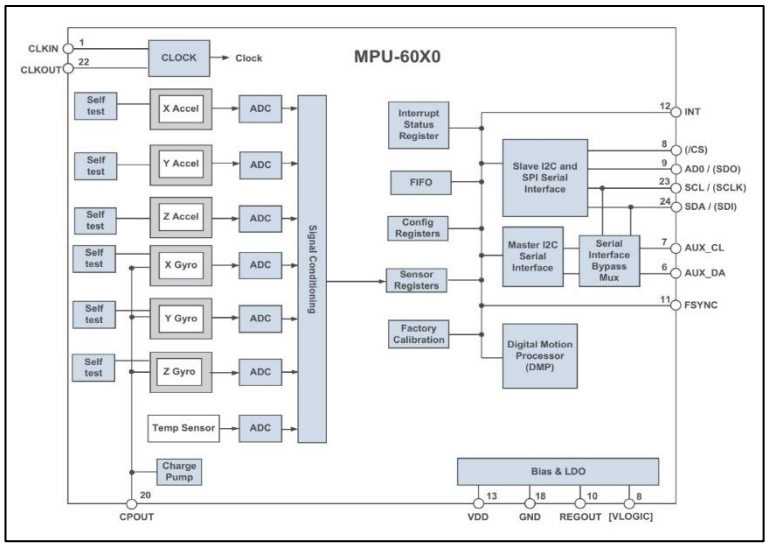

Fig. 5. 4: Block diagram of MPU6050 module.

Table 5. 1: Specifications of MPU6050 module

Parameters	**Range**
Operating Voltage	5V (typical)
Accelerometer Range	±2g, ±4g, ±8g, ±16g
Gyroscope Range	±250°/s, ±500°/s, ±1000°/s, ±2000°/s
Temperature Range	-40 to +85°C
Absolute Maximum Acceleration	Up to 10000g

The operation of a MEMS (Micro-Electro-Mechanical Systems) gyroscope is fundamentally rooted in the Coriolis effect, a phenomenon in physics. According to this principle, when a mass is in motion with a certain velocity along a particular path and is subjected to an external angular motion, a resultant force is generated, pushing the mass in a direction perpendicular to its original trajectory. It is worth noting that the magnitude of the angular motion directly influences the rate of displacement induced by this force. Inside the MEMS gyroscope, four proof masses are strategically incorporated and maintained in continuous oscillation. This continuous oscillation

sets the stage for the application of the Coriolis effect. As the system experiences angular motion, the Coriolis effect comes into play, altering the capacitance between these proof masses. Notably, the direction of this capacitance change depends on the direction of the applied angular motion. A pivotal aspect of the MEMS gyroscope's functionality is detecting this change in capacitance. This specific variation gives rise to a measurable reading, enabling the gyroscope to sense and record angular motion. In summary, the MEMS gyroscope exploits the Coriolis Effect to translate angular motion into changes in capacitance, thus providing a reliable and accurate means of detecting and quantifying angular motion.

5.2.1.2 Soil Moisture Sensor

Unquestionably, water is crucial to the chemical, physical, and mechanical characteristics of the soil. Understanding and analysing various processes involving soil, vegetation, and atmospheres, such as soil erosion, runoff, and soil water infiltration, depend on quantifying soil water content from the surface to greater depths. Due to the ability of aerial plant life to capture some of the water that falls as rain and the ability of plants to absorb moisture from the soil around them and release it to the atmosphere through evapotranspiration, soil vegetation alters the hydrological balance of the affected area. The latter mechanism could result in a decrease in the saturation level of the soil (an increase in suction), which would increase the soil’s shear strength. In other cases, water accumulation between the soil layer can cause the formation of the fluid zone, which may lead to a loss in shear strength causing slope failure. Thus, soil vegetation plays a vital role in stabilizing the slope to protect the environment.

With the help of this sensor, it is possible to track changes in soil moisture continuously. The soil moisture sensor consists of two probes to measure the volumetric water content by measuring the resistance or capacitance value through the soil material. The change in current or voltage is then calibrated to measure the water content. When the soil pores have more water, the resistance to current flow will be less as water provides better conductivity. Similarly, when less water is present in the pores, the resistance offered by the medium will be very high, reducing the current flow due to the poor conductivity offered between pores.

Compared to other sensors in the market which measure resistance, in this study, a capacitive soil moisture sensor version 2.0 is used to measure soil moisture levels through capacitive sensing. Version 2.0 has a better upgrade and offers a better service life than previously available versions, as it is corrosion-proof. The output of the capacitive moisture sensor is known to be

influenced by the complicated relative permittivity (ε_r^*) of the soil, i.e., dielectric medium [174], [175].

$$\varepsilon_r^* = \varepsilon_r' - j\varepsilon_r'' = \varepsilon_r' - j\left(\varepsilon_{relax}'' + \frac{\sigma_{dc}}{2\pi f \varepsilon_0}\right) \quad \text{Eq. 5. 1}$$

where, "ε_r' and ε_r'' are, respectively, the real and imaginary components of permittivity, σ_{dc} referred to the electrical conductivity, ε_{relax}'' is the contribution of molecular relaxation (dipolar rotation, atomic vibration, and electronic energy states), j indicates the imaginary number ($\sqrt{-1}$), and f is the frequency. The amount of energy from an external electric field that is stored in a material is measured by the real part of permittivity (ε_r'). The "loss factor," also known as the imaginary part of permittivity (ε_r''), predicts a material's susceptibility to dissipation or loss in the presence of an external electric field: $\varepsilon_r'' > 0$. Losses are linked to two main processes: electrical conductivity and molecular relaxation. The soil's salinity, ionic composition, frequency, and moisture affect permittivity.

The permittivity of a material is often represented by a complex number with a real part and an imaginary part. The real part of the permittivity represents the material's ability to store electric charge, while the imaginary part represents the material's ability to dissipate electric energy.

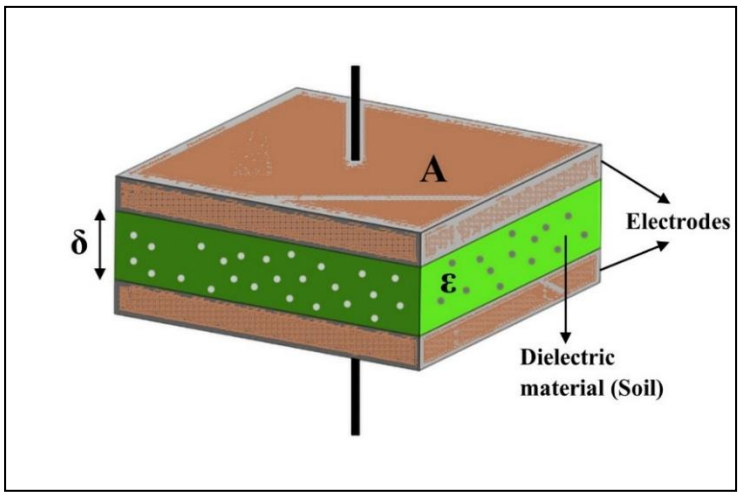

Fig. 5. 5: Parallel plate capacitor setup

Capacitive soil moisture sensors utilize the operation of a capacitor to provide an approximation of the amount of moisture present in the soil. The amount of charge a material can hold when subjected to a specific external electrical potential is referred to as its capacitance [176], [177]. The most common way to conceptualize capacitors is as parallel-plate setups, as shown in Fig. 5. 5.

The capacitance of an object can be expressed as a ratio of its charge to its electrical potential:

$$C = \frac{Q}{V} = \frac{\oint \varepsilon E \,.\, ds}{\int E \,.\, dl} \qquad \text{Eq. 5. 2}$$

The charge Q is defined by the integrating relationship between the generated electric field (E) and the relative permittivity of the surrounding dielectric material (ε) throughout the gross surface area of the probes. The line integral of the electric field is used in the definition of electric potential, abbreviated as V. δ is the distance between plates. For the capacitor with parallel plates, an assumption can be made that the electric field is uniform throughout the whole surface of the dielectric. This leads to the resulting simplification:

$$C = \frac{\varepsilon EA}{E\delta} = \frac{\varepsilon A}{\delta} \qquad \text{Eq. 5. 3}$$

This is usually believed to represent the relationship between the geometric parameters of a capacitor with parallel plates and the soil material having dielectric properties around the capacitor. The capacitance measured by a soil moisture sensor is distinct from that recorded by a capacitor with parallel plates, as the capacitor plates are coplanar rather than parallel. This indicates that the plates are not stacked on top, but are placed adjacent to one another and that the dielectric substance is the ground itself instead of a thin layer trapped between the plates. The following illustration demonstrates this point.

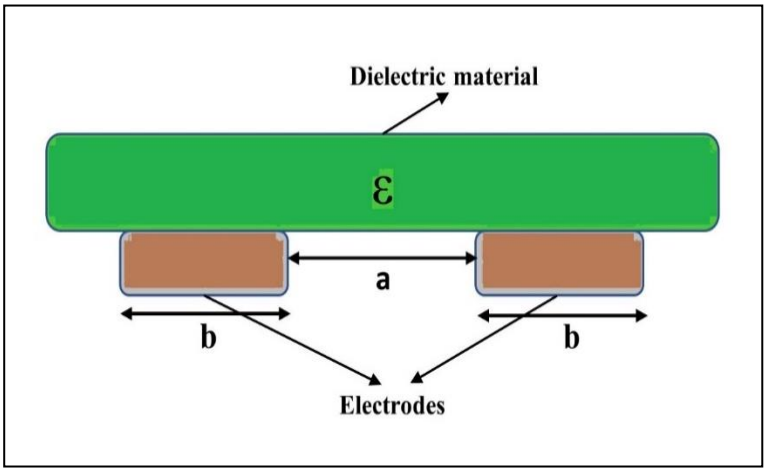

Fig. 5. 6: Illustration concept behind working of soil moisture sensor

Fig. 5. 6 clearly shows the arrangement of electrodes with the dielectric medium, which can be dry or wet soil and serves the same function similar to the plates of any capacitor. The capacitive soil moisture sensor works in conjunction with a timer circuit (TLC555, in the case of the selected sensor). The combination produces a duty cycle proportional to an analog voltage. This voltage

can be read off using a built-in microcontroller board. Capacitance for a flat capacitor is a complex function of dielectric constant and sensor shape that will not be investigated here. The only new component that has been added is G, a function that summarises the geometric qualities of the sensor. The relationship is:

$$C = \varepsilon G \qquad \text{Eq. 5. 4}$$

The geometrical and dielectric medium, along with surface line integration in planer configuration, makes the complex function, which can be simplified for better understanding by assuming a constant (*A*), and the solution to finding the dielectric constant is mentioned in below.

$$V = \frac{A}{C} \qquad \text{Eq. 5. 5}$$

In essence, this indicates that a correlation between the dielectric constant and the inverse of the voltage received by the sensor can be anticipated. Using the above relationship, the soil moisture sensor is calibrated to sense the moisture in soil pores in percentage or as the volumetric water content. Fig. 5. 7 shows the chosen, commercially available blade-shaped capacitive soil moisture sensor v2.0.

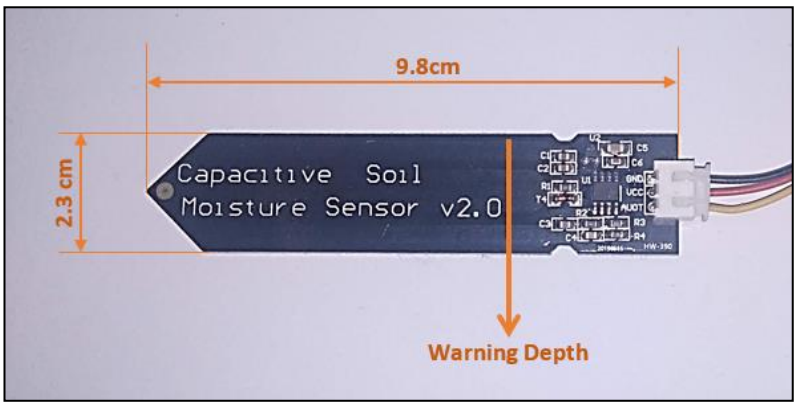

Fig. 5. 7: A capacitive soil moisture sensor v2.0

The most recent and reliable information for the version 2.0 soil moisture sensor developed by DFROBOT and sold under the SKU (stock keeping unit) designation of SEN0193 in various advertisements [178].

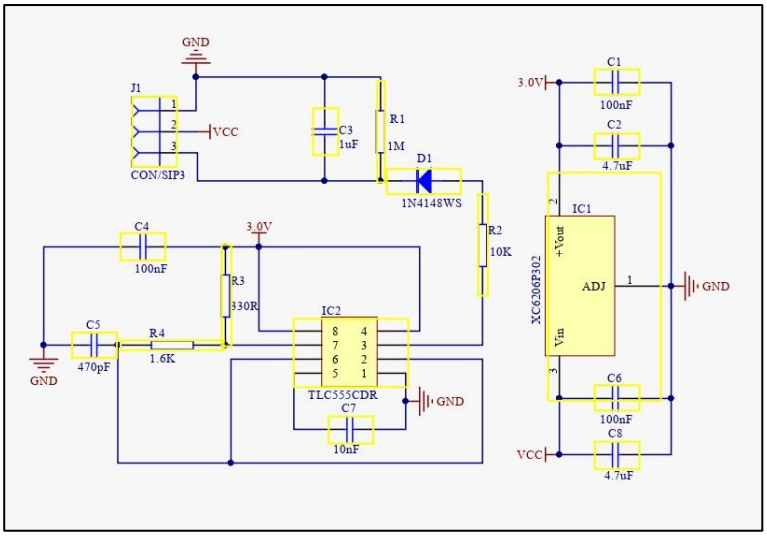

Fig. 5. 8: Circuit diagram of the capacitive sensors [178]

The sensor's datasheet suggests a suitable depth of penetration in soil, a working power supply between 3.3 and 5.5 volts, and an output voltage between 0 and 3.3 volts. Initially, a comprehensive investigation into the sensor's electrical circuits is carried out to get familiar with the functioning mechanism. The circuit diagram of the soil moisture sensor is shown in Fig. 5. 8.

5.2.1.3 Development Board

The development board is like the core of the monitoring system, as all the necessary parts are connected to it. The panel includes a microcontroller for reading and processing sensor values. The board consists of an input pin for analog and digital sensors, a power supply connecting headers, and a USB port to transfer the data. It can also be combined with various modules, like the Wi-Fi module, to transmit the data to the cloud or the memory card module to store it for further analysis. There are three types of boards available, namely Arduino uno board, Arduino nano board, and ESP8266 NodeMCU board, as shown in Fig. 5. 9(a), (b), and (c), respectively. There are three types of board available as shown in Fig. 5. 9.

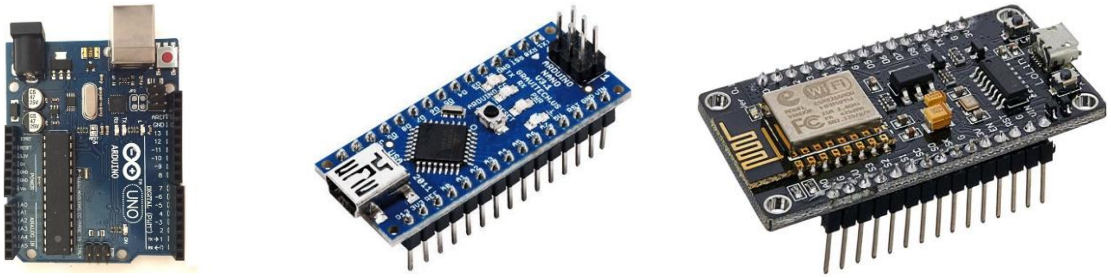

(a) **(b)** **(c)**

Fig. 5. 9: (a) Arduino Uno board, (b) Arduino Nano board, (c) ESP8266 NodeMCU board

5.2.1.4 Power Supply Unit

The power supply unit includes the power supply for all modules in the monitoring system. It consists of a battery with enough capacity of 10k mAh for the uninterrupted working of the system and a solar panel charging system for continuously charging the battery. The solar charging system is equipped with the overcharging protection of the battery to ensure the prolonged battery life.

5.2.1.5 Programming

Programming is the soul of any monitoring system. It communicates a program's intended functionality to a computer through a sequence of instructions. In this system, two types of sensors were used to monitor the landslide mechanism. Programming for the MPU6050 sensor has been done to compute the tilt angle, and any deviation induced by tilting can be recorded with time. The system has the capability to adjust itself by restarting to allow for better visualization. The second sensor is installed to monitor the volumetric water content of the soil, and programming is done to measure the moisture content in terms of percentage with time.

5.2.2 Data Logging Unit

This unit ensures the data collection acquired by the sensor. The data logging module can be attached to the development board using the USB hub or the memory card module to save the data. A Wi-Fi or GSM module can also be connected wirelessly to collect the sensor value on the internet cloud for further analysis. The development board is equipped with a Wi-Fi module to provide internet connectivity in the developed monitoring system. A GSM-based Wi-Fi modem is installed so that several monitoring sensors can be connected using the single modem according to the slope area and location, reducing the cost of individual GSM modules and the connectivity charge. The data collected from the sensors is stored using the Arduino cloud for further analysis.

5.2.3 Analysis Unit

In this section, the data collected from the sensors are analysed for better monitoring of slope movement. As the critical threshold value depends upon the geometry and material of the slope, it varies for individual slopes. After sufficient analysis and monitoring, a warning can be generated for each slope to reduce the catastrophic effects of slope failure by evacuating or strengthening stability.

5.2.4 IoT Based Monitoring System

The emergence of IoT-based monitoring systems represents a transformative advancement in technology and data-driven solutions. These systems utilize interconnected sensors, devices, and networks to gather and analyse data from various domains, including environmental conditions, machinery performance, healthcare metrics, and energy consumption. Their core objective is to offer real-time insights, improve decision-making, and enable proactive responses. Developing these systems requires a combination of hardware, software, and data analytics, often necessitating integration with existing infrastructure and communication networks. Moreover, the development process raises significant concerns regarding data privacy, security, and scalability in today's data-centric era.

In this section, the focus is on the process of measuring tilt angles with the MPU6050 sensor when paired with the NodeMCU ESP8266 board. This can be accomplished through the establishment of a connection between the MPU6050 6-axis Gyro/Accelerometer sensor and the ESP8266. The accelerometer generates X, Y, and Z acceleration data, which must be converted into 3D angles (X, Y, Z) to determine the sensor's 3D orientation. Subsequently, the tilt angle data is transmitted to the Blynk application via the Blynk cloud, facilitating remote monitoring via IoT.

The gyroscope is tasked with measuring the rotational velocity or the rate of change of angular position over time along the X, Y, and Z axes. It utilizes MEMS technology and the Coriolis effect for this purpose. The gyroscope provides outputs in degrees per second, and angular position data is obtained through integration of the angular velocity.

Blynk serves as a versatile application compatible with Android and iOS devices, facilitating control of various IoT applications via smartphones. It empowers users to create graphical user interfaces for IoT applications. In this context, the configuration of the Blynk application is outlined to enable monitoring of MPU6050 tilt angles over Wi-Fi using the NodeMCU ESP8266.

It begins by downloading and installing the Blynk Application from the Google Play Store. For iOS users, the App Store offers the download option. Upon the successful installation of the application, users have to launch and complete the registration process using an email address and password.

After completing the registration, the users have the option to display the values in various formats like gauges. Once the project is created successfully, one can navigate to the settings and

select the “Send Email” option. An authentication ID is received via email which is essential to retain as it is later required in the code.

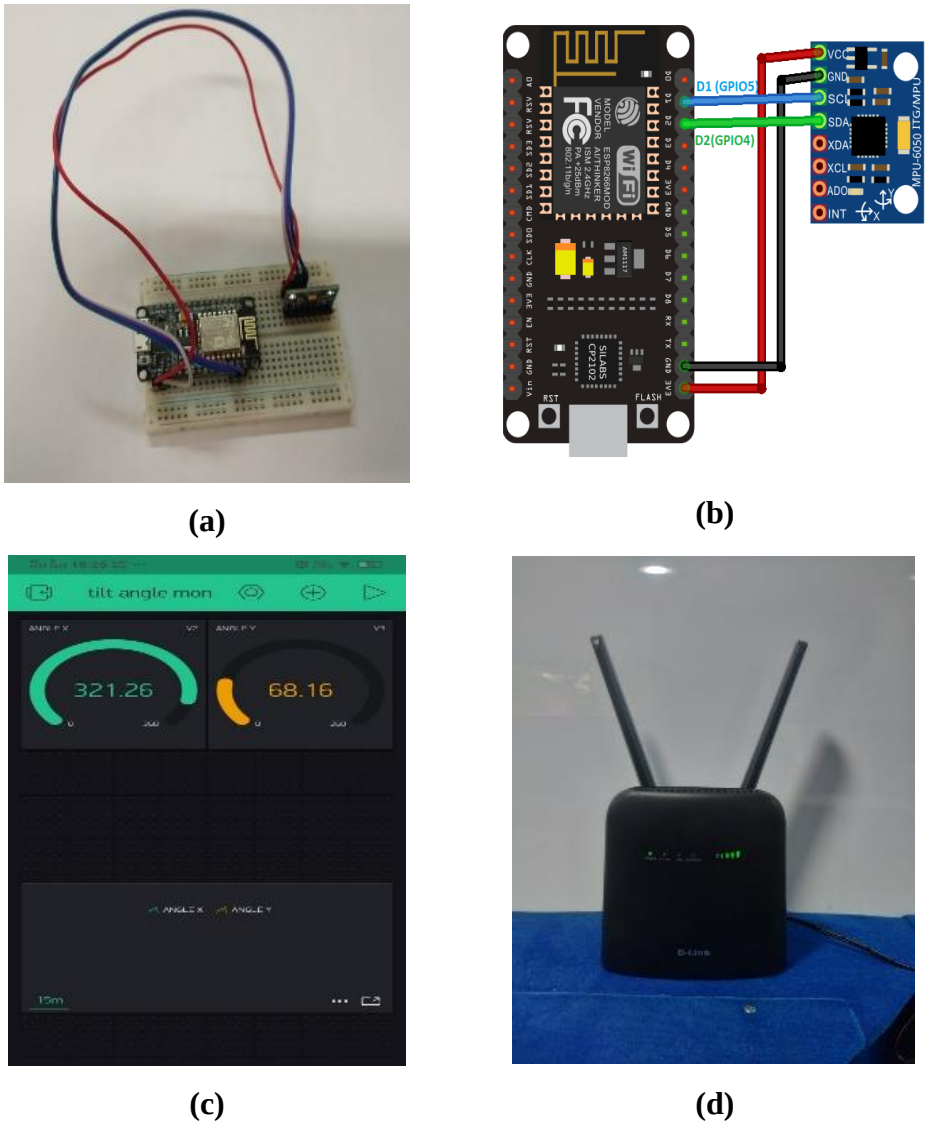

(a) **(b)**

(c) **(d)**

Fig. 5. 10: (a) ESP8266 module, (b) Connection diagram with the MPU6050 sensor, (c) Data transfer via IoT on a mobile device for monitoring and in-depth analysis, and (d) 4G GSM-based Wi-Fi router

Upon uploading the code, the serial monitor gets opened to review the outputs. To detect the angular position along the X, Y, and Z axes, the MPU6050 Gyro/Accelerometer must be tilted accordingly by the user. These tilt angles can also be observed on the computer display.

Given that the MPU6050 ESP8266 is connected to the internet, it will commence the transmission of data to the Blynk Application. The status can be conveniently monitored on the Blynk App, which will display gauges reflecting the changing X, Y, and Z angles.

In this system, wireless data transfer is facilitated using a WiFi module-based microcontroller (ESP8266). For internet connectivity, a GSM-based WiFi router is employed, capable of serving up to 10 devices. This allows for the interconnection of 10 sensor columns, creating an effective grid network for comprehensive slope monitoring at multiple points. Fig. 5. 10a and b depict the circuit diagram showcasing the interface between the MPU6050 Gyro/Accelerometer and the NodeMCU ESP8266. Meanwhile, Fig. 5. 10c illustrates the data reception on a mobile device through an internet connection, and Fig. 5. 10d presents the Wi-Fi module responsible for the internet connectivity of the module.

Previous research utilizing MEMS sensors and IoT-based networks has demonstrated the effectiveness of MEMS sensors and Arduino-based monitoring devices. However, challenges may arise concerning internet connectivity, particularly with modules relying on GSM-based internet connections. In remote locations, issues such as connection loss and missing data may occur. Addressing these issues could involve further development by implementing a more stable network [52], [69], [175], [179]–[181].

5.2.5 Cost Analysis

The developed system offers a cost-effective solution for slope monitoring, enabling users to easily install and oversee it. It incorporates a dedicated GSM-based Wi-Fi module capable of supporting up to 10 devices simultaneously, facilitating seamless data transfer for a grid of 10 sensor columns. This not only enhances monitoring efficiency but also reduces overall costs. The details of the components used and their respective unit prices are presented in Table 5. 2.

This proposed framework represents a comprehensive and budget-friendly solution, leveraging the existing GSM network infrastructure for communication. It is important to note that the framework is currently in a prototype stage, with plans for future deployment in real hillside landslide monitoring scenarios. The proposed cost-effective monitoring system offers a more budget-friendly solution compared to other currently available systems designed for landslide monitoring and early warning purposes [182]–[184].

Table 5. 2: Expenses associated with the materials utilized in creating the IoT framework for monitoring landslides [185]

Component	Cost per unit (in USD)	Quantity	Total cost (in USD)
MPU 6050	1.39	1	1.39
Soil Moisture sensor	0.75	1	0.75
Microcontroller Board	2.36	2	4.72
Wi-Fi Modem	42.14	1	42.14
Breadboard and wires	3.6	1	3.6
Power Supply with solar panel	22.28	1	22.28
Total			74.88

5.3 Methodology

In this chapter, a low-cost monitoring system that comprises a MEMS-based tilt sensor and soil moisture sensor developed to investigate the slope movements monitoring the tilting behaviour is discussed. A self-made testing platform has been designed to test the working of the monitoring system. A series of physical model tests have been conducted to assess the effectiveness of the sensor column monitoring process by evaluating the applied sensor column deformation behaviour with the observed tilt response. Landslide events have been modelled using a direct shear setup simulating first-time landslide failure experiment using a sensor column to analyse the performance of the developed system directly with relative deviation in angle; and the flow chart representing the methodology adopted for the present study is shown in Fig. 5. 11.

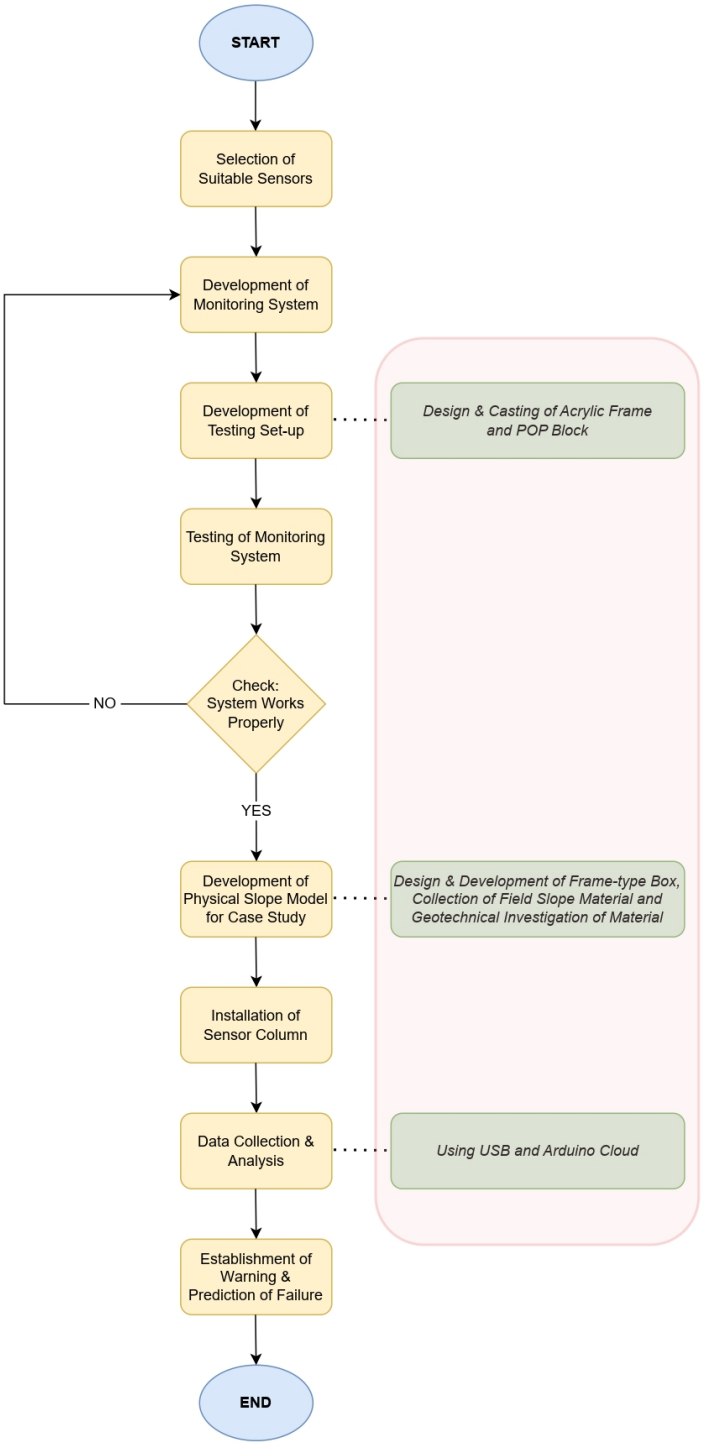

Fig. 5. 11: Flow chart of the development of EWS

5.3.1 Testing Setup

The testing method includes a predefined failure plane for simulating the slope failure to check the working and performance of the developed system. Fig. 5. 12 is the schematic representation of the physical model setup developed for studying slope failure. The setup has been used to analyze the displacement behavior using a tilt measurement by accelerating the top box relative to the bottom box. The setup includes a hydraulic jack to create a horizontal

movement to the upper block against the fixed wall support. The lower block is fixed to restrict any movement. Both blocks have holes throughout the depth where the sensor column is installed. An LVDT (Linear Variable Differential Transformer) sensor is also installed to measure the horizontal deformation induced by the external force applied by the hydraulic jack.

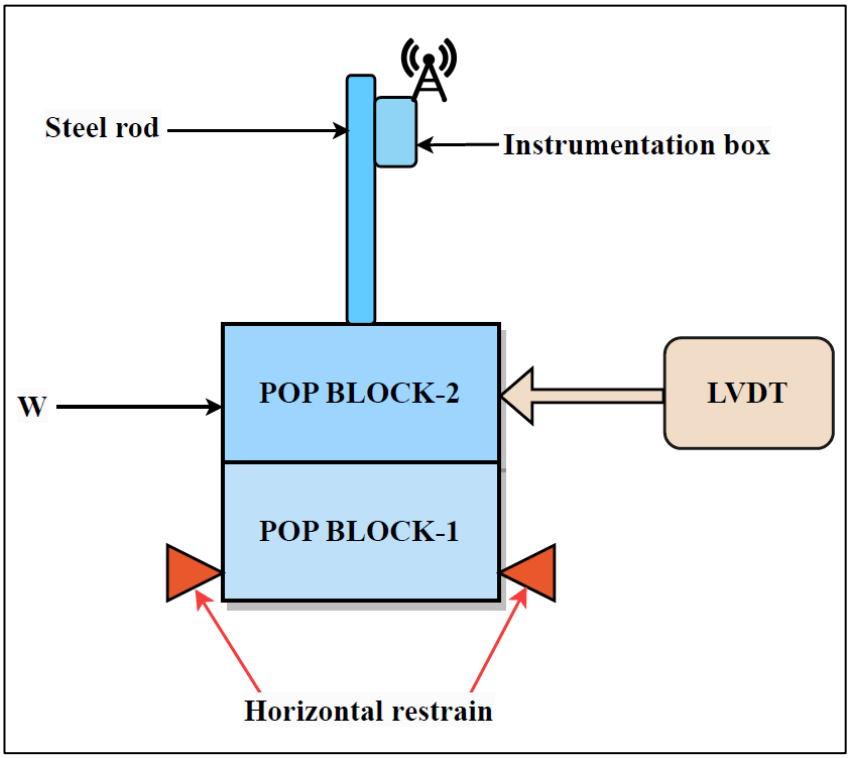

Fig. 5. 12: The schematic diagram of physical model setup

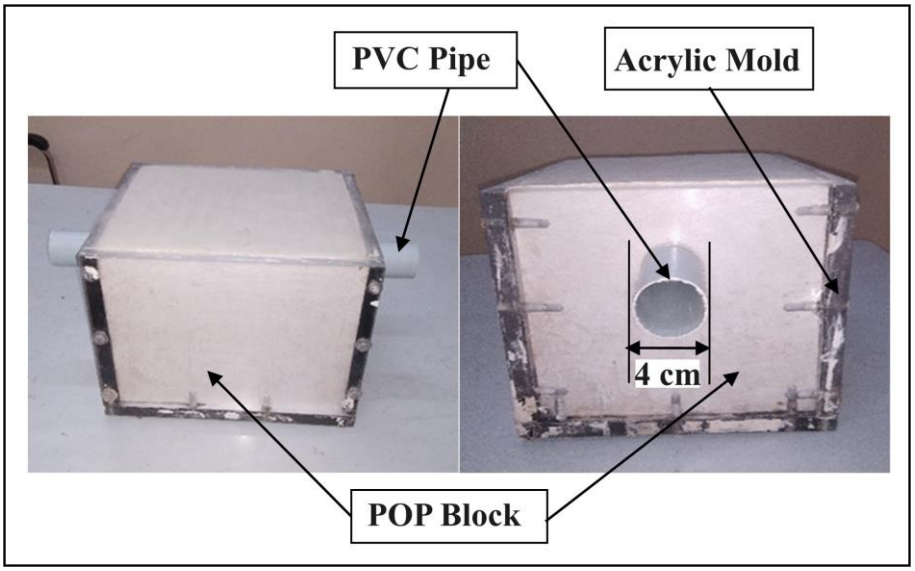

Fig. 5. 13: Casted POP blocks with boreholes of 4 cm

The blocks were made using the Plaster of Paris (POP) material, as it is easy to cast and move around in the lab. The casting was done using a mold of 20 cm × 20 cm × 30 cm made of acrylic sheet, and a hole of 4 cm diameter was made to place a PVC pipe longitudinally to create the borehole in the block for the placement of the sensor column. Fig. 5. 13 shows the casted POP block in a casing made of an acrylic sheet of thickness 18 mm and the borehole created using a plastic pipe of diameter 4 cm.

Fig. 5. 14 shows the components of the self-made block shear model setup comprised of POP blocks, restraining block, hydraulic jack, LVDT and tilt sensors, data logger, and data collection unit. The sensor is installed using the steel rod through the column of soil representing the in-situ soil of a slope. The joint made with POP blocks will act as a predefined failure plane. The lower blocks have been restricted to any movements, while the upper block is free to move when any external force has been applied. The upper block can be considered the failed soil mass, while the lower block is the base of the slab. This sensor has been tested by applying an external force with a hydraulic jack to cause a horizontal relative displacement of the top POP block with respect to the bottom block. The change in angle in the x and y directions is noted for further analysis. The experimental setup is designed in a way that various tests can be performed to evaluate how well the sensor functions under rapidly changing conditions.

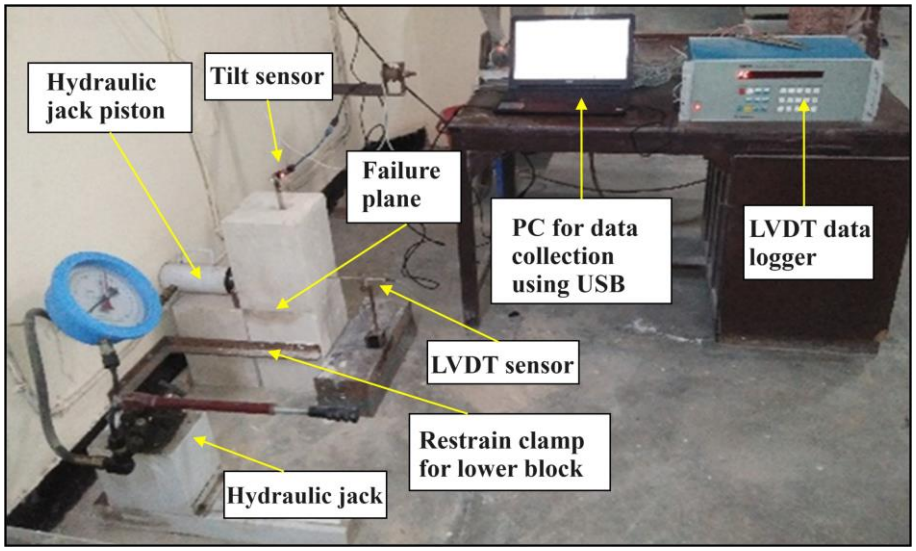

Fig. 5. 14: Self-developed large-scale direct shear setup

5.3.2 Results and Discussions

The findings of this investigation are summarized in this section. The results of the laboratory tests are discussed in greater detail in this article. To better understand the failure mechanism under rainfall, physical slope modelling is used to simulate and investigate the start-up mechanism of the slide. Testing and monitoring results are explained in this section.

5.3.2.1 Results of The Self-Developed Test Setup

The self-developed large-scale direct shear setup is used to test the working behavior of the developed sensor column for slope monitoring and failure prediction. Fig. 5. 15 shows the variation detected by the displacement induced using the hydraulic jack. A very small displacement has been induced to check if the system could detect a small deviation in angle. The maximum angle detected is only 0.5 degrees on the y-axis and 0.1 to 0.2 degrees on the x-axis. The system has some noise and variation in readings, but as it is very low limited to 0.01 to 0.05 degrees only thus can be ignored in further investigations or monitoring for better understanding.

In further testing, the displacement has been increased to a large extent to check the working of the sensor. The displacement recorded through LVDT can be seen in Fig. 5. 16. There is a limitation to the LVDT sensor that it could not measure such large deformation in this phase. Fig. 5. 17 shows the variation of angle when further displacement is introduced to the upper block. It shows that there is a large deviation detected in the y-axis as the slope usually moves downward against the y-axis. However, there is also some movement in the x-direction which can help in better monitoring of the slope.

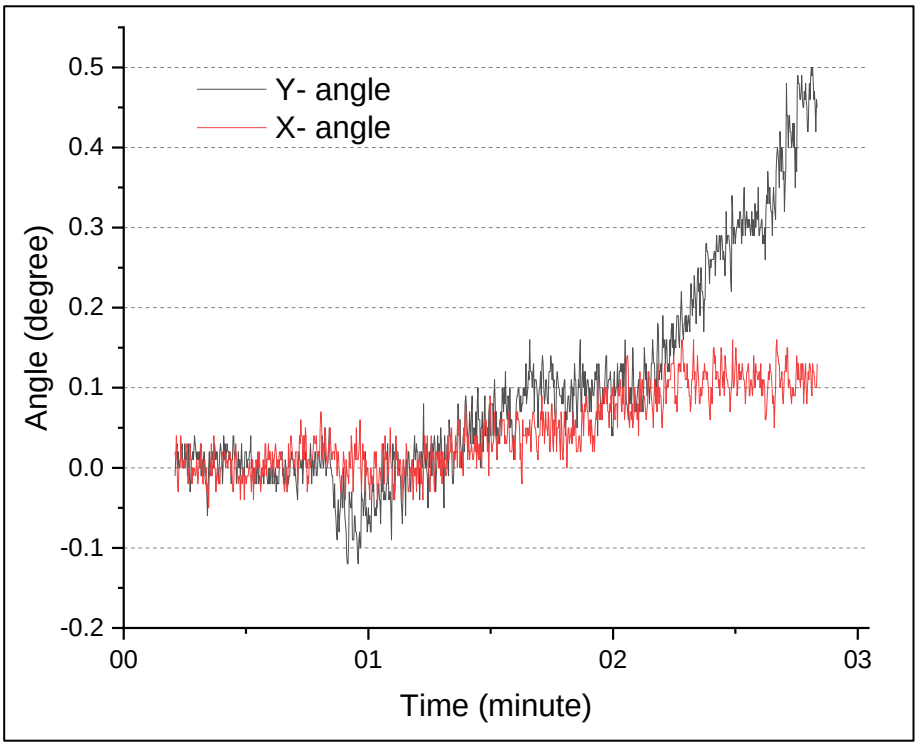

Fig. 5. 15: Variation of angle in X- and Y- direction

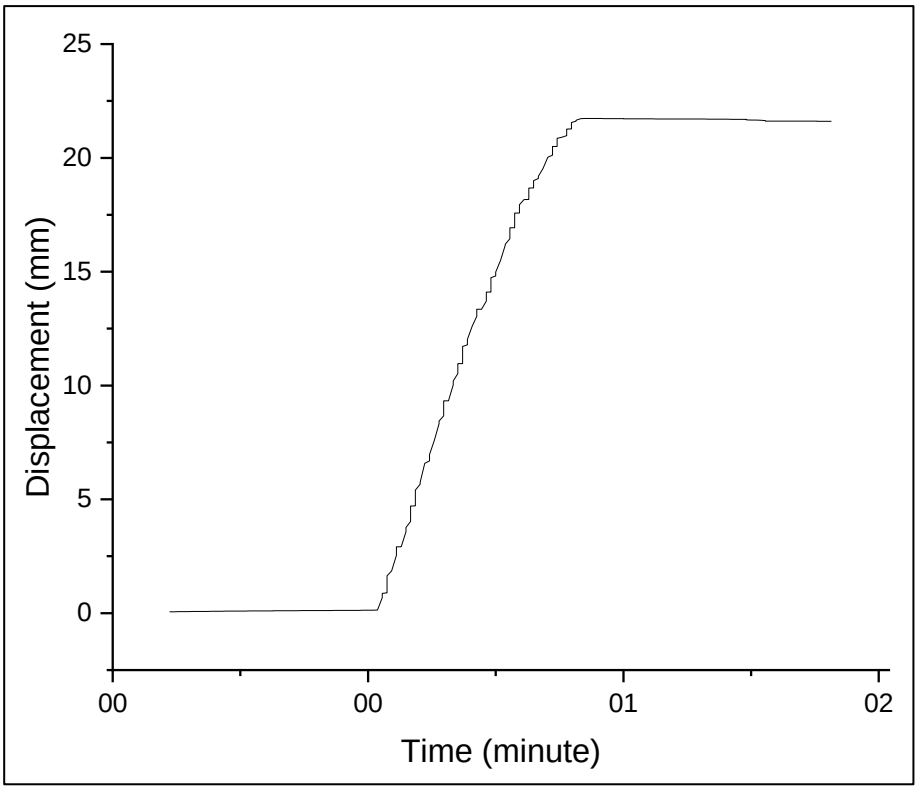

Fig. 5. 16: Linear displacement in X- direction using LVDT

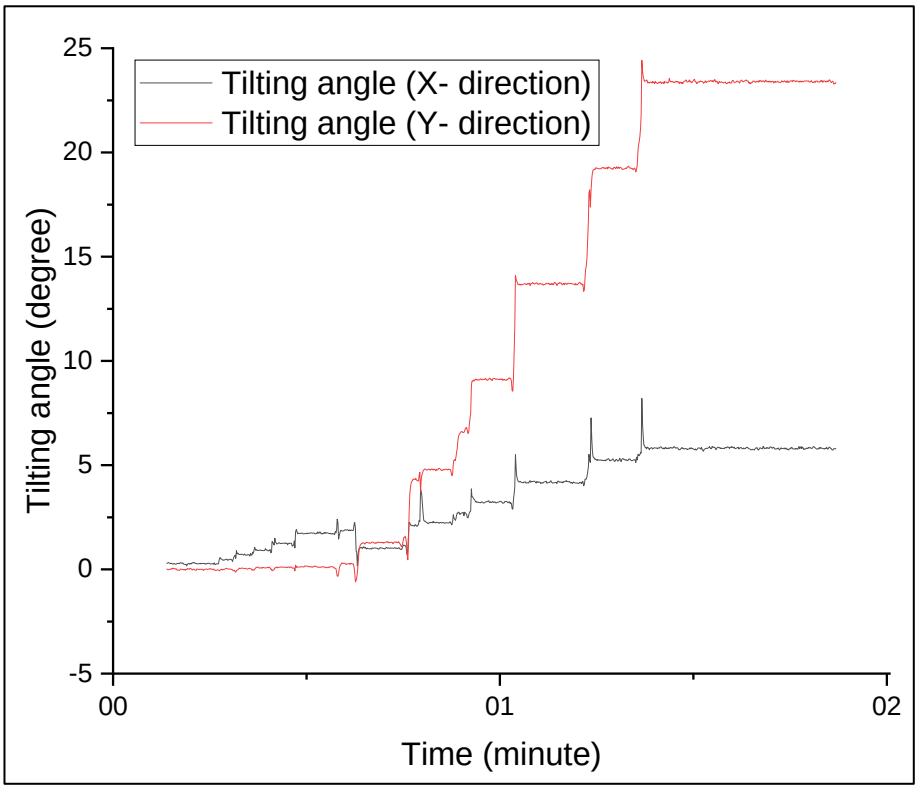

Fig. 5. 17: Variation of angle in X- and Y- direction

This chapter includes the development and testing of the low-cost landslide early warning system. The development is based on the MEMS tilt and soil moisture sensor which connects through the Arduino or NodeMCU boards as per requirements. Bhandari (2006) [66] utilized tilt base monitoring devise for continuous monitoring of rainfall led slides. Ramesh (2014) [68] developed wireless geological sensor network for multi-level LEWS by studying the collected data on rainfall, moisture, PWP, movement and soil properties. Uchimura et al. (2015) [69] also used MEMS based tilt and volumetric water content sensors to study the failure mechanism and the study proved that the MEMS sensor has the capability to effectively monitor the slopes. Intrieri et al. (2018) [72] developed low cost wireless network for ground instability monitoring. The system's limitations include precision (up to 2-5cm with data filtering and averaging) and battery duration (a few weeks with hourly data acquisition, depending on air temperature). Dikshit et al. (2018) [73] also designed a sturdy system using MEMS tilt sensors in conjunction with volumetric water content sensors for the purpose of monitoring both tilting angles and lateral displacement on slope surfaces. Madhusudhan et al. (2018) [74] designed an Arduino-based sensor network technology that can develop large-scale systems for real-time monitoring of landslide-prone areas and give warning signals. Berg et al. (2018) [75] and Dixon et al. (2018) [76] uses acoustic emission techniques to monitor the displacement of slopes. Purnomo et al.

(2019) [78] harnessed the capabilities of soil movement sensors, which effectively transformed spatial changes into stress measurements, and humidity sensors to record moisture levels. These sensors interfaced with a sophisticated 10-bit Analog to Digital Converter (ADC) embedded in the ATmega8535 microcontroller. Ribeiro and Lameiras (2019) [79] and Zhu et al. (2020) [82] also used MEMS based tilt sensor to monitor the slopes but also signifies the improved calibration techniques to improve the monitoring results. In this study the authors tested the developed system in to check its working principle which proved to be an important criterion in development of the respective EWS. Although the developed system has been primarily used only in the laboratory-controlled environment, few researchers [52], [69] also deployed the tilt-based sensors to the field and demonstrated that the developed system effectively records the data for monitoring purposes. The researchers have also asserted the presence of a connectivity issue resulting in the loss of data. Insights and findings of these studies mandate that such issues and limitations must be dealt with and prioritized in future development efforts.

5.4 Summary

The development of a landslide early warning system model is the main goal of this chapter. The following can be stated in accordance with the objectives:

1. The chapter includes the development of a landslide early warning system using low-cost MEMS sensors, such as 3-axis accelerometers and 3-axis gyroscopes, along with volumetric water content sensor. This approach allowed the creation of a cost-effective system utilizing affordable components.
2. A self-developed direct shear model has been used to examine the effectiveness of a rudimentary monitoring system designed. The proposed system achieved the development of a monitoring system with near real-time communication, facilitating continuous data transfer.
3. The monitoring system demonstrated autonomous operation for extended periods without significant issues.

CHAPTER 6

CONCLUSIONS AND RECOMMENDATIONS

6.1 General

The Himalayan region, known as ‘young fold’ and rugged mountains, experiences high rainfall and seismic activity, leading to a significant number of landslides in India, especially during the monsoon season. Factors such as over-exploitation of natural resources, deforestation, population growth, and climate change are expected to contribute to an increase in landslide-related disasters in the region. Despite numerous studies on landslides in the Himalayan region, the problem persists due to their frequent occurrences and severe consequences. Recent studies in India have focused on hazard zoning and establishing rainfall thresholds but often rely on heuristic or statistical methods, neglecting physical parameters and underlying processes.

To address this issue, an extensive study has been conducted to understand the root causes and mechanisms of landslides in the north Himalayan region through geological and geotechnical investigations and field instrumentation. Comprehensive data from various sources, combined with field and laboratory work, have been used to enhance the understanding.

Furthermore, the study introduced an innovative and cost-effective slope monitoring system incorporating MEMS-based tilt and moisture sensors. This system allows real-time data collection on tilt deformations and moisture content and is validated through self-developed direct shear testing and physical slope modelling methods.

6.2 Conclusions

The conclusion of this study based on experimental and numerical studies of rainfall-induced landslides are:

1. By varying the rainfall depth from 10 mm to 100 mm at 10 mm intervals, it has been observed that the slope of study area-I, underwent debris flow-type failure when the rainfall depth reached 80 mm with an intensity of 30 mm/hr. This conclusion highlights

the usefulness of physical model methods in determining critical thresholds and helps understand the failure mechanism of rainfall-induced landslides.

2. The adopted high intensity rainfall of 30 mm/hr has caused a notable impact on the slope. When rainfall is more intense, a significant portion of the rainwater infiltrates the soil on the hillslope. As a result, the water table rises, causing a noticeable decrease in the soil's strength. Consequently, higher intensity rainfall contributes significantly to the destabilization of the slope.

3. In the Jhakri study area, numerical modelling has been conducted on a slope with a 35° angle. Initially, the slope was stable, with a Factor of Safety (FOS) of 1.23. However, when subjected to rainfall with an intensity of 30 mm/hr, the FOS decreased to 0.626, signifying slope failure. Similarly, for the Kotrupi study area, where the slope angle was 47° under dry conditions, the FOS was 1.045. After the input rainfall, the FOS dropped to 0.670. These modelling results align with the outcomes observed in physical modelling, thereby validating the findings of the physical modelling.

4. The study proved that both gentle and steep slopes may fail to the influence of rainfall, confirming that rainfall is the primary triggering factor for landslides in the North Himalayan region, encompassing shallow and deep-seated failures across varying rainfall conditions. The results offer valuable insights in understanding the mechanism of rainfall-induced failure of landmass.

5. The tilt and volumetric water content sensors employed in the developed early warning and monitoring system provide accurate and precise measurements. The tilt sensor records even the slightest changes in the slope angle with a precision of 0.01 degree, enabling early detection of slope movement. Additionally, the volumetric water content sensor can detect percentage variations with a precision of 1 percent. aiding in the identification of critical conditions that could lead to landslides.

6. The results of physical modelling of the Jhakri landslide incorporating the use of tilt and moisture sensors indicated that the slope failed when subjected to significant moisture fluctuations and abrupt tilting, with a recorded tilt of approximately 3 degrees on the y-axis and around 2 degrees on the x-axis. This confirms the accuracy and working capabilities of the developed early warning and monitoring system.

7. The development of the IoT system, enables real-time data collection and monitoring for remote locations which are not easily accessible. The developed early warning and monitoring system facilitates real-time monitoring of slope conditions, allowing for prompt response and mitigation measures in the event of detected instabilities. The sensors of the developed IoT based landslide monitoring system transmit data wirelessly to a central monitoring station, enabling timely decision-making and minimizing potential risks associated with landslides.

8. The developed early warning system, designed for identifying impending slope failures, utilized a combination of tilt angle and moisture content variations. Through continuous monitoring, the system observed a gradual shift in the tilt angle of the slope over a two-hour period, displaying a variation ranging from approximately 0.5 degrees to 1.5 degrees. This specific range can be served as a predefined warning threshold. At the crucial second-hour mark, coinciding with the slope failure, there was a sudden and notable deviation 3 degrees to 3.5 degrees in the tilt angle.

9. The soil moisture sensor integrated into the system exhibited substantial variations of approximately 40% during periods of rainfall. These variations signalled a notable rise in soil saturation, reaching up to 95%, suggesting that elevated moisture levels may serve as a potential triggering factor for slope failure.

10. The developed low-cost monitoring system is a cost-effective solution for landslide monitoring compared to existing methods. The utilization of tilt and volumetric water content sensors allows for a more targeted and efficient monitoring approach, minimizing unnecessary expenses associated with complex monitoring systems.

6.3 Recommendations and Future Scope

Based on the findings of the current study, some critical recommendation in the existing guidelines and for monitoring of slopes as apart of early warning system for landslides are proposed in this section. Further, certain constraints of the present study are listed with prospective domains for future research.

1. In terms of the relative contributions of various causative factors to landslide hazards given in IS14496 part 2, the hydrological condition attribute is assigned only a 10% weight, alongside parameters such as lithology and land use/land cover (LULC). However, the significant findings of the current study sharply contrast with this

understanding, emphasizing that hydrological conditions, particularly rainfall, play a substantially more critical role in greatly amplifying vulnerability and subsequently leading to increased landslide occurrences, especially during the monsoonal seasons.

2. The implemented warning system can be field-tested on a natural slope for ongoing, real-time monitoring to evaluate its performance. Since the sensor is cost-effective, it can be deployed in numerous quantities across extensive slopes, enabling comprehensive spatial monitoring and ensuring accurate and effective surveillance to issue timely warnings and mitigate landslide disasters.

3. Uniform values were used for the geotechnical input parameters and applied rainfall across the entire study area. However, to enhance the realism of the study, it would be valuable to account for the spatial variations in geotechnical and hydrological characteristics at a regional scale.

4. It is possible to integrate numerous additional MEMS-based sensors, considering the contributing elements of landslides, in order to acquire more precise and targeted information. This approach enhances the comprehension of landslide mechanisms and strengthens the efficacy of early warning systems.

5. A variety number of physical modeling test can be employed in conjunction with tilt sensors to establish more accurate tilting thresholds, thereby enhancing the effectiveness of landslide failure warnings.

REFERENCES

[1] P. J. and A. N. Nirmala Jain, Priyom Roy, Tapas Ranjan Martha, "Landslide Atlas of India (Mapping, monitoring and advance techniques using space-based inputs)," 2023. [Online]. Available: https://www.isro.gov.in/media_isro/pdf/LandslideAtlas_2023.pdf.

[2] Geological Survey of India, "Landslide hazard zonation map of India," 2021. https://hpsdma.nic.in//admnis/admin/showimg.aspx?ID=1229 (accessed Sep. 10, 2021).

[3] S. Joshi, K. Kumar, V. Joshi, and B. Pande, "Rainfall variability and indices of extreme rainfall-analysis and perception study for two stations over Central Himalaya, India," *Nat. Hazards*, vol. 72, no. 2, pp. 361–374, 2014, doi: 10.1007/s11069-013-1012-4.

[4] M. T. Abraham, D. Pothuraju, and N. Satyam, "Rainfall thresholds for prediction of landslides in Idukki, India: An empirical approach," *Water (Switzerland)*, vol. 11, no. 10, 2019, doi: 10.3390/w11102113.

[5] P. Mandal and S. Sarkar, "Estimation of rainfall threshold for the early warning of shallow landslides along National Highway-10 in Darjeeling Himalayas," *Nat. Hazards*, vol. 105, no. 3, pp. 2455–2480, 2021, doi: 10.1007/s11069-020-04407-9.

[6] A. Dikshit, N. Satyam, B. Pradhan, and S. Kushal, "Estimating rainfall threshold and temporal probability for landslide occurrences in Darjeeling Himalayas," *Geosci. J.*, vol. 24, no. 2, pp. 225–233, 2020, doi: 10.1007/s12303-020-0001-3.

[7] R. K. Dahal and S. Hasegawa, "Representative rainfall thresholds for landslides in the Nepal Himalaya," *Geomorphology*, vol. 100, no. 3–4, pp. 429–443, 2008, doi: 10.1016/j.geomorph.2008.01.014.

[8] H. Rahardjo, T. H. Ong, R. B. Rezaur, and E. C. Leong, "Factors Controlling Instability of Homogeneous Soil Slopes under Rainfall," *J. Geotech. Geoenvironmental Eng.*, vol. 133, no. 12, pp. 1532–1543, 2007, doi: 10.1061/(asce)1090-0241(2007)133:12(1532).

[9] R. L. Baum and J. W. Godt, "Early warning of rainfall-induced shallow landslides and debris flows in the USA," *Landslides*, vol. 7, no. 3, pp. 259–272, 2010, doi: 10.1007/s10346-009-0177-0.

[10] D. G. Fredlund, H. Rahardjo, and M. D. Fredlund, *Unsaturated Soil Mechanics in Engineering Practice*. 2012.

[11] J. W. Godt, R. L. Baum, and N. Lu, "Landsliding in partially saturated materials," *Geophys. Res. Lett.*, vol. 36, no. 2, 2009, doi: 10.1029/2008GL035996.

[12] G. Zhang, R. Wang, J. Qian, J. M. Zhang, and J. Qian, "Effect study of cracks on behavior of soil slope under rainfall conditions," *Soils Found.*, vol. 52, no. 4, pp. 634–643, 2012, doi: 10.1016/j.sandf.2012.07.005.

[13] L. M. Highland, "The Landslide Handbook-A Guide to Understanding Landslides," *US Geol. Surv. Reston.*, pp. 4–42, 2008, [Online]. Available: http://landslides.usgs.gov/.

[14] ANI, “Landslide on Chaura to Wangtu National Highway,” 2023. https://www.aninews.in/news/national/general-news/himachal-pradesh-vehicular-movement-from-chaura-to-wangtu-national-highway-restored-after-landslide20230714185016/ (accessed Sep. 10, 2023).

[15] ANI, “NH-5 blocked in Shimla districts,” 2023. https://www.aninews.in/news/national/general-news/nh-5-blocked-in-three-areas-of-shimla-and-kinnaur-districts20230723112018/ (accessed Sep. 10, 2023).

[16] ANI, “Gangotri NH blocked due to landslide,” 2023. https://www.aninews.in/news/national/general-news/uttarakhand-gangotri-nh-blocked-due-to-landslide-restoration-underway20230720083843/ (accessed Sep. 10, 2023).

[17] ANI, “Mandi-Kullu National Highway blocked,” 2023. https://www.aninews.in/news/national/general-news/mandi-kullu-national-highway-blocked-other-routes-affected-himachal-traffic-police20230718225309/ (accessed Sep. 10, 2023).

[18] ANI, “Raigad (Maharashtra) landslide,” 2023. https://www.aninews.in/news/national/general-news/maharashtra-ndrf-calls-off-rescue-operation-in-raigad-death-toll-stays-at-2720230723232901/ (accessed Sep. 10, 2023).

[19] ANI, “Landslides in Kathua (Jammu and Kashmir),” 2023. https://www.aninews.in/news/national/general-news/j-k-8-killed-in-floods-landslides-in-upper-reaches-of-kathua20230719143935/ (accessed Sep. 10, 2023).

[20] A. Dikshit, R. Sarkar, B. Pradhan, S. Segoni, and A. M. Alamri, “Rainfall induced landslide studies in indian himalayan region: A critical review,” *Appl. Sci.*, vol. 10, no. 7, 2020, doi: 10.3390/app10072466.

[21] D. P. Kanungo and S. Sharma, “Rainfall thresholds for prediction of shallow landslides around Chamoli-Joshimath region, Garhwal Himalayas, India,” *Landslides*, vol. 11, no. 4, pp. 629–638, 2014, doi: 10.1007/s10346-013-0438-9.

[22] E. Can, “Investigation of landslide potential parameters on Zonguldak-Ereğli Highway and adverse effects of landslides in the region,” *Environ. Monit. Assess.*, vol. 186, no. 4, pp. 2435–2447, 2014, doi: 10.1007/s10661-013-3550-3.

[23] T. S. Teja, A. Dikshit, and N. Satyam, “Determination of rainfall thresholds for landslide prediction using an algorithm-based approach: Case study in the Darjeeling Himalayas, India,” *Geosci.*, vol. 9, no. 7, 2019, doi: 10.3390/geosciences9070302.

[24] A. Dikshit, R. Sarkar, and N. Satyam, “Probabilistic approach toward Darjeeling Himalayas landslides-A case study,” *Cogent Eng.*, vol. 5, no. 1, pp. 1–11, 2018, doi: 10.1080/23311916.2018.1537539.

[25] Y. Chen, B. Li, Y. Xu, Y. Zhao, and J. Xu, “Field Study on the Soil Water Characteristics of Shallow Layers on Red Clay Slopes and Its Application in Stability Analysis,” *Arab. J. Sci. Eng.*, vol. 44, no. 5, pp. 5107–5116, 2019, doi: 10.1007/s13369-018-03716-3.

[26] F. Guzzetti, S. Peruccacci, M. Rossi, and C. P. Stark, “The rainfall intensity-duration control of shallow landslides and debris flows: An update,” *Landslides*, vol. 5, no. 1, pp. 3–17, 2008, doi: 10.1007/s10346-007-0112-1.

[27] M. T. Abraham, N. Satyam, A. Rosi, B. Pradhan, and S. Segoni, “The Selection of rain gauges and rainfall parameters in estimating intensity-duration thresholds for landslide occurrence: Case study from Wayanad (India),” *Water (Switzerland)*, vol. 12, no. 4, 2020, doi: 10.3390/W12041000.

[28] S. Lari, P. Frattini, and G. B. Crosta, “A probabilistic approach for landslide hazard analysis,” *Eng. Geol.*, vol. 182, no. PA, pp. 3–14, 2014, doi: 10.1016/j.enggeo.2014.07.015.

[29] T. Glade, M. Crozier, and P. Smith, “Applying probability determination to refine landslide-triggering rainfall thresholds using an empirical ‘Antecedent Daily Rainfall Model,’” *Pure Appl. Geophys.*, vol. 157, no. 6–8, pp. 1059–1079, 2000, doi: 10.1007/s000240050017.

[30] M. T. Abraham, N. Satyam, B. Pradhan, and A. M. Alamri, “Forecasting of landslides using rainfall severity and soil wetness: A probabilistic approach for Darjeeling Himalayas,” *Water (Switzerland)*, vol. 12, no. 3, pp. 1–19, 2020, doi: 10.3390/w12030804.

[31] R. Tufano, M. Cesarano, F. Fusco, and P. De Vita, “Probabilistic approaches for assessing rainfall thresholds triggering shallow landslides. The study case of the peri-vesuvian area (Southern Italy),” *Ital. J. Eng. Geol. Environ.*, vol. 2019, no. Special Issue 1, pp. 105–110, 2019, doi: 10.4408/IJEGE.2019-01.S-17.

[32] G. Capparelli and D. Tiranti, “Application of the MoniFLaIR early warning system for rainfall-induced landslides in Piedmont region (Italy),” *Landslides*, vol. 7, no. 4, pp. 401–410, 2010, doi: 10.1007/s10346-009-0189-9.

[33] A. Dikshit and N. Satyam, “Application of FLaIR model for early warning system in Chibo Pashyor, Kalimpong, India for rainfall-induced landslides,” *Nat. Hazards Earth Syst. Sci.*, no. August, pp. 1–18, 2017, doi: 10.5194/nhess-2017-295.

[34] S. Panchal and A. K. Shrivastava, “A comparative study of frequency ratio, shannon’s entropy and analytic hierarchy process (Ahp) models for landslide susceptibility assessment,” *ISPRS Int. J. Geo-Information*, vol. 10, no. 9, 2021, doi: 10.3390/ijgi10090603.

[35] S. N. Selamat, N. A. Majid, M. R. Taha, and A. Osman, “Application of geographical information system (GIS) using artificial neural networks (ANN) for landslide study in Langat Basin, Selangor,” *IOP Conf. Ser. Earth Environ. Sci.*, vol. 1064, no. 1, 2022, doi: 10.1088/1755-1315/1064/1/012052.

[36] S. Panchal and A. K. Shrivastava, “Landslide hazard assessment using analytic hierarchy process (AHP): A case study of National Highway 5 in India,” *Ain Shams Eng. J.*, vol. 13, no. 3, p. 101626, 2022, doi: 10.1016/j.asej.2021.10.021.

[37] S. Panchal and A. K. Shrivastava, “Application of analytic hierarchy process in landslide susceptibility mapping at regional scale in GIS environment,” *J. Stat. Manag. Syst.*, vol. 23, no. 2, pp. 199–206, 2020, doi: 10.1080/09720510.2020.1724620.

[38] B. Pradhan, H. A. H. Al-Najjar, M. I. Sameen, M. R. Mezaal, and A. M. Alamri, “Landslide Detection Using a Saliency Feature Enhancement Technique from LiDAR-Derived DEM and Orthophotos,” *IEEE Access*, vol. 8, no. July, pp. 121942–121954, 2020, doi: 10.1109/ACCESS.2020.3006914.

[39] N. Singh, S. K. Gupta, and D. P. Shukla, “Analysis of landslide reactivation using satellite data: a case study of Kotrupi landslide, Mandi, Himachal Pradesh, India,” *Int. Arch. Photogramm. Remote Sens. Spat. Inf. Sci. - ISPRS Arch.*, vol. 42, no. 3/W11, pp. 137–142, 2020, doi: 10.5194/isprs-archives-XLII-3-W11-137-2020.

[40] B. Tiwari and B. Ajmera, “Physical Modelling of Rain-Induced Landslides,” pp. 277–285, 2018.

[41] V. Matziaris, A. M. Marshall, C. M. Heron, and H. S. Yu, “Centrifuge model study of thresholds for rainfall-induced landslides in sandy slopes,” *IOP Conf. Ser. Earth Environ. Sci.*, vol. 26, no. 1, 2015, doi: 10.1088/1755-1315/26/1/012032.

[42] C. Li *et al.*, “Model test on rainfall-induced loess–mudstone interfacial landslides in Qingshuihe, China,” *Environ. Earth Sci.*, vol. 75, no. 9, pp. 1–18, 2016, doi: 10.1007/s12665-016-5658-6.

[43] X. Huang and Y. Dong, “Study on Physical and Mechanical Properties of Soil in a Loess Landslide,” *J. Phys. Conf. Ser.*, vol. 2424, no. 1, p. 012010, 2023, doi: 10.1088/1742-6596/2424/1/012010.

[44] K. P. Acharya, N. P. Bhandary, R. K. Dahal, and R. Yatabe, “Seepage and slope stability modelling of rainfall-induced slope failures in topographic hollows,” *Geomatics, Nat. Hazards Risk*, vol. 7, no. 2, pp. 721–746, 2016, doi: 10.1080/19475705.2014.954150.

[45] A. K. Singh, J. Kundu, and K. Sarkar, “Stability analysis of a recurring soil slope failure along NH-5, Himachal Himalaya, India,” *Nat. Hazards*, vol. 90, no. 2, pp. 863–885, 2018, doi: 10.1007/s11069-017-3076-z.

[46] A. P. Paswan and A. K. Shrivastava, “Stability analysis of rainfall-induced landslide,” in *3rd International Online Conference on Emerging Trends in Multi-Disciplinary Research “ETMDR-2022,”* 2022, no. January, pp. 505–509.

[47] A. P. Paswan and A. K. Shrivastava, “Numerical modelling of rainfall-induced landslide,” in *International e-Conference on Sustainable Development & Recent Trends in Civil Engineering*, 2022, no. January, pp. 8–13.

[48] F. Jing, H. S. Ling, D. Xiuli, and W. Jinlong, “Influence of rainfall on transient seepage field of deep landslides: A case study of area II of Jinpingzi landslide,” *IOP Conf. Ser. Earth Environ. Sci.*, vol. 570, no. 2, 2020, doi: 10.1088/1755-1315/570/2/022056.

[49] R. Tufano, G. Formetta, D. Calcaterra, and P. De Vita, “Hydrological control of soil thickness spatial variability on the initiation of rainfall-induced shallow landslides using a three-dimensional model,” *Landslides*, vol. 18, no. 10, pp. 3367–3380, 2021, doi: 10.1007/s10346-021-01681-x.

[50] R. K. Dahal, S. Hasegawa, A. Nonomura, M. Yamanaka, T. Masuda, and K. Nishino, “Failure characteristics of rainfall-induced shallow landslides in granitic terrains of Shikoku Island of Japan,” *Environ. Geol.*, vol. 56, no. 7, pp. 1295–1310, 2009, doi: 10.1007/s00254-008-1228-x.

[51] E. Intrieri, G. Gigli, F. Mugnai, R. Fanti, and N. Casagli, “Design and implementation of a landslide early warning system,” *Eng. Geol.*, vol. 147–148, pp. 124–136, 2012, doi: 10.1016/j.enggeo.2012.07.017.

[52] M. T. Abraham, N. Satyam, B. Pradhan, and A. M. Alamri, “Iot-based geotechnical monitoring of unstable slopes for landslide early warning in the Darjeeling Himalayas,” *Sensors (Switzerland)*, vol. 20, no. 9, 2020, doi: 10.3390/s20092611.

[53] T. Uchimura *et al.*, “Simple monitoring method for precaution of landslides watching tilting and water contents on slopes surface,” *Landslides*, vol. 7, no. 3, pp. 351–357, 2010, doi: 10.1007/s10346-009-0178-z.

[54] S. Qiao *et al.*, “Investigation on surface tilting in the failure process of shallow landslides,” *Sensors (Switzerland)*, vol. 20, no. 9, 2020, doi: 10.3390/s20092662.

[55] A. Goyal and A. K. Shrivastava, “A novel heuristic and tunicate centered ANFIS and RCCRD optimization for soil nailing using a numerical approach,” *Soil Dyn. Earthq. Eng.*, vol. 176, no. October 2023, p. 108289, 2024, doi: 10.1016/j.soildyn.2023.108289.

[56] A. Goyal and A. K. Shrivastava, “Optimization of helical soil nailing behaviors by response surface methodology and hybrid Coot optimization,” *Int. J. Numer. Anal. Methods Geomech.*, vol. 47, no. 9, pp. 1658–1680, 2023, doi: https://doi.org/10.1002/nag.3533.

[57] A. Goyal and A. K. Shrivastava, “Analysis of conventional and helical soil nails using finite element method and limit equilibrium method,” *Heliyon*, vol. 8, no. 11, p. e11617, 2022, doi: 10.1016/j.heliyon.2022.e11617.

[58] K. Ben Sim, M. L. Lee, and S. Y. Wong, “A review of landslide acceptable risk and tolerable risk,” *Geoenvironmental Disasters*, vol. 9, no. 1, 2022, doi: 10.1186/s40677-022-00205-6.

[59] L. M. Lee, A. Kassim, and N. Gofar, “Performances of two instrumented laboratory models for the study of rainfall infiltration into unsaturated soils,” *Eng. Geol.*, vol. 117, no. 1–2, pp. 78–89, 2011, doi: 10.1016/j.enggeo.2010.10.007.

[60] R. L. Bates and J. A. Jackson, “Glossary of Geology,” *Am. Geol. Inst.*, p. 788, 1987.

[61] D. Cruden and D. Varnes, “Landslide Types and Processes, Transportation Research Board, US National Academy of Sciences, Special Report,” *Landslides Eng. Pr.*, vol. 24, no. December, pp. 20–47, 1996.

[62] M. J. Crozier, “Landslides,” in *Environmental Geology*, Dordrecht: Springer Netherlands, 1999, pp. 371–375.

[63] D.J Varnes, “Slope Movement types and Processes,” *Spec. Rep.*, pp. 68 & 76, 1978.

[64] D. M. Cruden and D. Varnes, “Landslide Types and Processes, Transportation Research Board, US National Academy of Sciences, Special Report, 247: 36-75,” *Landslides Eng. Pr.*, vol. 24, no. December, pp. 20–47, 1996.

[65] R. Von Huene, J. J. Miller, and P. Dartnell, “A possible transoceanic tsunami directed toward the U.S. west coast from the Semidi segment, Alaska convergent margin,” *Geochemistry, Geophys. Geosystems*, vol. 17, no. 3, pp. 645–659, 2016, doi: 10.1002/2015GC006147.

[66] R. K. Bhandari, “The Indian Landslide Scenario, Strategic Issues and Action Points,” *First India Disaster Manag. Congr.*, no. November, pp. 29–30, 2006.

[67] H. Alcik, O. Ozel, N. Apaydin, and M. Erdik, “A study on warning algorithms for Istanbul earthquake early warning system,” *Geophys. Res. Lett.*, vol. 36, no. 5, pp. 3–5, 2009, doi: 10.1029/2008GL036659.

[68] M. V. Ramesh, “Design, development, and deployment of a wireless sensor network for detection of landslides,” *Ad Hoc Networks*, vol. 13, no. PART A, pp. 2–18, 2014, doi: 10.1016/j.adhoc.2012.09.002.

[69] T. Uchimura *et al.*, “Precaution and early warning of surface failure of slopes using tilt sensors,” *Soils Found.*, vol. 55, no. 5, pp. 1086–1099, 2015, doi: 10.1016/j.sandf.2015.09.010.

[70] S. Biansoongnern, B. Plungkang, and S. Susuk, “Development of Low Cost Vibration Sensor Network for Early Warning System of Landslides,” *Energy Procedia*, vol. 89, pp. 417–420, 2016, doi: 10.1016/j.egypro.2016.05.055.

[71] J. A. Smethurst *et al.*, “Current and future role of instrumentation and monitoring in the performance of transport infrastructure slopes,” *Q. J. Eng. Geol. Hydrogeol.*, vol. 50, no. 3, pp. 271–286, 2017, doi: 10.1144/qjegh2016-080.

[72] E. Intrieri *et al.*, “Application of an ultra-wide band sensor-free wireless network for ground monitoring,” *Eng. Geol.*, vol. 238, no. March 2017, pp. 1–14, 2018, doi: 10.1016/j.enggeo.2018.02.017.

[73] A. Dikshit, D. N. Satyam, and I. Towhata, “Early warning system using tilt sensors in Chibo, Kalimpong, Darjeeling Himalayas, India,” *Nat. Hazards*, vol. 94, no. 2, pp. 727–741, 2018, doi: 10.1007/s11069-018-3417-6.

[74] Y. V Madhusudhan, D. Alfred, and B. Kavyashree, “Landslide and Rockslide Detection System with Landslide Early Warning System for Railways,” vol. 6, no. 13, pp. 1–9, 2018.

[75] N. Berg, A. Smith, S. Russell, N. Dixon, D. Proudfoot, and W. Andy Take, “Correlation of acoustic emissions with patterns of movement in an extremely slow-moving landslide at Peace River, Alberta, Canada,” *Can. Geotech. J.*, vol. 55, no. 10, pp. 1475–1488, 2018, doi: 10.1139/cgj-2016-0668.

[76] N. Dixon, A. Smith, J. A. Flint, R. Khanna, B. Clark, and M. Andjelkovic, “An acoustic emission landslide early warning system for communities in low-income and middle-income countries,” *Landslides*, vol. 15, no. 8, pp. 1631–1644, 2018, doi: 10.1007/s10346-018-0977-1.

[77] H. Kaur, S. Gupta, S. Parkash, R. Thapa, and A. Gupta, “Annals of GIS Evaluation of landslide susceptibility in a hill city of Sikkim Himalaya with the perspective of hybrid modelling techniques,” *Ann. GIS*, vol. 0, no. 0, pp. 1–20, 2019, doi: 10.1080/19475683.2019.1575906.

[78] F. A. Purnomo, N. M. Yoeseph, and G. W. Abisatya, “Landslide early warning system based on arduino with soil movement and humidity sensors Landslide early warning system based on arduino with soil movement and humidity sensors,” 2019, doi: 10.1088/1742-6596/1153/1/012034.

[79] R. R. Ribeiro and R. de M. Lameiras, “Evaluation of low-cost MEMS accelerometers for SHM: Frequency and damping identification of civil structures,” *Lat. Am. J. Solids Struct.*, vol. 16, no. 7 CILAMCE 2018, pp. 1–24, 2019, doi: 10.1590/1679-78255308.

[80] J. L. Soler-Llorens, J. J. Galiana-Merino, J. J. Giner-Caturla, S. Rosa-Cintas, and B. Y. Nassim-Benabdeloued, "Geophonino-W: A wireless multichannel seismic noise recorder system for array measurements," *Sensors (Switzerland)*, vol. 19, no. 19, 2019, doi: 10.3390/s19194087.

[81] O. Kafadar, "A geophone-based and low-cost data acquisition and analysis system designed to microtremor measurements," *Geosci. Instrumentation, Methods Data Syst. Discuss.*, no. 2016, pp. 1–10, 2020, doi: 10.5194/gi-2020-11.

[82] J. Zhu, W. Wang, S. Huang, and W. Ding, "An improved calibration technique for mems accelerometer-based inclinometers," *Sensors (Switzerland)*, vol. 20, no. 2, 2020, doi: 10.3390/s20020452.

[83] V. Supekar, P. Mote, P. Lohokane, and V. N.Kukre, "GSM based alert and warning system for LANDSLIDING and THUNDER activity," *Int. Res. J. Eng. Technol.*, vol. 05, no. 01, pp. 1442–1445, 2018, [Online]. Available: https://d1wqtxts1xzle7.cloudfront.net/56349092/IRJET-V5I1313.pdf?1524052132=&response-content-disposition=inline%3B+filename%3DGSM_based_alert_and_warning_system_for_L.pdf&Expires=1623055263&Signature=CaI~YdeQhhA9dNvVETk8h-Md~a8dgtgmu8EIVsvl-NXG2F9hIKENeA.

[84] D. P. Kanungo, A. K. Maletha, and M. Singh, "Ground Based Wireless Instrumentation and Real Time Monitoring of Pakhi Landslide, Garhwal Himalayas, Uttarakhand (India)," *Adv. Cult. Living with Landslides*, no. June 2018, 2017, doi: 10.1007/978-3-319-53487-9.

[85] G. Artese, M. Perrelli, S. Artese, S. Meduri, and N. Brogno, "POIS, a low cost tilt and position sensor: Design and first tests," *Sensors (Switzerland)*, vol. 15, no. 5, pp. 10806–10824, 2015, doi: 10.3390/s150510806.

[86] E. Intrieri, G. Gigli, N. Casagli, and F. Nadim, "Brief communication Landslide Early Warning System: Toolbox and general concepts," *Nat. Hazards Earth Syst. Sci.*, vol. 13, no. 1, pp. 85–90, 2013, doi: 10.5194/nhess-13-85-2013.

[87] G. T. Harilal, D. Madhu, M. V. Ramesh, and D. Pullarkatt, "Towards establishing rainfall thresholds for a real-time landslide early warning system in Sikkim, India," *Landslides*, vol. 16, no. 12, pp. 2395–2408, 2019, doi: 10.1007/s10346-019-01244-1.

[88] M. T. Abraham, N. Satyam, S. Kushal, A. Rosi, B. Pradhan, and S. Segoni, "Rainfall threshold estimation and landslide forecasting for Kalimpong, India using SIGMA model," *Water (Switzerland)*, vol. 12, no. 4, 2020, doi: 10.3390/W12041195.

[89] H. Yang, F. Wei, Z. Ma, H. Guo, P. Su, and S. Zhang, "Rainfall threshold for landslide activity in Dazhou, southwest China," *Landslides*, vol. 17, no. 1, pp. 61–77, 2020, doi: 10.1007/s10346-019-01270-z.

[90] A. Dikshit, R. Sarkar, B. Pradhan, S. Acharya, and K. Dorji, "Estimating rainfall thresholds for landslide occurrence in the Bhutan Himalayas," *Water (Switzerland)*, vol. 11, no. 8, pp. 10–13, 2019, doi: 10.3390/w11081616.

[91] S. Naidu, K. S. Sajinkumar, T. Oommen, V. J. Anuja, R. A. Samuel, and C. Muraleedharan, "Early warning system for shallow landslides using rainfall threshold and slope stability analysis," *Geosci. Front.*, vol. 9, no. 6, pp. 1871–1882, 2018, doi: 10.1016/j.gsf.2017.10.008.

[92] A. Dikshit and D. N. Satyam, “Estimation of rainfall thresholds for landslide occurrences in Kalimpong, India,” *Innov. Infrastruct. Solut.*, vol. 3, no. 1, 2018, doi: 10.1007/s41062-018-0132-9.

[93] M. Melillo, M. T. Brunetti, S. Peruccacci, S. L. Gariano, A. Roccati, and F. Guzzetti, “A tool for the automatic calculation of rainfall thresholds for landslide occurrence,” *Environ. Model. Softw.*, vol. 105, pp. 230–243, 2018, doi: 10.1016/j.envsoft.2018.03.024.

[94] A. Rosi, T. Peternel, M. Jemec-Auflič, M. Komac, S. Segoni, and N. Casagli, “Rainfall thresholds for rainfall-induced landslides in Slovenia,” *Landslides*, vol. 13, no. 6, pp. 1571–1577, 2016, doi: 10.1007/s10346-016-0733-3.

[95] M. N. Papa, V. Medina, F. Ciervo, and A. Bateman, “Derivation of critical rainfall thresholds for shallow landslides as a tool for debris flow early warning systems,” *Hydrol. Earth Syst. Sci.*, vol. 17, no. 10, pp. 4095–4107, 2013, doi: 10.5194/hess-17-4095-2013.

[96] D. Tiranti and D. Rabuffetti, “Estimation of rainfall thresholds triggering shallow landslides for an operational warning system implementation,” *Landslides*, vol. 7, no. 4, pp. 471–481, 2010, doi: 10.1007/s10346-010-0198-8.

[97] A. Sengupta, S. Gupta, and K. Anbarasu, “Rainfall thresholds for the initiation of landslide at Lanta Khola in north Sikkim, India,” *Nat. Hazards*, vol. 52, no. 1, pp. 31–42, 2010, doi: 10.1007/s11069-009-9352-9.

[98] N. Caine, “The Rainfall Intensity: Duration Control of Shallow Landslides and Debris Flows,” *Geogr. Ann. Ser. A, Phys. Geogr.*, vol. 62, no. 1/2, p. 23, 1980, doi: 10.2307/520449.

[99] G. Capparelli and P. Versace, “FLaIR and SUSHI: Two mathematical models for early warning of landslides induced by rainfall,” *Landslides*, vol. 8, no. 1, pp. 67–79, 2011, doi: 10.1007/s10346-010-0228-6.

[100] C. Lepore, E. Arnone, L. V. Noto, G. Sivandran, and R. L. Bras, “Physically based modeling of rainfall-triggered landslides: A case study in the Luquillo forest, Puerto Rico,” *Hydrol. Earth Syst. Sci.*, vol. 17, no. 9, pp. 3371–3387, 2013, doi: 10.5194/hess-17-3371-2013.

[101] T. R. Martha, P. Roy, K. B. Govindharaj, K. V. Kumar, P. G. Diwakar, and V. K. Dadhwal, “Landslides triggered by the June 2013 extreme rainfall event in parts of Uttarakhand state, India,” *Landslides*, vol. 12, no. 1, pp. 135–146, 2015, doi: 10.1007/s10346-014-0540-7.

[102] H. Yang, F. Wang, V. Vilímek, K. Araiba, and S. Asano, “Investigation of rainfall-induced shallow landslides on the northeastern rim of Aso caldera, Japan, in July 2012,” *Geoenvironmental Disasters*, vol. 2, no. 1, 2015, doi: 10.1186/s40677-015-0028-3.

[103] V. Gupta, R. K. Bhasin, A. M. Kaynia, R. S. Tandon, and B. Venkateshwarlu, “Landslide Hazard in the Nainital township, Kumaun Himalaya, India: the case of September 2014 Balia Nala landslide,” *Nat. Hazards*, vol. 80, no. 2, pp. 863–877, 2016, doi: 10.1007/s11069-015-2002-5.

[104] S. KS and S. K, “A Geological Appraisal of Slope Instability in Upper Alaknanda Valley, Uttarakhand Himalaya, India,” *J. Geol. Geophys.*, vol. 5, no. 5, 2016, doi: 10.4172/2381-8719.1000258.

[105] J. L. Innes, “Debris Flows / Avalanches :,” vol. 7, pp. 469–501, 1987.

[106] G. B. Crosta and P. Frattini, “Distributed modelling of shallow landslides triggered by intense rainfall,” *Nat. Hazards Earth Syst. Sci.*, vol. 3, no. 1–2, pp. 81–93, 2003, doi: 10.5194/nhess-3-81-2003.

[107] A. Dikshit and N. Satyam, “Rainfall Thresholds for Landslide Occurrence in Kalimpong using Bayesian Approach,” no. December, pp. 14–17, 2017, [Online]. Available: http://www.scirp.org/journal/nr.

[108] B. Mandal, S. Mondal, and S. Mandal, “GIS-based landslide susceptibility zonation (LSZ) mapping of Darjeeling Himalaya, India using weights of evidence (WoE) model,” *Arab. J. Geosci.*, 2023, doi: 10.1007/s12517-023-11523-w.

[109] Z. Liao *et al.*, “Prototyping an experimental early warning system for rainfall-induced landslides in Indonesia using satellite remote sensing and geospatial datasets,” *Landslides*, 2010, doi: 10.1007/s10346-010-0219-7.

[110] A. M. Nanda, P. Ahmed, T. A. Kanth, and Z. ul Hassan, “Landslide Susceptibility Zonation along National Highway 1D from Sonamarg to Kargil, North Western Himalaya,” *J. Geol. Soc. India*, 2023, doi: 10.1007/s12594-023-2346-5.

[111] A. Gokul *et al.*, “Landslide Susceptibility Assessment of a Part of the Western Ghats (India) Employing the AHP and F-AHP Models and Comparison with Existing Susceptibility Maps,” *Land*, 2023, doi: 10.3390/land12020468.

[112] M. Makonyo and Z. Zahor, “GIS-based analysis of landslides susceptibility mapping: a case study of Lushoto district, north-eastern Tanzania,” *Nat. Hazards*, 2023, doi: 10.1007/s11069-023-06038-2.

[113] M. Liu *et al.*, “Landslide Susceptibility Zoning in Yunnan Province Based on SBAS-InSAR Technology and a Random Forest Model,” *Remote Sens.*, 2023, doi: 10.3390/rs15112864.

[114] A. Bhadran, A. L. Achu, G. Gopinath, N. Jesiya, and U. P. Surendran, “Ensemble of fuzzy-analytical hierarchy process in landslide susceptibility modeling from a humid tropical region of Western Ghats, Southern India,” *Environ. Sci. Pollut. Res.*, 2023, doi: 10.1007/s11356-023-27377-4.

[115] L. Zhang *et al.*, “A comparative study of different neural network models for landslide susceptibility mapping,” *Adv. Sp. Res.*, vol. 70, Jul. 2022, doi: 10.1016/j.asr.2022.04.055.

[116] L. Shano, M. Meten, and T. K. Raghuvanshi, “Landslide susceptibility mapping using frequency ratio model: the case of Gamo highland, South Ethiopia,” *Arab. J. Geosci.*, vol. 14, Mar. 2021, doi: 10.1007/s12517-021-06995-7.

[117] A. Saha, S. Mandal, and S. Saha, “Geo-spatial approach-based landslide susceptibility mapping using analytical hierarchical process, frequency ratio, logistic regression and their ensemble methods,” *SN Appl. Sci.*, vol. 2, Sep. 2020, doi: 10.1007/s42452-020-03441-3.

[118] P. Sestraș *et al.*, “Landslides susceptibility assessment based on GIS statistical bivariate analysis in the hills surrounding a metropolitan area.,” *Sustainability*, 2019, doi: 10.3390/su11051362.

[119] W. Chen *et al.*, “Spatial prediction of landslide susceptibility using data mining-based kernel logistic regression, naive Bayes and RBFNetwork models for the Long County area (China),” *Bull. Eng. Geol. Environ.*, 2019, doi: 10.1007/s10064-018-1256-z.

[120] S. Mondal and S. Mandal, “Landslide susceptibility mapping of Darjeeling Himalaya, India using index of entropy (IOE) model,” *Appl. Geomatics*, 2019, doi: 10.1007/s12518-018-0248-9.

[121] G. Chen, L. Qiao, L. Tan, X. Meng, Y. Zhang, and Z. Xie, “A comparative study of landslide susceptibility mapping using weight of evidence, logistic regression and support vector machine and evaluated by SBAS-InSAR monitoring: Zhouqu to Wudu segment in Bailong River Basin, China,” *Environ. Earth Sci.*, vol. 76, Apr. 2017, doi: 10.1007/s12665-017-6640-7.

[122] L. Lin, Q. Lin, and Y. Wang, “Landslide susceptibility mapping on a global scale using the method of logistic regression,” *Nat. Hazards Earth Syst. Sci.*, vol. 17, Aug. 2017, doi: 10.5194/nhess-17-1411-2017.

[123] C. Chalkias, C. Polykretis, E. Karymbalis, and M. Ferentinou, “Integrating Expert Knowledge with Statistical Analysis for Landslide Susceptibility Assessment at Regional Scale,” *Geosciences*, vol. 6, Mar. 2016, doi: 10.3390/geosciences6010014.

[124] A. K. Saha, C. C. Pant, D. C. Sharma, and S. Kundu, “Remote Sensing and GIS Based Landslide Susceptibility Assessment using Binary Logistic Regression Model: A Case Study in the Ganeshganga Watershed, Himalayas,” *J. Indian Soc. Remote Sens.*, vol. 41, Jan. 2013, doi: 10.1007/s12524-012-0255-y.

[125] A. K. Roy, S. Sarkar, and T. R. Martha, “Landslide susceptibility assessment using Information Value Method in parts of the Darjeeling Himalayas,” *J. Geol. Soc. India*, vol. 82, Oct. 2013, doi: 10.1007/s12594-013-0162-z.

[126] S. S. Chandrasekaran, R. Sayed Owaise, S. Ashwin, R. M. Jain, S. Prasanth, and R. B. Venugopalan, “Investigation on infrastructural damages by rainfall-induced landslides during November 2009 in Nilgiris, India,” *Nat. Hazards*, vol. 65, no. 3, pp. 1535–1557, 2013, doi: 10.1007/s11069-012-0432-x.

[127] A. P. Paswan and A. k. Shrivastava, “Modelling of rainfall-induced landslide: a threshold-based approach,” *Arab. J. Geosci.*, vol. 15, no. 8, p. 795, 2022, doi: 10.1007/s12517-022-10024-6.

[128] K. Singh and V. Kumar, “Slope stability analysis of landslide zones in the part of Himalaya, Chamba, Himachal Pradesh, India,” *Environ. Earth Sci.*, vol. 80, no. 8, pp. 1–15, 2021, doi: 10.1007/s12665-021-09629-z.

[129] S. J. Harris, R. P. Orense, and K. Itoh, “Back analyses of rainfall-induced slope failure in Northland Allochthon formation,” *Landslides*, vol. 9, no. 3, pp. 349–356, 2012, doi: 10.1007/s10346-011-0309-1.

[130] R. K. Dahal, “Rainfall-induced Landslides in Nepal,” *Int. J. Eros. Control Eng.*, vol. 5, no. 1, pp. 1–8, 2012, doi: 10.13101/ijece.5.1.

[131] M. L. Lee, K. Y. Ng, Y. F. Huang, and W. C. Li, “Rainfall-induced landslides in Hulu Kelang area, Malaysia,” *Nat. Hazards*, vol. 70, no. 1, pp. 353–375, 2014, doi: 10.1007/s11069-013-0814-8.

[132] L. Zhang, F. Wu, H. Zhang, L. Zhang, and J. Zhang, “Influences of internal erosion on infiltration and slope stability,” *Bull. Eng. Geol. Environ.*, vol. 78, no. 3, pp. 1815–1827, 2019, doi: 10.1007/s10064-017-1185-2.

[133] N. Kumar, A. K. Verma, S. Sardana, K. Sarkar, and T. N. Singh, “Comparative analysis of limit equilibrium and numerical methods for prediction of a landslide,” *Bull. Eng. Geol. Environ.*, vol. 77, no. 2, pp. 595–608, 2018, doi: 10.1007/s10064-017-1183-4.

[134] I. Jamir, V. Gupta, V. Kumar, and G. T. Thong, “Evaluation of potential surface instability using finite element method in Kharsali Village, Yamuna Valley, Northwest Himalaya,” *J. Mt. Sci.*, vol. 14, no. 8, pp. 1666–1676, 2017, doi: 10.1007/s11629-017-4410-3.

[135] V. Senthilkumar, S. S. Chandrasekaran, and V. B. Maji, “Geotechnical characterization and analysis of rainfall—induced 2009 landslide at Marappalam area of Nilgiris district, Tamil Nadu state, India,” *Landslides*, vol. 14, no. 5, pp. 1803–1814, 2017, doi: 10.1007/s10346-017-0839-2.

[136] S. Jeong, K. Lee, J. Kim, and Y. Kim, “Analysis of rainfall-induced landslide on unsaturated soil slopes,” *Sustain.*, vol. 9, no. 7, pp. 1–20, 2017, doi: 10.3390/su9071280.

[137] V. Gupta *et al.*, “Finite element analysis of failed slope by shear strength reduction technique: a case study for Surabhi Resort Landslide, Mussoorie township, Garhwal Himalaya,” *Geomatics, Nat. Hazards Risk*, vol. 7, no. 5, pp. 1677–1690, 2016, doi: 10.1080/19475705.2015.1102778.

[138] O. Igwe, W. Mode, O. Nnebedum, I. Okonkwo, and I. Oha, “The analysis of rainfall-induced slope failures at Iva Valley area of Enugu State, Nigeria,” *Environ. Earth Sci.*, vol. 71, no. 5, pp. 2465–2480, 2014, doi: 10.1007/s12665-013-2647-x.

[139] B. D. Collins and D. Znidarcic, “Stability Analyses of Rainfall Induced Landslides,” *J. Geotech. Geoenvironmental Eng.*, vol. 130, no. 4, pp. 362–372, 2004, doi: 10.1061/(asce)1090-0241(2004)130:4(362).

[140] Y. M. Cheng and C. K. Lau, “A study on factor of safety evaluation in slope stability analysis,” *HKIE Trans. Hong Kong Inst. Eng.*, vol. 8, no. 1, pp. 28–34, 2013, doi: 10.1080/1023697X.2001.10667838.

[141] D. G. Fredlund, Anqing Xing, and Shangyan Huang, “Predicting the permeability function for unsaturated soils using the soil-water characteristic curve,” *Can. Geotech. J.*, vol. 31, no. 4, pp. 533–546, 1994, doi: 10.1139/t94-062.

[142] C. W. W. Ng, B. Wang, and Y. K. Tung, “Three-dimensional numerical investigations of groundwater responses in an unsaturated slope subjected to various rainfall patterns,” *Can. Geotech. J.*, vol. 38, no. 5, pp. 1049–1062, 2001, doi: 10.1139/cgj-38-5-1049.

[143] D. Dudeja, S. P. Bhatt, and A. K. Biyani, “Stability assessment of slide zones in Lesser Himalayan part of Yamunotri pilgrimage route, Uttarakhand, India,” *Environ. Earth Sci.*, vol. 76, no. 1, pp. 1–18, 2017, doi: 10.1007/s12665-016-6366-y.

[144] D. P. Kanungo, A. Pain, and S. Sharma, “Finite element modeling approach to assess the stability of debris and rock slopes: A case study from the Indian Himalayas,” *Nat. Hazards*, vol. 69, no. 1, pp. 1–24, 2013, doi: 10.1007/s11069-013-0680-4.

[145] K. Sarkar, T. N. Singh, and A. K. Verma, “A numerical simulation of landslide-prone

slope in himalayan region—A case study," *Arab. J. Geosci.*, vol. 5, no. 1, pp. 73–81, 2012, doi: 10.1007/s12517-010-0148-8.

[146] N. A. Hammouri, A. I. Husein Malkawi, and M. M. A. Yamin, "Stability analysis of slopes using the finite element method and limiting equilibrium approach," *Bull. Eng. Geol. Environ.*, vol. 67, no. 4, pp. 471–478, 2008, doi: 10.1007/s10064-008-0156-z.

[147] T. N. Singh, A. Gulati, L. Dontha, and V. Bhardwaj, "Evaluating cut slope failure by numerical analysis - A case study," *Nat. Hazards*, vol. 47, no. 2, pp. 263–279, 2008, doi: 10.1007/s11069-008-9219-5.

[148] D. Y. Zhu, C. F. Lee, and H. D. Jiang, "Generalised framework of limit equilibrium methods for slope stability analysis," *Geotechnique*, vol. 53, no. 4, pp. 377–395, 2003, doi: 10.1680/geot.2003.53.4.377.

[149] S. Guan, Z. Shi, and H. Zheng, "Effects of soil properties and geomorphic parameters on the breach mechanisms of landslide dams and prediction of peak discharge," *Acta Geotech.*, vol. 2, 2023, doi: 10.1007/s11440-023-01908-2.

[150] J. Cogan and I. Gratchev, "A study on the effect of rainfall and slope characteristics on landslide initiation by means of flume tests," *Landslides*, vol. 16, no. 12, pp. 2369–2379, 2019, doi: 10.1007/s10346-019-01261-0.

[151] Z. Zhang, T. Wang, S. Wu, H. Tang, and C. Liang, "Investigation of dormant landslides in earthquake conditions using a physical model," *Landslides*, vol. 14, no. 3, pp. 1181–1193, 2017, doi: 10.1007/s10346-017-0813-z.

[152] B. P. Wen and L. He, "Influence of lixiviation by irrigation water on residual shear strength of weathered red mudstone in Northwest China: Implication for its role in landslides' reactivation," *Eng. Geol.*, vol. 151, pp. 56–63, 2012, doi: 10.1016/j.enggeo.2012.08.005.

[153] Y. F. Zhou, L. G. Tham, W. M. Yan, F. C. Dai, and L. Xu, "Laboratory study on soil behavior in loess slope subjected to infiltration," *Eng. Geol.*, vol. 183, pp. 31–38, 2014, doi: 10.1016/j.enggeo.2014.09.010.

[154] X. gang Wang, B. qin Lian, L. Kai, and L. Li, "Trigger mechanism of loess-mudstone landslides inferred from ring shear tests and numerical simulation," *J. Mt. Sci.*, vol. 18, no. 9, pp. 2412–2426, 2021, doi: 10.1007/s11629-021-6791-6.

[155] S. Li, C. Li, D. Yao, C. Liu, and Y. Zhang, "Multiscale nonlinear analysis of failure mechanism of loess-mudstone landslide," *CATENA*, vol. 213, p. 106188, 2022, doi: https://doi.org/10.1016/j.catena.2022.106188.

[156] H. Ling and H. I. Ling, "Centrifuge Model Simulations of Rainfall-Induced Slope Instability," *J. Geotech. Geoenvironmental Eng.*, vol. 138, no. 9, pp. 1151–1157, 2012, doi: 10.1061/(asce)gt.1943-5606.0000679.

[157] a Askarinejad *et al.*, "Physical modelling of rainfall induced landslides under controlled climatic conditions," *Eurofuge 2012*, vol., no., 2012, [Online]. Available: http://repository.tudelft.nl/assets/uuid:8105d54f-89af-49b9-9eb1-99e8f5729527/Askarinejad-_Physical_modelling_of_rainfall_induced_landslides_under_controlled_climatic_conditions.pdf.

[158] J. Peranić, N. Čeh, and Ž. Arbanas, “The Use of Soil Moisture and Pore-Water Pressure Sensors for the Interpretation of Landslide Behavior in Small-Scale Physical Models,” *Sensors*, vol. 22, no. 19, 2022, doi: 10.3390/s22197337.

[159] Q. Zhan, S. Wang, F. Guo, Y. Chen, L. Wang, and D. Zhao, “Early warning model and model test verification of rainfall-induced shallow landslide,” *Bull. Eng. Geol. Environ.*, vol. 81, no. 8, 2022, doi: 10.1007/s10064-022-02827-4.

[160] M. Vivoda Prodan, J. Peranić, S. Pajalić, and Ž. Arbanas, “Physical Modelling of Rainfall-Induced Sandy and Clay-Like Slope Failures,” *Adv. Mater. Sci. Eng.*, vol. 2023, 2023, doi: 10.1155/2023/3234542.

[161] J. Peranić, V. Jagodnik, N. Čeh, M. Vivoda Prodan, S. Pajalić, and Ž. Arbanas, “Small-scale physical landslide models under 1g infiltration conditions and the role of hydrological monitoring,” *Proc. 5th ReSyLAB ’Landslide Model. Appl.* , no. March, pp. 171–180, 2022.

[162] Ž. Arbanas, V. Jagodnik, J. Peranić, S. Pajalić, M. V. Prodan, and N. Čeh, “Physical Model of Rainfall Induced Landslide in Flume Test : Preliminary Results,” *4th Eur. Conf. Phys. Model. Geotech. - ECPMG 2020At Luleå, Sweden*, no. September, pp. 115–122, 2020, [Online]. Available: https://www.researchgate.net/publication/344174593.

[163] H. Wang, B. Xu, J. Zhang, X. Guo, Q. Zeng, and L. Zhang, “Rainfall thresholds of debris flows based on varying rainfall intensity types in the mountain areas of Beijing,” *Geomatics, Nat. Hazards Risk*, vol. 13, no. 1, pp. 2166–2181, 2022, doi: 10.1080/19475705.2022.2111281.

[164] Y. Zhang, Y. Zhu, X. Yan, S. Li, Q. Yu, and Y. Wang, “A determination method of rainfall type based on rainfall-induced slope instability,” *Nat. Hazards*, vol. 113, no. 1, pp. 315–328, 2022, doi: 10.1007/s11069-022-05301-2.

[165] C. Arnhardt *et al.*, “based Landslide Early Warning System -- SLEWS. Development of a geoservice infrastructure as basis for early warning systems for landslides by integration of,” *Geotechnol. Sci. Report. Early Warn. Syst. Earth Manag. Kick-Off-Meeting 10 Oct. 2007 Tech. Univ. Karlsruhe*, no. October, pp. 75–88, 2007, [Online]. Available: http://www.winsoc.org/pdf/ATT00010.pdf.

[166] J. S. Gidon and S. Sahoo, “Hydrological effects on Rainfall-Induced Slope instability: A Case Study,” *Res. Sq.*, pp. 1–27, 2023.

[167] V. Menon, “Effects of pore water pressure on the slope profile of a laboratory simulated rainfall-induced landslides,” pp. 1–18, 2023.

[168] M. Kuradusenge, S. Kumaran, M. Zennaro, and A. Niyonzima, “Experimental Study of Site-Specific Soil Water Content and Rainfall Inducing Shallow Landslides: Case of Gakenke District, Rwanda,” *Geofluids*, vol. 2021, 2021, doi: 10.1155/2021/7194988.

[169] J. Uwihirwe, M. Hrachowitz, and T. A. Bogaard, “Landslide precipitation thresholds in Rwanda,” *Landslides*, vol. 17, no. 10, pp. 2469–2481, 2020, doi: 10.1007/s10346-020-01457-9.

[170] H. Wu and T. Song, “An evaluation of landslide susceptibility using probability statistic modeling and GIS’s spatial clustering analysis,” *Hum. Ecol. Risk Assess.*, vol. 24, no. 7, pp. 1952–1968, 2018, doi: 10.1080/10807039.2018.1435253.

[171] F. Rollo and S. Rampello, “Probabilistic assessment of seismic-induced slope displacements: an application in Italy,” *Bull. Earthq. Eng.*, vol. 19, no. 11, pp. 4261–4288, 2021, doi: 10.1007/s10518-021-01138-5.

[172] BIS, “IS 14496 (Part 2) : 1998,” 1998.

[173] P. Roshan and S. Pal, “Structural challenges for seismic stability of buildings in hilly areas,” *Environ. Sci. Pollut. Res.*, no. 0123456789, 2022, doi: 10.1007/s11356-022-23263-7.

[174] T. J. Kelleners, R. W. O. Soppe, D. A. Robinson, M. G. Schaap, J. E. Ayars, and T. H. Skaggs, “Calibration of Capacitance Probe Sensors using Electric Circuit Theory,” *Soil Sci. Soc. Am. J.*, vol. 68, no. 2, pp. 430–439, 2004, doi: 10.2136/sssaj2004.4300.

[175] P. Placidi, L. Gasperini, A. Grassi, M. Cecconi, and A. Scorzoni, “Characterization of low-cost capacitive soil moisture sensors for IoT networks,” *Sensors (Switzerland)*, vol. 20, no. 12, pp. 1–14, 2020, doi: 10.3390/s20123585.

[176] J. Hrisko, “Capacitive Soil Moisture Sensor Calibration with,” *Mak. Portal LLC*, no. 0, pp. 1–24, 2020.

[177] N. Ida, *Engineering Electromagnetics*. 2015.

[178] DFRobot, “Capacitive Soil Moisture Sensor,” pp. 1–6, 2018, [Online]. Available: https://www.sigmaelectronica.net/wp-content/uploads/2018/04/sen0193-humedad-de-suelos.pdf.

[179] A. Joshi, J. Grover, D. Prasanna Kanungo, and R. Kumar Panigrahi, “Real-time Landslide Monitoring, Detection and Early Warning System for Tangni Landslide,” *SSRN Electron. J.*, pp. 1–6, 2020, doi: 10.2139/ssrn.3511001.

[180] M. Gamperl, J. Singer, and K. Thuro, “Internet of things geosensor network for cost-effective landslide early warning systems,” *Sensors*, vol. 21, no. 8, pp. 1–23, 2021, doi: 10.3390/s21082609.

[181] P. Chaturvedi *et al.*, “A Low-Cost IoT Framework for Landslide Prediction and Risk Communication,” *Internet Things A to Z*, no. March, pp. 593–610, 2018, doi: 10.1002/9781119456735.ch21.

[182] A. Pathania *et al.*, “A Low Cost, Sub-Surface IoT Framework for Landslide Monitoring, Warning, and Prediction,” *2020 Int. Conf. Adv. Comput. Commun. Embed. Secur. Syst.*, no. March, 2020, [Online]. Available: https://www.researchgate.net/publication/339850328_A_Low_Cost_Sub-Surface_IoT_Framework_for_Landslide_Monitoring_Warning_and_Prediction.

[183] T. Gracchi, “International Doctorate in Civil and Environmental Engineering Wireless sensor networks for landslide monitoring : application and optimization by visibility analysis on 3D point clouds Teresa Gracchi,” 2019.

[184] Asian Development Bank, “Landslide Risk Management Sector Project,” 2021. [Online]. Available: https://www.adb.org/sites/default/files/linked-documents/53022-001-sd-05.pdf.

[185] Robu, “MEMS sensor and components,” 2023. https://robu.in/ (accessed Oct. 05, 2023).

[186] Y. Luo, S. ming He, F. zhu Chen, X. po Li, and J. chuan He, "A physical model considered the effect of overland water flow on rainfall-induced shallow landslides," *Geoenvironmental Disasters*, vol. 2, no. 1, 2015, doi: 10.1186/s40677-015-0017-6.

[187] A. W. Skempton, "Residual strength of clays in landslides, folded strata and the laboratory," *Geotechnique*, vol. 35, no. 1, pp. 3–18, 1985, doi: 10.1680/geot.1985.35.1.3.

[188] S. T. Y. Wong, D. E. L. Ong, and R. G. Robinson, "Behaviour of MH silts with varying plasticity indices," *Geotech. Res.*, vol. 4, no. 2, pp. 118–135, 2017, doi: 10.1680/jgere.17.00002.

[189] R. M. Iverson, "Landslide triggering by rain infiltration," *Water Resour. Res.*, vol. 36, no. 7, pp. 1897–1910, 2000, doi: 10.1029/2000WR900090.

[190] K. Sarkar, A. K. Singh, A. Niyogi, P. K. Behera, A. K. Verma, and T. N. Singh, "The assessment of slope stability along NH-22 in Rampur-Jhakri Area, Himachal Pradesh," *J. Geol. Soc. India*, vol. 88, no. 3, pp. 387–393, 2016, doi: 10.1007/s12594-016-0500-z.

[191] S. K. Mittal, M. Singh, and B. Singh, "Monitoring of Jhakri Landslide in Bari Village Area of Himachal Pradesh," pp. 129–134, 2013.

[192] C. Prakasam, R. Aravinth, B. Nagarajan, and V. S. Kanwar, "Site-specific geological and geotechnical investigation of a debris landslide along unstable road cut slopes in the Himalayan region, India," *Geomatics, Nat. Hazards Risk*, vol. 11, no. 1, pp. 1827–1848, 2020, doi: 10.1080/19475705.2020.1813812.

[193] Bhukosh - Geological Survey of India, "Lithological map," *GSI*. https://bhukosh.gsi.gov.in/Bhukosh/MapViewer.aspx (accessed Oct. 10, 2023).

[194] IS:2720 (Part 4), "Indian Standard, Methods of Test for Soils, Part 4: Grain Size Analysis," *Bur. Indian Stand. New Delhi, India.*, vol. Reaffirmed, no. 2006, pp. 1–38, 1985.

[195] HPSDMA, "GOVERNMENT OF HIMACHAL PRADESH (DISASTER MANAGEMENT CELL) MEMORANDUM OF DAMAGES DUE TO FLASH FLOODS , CLOUDBURSTS AND LANDSLIDES DURING MONSOON SEASON – 2022," 2022, [Online]. Available: https://hpsdma.nic.in/admnis/admin/showimg.aspx?ID=3516.

[196] BIS, "IS 14496 (Part 2) : 1998," 2007.

[197] G. F. Wieczorek, *Landslide Triggering mechanism*. 1996.

[198] R. K. Sharma, B. S. Mehta, and C. S. Jamwal, "Cut slope stability evaluation of NH-21 along Nalayan-Gambhrola section, Bilaspur district, Himachal Pradesh, India," *Nat. Hazards*, vol. 66, no. 2, pp. 249–270, 2013, doi: 10.1007/s11069-012-0469-x.

[199] P. T. Ilamkar and A. Kohli, "Report on geological assessment of Kotrupi landslide, Mandi - Jogindernagar - Pathankot National Highway (N.H.-154), tehsil Padhar, district Mandi, Himachal Pradesh," *Geol. Surv. India*, vol. 6, pp. 5–9, 2017.

[200] P. Sharma, S. Rawat, and A. K. Gupta, "Study and Remedy of Kotropi Landslide in Himachal Pradesh, India," *Indian Geotech. J.*, vol. 49, no. 6, pp. 603–619, 2019, doi: 10.1007/s40098-018-0343-1.

[201] ISRO, “Kotrupi landslide, Mandi district, Himachal Pradesh, (A preliminary report) National Remote Sensing Centre / ISRO , Hyderabad,” vol. 2, pp. 4–6, 2017.

[202] S. Prakash and A. Kathait, *A Case Study on Kotrupi Landslide 2017, Mandi District, Himachal Pradesh National*. National Institute of Disaster Management (NIDM), Ministry of Home Affairs, Government of India, New Delhi-110042, 2021.

[203] IS: 2720 (part 5), “Determination of liquid and plastic limit,” *Bur. Indian Stand. New Delhi, India.*, vol. Reaffirmed, no. 2006, pp. 1–16, 1985.

[204] IS : 2720 (Part 7-1980), “determination of water content -dry density relation using light compaction,” *Bur. Indian Stand. (BIS), IS.2720-11*, pp. 1–16, 2011.

[205] S. A. Anderson and N. Sitar, “Analysis of rainfall-induced debris flows,” *J. Geotech. Eng.*, vol. 121, no. 7, pp. 544–552, 1995, doi: 10.1061/(ASCE)0733-9410(1995)121:7(544).

[206] IS: 2720 (part 11), “Determination of the shear strength parameters of a specimen tested in Unconsolidated Undrained triaxial compression without the measurement of pore water pressure,” *Bur. Indian Stand. (BIS), IS.2720-11*, 1993.

[207] IS.2720 (Part 3):1980, “Indian Standard, Determination of specific gravity, Part 3 (Section II)- Fine, medium and coarse grained soils,” *Bur. Indian Stand. New Delhi, India.*, vol. Reaffirmed, no. 2002, pp. 1–8, 1980.

[208] IS: 2720 (part 12), “Determination of shear strength parameters of soil from consolidated undrained triaxial compression test with measurement of pore water pressure,” *Is 2720*, vol. Part XII, 1981.

[209] IS:2720 (Part 2), “Indian standard, Methods of test for soils, Part 2: Determination of water content,” *Bur. Indian Stand. New Delhi, India.*, vol. Reaffirmed, no. 2010, pp. 1–17, 1973.

[210] IS:2720 (Part 1): 1983, “Methods of test for soils, Part 1: Preparation of dry soil samples for various tests,” *Bur. Indian Stand. New Delhi*, vol. Reaffirmed, no. 2006, pp. 1–10, 1983, [Online]. Available: https://ia800900.us.archive.org/29/items/gov.in.is.2720.1.1983/is.2720.1.1983.pdf.

[211] Bureau of Indian Standards, “Determination of water content-dry density relation using heavy compaction,” *Is 2720*, vol. Part VIII, pp. 3562–3577, 1983.

[212] C. Kristo, H. Rahardjo, and A. Satyanaga, “Effect of variations in rainfall intensity on slope stability in Singapore,” *Int. Soil Water Conserv. Res.*, vol. 5, no. 4, pp. 258–264, 2017, doi: 10.1016/j.iswcr.2017.07.001.

[213] S. P. Pradhan, S. D. Panda, A. R. Roul, and M. Thakur, “Insights into the recent Kotropi landslide of August 2017, India: a geological investigation and slope stability analysis,” *Landslides*, vol. 16, no. 8, pp. 1529–1537, 2019, doi: 10.1007/s10346-019-01186-8.

[214] N. Mali, D. P. Shukla, and V. U. Kala, “Identifying Geotechnical Characteristics for Landslide Hazard Indication: A Case Study in Mandi, Himachal Pradesh, India,” *Arab. J. Geosci.*, vol. 15, no. 2, 2022, doi: 10.1007/s12517-022-09475-8.

[215] S. Chakraborty, R. Hore, A. M. Shuvon, K. Kamrul, and M. A. Ansary, “Physical and numerical analysis of reinforced soil wall on clayey foundation under repetitive loading: effect of fineness modulus of backfill material,” *Arab. J. Geosci.*, vol. 14, no. 12, 2021, doi: 10.1007/s12517-021-07317-7.

[216] A. P. Paswan and A. K. Shrivastava, “Modelling of rainfall - induced landslide : a threshold - based approach,” *Arab. J. Geosci.*, vol. 15, pp. 1–19, 2022, doi: 10.1007/s12517-022-10024-6.

[217] J. Burland, “The Geotechnical Triangle,” *ICE Man. Geotech. Eng.*, vol. 1, pp. 17–26, 2012, doi: 10.1680/moge.57074.0017.

[218] H. Lin and W. Zhong, “Influence of Rainfall Intensity and Its Pattern on the Stability of Unsaturated Soil Slope,” *Geotech. Geol. Eng.*, vol. 37, no. 2, pp. 615–623, 2019, doi: 10.1007/s10706-018-0631-7.

[219] Y. Zhao, “Transient stability analysis method and sensitivity study of unsaturated soil slopes under consideration of rainfall conditions,” *Arab. J. Geosci.*, vol. 14, no. 12, 2021, doi: 10.1007/s12517-021-07514-4.

[220] GEO-SLOPE International Ltd, “Seepage Modeling with SEEP / W 2012,” *Geostudio*, no. July, p. 199, 2012, [Online]. Available: http://www.geo-slope.com.

[221] V. Jagodnik, “Rainfall infiltration and stability analysis of an unsaturated slope in residual soil from flysch rock mass Infiltration pluviale et analyse de la stabilité d ’ une pente non saturée,” 2019, doi: 10.32075/17ECSMGE-2019-0906.

[222] N. R. Morgenstern and V. E. Price, “A Numerical Method for Solving the Equations of Stability of General Slip Surfaces,” *Comput. J.*, vol. 9, no. 4, pp. 388–393, 1967, doi: 10.1093/comjnl/9.4.388.

[223] D. G. Fredlund and J. Krahn, “Comparison of slope stability methods of analysis,” *Can. Geotech. J.*, vol. 14, no. 3, pp. 429–439, 1977, doi: 10.1139/t77-045.

[224] D. G. Fredlund, J. Krahn, and D. E. Pufahl, “The relationship between limit equilibrium slope stability methods.,” *Soil Mech. Found. Eng. Proc. 10th Int. Conf. Stock. June 1981. Vol. 3*, no. June 1981, pp. 409–416, 1981, doi: 10.1016/0148-9062(84)91799-6.

[225] E. Spencer, “A Method of analysis of the Stability of Embankments Assuming Parallel Inter-Slice Forces,” *Géotechnique*, vol. 17, no. 1, pp. 11–26, 1967, doi: 10.1680/geot.1967.17.1.11.

[226] N. R. Morgenstern and V. E. Price, “The Analysis of the Stability of General Slip Surfaces,” *Géotechnique*, vol. 15, no. 1, pp. 79–93, 1965, doi: 10.1680/geot.1965.15.1.79.

[227] GEO-SLOPE, “Stability modeling with Slope/W,” *... Methodol. Calgary, Canada, Geo-Slope/W ...*, no. June, 2012, [Online]. Available: http://www.eng.uwo.ca/people/tnewson/Lectures/SLOPEW Engineering Book.pdf.

[228] M. Aubertin, M. Mbonimpa, B. Bussière, and R. P. Chapuis, “A model to predict the water retention curve from basic geotechnical properties,” *Can. Geotech. J.*, vol. 40, no. 6, pp. 1104–1122, 2003, doi: 10.1139/t03-054.

[229] D. G. Fredlund and Anqing Xing, “Equations for the soil-water characteristic curve,” *Can. Geotech. J.*, vol. 31, no. 4, pp. 521–532, 1994, doi: 10.1139/t94-061.

[230] E. C. Leong and H. Rahardjo, “PERMEABILITY FUNCTIONS FOR UNSATURATED SOILS By E. C. Leong,” *J. Geotech. Geoenvironmental Eng.*, vol. 123, no. 12, pp. 1118–1126, 1998.

[231] GEO-SLOPE International Ltd, “Seepage Modeling with SEEP / W 2015,” *Geostudio*, no. July, p. 199, 2012, [Online]. Available: http://www.geo-slope.com.

[232] T. C. Hopkins, D. L. Allen, and R. C. Deen, “Effects of Water on Slope Stability,” p. 45p, 1975.

[233] X. Luo, J. Yuan, and T. Gu, “Study on the stability of slopes on both sides of highway in rock area under rainfall,” *Arab. J. Geosci.*, vol. 14, no. 6, 2021, doi: 10.1007/s12517-021-06857-2.

[234] T. T. Lim, H. Rahardjo, M. F. Chang, and D. G. Fredlund, “Effect of rainfall on matric suctions in a residual soil slope,” *Can. Geotech. J.*, pp. 618–628, 1996.

LIST OF PUBLICATIONS

Journals SCI/SCIE

1. Paswan, A. P., & Shrivastava, A. K. (2022). Modelling of rainfall - induced landslide: a threshold - based approach. Arabian Journal of Geosciences, 15, 1–19. https://doi.org/10.1007/s12517-022-10024-6
2. Paswan, A. P., & Shrivastava, A. K. (2023). Evaluation of a Tilt-Based Monitoring System for Rainfall-Induced Landslides: Development and Physical Modelling. Water, 15(10), 1862. https://doi.org/10.3390/w15101862
3. Paswan, A.P., Shrivastava, A.K., Study of rainfall-induced landslide using self-developed tilt monitoring system: a physical and numerical modelling approach. Journal of Applied and Regional Geology. (Under Review)
4. Paswan, A.P., Shrivastava, A.K., Influence of transient seepage conditions on stability of rainfall-induced landslide: a numerical approach. Advances in Civil Engineering. (Under Review)

Conference Presented

1. Presented the paper titled “Stability Analysis of Slope Induced with Coal Ash Dykes” into 4th International Conference on Inventive Research in Material Science and Technology ICIRMST 2023 held during 20-21, January 2023 organized by RVS Technical Campus Coimbatore, India
2. Presented the paper titled, “Study of Rainfall-Induced Landslide Using Modelling Methods” into 27th International Conference on Hydraulics, Water Resources, Environmental and Coastal Engineering 22nd-24th December, 2022 Under the Aegis of Punjab Engineering College, Chandigarh & The Indian Society for Hydraulics (ISH), Pune, India
3. Presented the paper titled “Stability analysis of rainfall-induced landslide” into 3rd international conference on Emerging Trends in Muti-Disciplinary Research “ETMDR-2022 organized by Poornima University, Jaipur, India.
4. Presented the paper titled “Numerical modelling of rainfall-induced landslide” into International Conference on Sustainable Development and Recent Trends in Civil

Engineering held during 4th – 5th January, 2022 organized by Dr. Akhilesh Das Gupta Institute of Technology & Management, New Delhi, India and won the Best Paper Award.

Conference Proceeding

1. Paswan, A.P., Shrivastava, A.K.: Stability analysis of rainfall-induced landslide. In: 3rd International Online Conference on Emerging Trends in Multi-Disciplinary Research "ETMDR-2022." pp. 505–509 (2022)
2. Paswan, A.P., Shrivastava, A.K.: Numerical modelling of rainfall-induced landslide. In: International e-Conference on Sustainable Development & Recent Trends in Civil Engineering. pp. 8–13 (2022)

***